U.PORTO
FACULDADE DE CIÊNCIAS
UNIVERSIDADE DO PORTO

FACULDADE DE
CIÊNCIAS E TECNOLOGIA
UNIVERSIDADE NOVA DE LISBOA

Design of novel 3-hydroxy-4-pyridinone iron chelators to fight mycobacterium infection

Tânia Moniz

Tese de Doutoramento apresentada à
Faculdade de Ciências da Universidade do Porto,
Faculdade de Ciências e Tecnologia da Universidade Nova de Lisboa,
Química Sustentável

2016

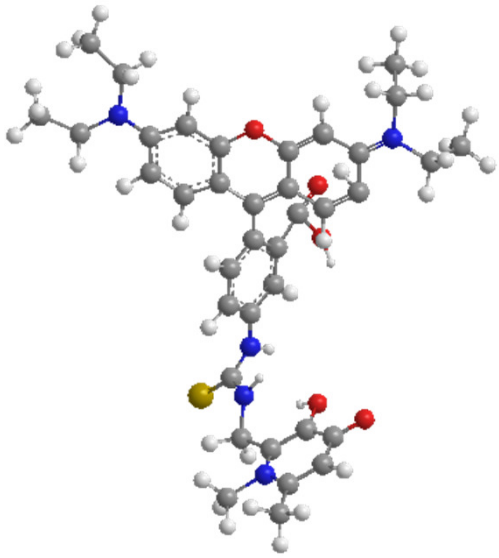

Design of novel 3-hydroxy-4-pyridinone iron chelators to fight mycobacterium infection

Tânia Moniz

Doutoramento em Química Sustentável

Departamento Química e Bioquímica

2016

Orientador

Professora Doutora Maria da Conceição Rangel, Professora Associada Agregada, Instituto de Ciências Biomédicas Abel Salazar

Coorientador

Professor Doutor Baltazar Manuel Romão de Castro, Professor Catedrático, Faculdade de Ciências da Universidade do Porto

This work was conducted at REQUIMTE, Department of Chemistry and Biochemistry, University of Porto, Portugal, under the supervision of Professor Doctor Maria Rangel and Professor Doctor Baltazar de Castro.

The work presented in this dissertation was supported by a PhD fellowship from the Portuguese Foundation for Science and Technology (FCT) to the author (SFRH/BD/79874/2011).

ACKNOWLEGDMENTS / AGRADECIMENTOS

À Fundação para a Ciência e Tecnologia (FCT), a atribuição da Bolsa de Doutoramento, SFRH/BD/79874/2011.
À Faculdade de Ciências da Universidade do Porto e à Faculdade de Ciências e Tecnologia da Universidade Nova de Lisboa por me terem aceite como estudante do Programa Doutoral em Química Sustentável (PDQS). Ao PDQS um especial agradecimento pelos conteúdos lecionados e pelas atividades organizadas.

À Professora Doutora Maria Rangel agradeço a excecional orientação e tudo o que me tem ensinado, a todos os níveis, ao longo destes anos de estudo. Obrigada pelas discussões tão construtivas, por todo o rigor que me incute e por despertar sempre em mim o espírito crítico. Agradeço todo o carinho, paciência e preocupação sempre presentes e sobretudo por ser sempre muito mais do que uma orientadora.
Ao Professor Doutor Baltazar de Castro, co-orientador da presente tese, agradeço a orientação, as suas críticas tão valiosas e a sua boa disposição sempre contagiante.

Ao Luís Cunha-Silva pela obtenção das estruturas de Raios-X e por toda a sua dedicação no tratamento dos dados.
À Professora Doutora Paula Gameiro, por me ter recebido no seu laboratório e por toda a ajuda no trabalho respeitante à utilização de lipossomas como modelos membranares.
À Doutora Maria José Feio pela sua dedicação na realização dos testes inibição de crescimento com outras espécies bacterianas.
Ao Laboratório de Análise Estrutural da Universidade do Porto (CEMUP), em particular à Mariana Andrade pela disponibilidade na obtenção dos espetros de NMR e ao André Silva e à Sílvia Maia pela aquisição dos MS.
A special acknowledgment to Galya Ivanova, for the enthusiasm in the NMR experiments with liposomes, for the precious help in the spectra interpretation and for everything that I learn with you about NMR. Thanks for your friendship and good ideas.

À Professora Doutora Salomé Gomes e ao Professor Doutor Pedro Rodrigues por me terem recebido sempre tão bem no seu grupo de investigação e me terem permitido realizar os estudos microbiológicos em *M. avium*. Agradeço por toda a disponibilidade sempre demonstrada durante os ensaios e na discussão de resultados.

Ao Grupo da Química Teórica, liderado pela Professora Doutora Maria João Ramos e pelo Professor Doutor Pedro Fernandes, agradeço toda a disponibilidade e empenho na execução dos cálculos teóricos realizados. Um especial agradecimento aos colegas Natércia Teixeira e João Coimbra.

À Professora Doutora Lourdes Basto e ao Professor Doutor Fernando Remião agradeço a enorme disponibilidade em me receberem no seu laboratório e me permitirem realizar os estudos de toxicidade. Agradeço a todas as colegas de laboratório por toda a ajuda prestada e em especial à Diana Dias da Silva por tudo o que me ensinou, pela sua enorme dedicação, em todas as horas e qualquer dia da semana, pelo seu enorme companheirismo e ajuda no tratamento e discussão dos resultados.

A todos os colegas de laboratório da FCUP, agradeço o companheirismo, boa disposição e excelente companhia nas pausas para almoço.

Não podia deixar de agradecer em particular aos colegas de grupo, que foram sempre muito mais do que colegas. À Ana Margarida, agradeço a toda a disponibilidade e dedicação na síntese de compostos. Obrigada sobretudo pela boa energia e a alegria contagiante das tuas gargalhadas. Ao André Silva, agradeço o companheirismo no laboratório, todo o enorme e estimulante apoio na escrita da tese e pelo espírito crítico na discussão de resultados. À Carla e ao Filipe agradeço por todo o carinho e por estarem, incondicionalmente, sempre tão prontos a ajudar. À Cláudia pelo enorme apoio e amizade, e todas as conversas tão estimulantes e pelas excelentes ideias. À Daniela agradeço toda a ajuda na bancada sobretudo pela tranquilidade que consegues transmitir.

A todos os colegas de laboratório no IBMC, em particular, Ana, Carolina, Inês, João, Miguel, Tânia Magalhães e Tânia Silva, pela imensa ajuda na bancada e pela diversão na hora do almoço. Um especial agradecimento por me tratarem sempre como *"one of us"*. À Tânia Silva agradeço especialmente, tudo o que contigo aprendi no laboratório e por toda a tua paciência e pelas nossas "teimosas" discussões que tanto nos fazem crescer.

Aos colegas do PDQS agradeço o companheirismo nas viagens realizadas e a enorme entreajuda que sempre se fez notar.

Aos todos os meus amigos pelos bons momentos de diversão e descontração. Obrigada por estarem sempre presentes, nos bons e nos maus momentos. Thiago, Pedrinho, Mário e Vânia, Pedro (e Francisco), é muito bom ter-vos sempre por perto. À Isabel, como tu disseste, "a amizade inesperada", obrigada por seres a amiga sempre disponível que és e por podermos estar sempre juntas, mesmo a uns quilómetros de distância.

Às meninas do “Clube da Tupperware”, vocês são únicas. Nunca poderei agradecer todo o que fazem por mim! Obrigada pela vossa ajuda a todos os níveis e pelos momentos únicos que vivemos. À Ana, obrigada por essa paz contagiante, à Inês, obrigada por todas as boas conversas e pela tua companhia e insistência no ginásio. À Tânia Silva, por me contagiares sempre com essa tua garra. Às mais recentes na minha história, Carolina e Tânia Magalhães, quero agradecer por terem deixado entrar nas vossas vidas e pela vossa entrega e amizade únicas. Carolina, obrigada por me teres ajudado a desbloquear muitos pensamentos e Maga, obrigada por essa boa energia e força que partilhas comigo. Obrigada aos maridos do “Clube” por nos aturarem sempre nas nossas festas. E que bom que foi ver o club multiplicar-se durante este tempo de doutoramento!

Aos meus Tios e Priminhos, e à minha pequenina afilhada, obrigada por todo o carinho. Ao meu Tio Pedro que já não estando connosco, está sempre a olhar por mim. Um especial agradecimento à Lenita: és das pessoas mais generosas que conheço!
Aos meus sogros Deli e Jorge, e à avó Elvira, obrigada por me tratarem sempre tão bem, por tudo o que me proporcionam, por todo o apoio e carinho que me dão diariamente e pelos bons momentos que temos passado juntos.

Aos meus Avós, agradeço todo o apoio e suporte desde sempre, por me terem criado e educado e me terem tornado a pessoa que sou hoje. Que bom que é ter-vos ao meu lado. À minha Avó Maria, que perdi fisicamente durante o tempo desta tese, obrigada por tudo o que me ensinaste.

Aos meus Pais, de quem tanto gosto, faltam-me palavras para descrever o quanto vos agradeço. Nas dificuldades foram sempre fortes e tudo superam. Obrigada por se preocuparem sempre tanto, por estarmos sempre juntos e por todo o amor incondicional que me dão. À minha mana, a minha mais pequena, quero agradecer-te por me alegrares sempre, pela tua rebeldia e por te teres crescido tanto valorizando o que te tentei ensinar. És o meu orgulho.

E a ti Zé, já uma vez te escrevi que “os resultados são também teus” e é mais uma vez tão verdade. Obrigada por me ouvires todos os dias com os meus problemas e vitórias. Obrigada por estares sempre aqui para me confortar e aturares as minhas irritações. Obrigada por essa calma, por todo o amor e por partilhares a tua vida comigo.

A todos os que de alguma forma contribuíram para a realização deste trabalho, o meu muito obrigada.

PUBLISHED WORK

Part of the work presented in this thesis is already published in peer-review international scientific journals, as follows:

T. Moniz, A. Nunes, A. M. G. Silva, C. Queirós, G. Ivanova, M. S. Gomes and M. Rangel, *Rhodamine labelling of 3-hydroxy-4-pyridinone iron chelators is an important contribution to target Mycobacterium avium infection*, Journal of Inorganic Biochemistry, **2013**, *121*, 156-166. DOI: 10.1016/j.jinorgbio.2013.01.002.

J. T.S. Coimbra[#], **T. Moniz[#],** N. F. Brás[#], G. Ivanova[#], P. A. Fernandes, M. J. Ramos and M. Rangel, *Relevant Interactions of Antimicrobial Iron Chelators and Membrane Models Revealed by Nuclear Magnetic Resonance and Molecular Dynamics Simulations*, The Journal of Physical Chemistry B, **2014**, *118*, 14590−14601. DOI: 10.1021/jp509491p. ([#]The authors contributed equally)

R. B. R. Mesquita[#], **T. Moniz[#]**, J. L. A. Miranda[#], V. Gomes[#], A. M. N. Silva, J. E. Rodriguez-Borges, A. O. S. S. Rangel and M. Rangel*, Synthesis and characterization of a 3-hydroxy-4-pyridinone chelator functionalized with a polyethylene glycol (PEG) chain aimed at sequential injection determination of iron in natural waters*, Polyhedron, **2015**, 101, 171-178. DOI: 10.1016/j.poly.2015.09.015. ([#]The authors contributed equally)

T. Moniz, D. Silva, T. Silva, M. S. Gomes and M. Rangel, *Antimycobacterial activity of rhodamine 3,4-HPO iron chelators against Mycobacterium avium: analysis of the contribution of functional groups and of chelator´s combination with ethambutol*, MedChemComm, **2015**, 6, 2194-2203.

T. Moniz, J. T.S. Coimbra, N. F. Brás, L. Cunha-Silva, M. J. Ramos, P. A. Fernandes, B. de Castro and M. Rangel, *Synthesis and structural characterization, by spectroscopic and computational methods, of two fluorescent 3-hydroxy-4-pyridinone chelators bearing sulphorhodamine b and naphthalene*, RSC Advances, **2016**, 6, 4200-4211.

T. Moniz, B. de Castro, M. Rangel and G. Ivanova**,** *NMR study of the interaction of fluorescent 3-hydroxy-4-pyridinone chelators with DMPC liposomes*, Physical Chemistry Chemical Physics, **2016**, accepted manuscript.

Related work, comprising the design of fluorescent 3,4-HPO for applications as sensors, was published during the PhD period and is not discussed in the present dissertation:

T. Moniz, C. Queirós, R. Ferreira, A. Leite, P. Gameiro, A. M. G. Silva and M. Rangel, *Design of a water soluble 1,8-naphthalimide/3-hydroxy-4-pyridinone conjugate: investigation of its spectroscopic properties at variable pH and in the presence of* Fe^{3+}*,* Cu^{2+} *and* Zn^{2+}, Dyes and Pigments, **2013**, *98*, 201-211. DOI: 10.1016/j.dyepig.2013.02.020.

C. Queirós, A. Leite, M. G. M. Couto, **T. Moniz**, L. Cunha-Silva, P. Gameiro, A. M. G. Silva and M. Rangel, *Tuning the limits of pH interference of a rhodamine ion sensor by introducing catechol and 3-hydroxy-4-pyridinone chelating units*, Dyes and Pigments, **2014**, *110*, 193-202. DOI: 10.1016/j.dyepig.2014.04.007.

ABSTRACT

Previous results obtained by our research group demonstrated that rhodamine-labelled 3-hydroxy-4-pyridinone (3,4-HPO) chelators exhibit antimycobacterial activity, related but not limited to their iron binding capacity. The results suggested that the inhibition of bacterial growth is dependent on the fluorophore, namely on the substituents of the amino groups of the xanthene ring, and on the type of linkage between rhodamine and the chelating unit, thus pointing out the importance of the hydrophilic/lipophilic balance of the fluorescent chelator's structure.

In the present thesis we evaluate the antimycobacterial activity of new chelators (**MRB2**, **MRB4**, **MRB20**, **MRH10** and **MRB9**) expressly designed to allow: (a) the direct comparison of the influence of the functional groups *per se* on the antimycobacterial effect; (b) the establishing of the best conjunction of fluorophore substituents and type of linkage; (c) the identification of the finest combination of rhodamine 3,4-HPO chelators with other antibiotics to achieve a higher biological activity. The activity of the chelators was assessed by measuring their effect against *M. avium*. In this study we also report the antimycobacterial effect of **MRH7**, which proved to be the best performer of the set of chelators under study, in combination with ethambutol, which is one of the antibiotics currently in use to treat mycobacterial infections. The results are indicative that a combination of 3,4-HPO iron chelators with an antibiotic is a promising strategy to fight *M. avium* infections.

As the antibacterial activity seems to be associated with the differential interaction of the chelators with biological membranes we investigate the interaction of the compounds with membrane by using spectroscopic methods such as Fluorescence, Nuclear Magnetic Resonance and Electron Paramagnetic Resonance. The results show that the more active compounds strongly interact with the lipid phase while the less-active do not. Fluorescence confocal microscopy experiments were also performed to get insight on the cellular distribution of the fluorescent chelators inside bone marrow derived macrophages and peripheral blood mononuclear cells. The results show that both in macrophages and in PBMC's the uptake of the more active compounds seems to be facilitated and a higher quantity reaches the cytosol. Co-localization studies showed that once inside the cell the rhodamine labelled chelators have access to their targets, namely the phagosome.

The *in vitro* toxicity of the rhodamine derived 3,4-HPO chelators was investigated by the evaluation of the viability of HepG2 cells by performing MTT reduction and LDH leakage assays. The results achieved by both methodologies were compared and the data obtained provides evidence that hexadentate chelators seem to be more toxic than the bidentate related chelators.

As a final goal, experiments concerning the development of modified 3,4-HPO with improved water solubility were performed and a 3,4-HPO functionalized with a PEGylated chain was synthesized. The analytical application of this molecule was compared with the previously used 3,4-HPO ligands and the results show that the new chelator provides better sensitivity and a lower LOD for iron determination in aqueous samples.

In conclusion, the current results are relevant for the selection of the chelator with best antimycobacterial effect and also for the design of novel molecular architectures intended for application in the different fields of research.

KEYWORDS: 3-hydroxy-4-pyridinone; Iron(III) chelators; fluorescent ligands; rhodamine; spectroscopy; biological membranes; infection; *Mycobacterium avium*; bacteria; antibiotics.

RESUMO

O grupo de investigação onde se insere a presente dissertação tem vindo a desenvolver moléculas quelantes capazes de remover ferro e assim controlar o crescimento de bactérias patogénicas. Estudos anteriores mostraram que quelantes do tipo 3-hidroxi-4-piridinonas (3,4-HPO) funcionalizados com diferentes rodaminas são eficazes na inibição do crescimento bacteriano de *Mycobacterium avium*. Os resultados obtidos demonstraram ainda que este efeito é dependente da natureza do fluoróforo, em particular dos substituintes ligados ao átomo de azoto dos anéis xanteno bem como do grupo funcional presente na ligação entre o fluoróforo e a unidade quelante. Estes resultados evidenciam a importância do balanço hidro/lipofílico do quelante para o seu efeito antimicobacteriano.

Neste trabalho, um conjunto de novos quelantes estruturalmente relacionados, **MRB2**, **MRB4**, **MRB20**, **MRH10** e **MRB9**, foram desenhados de modo a (a) avaliar a influência de diferentes grupos funcionais no efeito antimicobacteriano; (b) estabelecer a melhor conjugação entre os substituintes dos anéis xanteno e o grupo funcional da ligação fluoróforo-unidade quelante; e (c) estabelecer a combinação mais vantajosa de co-administração de quelantes concomitantemente com antibióticos de uso clássico no tratamento deste tipo de infeções.
O efeito destes quelantes no controlo da infeção causada por *M. avium* foi avaliado e o quelante que se mostrou mais eficaz, **MRH7**, foi testado em combinação com um antibiótico habitualmente utilizado no controlo de infeções causadas por micobactérias, o Etambutol. Os resultados mostraram que a co-administação deste tipo de quelantes com antibióticos utilizados na clínica é uma estratégia vantajosa no combate a infeções provocadas por estes patogénios.

A atividade antibacteriana dos quelantes funcionalizados com rodaminas parece estar relacionada com a diferente capacidade dos ligandos em interagir com membranas biológicas. Desta forma, diferentes técnicas espectroscópicas, Fluorescência, Ressonância Magnética Nuclear e Ressonância Paramagnética Eletrónica, foram utilizadas para estudar a interação destes quelantes com modelos membranares de lipossomas.
Os resultados mostraram que os compostos com maior efeito no controlo do crescimento de *M. avium* são os que possuem maior capacidade para interagir com membranas,

enquanto que os que apresentaram menor atividade antimicobacteriana são os que têm menor afinidade para membranas.

De modo a avaliar a distribuição dos quelantes em macrófagos derivados da medula óssea de ratinho e em células mononucleares do sangue periférico de humanos realizaram-se estudos de Microscopia Confocal de Fluorescência. Os resultados mostraram que todos quelantes testados são capazes de atingir o citoplasma das células embora os ligandos com maior atividade antimicobacteriana tenham mais facilidade em atravessar a membrana celular. Nos estudos de co-localização com diferentes organelos celulares foi possível concluir que estes quelates, uma vez no interior das células, conseguem atingir potenciais alvos celulares, nomeadamente o fagossoma, onde reside a bactéria.

O estudo *in vitro* da toxicidade dos quelantes funcionalizados com rodamina foi avaliada numa linha celular de fígado, células HepG2, com recurso a diferentes métodos, nomeadamente estudos de redução de "MTT" e de libertação da enzima citoplasmática "LDH". Os resultados obtidos em ambos os testes foram comparados e estes sugerem que os quelantes hexadentados parecem induzir maior toxicidade do que os ligandos bidentados.

Por último, considerou-se o desenho de 3,4-HPO modificadas de modo a aumentar a solubilidade destes quelantes em solução aquosa, tendo-se sintetizado um ligando funcionalizado com uma cauda derivada de uma molécula de polietilenoglicol (PEG).
A aplicação deste quelante em testes analíticos para a determinação da concentração de ferro em amostras de águas foi avaliada e comparada com os resultados obtidos anteriormente pelo grupo de investigação, com a utilização de outros ligandos do tipo 3,4-HPO. O novo ligando mostrou maior sensibilidade e menor limite de deteção na determinação de ferro em águas.

Em suma, os resultados descritos no presente trabalho contribuem com informação relevante para a escolha de quelantes que possam apresentar um maior efeito no combate a infeções causadas por *M. avium* bem como no desenho de novas arquiteturas moleculares para diferentes aplicações, nas mais diversas áreas de interesse científico.

PALAVRAS-CHAVE: 3-hidroxi-4-piridinona; quelantes de ferro(III); ligandos fluorescentes; rodamina; espectroscopia; membranas biológicas; infeção; *Mycobacterium avium*; bactéria; antibióticos.

TABLE OF CONTENTS

LIST OF TABLES

LIST OF FIGURES

LIST OF ABBREVIATIONS

16-DSA	16-doxyl-stearic acid, free radical
$2A_{max}$	Maximum hyperfine splitting
2D	Bidimensional
3,4-HPO	3-hydroxy-4-pyridinone
5-DSA	5- doxyl-stearic acid, free radical
ABC-transporter	ATP-binding cassette transporter
ACD	Anaemia of chronic disease
AD	Alzheimer's disease
AG	Arabinogalactan
AI	Anaemia of inflammation
AIDS	Acquired immune deficiency syndrome
ANOVA	Analysis of variance
Asu	Asymmetric unit
ATP	Adenosine triphosphate
BBB	Blood/brain barrier
BCG	Calmette-guérin bacillus
BMM	Bone marrow derived macrophages
BMP	Bone morphogenetic protein
bs	Broad singlet
CFU	Colony forming unit
CHELu	Bidentate chelating unit
CM1	1-(*N*-acetyl-6-aminohexyl)-3-hydroxy-2-methylpyridin-4-one
CNS	Central nervous system
COSY	1H/1H correlation spectra
CP	Compounds' partition
Cq	Quaternary carbon
CR3	Complement receptor 3
ctrl	Control
d	Duplet
D	Diffusion coefficient
DCC	Dicyclohexylcarbodiimide
DC-SIGN	Dendritic Cell-Specific Intercellular adhesion molecule-3-G Non--integrin integrin
DCU	*N, N*-dicyclohexylurea
DCYTB	Duodenal cytochrome b
dd	Double duplet
DFO	Desferrioxamine B
DFP	Deferiprone
DFT	Desferrithiocin

DFX	Desferasirox
DLS	Dynamic light scattering
DMEM	Dulbecco's modified eagle's medium
DMF	*N, N*-dimetylformamide
DMPC	1,2-dimyristoyl-*sn*-glycero-3-phosphocholine
DMPG	1,2-dimyristoyl-*sn*-glycero-3-phospho-(1'-rac-glycerol)
DMSO	Dimethylsulfoxide
DMSO-d_6	Deuterated dimethylsulfoxide
DMT1	Divalent metal transporter 1
DNA	Deoxyribonucleic acid
DOSY	Diffusion NMR spectroscopy
Dp44mT	Thiosemicarbazone
DPH	1,6-Diphenyl-1,3,5-hexatriene
DTPA	Diethylene triamine pentaacetic acid
DtxR	Diphtheria toxin repressor
ECGg	Epigallocatechingallate
EC_{50}	Half maximal effective concentration
EDHPA	Ethylene diamine hydroxy phenylacetic acid
EDTA	Ethylenediaminetetraacetic acid
EPR	Electron paramagnetic resonance
ER	Endoplasmic reticulum
Escherichia coli	*E. Coli*
ESI-MS	Electrospray ionisation mass spectrometry
ETH	Ethambutol
FBS	Fetal bovine serum
FBS0701	Deferitazole
FCS	Fetal calf serum
FDA	U.S. Food and Drug Administration
FPN	Ferroportin
Fur	Ferric uptake regulator
Fxu	Ferri-exochelin uptake
GFP	Green fluorescence protein
GTP	Guanosine triphosphate
HBED	*N, N'*-Di(2-hydroxybenzyl)ethylenediamine-*N, N'*-diacetic acid monohydrochloride
HBSS	Hank's balanced salt solution
HCP-1	Haem carrier protein 1
Hdmpp	2- dimethyl-3-hydroxy-4-pyridinone or L1
HEPES	4-(2-hydroxyethyl)-1-piperazineethanesulfonic acid buffer
HepG2	Human hepatoma cell line
HFE	Haemochromatosis protein
HH	Hereditary haemochromatosis
HIF-1a	Hypoxia-inducible factor-1a
HJV	Hemojuvelin
HLB	Hydro-lipophilic balance
HMBC	1H/13C heteronuclear multiple bond coherence

HO-1	Haem oxygenase-1
HPCIH	Isonicotinoyl hydrazone
HPO	Hydroxypyridinone
HSQC	1H/13C heteronuclear single quantum coherence
HSV	Herpes simplex virus
I	Ionic strength
IDA	Iron deficiency anaemia
IFNγ	Interferon gamma
IL	Interleukin
iNOS	Inducible nitric oxide synthase
IREs	Iron regulatory elements
IRPs	Regulatory proteins
ITCs	Isothiocyanates
IUPAC	International Union of Pure and Applied Chemistry
J	Coupling constant (NMR)
Jak2	Janus kinase 2
K_f	Formation constant
K_p	Partition constant
K_{sp}	Solubility product constant
K_{sv}	Stern–Volmer constant
LAM	Lipoarabinomannan
LCCM	L929 cell conditioned medium
LDH	Lactate dehydrogenase
Lf	Lactoferrin
LM	Lipomannan
LOD	Limit of detection
log *D*	Logarithmic distribution coefficient values
log*β*	Affinity constant
LUVs	Large unilamellar vesicles
m	Multiplet
m-	*Meta- position*
M. bovis BCG	*Mycobacterium bovis* BCG
M. leprae	*Mycobacterium leprae*
M. smegmatis	*Mycobacterium smegmatis*
M. tuberculosis	*Mycobacterium tuberculosis*
m/z	Mass-to-charge ratio
MAC	*M. avium* complex
maltol	2-methyl-3-hydroxy-4-pyrone
Man4	Mannose units
M-CSF	Macrophage colony stimulating factor
MD	Molecular Dynamics
MeOD-d_4	Deuterated methanol
MHC	Major histocompatibility complex
MIC	Minimum inhibitory concentration
MLVs	Multilamellar liposomes

MOPS	3-(*N*-morpholino)propanesulfonic acid buffer
MR	Mannose receptors
MRAMP	Homologue Nramp protein in *Mycobacterium tuberculosis*
mRNA	Messenger ribonucleic acid
MS	Mass spectrometry
MTT	3-[4,5-dimethylthiazol-2-yl]-2,5 diphenyl tetrazolium bromid
MW	Microwave
n	Mole
NAD(P)	Nicotinamide adenine dinucleotide phosphate in oxidized form
NAD(P)H	Nicotinamide adenine dinucleotide phosphate in reduced form
NAD+	Nicotinamide adenine dinucleotide in oxidized form
NADH	Nicotinamide adenine dinucleotide in reduced form
NHS	*N*-hydroxysuccinimide
NMR	Nuclear magnetic resonance
NRAMP1	Natural resistance-associated macrophage protein 1
NTBI	Non-transferrin bound iron
o-	*Ortho-position*
OEG	Oligo(ethylene glycol)
p-	*Para- position*
p.a.	*Pro-analysis*
PAS	Paminosalicylic acid
PBMCs	Peripheral blood mononuclear cells
PBS	Phosphate buffered saline
PD	Parkinson's disease
PE	Phosphatidylethanolamine
PEG	Polyethylene glycol
PEG-HPO	Pegylated 3-hydroxy-4-pyridinone ligand
PG	Phosphatidylglycerol
PIH	Pyridoxal isonicotinoyl hydrazone
PIM	Phosphatidylinositol mannosides
ppm	Parts per million
Pseudomonas aeruginosa	*P. Aeruginosa*
Q	Quencher
RBCs	Red blood cells
RNA	Ribonucleic acid
ROS	Reactive oxygen species
rpm	Revolutions per minute
r_s	Steady-state fluorescence anisotropy
RSD	Relative standard deviation
SAR	Structure activity relationships
Scn	Siderocalin
SI	Sequential injection
SIH	Salicylaldehyde isonicotinoyl hydrazone
SmT	Smooth-transparent

Staphylococcus aureus	*S. Aureus*
Staphylococcus epidermis	*S. Epidermis*
STAT	Signal transducer and activator of transcription
t	Triplet
$T1$	Spin-lattice relaxation time
TB	Tuberculosis
Tf	Transferrin
TfR	Transferrin receptor
TLC	Thin layer chromatography
TLR	Toll-like receptor
T_m	Phase transition temperature
TMA-DPH	Trimethylammoniumdiphenylhexatriene
TNF-α	Tumour necrosis factor alpha
UV-Vis	Ultraviolet-visible
V/V	Volume/volume
Vibrio vulnificus	*V. Vulnificus*
β-NADH	β -nicotinamide adenine dinucleotide
δ	Chemical shift
ε	Molar extinction coefficient
λ	Wavelength
τ	Rotation correlation time

AIMS AND SCOPE

AIMS AND SCOPE

In face of an urgent need to develop novel therapies to fight mycobacterial infections, our research group has been particularly interested in the development of iron(III) chelators, based on 3-hydroxy-4-pyridinone (3,4-HPOs) units that may be used to deprive *M. avium* of iron.

The research started in 2007 and the inhibitory effect of several bidentate and hexadentate 3,4-HPO chelators on the growth of *M. avium* inside bone marrow derived macrophages (BMM) has been investigated [1]. The present PhD thesis follows the latter studies which include the work developed under the author's Master thesis investigation project [2].

From the previous studies it is known that:

- Amongst all the ligands tested, the most active chelator includes a hexadentate chelating unit labelled with a rhodamine B isothiocyanate moiety. Its antimycobacterial activity is associated with the iron chelating capacity of the ligand but this property is not sufficient *per se*, since the non-functionalized chelating units were not effective [1];

- The partition and distribution of chelators functionalized with either rhodamine or fluorescein fragments on model membranes and cells are distinctive.
  The most biologically active compounds were those which interact more strongly with lipid phases and most easily cross cell membranes [3];

- Fluorescent chelators, with different denticity and functionalized with diverse rhodamine frameworks, have been synthesized. All the chelators were capable of restricting the intramacrophagic growth of *M. avium* and their activity is dependent on the structural differences on the molecular framework of the rhodamine. The most significant inhibitory effect was obtained with rhodamine B isothiocyanate labelled compounds. The effect is superior to that observed for other two chelators functionalized with carboxyrhodamine [2, 4].

The aim of the present PhD project is to answer the following questions:

Q1 - Is the biological effect dependent on the functional groups of the rhodamine moiety present in the chelator structure, namely the isothiocyanate group?

Q2 - Are the substituents linked to the nitrogen of the xanthene ring important for the biological effect?

Q3 - Are the structural characteristics on the rhodamine framework determinant for the interaction of the chelators with biological membranes?

Q4 - Is the biological effect related with interaction of the chelators with biological membranes?

In the figure below (Figure AS.1) the connection of the raised questions is represented graphically.

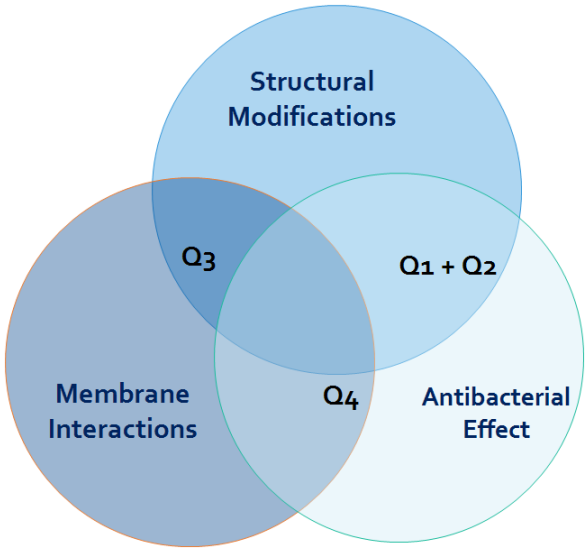

Figure AS.1. Schematic representation of the questions aimed to be answered in the present work.

To answer the above questions, we chose to design parent chelators in which different structural groups are introduced in order to establish structure/activity relationships and to increase biological activity. We finally expect to identify key molecular structures that may be relevant for the development of novel therapeutic tools to treat infection through iron deprivation.

The antimicrobial activity of the new compounds was assessed in *M. avium* infection model. Partition properties of the most active compounds were investigated in liposomes and their distribution within the cells was monitored by confocal microscopy. *In vitro* safety studies for the tested chelators were also carried out.

The particular objectives of the present work are:

- The synthesis and characterization of 3,4-HPO labelled with different fluorophores, global charge and hydro-lipophilic balance (HLB) (Chapter 2);
- The evaluation of *in vitro* activity of the new chelators in the control of *M. avium* growth and the investigation of the effect of the most active chelator, alone and in combination with a classic antibiotic, Ethambutol (ETH) (Chapter 3);
- The study of the partition and distribution properties of the most active chelators in lipid bilayers using fluorescence, NMR and EPR spectroscopies (Chapter 4);
- The investigation of the interaction of most active chelators and their distribution within cells by fluorescence confocal microscopy (Chapter 4);
- *In vitro* safety studies for the synthesized chelators; in hepatocytes (HepG2) (Chapter 5).
- The design of iron(III) chelators with increased hydrophilicity for further application in aqueous systems, namely in analytical processes of iron(III) determination and quantification in water samples (Chapter 6).

As a final goal we aim to get molecular architectures that combine all the features required to target the sites where infectious processes take place and consequently exert a higher antimicrobial activity.

1 | GENERAL INTRODUCTION

1. GENERAL INTRODUCTION

1.1 Iron, an essential element for life

1.1.1 Biochemistry of iron

Iron is the 26th element of the Periodic Table, one of the most abundant elements in the earth crust and an essential micronutrient for the growth of almost all living organisms, with few exceptions such as *Lactobacilli* and *Borrelia burgorferi* [5]. Iron is involved in a large number of biological functions, as a cofactor of many metalloproteins [6]. Due to the exceptional capacity of the element to act as an electron donor and acceptor, more than 100 enzymes require iron for their function and iron is as a component of iron-sulfur clusters, [Fe-S], or haem groups [7]. Among others, iron is crucial for haemoproteins, such as haemoglobin, responsible for the oxygen transport, for oxidases, peroxidases or catalases involved in oxygen metabolism and electron transfer performed by cytochromes. Iron is also essential for non-haem proteins, including those that require [Fe-S] clusters in mitochondrial electron transport chain and for ribonucleotide reductase required in the DNA biosynthesis.
In biological systems, iron is most commonly found in three oxidation states: Fe(II), Fe(III), and in a much lower amount Fe(IV). In an aqueous environment, Fe(II) is oxidized to Fe(III) to precipitate in the form of ferric hydroxide [8] and at physiological pH, Fe(II) is more soluble than Fe(III) (K_{sp} of Fe $(OH)_3 < 10^{-38}$) (as reviewed in [9-13]).
Although essential for life, iron is also toxic due to its ability to participate in Fenton/Haber–Weiss type reactions. These reactions lead to the generation of free radicals, reactive oxygen species (ROS), which damage cells, tissues and organs by reacting with several biomolecules, resulting in protein oxidation, DNA oxidation, mitochondrial damage and peroxidation of membrane lipids, through the production of alkoxyl and peroxyl radicals by reaction with unsaturated lipids [14-16].
In the Haber-Weiss cycle, the Fe(II) cation reacts with hydrogen peroxide (H_2O_2) and oxygen (O_2) to yield free radicals such as superoxide (O_2^-) and hydroxyl ($^{\bullet}OH$) [14, 16-20]. At the physiological pH value, superoxide dismutates to form hydrogen peroxide which in turn may be decomposed by the enzyme catalase into water and oxygen [21]. These reactions are illustrated in Figure 1.1.

The formation of ROS may contribute to the development of several diseases such as hepatitis, haemochromatosis, liver cirrhosis, cancer, and neurodegeneration [21, 22].

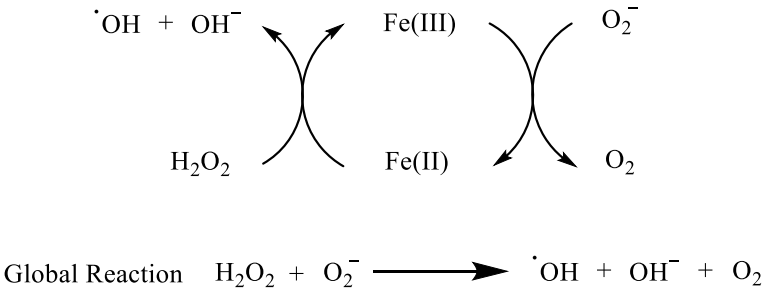

Figure1.1 – Chemical reactions involved in the formation of ROS in the presence of iron. Adapted from [2, 18].

1.1.2 Body iron homeostasis

The amount of iron in the body of a healthy adult human being is around 3–5 g (45 and 55 mg/kg of body weight in adult women and men, respectively). The greater part, *ca* 2 g, is incorporated in haemoglobin and the remaining amount of iron is distributed between macrophages (~600 mg) or stored in hepatocytes (~1 g) incorporated in ferritin. Approximately 8 mg of the total iron is found in muscle myoglobin and a smaller amount is present in other cells and tissues as a constituent of haem- and non-haem proteins (~350 mg). Very low levels of iron remain in intracellular labile iron pools [6, 15, 23, 24].

Nearly 20 to 25 mg of iron are in daily circulation in the human body although only a small amount, about 1–2 mg, is normally absorbed from the diet, in order to re-establish regular losses caused by desquamation of the skin and intestine cells, and by menstruation in women. The highest amount of circulating iron comes from the spleen, resulting from the degradation of senescent red blood cells (RBCs) by macrophages. This iron is efficiently recycled, returning to the bone marrow via the transporter protein, transferrin (Tf) [6, 25].

The regulation of absorption, transport and storage processes required to maintain the basal iron level in the body is crucial to prevent iron deficiency and iron excess derived disorders. The metal homeostasis is regulated with high precision and requires several molecular mechanisms and proteins [26], summarized in Figure 1.2.

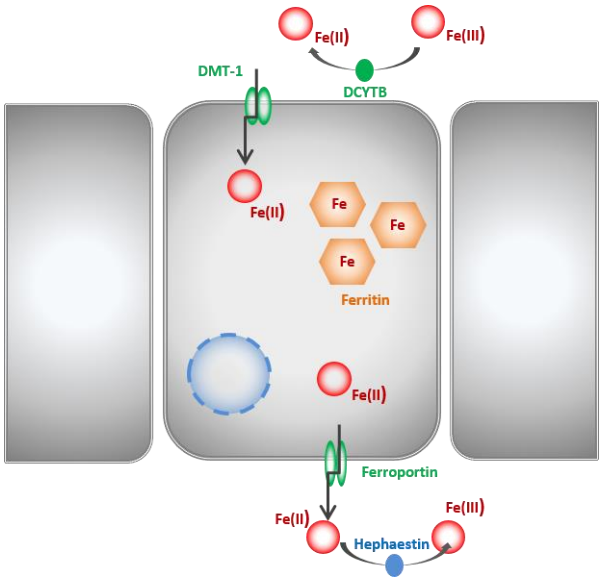

Figure 1.2 – Iron transport along the enterocyte. Iron absorbed from the diet in converted to Fe(II) by DCYTB and further transported via DMT1. In the cytosol, iron can be stored in ferritin or exported to the plasma by ferroportin to be transported bounded to transferrin, after conversion to Fe(III) by Hephaestin. Adapted from [2, 27].

Iron obtained from haem and non-haem sources is absorbed at the duodenum by distinct mechanisms. The intestinal haem iron absorption seems to require a specialized haem carrier, although this has not been definitely identified. Haem carrier protein 1, HCP1, is a strong candidate, but evidence has been accumulated that this protein has a predominant role as a folate rather than haem transporter [24].

Non-haem iron predominates in the oxidized form, Fe(III), and therefore to cross the apical membrane it has to be reduced to Fe(II) by ferrireductases, namely duodenal cytochrome b (DCYTB), and subsequently transported by the proton-coupled divalent metal transporter 1, DMT1, (also known as SLC11A2, NRAMP2 and DCT1) [24, 28, 29]. Mutation of the murine *DMT1* gene (*Slc11a2−/−* mice) has put in evidence the functions for DMT1 in intestinal iron absorption and erythroid iron uptake [30].

In order to enter the circulation, the absorbed iron is exported by enterocytes through the only known iron efflux transmembrane transporter: ferroportin (FPN1, also known as Ireg1, MTP1 or SLC40A1). FPN1 is located in the basolateral membrane in association with transmembrane ferroxidase hephaestin and performs the oxidation of Fe(II) to Fe(III), the form incorporated in transferrin [31]. Ferroportin is mainly expressed in enterocytes and is also present in macrophages and placenta [5].

The iron absorbed may be stored or kept in circulation bound to the serum protein transferrin (Tf), for further delivery to other cells and organs by receptor-mediated endocytosis *via* transferrin receptor-1 (TfR1). This transmembrane glycoprotein forms a homodimer linked by a disulphide bridge, binding one Tf molecule at each of its subunits.
After endocytosis of the complex Tf/TfR1, the endosome is acidified by the action of a proton pump ATPase to reach pH 5.5 and a conformational change occurs conducing to release of iron in the oxidized form Fe(III). This is subsequently reduced to Fe(II) to allow the transport by DMT1 to the cytosol of the cells. After iron release, the apo-Tf/TfR1 complex returns to the membrane and apo-Tf is recycled to bind more iron [24, 26, 28, 29].
In healthy adults, only approximately 30% Tf binding sites are saturated with iron. Levels of saturation below 15% are associated to iron deficiency and conversely levels above 45% indicate iron overload. This excessive Tf saturation is associated to the existence of non-bound and highly reactive iron, called as non-transferrin bound iron (NTBI). NTBI is predominantly deposited in the liver and can also accumulate in other organs, such as heart and pancreas, leading to organ damage [24].

Inside cells, iron which is not immediately required for cellular function is stored inside ferritin. One ferritin molecule contains 24 subunits organized in a spherical shell-like moiety with the ability to capture more than 4000 iron cations [14, 24, 26, 32]. While in most tissues ferritin is present as a cytosolic protein, composed of variable proportions of H- and L- ferritin chains, some tissues also have a mitochondrial ferritin [33].
In addition to cytosolic and mitochondrial ferritin incorporation, iron can also be stored in the lysosomes, in the form of haemosiderin, representing a small fraction of body iron stocks [23].

1.1.3 Regulation of cellular and systemic iron homeostasis

The regulation of the mechanisms to maintain iron balance in the organism occurs both at cellular and systemic levels and these two distinct systems are complementary and function in a coordinated manner [34].

In cellular processes, the regulation is primarily obtained by the sequestration of iron by ferritin, keeping the excess of iron protected from the development and formation of ROS and allowing this micronutrient to be mobilized when needed. The second level of cellular regulation comprises the iron regulatory proteins (IRPs). IRPs respond to different iron conditions and in a scenario of iron deficiency, they bind to iron regulatory elements (IREs) present in the untranslated regions of mRNAs and regulate the expression of iron transport

and storage proteins at a post-transcriptional level, leading ultimately to an increase of TfR1 expression and decreased ferritin expression, in order to facilitate an increase of intracellular iron levels. IRE-containing mRNAs encode several proteins involved in the iron metabolism, such as ferritin, DMT1, FPN and others [24, 28, 31, 35].

The systemic regulation of iron levels is mainly governed by the hormone hepcidin, which was firstly described as an antimicrobial peptide [28]. Biologically active hepcidin is a 25-amino-acid peptide (part of an 84-amino-acid entire precursor) and is essentially produced in the liver by hepatocytes but can also be produced by the heart, pancreas, and hematopoietic cells.

Hepcidin is involved in iron metabolism and the disruption of the respective gene (*Hamp1−/−* mice) resulted in an iron overload profile [36]. Hepcidin acts as a negative regulator of iron metabolism and its expression changes according to the body iron requirements.

The expression of hepcidin decreases, in conditions of increased need of iron, causing an increase in the levels of FPN and consequently in iron levels. In opposition, when the levels of iron are high, the production of hepcidin increases leading to a decrease in FPN expression and thus reducing the amount of iron in circulation [6, 35, 37].

Hepcidin binds directly to FPN, the only known cellular iron export protein. It induces Janus kinase 2 (Jak2)-dependent phosphorylation, internalization and lysosomal degradation of FPN, thereby decreasing cellular iron efflux from these cells [35].

Under basal conditions, the expression of hepcidin is regulated by mechanisms requiring the bone morphogenetic protein (BMP)/SMAD pathway signalling mechanisms. In a scenario of inflammation, there is an induction of hepcidin expression mainly dependent on interleukin-6 (IL-6) and the activation of STAT3 (signal transducer and activator of transcription 3) [24, 38, 39].

Another important contributor for the systemic regulation of iron levels is the protein HFE, expressed in hepatocytes. It is encoded by the gene *hfe*, a homologue of the major histocompatibility complex (MHC) class 1 antigen and interacts with TfR1 and TfR2. TfR2 is a homolog of TfR1 and is expressed in hepatocytes and in erythroid precursor cells.

TfR2 acts mainly as an iron sensor and when serum iron levels are high, the binding of Tf-Fe to TfR1 displaces HFE, which in turns binds TfR2. The HFE-TfR2 complex interacts with signals induced by the binding of bone morphogenetic protein 6 (BMP6) to increase the expression of hepcidin [26, 28, 29]. This process also requires other co-factors, namely hemojuvelin (HJV) to amplify the BMP6 signal [31, 35, 40].

Moreover, under conditions of low levels of iron, such as hypoxia and aneamia, other mechanisms are initiated in order to decrease hepcidin levels, namely the induction of the transcription factor hypoxia-inducible factor (HIF)-1a and cleavage of membrane HJV [35].

The described cellular and systemic mechanisms performed by the well regulated control systems, IRE/IRP and hepcidin/FPN, have a high degree of coordination and the intercommunication of the overall proteins involved efficiently contribute to maintain the iron homeostasis and prevent the scenarios of iron deficiency or iron overload.

1.1.4 Deregulation of iron levels

When one of the players in the regulation of iron homeostasis does not work properly, the levels of iron in the body become deregulated which can induce the development of several diseases.

Although iron is essential for life, if present in forms susceptible to generate ROS, it can induce cell and tissues damage and compromise the normal functions of organs. As reviewed in the literature [6], free radicals are associated with the development of several diseases such as cancer, diabetes, cardiovascular, neurodegenerative and ophthalmologic diseases, and aging [41]. Iron deposition is highly associated to the development of diverse neurodegenerative diseases, such as Parkinson and Alzheimer [28]. There are numerous reports of iron overload derived diseases [6, 31].

Iron overload diseases can be categorized into primary or secondary disorders. The first are associated to hereditary deficiency in the mechanism of iron regulation and the second are related to acquired alterations [6].
The most prevalent iron overload disorder is hereditary haemochromatosis (HH). HH is an autosomal recessive disease characterized by an excessive absorption of dietary iron, which accumulates mainly in liver, heart, and pancreas. The disease is associated to the mutation in genes that encode proteins involved in iron homeostasis and the most frequent form of hereditary haemochromatosis (classified as type 1) (~90%) is associated with mutations, a C282Y substitution, in *hfe* gene [6, 31].

Several other haemochromatosis forms can occur, such as juvenile haemochromatosis, TfR2 haemochromatosis, ferroportin haemochromatosis, derived from mutations in genes that encode for HJV, TfR2, FPN, respectively. Other hereditary disorders of systemic iron overload unrelated to the hepcidin/ferroportin axis are described, such as DMT1 deficiency, HO-1 (Haem oxygenase 1) deficiency, aceruloplasminemia and atransferrinemia, and occur

in consequence of mutations in genes that codify for DMT1, HO-1, ceruloplasmin and Tf. Hereditary disorders of mitochondria are also related with iron overload and patients suffer from local mitochondrial accumulation of iron in specific tissues. The disease is associated with mutations in proteins required for haem and iron–sulfur cluster biosynthesis [31].

High levels of iron in the central nervous system (CNS) are relevant for the development of several diseases. Along the aging process, iron tends to deposit in the brain and oxidative stress increases, as reported in Friedreich ataxia and Parkinson and Alzheimer diseases. This deposition is also reported for less common diseases such as multiple sclerosis, amyotrophic lateral sclerosis, Huntington disease, ischemic stroke, cerebral haemorrhage and cerebral contusion (reviewed in [10, 31, 42]).

Secondary iron overload is derived from several pathologies, such as deficient erythropoiesis, ingestion of iron in excessive amounts and chronic liver diseases (hepatitis, alcoholic liver disease, etc.) in which iron overload acts as a stimulus for the progression of the diseases. The most common example of secondary iron overload disorders is thalassemia. The disease is characterized by a chronic anaemia due to the non-efficient erythropoiesis as a result of defects in the synthesis of globin chains of haemoglobin. The iron overload scenario in this disease is a consequence of the clinical treatment used, which consists in blood transfusions to correct the anaemia in the patients (reviewed in [31]).

The excess of iron causes several complications to the organism, an iron deficiency is also problematic, and may result from excessive loss and / or lower absorption of iron.
Anaemia, characterized by low levels of circulating haemoglobin, is caused by impaired RBC destruction or production or blood loss. Due to the fact that iron is crucial for haemoglobin synthesis, deficiency of iron is the most common cause of anaemia [43]. Several consequences of iron deficiency anaemia (IDA) are reported, such as defects in development (cognitive and motor), reduced work capacity, delay in the growth of body and organs, defective bone mineralization and less effective immune response [6].
Another type of anaemia has been described, the so-called anaemia of inflammation (AI) or anaemia of chronic disease (ACD). ACD occurs in response to several conditions such as extended inflammatory scenarios, resultant from autoimmune disorders or cancer, and mainly during infections, due to the importance of iron for the growth of pathogens (as discussed later in this chapter). ACD is characterized by hypoferremia, increased levels of ferritin and impaired erythropoiesis, decreasing the iron levels in circulation [43, 44].

1.2 Iron and bacterial infection

1.2.1 Bacterial iron acquisition

As iron is an essential metal for bacterial growth, these microorganisms developed diverse strategies to efficiently scavenge iron from the environment and also mechanisms to regulate the levels of iron for their needs and to prevent an eventual toxic effect [5, 6, 45].

Some bacterial strains can remove iron from haem proteins, namely haemoglobin. These microorganisms are able to take out the haem from haemoglobin, transport it into the cytoplasm and promote iron release by means of haem oxygenases [46].
Some bacteria can also acquire iron from proteins involved in iron storage, namely lactoferrin, ferritin and Tf [18]. These organisms express transferrin receptors such as TbpA and while the host organism develops mutations in transferrin to alter the binding of Tf to this receptor, bacteria counteract by performing other mutations in the receptor to re-establish the specificity of the binding [47].

Alternatively, in response to iron needs, bacteria produce specialized low molecular weight molecules, called siderophores, which are high affinity iron(III) ligands (logβ from ~12 - 49). Fungi and plants also synthesize siderophores to obtain the amount of this nutrient essential for their biological functions.
More than 500 siderophores have been described and the chemical structure of approximately 260 siderophores is known [48, 49].
The synthesis of bacterial siderophores is of remarkable importance. The fact that the enzymatic inhibition of their biosynthesis helps controlling bacterial growth provides evidence for its importance. Thus, the development of chemical inhibitors for the enzymes involved in siderophore synthesis has been suggested as a strategy for the control of infection [50].

1.2.1.1 Siderophores: physicochemical properties, biosynthesis and transport

Most siderophores are hexadentate ligands possessing six oxygen donor atoms that coordinate iron and the most common geometry for siderophore-iron complex is octahedral or pseudo- octahedral, favoring the formation of thermodynamically stable high-spin iron(III) complexes. Less frequently, iron complex geometry can also be a distorted octahedron, with nitrogen or sulfur donor atoms [49].

The most common bidentate chelating units in siderophores are catecholate, hydroxamate and α-hydroxycarboxylate. [51] (Figure 1.3). Enterobactin, desferoxamine and citrate are examples of siderophores that represent these classes of chelating units [52] (Figure 1.4). The existence of mixed-ligand siderophores, such as yersiniabactin, in which more than one type of chelating units are present in the ligand structure, has also been reported (reviewed in [7, 52]) (Figure 1.4).

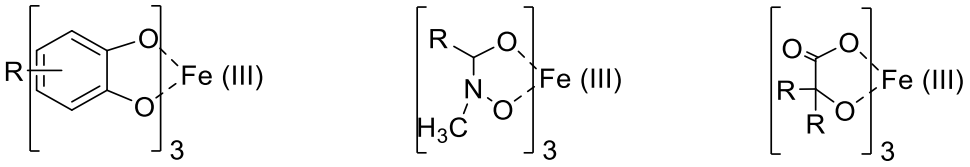

Figure 1.3 – The most common chelating units of siderophores: catechol (left), hydroxamate (centre) and α-hydroxycarboxylate (right) (Adapted from [2]).

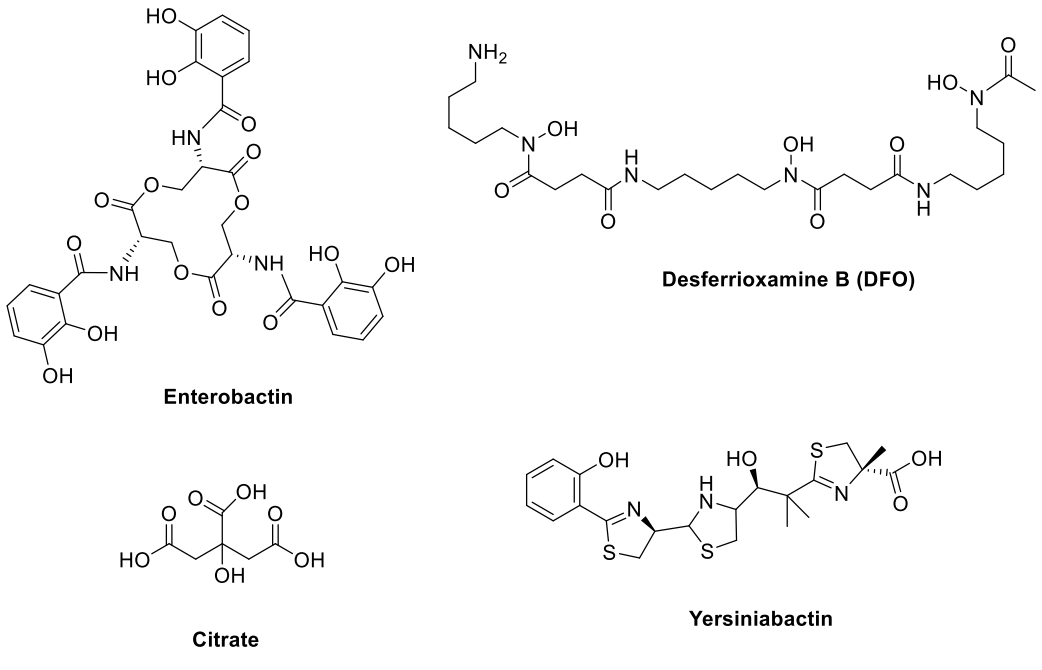

Figure 1.4 - Representative structures of siderophores possessing catecholate, hydoxamate, α-hydroxyacid units or mixed type siderophores: enterobactin, desferrioxamine, citrate and yersiniabactin. Adapted from [52].

Siderophores can also be bidentate ligands although this type is less frequent in natural siderophores, mainly due to the fact that bidentate chelators form less stable iron complexes. Thermodynamically, the formation constant, K_f, of the complex with a hexadentate ligand is higher than for bidentate chelators due to the entropy changes in the formation of complexes with hexadentate ligands which are higher than those observed with

bidentate ligands. Moreover, from a kinetic point of view, complexes formed by bidentate chelators are much more labile than those formed by hexadentate ligands and consequently ligands are more easily released from the complex [3, 49].
Natural siderophores are selective towards iron(III) over iron(II) and the higher the affinity for iron(III), the more negative the redox potential of the complex. The standard redox potential of the Fe(III)/Fe(II) pair in water is +0.77 V but iron chelation usually decreases this value and consequently guarantees the redox stability of the complex, which means that iron will not easly participate in the generation of free radicals. Coordination of iron with some siderophores can significantly decrease the redox potential, such as for the iron complex with the siderophore ferrioxamine B (to -0.45 V), and consequently renders iron inaccessible to reduction by biological agents, namely NAD(P)H (-0,32 V) [7, 49].
Moreover, the cyclization of the ligand is advantageous for the siderophore structure because it contributes to a higher stability of the complex and also improves the diffusion across cellular membranes and protects the ligand from the action of degrading enzymes.
According to these facts, cyclic hexadentate ligands seem to show advantage in siderophore evolution [51].

The biosynthesis of siderophores is performed by nonribosomal peptide synthetases, which sense the levels of iron. The mechanism of bacterial iron acquisition is controlled by different regulators, namely ferric uptake regulator (Fur), the diphtheria toxin repressor (DtxR) and small RNAs [46].

After iron sequestration by siderophores, the ferri-siderophore complexes have to cross the membrane by active transport through siderophore receptors. The biosynthesis of these receptors is co-regulated with siderophore biosynthesis in response to low iron levels [53].
In the next step, the iron is released in the cytoplasm after reduction to Fe(II), due to less affinity than for Fe(III). The reduction is catalyzed by ferri-siderophore reductases [7].
The transport mechanism differs in Gram-positive and Gram-negative bacteria as the first only possess a single membrane, whereas Gram-negative bacteria possess outer and inner membranes. In Gram-positive bacteria, the receptors are associated to the cell wall while in Gram-negative organisms the receptors are located in the outer membrane and ferri-siderophore complex are translocated into the periplasmic space by interaction with the TonB system [46, 52]. Then, periplasmic binding proteins transport ferri-siderophore complexes to a cytoplasmic membrane protein belonging to the ATP-binding cassette transporter (ABC-transporter) superfamily, which hydrolyses ATP to drive iron to the

bacterial cytosol, while the iron-free siderophore is degraded or recycled by excretion through an efflux pump system [52].

1.2.1.2 Siderophore-based antibiotics

Several antibacterial molecules have been developed which act by inhibiting iron uptake. Numerous iron chelators have been synthesized, inspired in the structure of natural siderophores. These antibacterial molecules may sequester the iron available for bacterial growth, as discussed later (chapter 1.3). Otherwise, ferri-siderophore receptors can be inhibited by a non-functional structural analogue or by giving siderophores coordinated to other metal ions with lower toxicity to the host organism [cited in 12, 54].

A related therapeutic approach is the use of siderophore-drug conjugates, which consists in coupling antibiotics to natural siderophores or their synthetic analogues. These conjugates are recognized by bacteria due to the similarities with their natural ligands, thus acting like “Trojan horses” [55, 56]. Miller co-workers have been developing this field and designed a new antimycobacterial that combines mycobactin and artemisinin molecule. The idea was the use of the siderophore ability to drive this conjugate to the mycobacterial cell and at the same time taking advantage of artemisinin function of generating ROS producing warhead [57].
Another examples are sideromycins, such as albomycin and salmycin, which are naturally occuring antibiotics covalently attached to siderophores with increased antibacterial activity [49].

1.2.2 Iron deprivation as immune response

The relevance of iron for the growth of several pathogens has been extensively investigated. It is well documented that an increase in iron levels may be disadvantageous for the control of the infection by the host [45]. Iron overload is associated to an increase in the susceptibility to infection and several examples have been reported [37, 58, 59].

Due to high levels of iron available in a scenario of Haemochromatosis, the disease has been associated with an increased susceptibility to infection by several bacteria [46] such as *Yersinia enterocolitica [60]* and *Vibrio vulnificus* [61].
Patients with low levels of iron are less susceptible to malaria [62] and iron availability increases the growth of enteric pathogenic bacteria such as *Salmonella typhimurium* [63]. The importance of iron for intracellular bacteria such as *Listeria monocytogenes* [64] and *Mycobacterium* [44] has also been described.

Recently, it has been described that apo-Tf inhibits the growth of bacteria, such as *Staphylococcus aureus* and *Acinetobacter baumannii*, and fungi *Candida albicans* by iron sequestration [65]. Conversely, for other pathogens such as *Leishmania*, iron may have an opposite effect, generating toxicity for the microorganisms, protecting the host from the infection (reviewed in [44, 66]).

In response to infections, the infected organisms developed several strategies to regulate the absorption, transport and storage of iron in order to achieve an overall decrease in the amount of iron available for bacterial (or even protozoal and fungal) growth, thus controlling the infection [29]. This adaptive approach of hosts to defend themselves from the invaders by restricting access to essential transition metals, namely iron, is referred in the literature as “nutritional immunity” [46].
Taking advantage of the knowledge on the iron-related interplay between host and the pathogen for iron and the evidence of a nutritional immunity, the development of antibacterial approaches based on the destabilisation of iron concentrations accessible for bacteria has been reported [10, 29, 52, 67, 68].

The withholding of iron from pathogens can be achieved namely by the regulation of the expression of proteins required for iron homeostasis (described in section 1.1.3) and by the participation of several other proteins involved in the immune response.

NRAMP1, natural resistance-associated macrophage protein 1, participates in the host iron related innate immunity. This protein is localized in the phagosomal membrane and exports Fe (and Mn) from the phagosome into the cytosol, to consequently reduce iron bioavailability for intracellular pathogens harboured in phagosomes [45]. Some authors have conversely suggested that NRAMP1 can import iron into phagosome to generate the ROS to combat the pathogens [5, 18]. NO production by iNOS is modulated by NRAMP1 and contributes to the host defence against bacteria [69].

Lactoferrin (Lf), an iron containing protein that is present inside neutrophil granules at sites of inflammation and bioavailable in saliva, breast milk and tears, participates in the regulation of the proliferation and activation of immune cells such as lymphocytes, monocytes, and natural killer cells. Lf is considered a bacteriostatic agent due to its function as an inhibitor of pathogens growth by iron deprivation [39, 46].

Lipocalin-2 (also known as siderocalin, Scn) is expressed in hepatocytes, neutrophils and infected macrophages and binds ferri-siderophore complexes, thus recovering the iron

sequestered by siderophores for bacterial utilization. Lipocalin-2 complements the activity of Lf because lipocalin-2 binds the iron already earmarked for bacterial use [39, 70, 71].

Hepcidin has crucial functions in the regulation of iron levels during inflammatory processes. Interleukin 6, IL-6, induces hepcidin expression via JAK-STAT signalling pathway and hepcidin is produced in response to toll-like receptor 4 (TLR4) activation by bacterial pathogens. Increased production of this hormone leads to the downregulation of Fpn1 mRNA expression in macrophages, in order to decrease the amount of iron available for bacterial growth [5, 66, 72].
A recent work, in which the authors demonstrate that hepcidin participates in host defence against *V. vulnificus* by reducing iron levels during infection provides evidence of the involvement of hepcidin in the iron metabolism and infection. They also have shown that treatment of susceptible mice to this infection with hepcidin agonists decreases the mortality of the host caused by the bacteria [73].
Ferritin expression is also increased during infection in order to sequester iron in macrophages and protect from bacterial utilization [5].

Several other hepcidin-independent defence pathways are reported, modulated by cytokines such as TNF-α, and also IFNγ, interleukin-1 (IL-1), IL-6 and IL-10, that regulate iron levels to combat bacterial infections. These pro- and anti-inflammatory cytokines regulate the expression of DMT1, TfR1, Fpn1 and Ft in macrophages (reviewed in [43, 74]).

The cytokine IFNγ conduces to the reduction of the expression of TfR1 during bacterial infection to inhibit iron uptake by macrophages and potentiate a hypoferremia status [58, 75]. IFNγ stimulates the synthesis of NO by iNOS (reviewed in [74]) and *in vivo* studies have shown that an iron enriched diet leads to a decrease of IFNγ expression (reviewed in [29]). *In vitro* studies also referred that IFNγ increases the synthesis of hepcidin in *M. tuberculosis* infected macrophages, thus reinforcing the relation between iron and host response to infections (reviewed in [76]).

In summary, while bacteria require iron and have developed strategies to acquire this nutrient, host organisms have also established several approaches to regulate iron levels and prevent bacteria from gaining access to iron. Such mechanism of iron regulation constitute an efficient strategy of the hosts to control infections.

1.2.3 Iron and mycobacterial infection

Since one of the aims of the present PhD work is the design of iron(III) chelators to be used as potential antibacterial agents to control *M. avium* infection, the characteristics of this pathogen and the relationship between iron and mycobacterial infection will be discussed in more detail in this chapter.
M. avium is the causative agent of avian tuberculosis and disease in immunocompromised patients. Due to the emergence of several diseases, such as chronic obstructive pulmonary disease, AIDS (Acquired Immune Deficiency Syndrome) and cancer, their associated immunodeficiency condition increases the prevalence of *M. avium* infections worldwide justifying the relevance of studying the infection caused by this pathogen [18, 77-79].

1.2.3.1 Mycobacteria

Mycobacterium is a genus of bacteria that comprises several species, namely the pathogens *Mycobacterium tuberculosis* and *Mycobacterium leprae*, responsible for tuberculosis and leprosy, respectively. Other mycobacteria are responsible for opportunistic infections in humans and other animals, such as *Mycobacterium avium*.
M. avium complex (MAC) includes *M. avium* and also the non-tuberculous mycobacteria, such as *Mycobacterium intracellulare. M. avium* is the second most important group of opportunistic pathogens responsible for pulmonary disease, leading to respiratory failure [80-82].

Mycobacterium species can be classified in different groups, according to their growth rate, as slow growers and fast growers. The first group requires longer proliferation times and is associated with the development of pulmonary and lymphonodal diseases while the second group forms visible colonies in solid media within 7 days and usually affect cutis, bones and joints. Both *M. tuberculosis* and *M. avium* are slowly growing mycobacteria while other mycobacteria such as *Mycobacterium smegmatis* comprises the fast growers group [83].
Mycobacteria can also be classified according to their morphotypes as smooth or rough, transparent or opaque. The smooth transparent morphotype is usually related with virulence in mouse while the rough opaque morphotypes was found in AIDS patients [84].

The lipidic composition and the architecture of the complex and unique structure of the mycobacterial cell envelope contribute to the pathogenicity of these microorganisms [85]. Mycobacteria's cell envelope is composed by the plasma membrane, the cell wall and the capsule (Figure 1.5) [86].

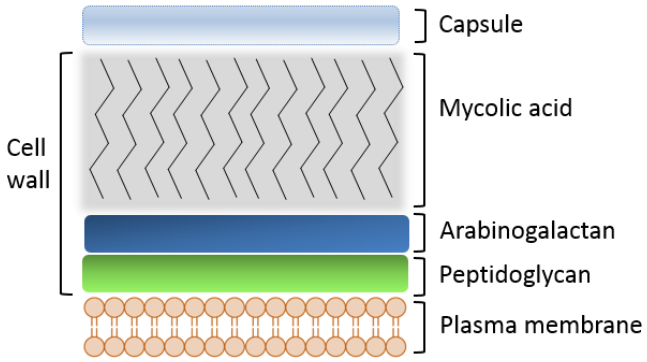

Figure 1.5 - Schematic representation of the cell envelope of pathogenic mycobacteria. (Adapted from [86]).

The lipidic composition of the plasma membrane includes different phospholipids, namely phosphatidylglycerol (PG), phosphatidylethanolamine (PE) and phosphatidylinositol mannosides (PIM). Other glycolipids are also embedded in the plasma membrane, such as lipoarabinomannan (LAM) and lipomannan (LM), and also some proteins and glycoproteins. Mycobacteria are unusual Gram-positive bacteria in which the cell wall contains peptidoglycan covalently bound to arabinogalactan (AG) esterified with long chain mycolic acids.
The more external layer of the mycobacterial cell envelope, the capsule, is predominantly composed by glycoproteins, arabinomannan and mannan derived polysaccharides [86, 87].

The particular characteristics, mainly the hydrophobicity and impermeability of the cell envelope of mycobacteria, contribute to the virulence of these pathogens as the complex cell envelope constitutes a barrier that compromises the uptake of many antibiotics and the treatment of mycobacterial infections.

The saccharides present in the cell envelope of mycobacteria are involved in the recognition and uptake by host cell phagocytic receptors. The complement receptor 3 (CR3) recognizes *M. tuberculosis* by PIM present in the mycobacterial membrane while mannose receptors (MR) detect the mannose residues. Other receptors such as the human DC-SIGN of dendritic cells and macrophages recognize LAM. TLRs of macrophages and dendritic cells recognized cell envelope constituents, such as LAM, and activate signalling pathways in the cells [86, 87].

Both *M. tuberculosis* and *M. avium* are facultative intracellular pathogens that reside primarily inside mononuclear phagocytes, namely macrophages and monocytes. These pathogens grow inside vacuoles, the phagosomes, and developed several strategies to survive and resist to host defences [88-90].

Upon formation of the phagosome, the vacuole undergoes a stepwise maturation process, which consists of acidification and several fusion events. The last step is the fusion with lysosomes leading to the formation of a phagolysosome that contains enzymes conducting to the establishment of an acidic environment (~pH = 5) by intervention of the hydrolases required to degrade the pathogens [91, 92].

To ensure survival and replication inside the phagosome in infected macrophages, mycobacteria developed strategies to retard phagosome maturation, namely by manipulating the host cell endocytic pathways in order to prevent the fusion of the phagosome with late endosomes and lysosomes [88, 91]. Thus, the mycobacteria-containing phagosomes remain with characteristics of an early endosome. The levels of ATPase are low and the vacuole is not acidified (the neutral pH value is maintained) which may be due to the exclusion of the enzyme from the membrane. Moreover, the phagosome infected with mycobacteria, namely *M. avium,* does not follow the normal course of maturation, modulating GTPase expression, excluding Rab7 and maintaining Rab5. Rab5 and Rab7 are involved in early and late endosome fusion, respectively [84, 91-94].

Consequently and due to these mechanisms of subversion, mycobacteria can survive inside phagosomes for longer periods of time without being delivered to lysosomes.

1.2.3.2 Treatment of mycobacterial infections

As a result of the highly impermeable cell wall of mycobacteria, the infections caused by these pathogens are difficult to treat. Additionally, mycobacteria have developed different mechanisms of antibiotic resistance conducting to an urgent need to develop new chemotherapeutic agents to control the multidrug-resistant mycobacteria [80, 95].

The classic approach to treat lung disease caused by MAC infections usually includes a multidrug combination of isoniazid, rifampicin (also known as rifampin) and ethambutol. Several other drugs, such as pyrazinamide, streptomycin (and other aminoglycosides), cycloserine, fluoroquinolones and ethionamide, are also used [96].

In addition to the need of combining several drugs to treat mycobacterial infections, the therapies require long treatment durations of at least 6 months and consequently the development of more efficient drugs to reduce the treatment period remains crucial [97].

More recently, macrolides, such as clarithromycin or azithromycin, have been proposed as antibiotics against mycobacterial infections [80] and the combination of clarithromycin or azithromycin, ethambutol and a rifamycin (rifampicin or rifabutin) has already been suggested, despite the treatment still needs an optimization process [81].

Although rifampicin is known to affect the metabolism of the newer macrolides, the combination of these drugs is still used [81].
Several other compounds have been investigated to treat mycobacterial infections. The nitroimidazoles are one of the most recent advances in the design of new drugs that have revealed success in the control of these infections [98, 99].

The impairment of the biosynthetic siderophore production is also a target to the development of new antimycobacterial drugs. *P*-aminosalicylic acid (PAS) is one of the oldest described drugs that has an inhibitory effect in the synthesis of mycobactin [100, 101]. The effect of new compounds that act by inhibiting the enzymes required for synthesis of mycobactin has also been reported [50, 102].
The mycobacterial fatty acid biosynthesis pathway is also a clinically validated target in drug discovery. Recently, the activity of 4-hydroxy-2-pyridones against *Mycobacterium tuberculosis* infection has been reported. This class of compounds inhibits the enzyme InhA, the enoyl reductase required for this biological process. In this study, those HPO chelators showed potent bactericidal effect against common isoniazid-resistant TB clinical isolates [103].

The mechanism of action and drug targets of the most used drugs (referred above) for treatment of mycobacterial infection are summarized in Table 1.1.

Table 1.1 – Drugs used for treatment of mycobacterial infections and their mechanisms of action.

Target	Mechanism of Action	Drug	Reference
Nucleic acids	DNA damage	Nitroimidazole	[104, 105]
	Inhibition of bacterial DNA replication	Fluoroquinolones	[106]
	Inhibition of bacterial RNA synthesis	Rifamycins (eg.: rifampicin, rifabutin)	[107]
Inhibition of protein synthesis	Binding to 30S ribosomal subunit	Aminoglycosides (eg.: treptomycin)	[108, 109]
	Binding to 50S ribosomal subunit	Macrolides (eg.: clarithromycin or azithromycin)	[110]
Cell envelope	Inhibition of arabinofuranosyl transferases	Ethambutol	[111-113]
	Inhibition of mycolic acid biosynthesis	Isoniazid	[114, 115]
		Ethionamide	[116]
	Inhibition of bacterial fatty acid biosynthesis	Pyrazinamide	[117]
	Inhibition of peptidoglycan biosynthesis	Cycloserine	[118]
Siderophore biosynthesis	Inhibition of biosynthesis of mycobactin	*P*-aminosalicylic acid	[100, 101]

1.2.3.3 Iron status and mycobacterial infections

As described above, iron has an impact in the growth of all organisms and in particular mycobacteria, namely, *M. tuberculosis* and *M. avium*. Several reviews reporting the relation between the bioavailability of this metal and the progress of infection have been published (see reference [44] as an example). However, other elements may also be important for mycobacterial infections. Other metals such as Zn, Mn or Cu are also relevant, either as an essential nutrient or due to a toxic effect for the bacteria [46, 119, 120].

The seminal reports of an iron deprivation effect in mycobacterial growth dates from 1960's [121, 122], but several studies have followed and reinforced this evidence.
It has been reported that an iron deficient diet leads to a decrease in *M. avium* growth in mice [123] and iron limitation *in vitro* has been shown to restrict the growth of mycobacteria, including *M. tuberculosis* [124]. Conversely, a supplementation with iron-dextran [125, 126], or polymaltose ferric hydroxide [127] or also with iron citrate was shown to increase the growth of the pathogen in treated mice [128]. High levels of iron acquired from the diet lead to an exacerbation of *M. tuberculosis* infection symptoms in humans and mice [129].

Moreover, it has been shown that iron overloaded haemochromatosis protein (HFE) - deficient mice are more susceptible to *M. avium* infection [130]. These findings were reproduced in macrophages isolated from mice and infected with *M. avium* [126].

Several studies correlate the iron status in AIDS patients and the susceptibility to mycobacterial infections and experiments have shown that iron overload increases mycobacterial growth in immunodeficient mice [78, 126]. Iron redistribution towards macrophages in AIDS patients favored the progress of tuberculosis [131], thus corroborating this relation between iron and mycobacterial infection.

According to these results, the influence of iron in the development of mycobacterial infections is clear and it seems plausible that iron metabolism is considered a target to develop new drugs to fight infections.

1.2.3.4 Iron acquisition by mycobacteria

Mycobacteria, like other pathogens, developed systems for sensing and regulating iron levels in the intracellular medium. They produce siderophores for iron acquisition and transport and synthesize proteins to store the iron recruited from the host and the environment [132].

Concerning the synthesis of siderophores, mycobacteria, differ from other bacteria because they are able to produce intracellular and extracellular siderophores, with the exception of *M. leprae* which only produces the extracellular ligands [132].

Mycobactins are lipophilic and salicylate-containing siderophores that remain associated to the bacterial membrane. The extracellular siderophores are exochelins, which are hydrophilic and have a peptide-based structure, and/or carboxymycobactins, in which the long alkyl chain of mycobactin is substituted with a short acyl (Figure 1.6). Mycobacterial siderophores are hexadentate ligands possessing chelating units based on the phenyloxazolidine ring, ornithine- derived hydroxamates and salycilates [3, 133].
Non-pathogenic species, such as *Mycobacterium smegmatis* and *Mycobacterium neoaurum*, produce exochelins while pathogenic mycobacteria synthesize carboxymycobactins [101, 133]. Salicylic and citric acid are also produced by mycobacteria and also have a role in mycobacterial iron acquisition [124].
The different structural characteristics and lipophilicity of mycobactins and exochelins/ carboxymycobactins influence the localization of these molecules. The intracellular siderophores chelate iron in the cell envelope while the extracellular are able to coordinate iron in aqueous environment, such as the cytosol of host cells.

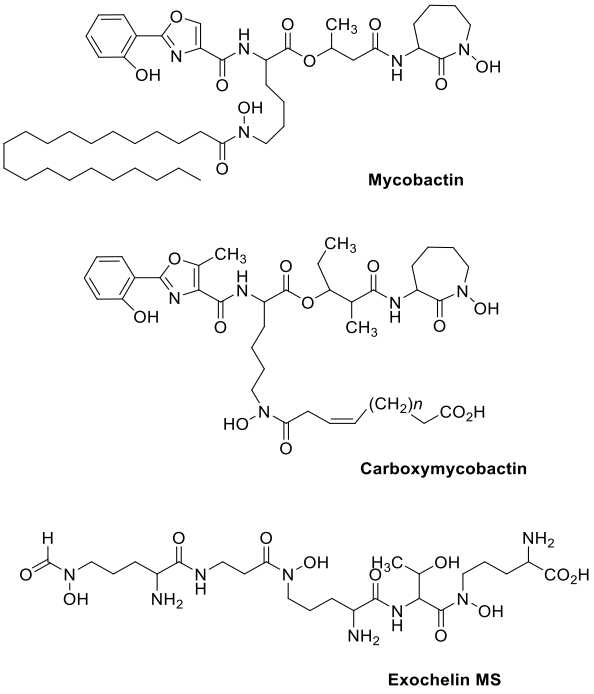

Figure 1.6 – Structure of mycobacterial siderophores. Mycobactin T produced by *M. tuberculosis* (MB T); Carboxymycobactin synthetized for *M. avium*, *M tuberculosis* e *M. bovis* (*n*=2-9); Exochelin MS produced for *M. smegmatis*. (Adapted from [2, 12, 18, 134]).

The biosynthesis of mycobacterial siderophores is performed by non-ribosomal peptide synthetases in response to iron needs of the bacteria [135]. In the case of the biosynthesis of mycobactin, several enzymes are required, such as MbtA, MbtB, MbtC, MbtD, MbtE, MbtF and MbtI. The incorporation of salicylic acid into the mycobactin framework is mediated by MbtA [18, 50].

The regulation of iron metabolism in bacteria is performed at a transcriptional level and is mediated by iron-dependent regulatory proteins, namely the Fur and DtxR families. Fur proteins regulate iron concentration but also several other biological processes such as the oxidative stress response, general metabolism and the synthesis of bacterial virulence factors [135]. DtxR is described as the iron-dependent toxin regulator and mycobacteria produce two proteins of this family, SirR and IdeR, which work as a repressor for the synthesis of siderophores and as activator for the production of storage proteins, respectively, when iron is available in the environment for bacterial use [136, 137].

After production of siderophores and efficient binding of iron, mycobacteria uptake this element for usage or storage and the mechanism of transport differs according to the type of siderophore and its localization.

Mycobactins, located in the membrane, bind Fe(III) which is subsequently transferred through the membrane into the bacterial cell and reduced to Fe(II), by ferri-reductases, to promote metal ion release [18, 133].
Mycobactins provide high stability constants for the formation of iron complex (log β ~ 31) [3] and these siderophores may be able to remove iron from host proteins, such as transferrin and ferritin. However, due to the localization of mycobactins, the access to these proteins is difficult which compromises acquisition of such iron sources. Thus, mycobactins may act in collaboration with extracellular siderophores: mycobactins bind iron previously bound by carboxymycobactins and then transfer it through the bacterial membrane [18, 101].

Often, other mechanisms to acquire and transport iron bound to mycobactins are also suggested [132, 138]. The authors suggest that mycobactins may diffuse into the host macrophage and then mobilize iron available in the intracellular pools of the macrophage. The ferri-mycobactins are then associated to lipid droplets and return to the phagosomes (Figure 1.7).

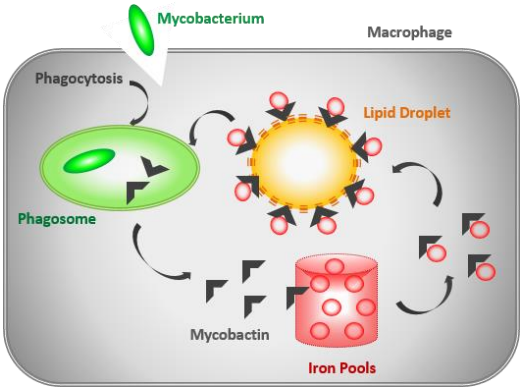

Figure 1.7 – Mechanism suggested for iron transport by mycobactins. The lipophilic siderophores diffuse into the host macrophage and then mobilize iron available in the intracellular pools in the macrophage. The ferri-mycobactins are then associated to lipid droplets and return to the phagosomes. (Adapted from [2, 138]).

In the case of exochelins, these ligands are able to transport iron through the cell membrane [79, 133]. Exochelins, similarly to carboxymycobactins, may also transfer iron to mycobactins. Moreover, it is also described in the literature that exochelins are taken up by active transport and access iron from ferritin, Tf and Lf [18, 139].

Several proteins are required for the transport of ferri-exochelin. The complex is recognized by specific receptors, FxuD, in the cell envelope and is transferred through the cytoplasm with the participation of other proteins such as FxuA, FxuB and FxuC. Finally, iron is released in the cytoplasm after reduction of Fe(III) to Fe(II) by a reductase, namely the ferri-mycobactin reductase. The free siderophore is recycled and transferred back to the extracellular medium by active transport involving a specific protein, ExiT [101, 140].

The transport of iron mediated by carboxymycobactins may require a specific system of transporters for the uptake of ferri- carboxymycobactins, the ATP binding cassette (ABC) transporters. However, due to the size of carboxymycobactins, it is also suggested the uptake of the iron complex may occur by passive or facilitated diffusion. In the interior of the bacterial cell, iron is released by action of reductases, in a similar manner to that described for exochelins and mycobactins. Similarly to exochelins, carboxymycobactins can also access iron from host proteins, such as ferritin and Tf [18, 88, 101, 137].

After recruitment of iron from the host to mycobacteria, the metal is stored in order to prevent undesirable toxic effects to the pathogens. Mycobacteria, as other Gram-positive and Gram-negative bacteria, synthesize an iron storage protein, bacterioferritin, which has several similarities with the human storage protein, ferritin. Bacterioferritin, is located in the cytoplasm of mycobacteria and the protein provides iron for mycobacterial needs such as their metabolic processes [101, 132, 140].

In addition to the mechanisms described above to regulate iron levels in mycobacteria, these pathogens have developed other strategies to maintain optimal iron concentrations and prevent toxic effects and the protein MRAMP is suggested to be involved in this process. MRAMP is a homologue to the host protein NRAMP and its expression increases when iron is in excess in the environment. MRAMP is a transporter of divalent metal ions, such as iron and zinc although the direction of the flux is not yet clearly established. MRAMP may act as importer for mycobacterial iron acquisition or as an iron exporter to prevent oxidative stress associated with high iron levels [74, 132]. Moreover, these microorganisms, namely *M. tuberculosis*, developed metal efflux systems, such as P-type ATPases and oxidases in order to resist metal intoxication [88].

The combination of the different strategies developed by mycobacteria to sense, acquire and regulate iron levels allowed these microorganisms to grow, survive and resist to the host defences.

1.2.3.5 Host defence mechanisms against mycobacteria

Iron homeostasis and macrophages are closely interconnected as the phagocytosis and degradation of senescent erythrocytes is performed by macrophages and the iron is recycled to guarantee the normal iron levels in the organism. These cells also express several proteins involved in iron regulation, where production is regulated by iron levels and inflammatory signals, as previously described [74].

This interaction is particularly relevant for mycobacteria, as these pathogens are phagocytized by macrophages and reside inside these cells.
Macrophages recognise mycobacterial components by TLR2 or TLR4 [85, 141] and these cells represent one of the innate immune defences against bacterial invaders, namely against *M. avium* and *M. tuberculosis*.
Macrophages also produce pro-inflammatory cytokines, such as TNFα, IL-1, IL-6, IL-12, IL-18, and IL-23, that lead to the activation of T-cells and therefore contribute to the combat of the infection [91, 142].

In addition to the iron depriving strategies, host cells have also developed several other mechanisms of defence as the formation of toxic species, namely nitric oxide (NO) and ROS. The cytokine IFNγ induces the phagocyte NADPH oxidase and the iNOS2 to produce ROS [88, 91, 141].
Although the ROS produced by NADPH oxidase are relevant to control some bacterial infections caused by species such as *Staphylococus aureus* and *Salmonella typhimurium*

[143, 144], it has been demonstrated that the production of toxic species by NADPH oxidase was not effective in the decrease of *M. avium* growth inside BMM [145].

The importance of NO in the control of *M. tuberculosis* infection has also been demonstrated [141, 146]. *M. tuberculosis* infected mice treated with iNOS inhibitors showed increased mortality associated to an increased bacterial growth [147]. Similar results were obtained with iNOS gene-disrupted mice that have shown increased susceptibility to *M. tuberculosis* infection [148]. Conversely, iNOS knock-out mice are not more susceptible to *M. avium* infection [84, 149] and even though, the *in vitro* growth of *M*. *avium* inside macrophages is not inhibited by NO [126, 146].

As described for other bacterial infections, NRAMP1, participates in the host response against mycobacteria although the function of this protein is not well established. Mutation in the gene that encodes for this proteins, in humans, increase the susceptibility to *M. tuberculosis* infections [142]. Moreover, mice mutant for this gene are also more susceptible to *M. avium* infection [126, 150]. However, other studies have shown that mice in which this gene was deleted are equally resistant to *M. tuberculosis* infection [151].

The expression of several other proteins is regulated in response to mycobacterial infection, in order to deprive mycobacteria from iron and it has been demonstrated that: (a) the levels of ferritin inside macrophages increase upon *M. avium* infection [74, 152]; (b) *in vitro*, hepcidin also has a crucial function in iron deprivation during mycobacterial infections as demonstrated in a study in which the levels of hepcidin increase in *M. avium* and *M. tuberculosis* infected macrophages [153]; (c) overexpression of ferroportin inhibits intramacrophagic growth of *M. tuberculosis* [154]; (d) upon macrophages infection with *M. avium*, the expression of DMT-1 is induced and the expression of TfR-1 is repressed [74, 155]; (e) lipocalin-2 may also plays a critical function in iron depriving strategies as it binds carboxymycobactins produced by mycobacteria [156], as it has also been described that lipocalin-2 can inhibit the axenic growth of *M. tuberculosis* and *M. bovis* BCG. Other evidence of the involvement of lipocalin-2 in the control of mycobacterial infection is the fact that mice deficient in this protein are highly susceptible to *M. tuberculosis* infection [157].

Taken together, all of these mechanisms may contribute to the ability of a host to control the infection caused by mycobacteria.

1.3 Iron chelators

Iron is usually bound to different atoms or molecules, namely to chelators that act as entities to which metal ions are bound to avoid its toxicity.
To maintain optimal metal ion levels in animals, chelators or their complexes can be administered in order to remove the excess of ions [158] or to deliver ions to the organisms [159-161].
The administration of chelating agents has proved to be advantageous for the treatment of several diseases associated with elevated levels of metal ions, namely for iron associated disorders and infection, therefore pointing out the importance of the development of new chelators for therapeutic application. The therapeutic methodologies in which chelators are administered to regulate metal ion concentrations are usually designated as “chelation therapy” [158].

According to IUPAC nomenclature, “chelation” is defined as *“The formation or presence of bonds (or other attractive interactions) between two or more separate binding sites within the same ligand and a single central atom”* and the term “chelator” (or “chelate”) corresponds to the *“molecular entity in which there is chelation”*. Chelators are classified accordingly to the number of coordinating atoms in the chelator structure involved in metal ion coordination. Chelators can be multidentate: bidentate, tridentate, tetradentate, hexadentate, etc., if in their structure two, three, four or six coordinating atoms are present [162].

In the design iron chelators, several aspects to be taken into consideration.
The properties of the metal ion are relevant in order to develop ligands with high affinity and selectivity for this metal ion. As iron(III) is classified a hard Lewis acid, this metal ion forms high-stable complexes with hard ligands, such as oxygen, and therefore ligands with oxygen as coordinating atoms are preferred over other atoms such as nitrogen [48, 163].

The thermodynamic stability of an iron(III) complex which is formed with a certain ligand is also a relevant property to be taken in consideration. High spin iron(III) prefers an octahedral arrangement composed by six donor atoms and generally hexadentate chelators form complexes with higher thermodynamic stability than those with tridentate or bidentate ligands.

From a kinetic point of view, bidentate and tridentate ligands are more labile and the iron(III) complexes tend to dissociate at low ligand concentrations [48].

Inspired in the naturally occurring siderophore chelating units, the majority of the synthetic chelators are based on catechol and hydroxamate chelating units.
Hydroxypyridinones (HPOs), which are ligands that embrace characteristics of both hydroxamate and catechol groups, have also been reported [164] and a detailed description of this type of compounds will be discussed later, in section 1.3.1.
Although HPOs have lower values of affinity constant, the corresponding pFe(III) values are higher when compared with those of catechol ligands, thus increasing the interest on this type of ligands. The concept of pFe(III) value was introduced by Kenneth Raymond and is used to compare the Fe(III) chelating properties of chelators at physiological conditions (pH 7.4 with a total ligand concentration of 10^{-5} M and a total Fe(III) concentration of 10^{-6} M) [165] in opposition to the standard conditions considered for the determination of the affinity constant [48, 166].

Other ligand types are also described, namely hydroxyquinolines, aminocarboxylates and hydroxycarboxylates. Aminocarboxylates chelators, namely ethylenediaminetetraacetic acid (EDTA), efficiently bind iron(III) but these ligands have low iron(III) selectivity. Hydroxycarboxylates are more selective for iron(III) than aminocarboxylates as a consequence of the nature of the coordinating atoms, as these ligands have oxygen donor ligands [48, 164, 167].

The hydro-lipophilic balance (HLB), charge and molecular weight of chelating agents are also important properties to be considered in the design of chelators. These properties are particularly relevant if the ligand is expected to be administered orally as chelators have to be absorbed from the gastrointestinal tract and cross biological membranes until they are able to reach their targets.
Ligands must possess a HLB that allows their cross through membranes and simultaneously be soluble in aqueous biological environments. Due to the ion trapping effect, uncharged ligands diffuse easily in biological membranes and smaller molecules (molecular weights <200) cross membranes by non-facilitated diffusion [48, 167].
Smaller ligands, as bidentate and tridentate, have good oral bioavailability due to their facility to cross biological membranes, although this property can also be disadvantageous because these molecules can be toxic if they are able to cross the blood/brain barrier (BBB) and remove the iron needed for biological processes in the brain.

1.3.1 3-hydroxy-4-pyridinones as iron chelators

Hydroxypyridinones (HPOs) are *N*-heterocyclic compounds in which the metal ion is coordinated by two oxygen atoms of the carbonyl and hydroxyl groups in the ligand structure. Among other HPOs, namely 1-hydroxypyridin-2-one and 3-hydroxypyridin-2-one, the 3-hydroxy-4-pyridinone class is the most studied type of ligands [168, 169].

3,4-HPOs have low toxicity and good biocompatibility and are versatile molecules that can be functionalized in order to confer specific physicochemical or biological characteristics, without changing their chelating capacity.
These ligands form high stable complexes (high affinity constant) with trivalent hard metal ions, such as Fe(III), Al(III), Ga(III) as well with divalent metal ions, namely Zn(II), Cu(II) e VO(II).
The 3,4-HPO chelating units possess two dissociable protons whose characteristic pKa values are centred at 3.2 and 9.6 as previously described by our research group [170] (Figure A.2 in Appendix). Accordingly, depending on pH value, 3,4-HPO may be present in enol or keto forms. In aqueous solution, and in particular at pH=7.4, characteristic of biological fluids, the ligands are present in the keto form. Consequently, at the refered pH value, 3,4-HPOs form neutral 1:3 complexes with M(III) ions [168, 169, 171, 172].

Our research group has been working on the design of 3,4-HPOs ligands with different denticity to be used in several applications [159, 173-176].
Fluorescent chelators have been prepared by conjugating 3,4-HPO chelating units with fluorophores derived from different families of molecules such as naphthalene [170], 1,8-naphtalimide [177], fluorescein [3] and rhodamine [3, 4, 178, 179], in order to provide final fluorescent chelators with different physicochemical properties, namely the fluorescence emission spectrum, charge at physiological pH and distinct HLB due to the different nature of the fluorescent substituents linked to the chelating unit.

3,4-HPO chelators are obtained by reaction of 3-hydroxy-4-pyrones with primary amines (Figure 1.8) and the metal ion complexes formed by 3,4-HPO ligands exhibit higher values of stability constants than those determined for the respective 3-hydroxy-4-pyrones used as precursors [2, 168].

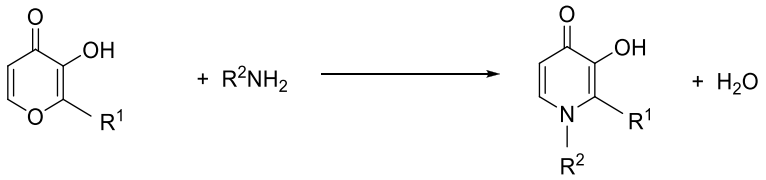

Figure 1.8 – Reaction scheme for synthesis of 3,4-HPOs by reaction of 3-hydroxy-4-pyrones with primary amines. (Adapted from [2]).

3,4-HPOs are characterized by their high affinity for iron(III) associated to extensive delocalisation of the lone pair of electrons of nitrogen atom in the 3,4-HPO ring (Figure 1.9). Moreover, the hydroxyl group is situated in *ortho* position in relation with the carbonyl group of the ring, thus leading to ideal geometry for iron(III) binding [180].

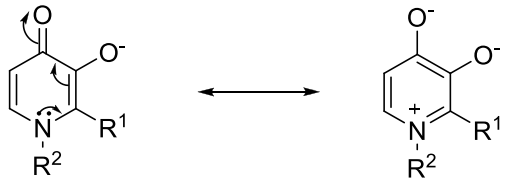

Figure 1.9 - Electronic delocalization in the 3,4-HPO ring. (Adapted from [2]).

Although HPOs are used to chelate and remove metals in excess in the organisms, metallodrugs based on these ligands are also described in the literature and metal ion complexes of HPOs are referred as potential pharmaceutical agents. These structures may be useful in many medical areas such as nuclear magnetic resonance probes [181] for diagnosis, or as active compounds for the treatment of diabetes [159] and cancer (see [168] for a review).

Several examples of applications of 3,4-HPOs for chelation therapy are described, namely in the treatment of infections caused by different pathogens and in disorders associated with oxidative stress, such as neurodegenerative diseases, in particular Alzheimer's disease (AD) and Parkinson's disease (PD). This topic will be discussed in the next sections (1.3.2 and 1.3.3).

1.3.2 Examples of chelators used in clinics for iron removal

Iron(III) chelators, either naturally occurring or synthetic, are clinically used for the treatment of iron overload associated with several diseases and also to control infections caused by diverse pathogens.

The first iron chelator approved by FDA (U.S. Food and Drug Administration) was Desferrioxamine B (DFO, also known as Desferal), a naturally occurring siderophore

produced by *Streptomyces pilosus.* DFO is a hexadentate ligand that includes three hydroxamate groups for iron(III) coordination [163] (Figure 1.10). DFO is one of the chelators currently used in the treatment of β-thalassaemia major [182].
This molecule has several disadvantages, namely low bioavailability and short half-life time in plasma and therefore the therapeutic includes subcutaneous infusions administered twice a day, three to seven times a week, which causes discomfort to the patients [54, 183].

In 1982, Deferiprone (DFP, also known as 1,2- dimethyl-3-hydroxy-4-pyridinone, L1, Hdmpp, CP20 or Ferriprox) was discovered and in 1999 this ligand was approved for use in the treatment of β-thalassemia patients [182] (Figure 1.10). DFP is a bidentate 3,4-HPO that forms highly stable complexes with iron(III) (pFe(III) value of ~19) but some side-effects have been reported, namely the occurrence of neutropenia and agranulocytosis events [48, 158, 168, 184]. Recently, the oral administration of DFP to hepcidin-knockout mice has shown protective effect against retinal degeneration caused by chronic systemic iron overload [185].

In order to overcome these drawbacks, several ligands have been proposed. Deferasirox (DFX, commercialized as Exjade, by Novartis) was approved in 2005 by the FDA as the first iron chelator for orally administration [15] (Figure 1.10). DFX has also shown positive effects in the treatment of patients with myelodysplastic syndrome, in which iron overload is a frequent consequence of the blood transfusions needed in the treatment of this disorder [186]. However, this drug has shown toxicity, namely affecting renal function and gastrointestinal disturbances in patients with β-thalassemia major [187].

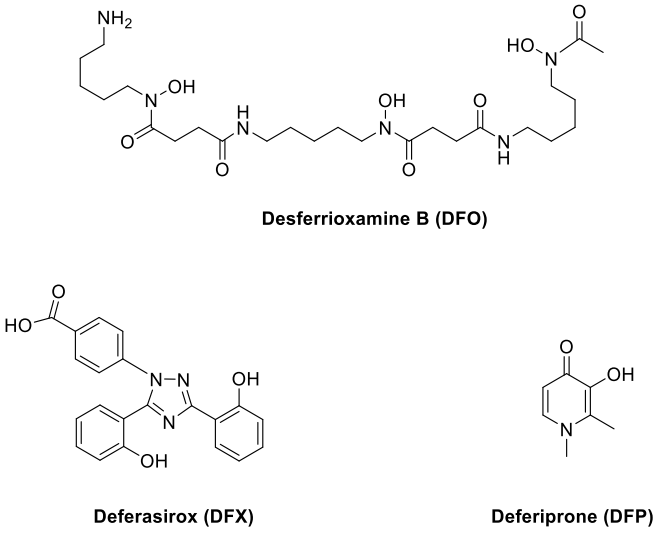

Figure 1.10 – Most clinically used iron chelators: Desferrioxamine B (DFO), Deferasirox (DFX) and Deferiprone (DFP) [15].

Recently, a new 3,4-HPO candidate has also been reported, 1-(*N*-acetyl-6-aminohexyl)-3-hydroxy-2-methylpyridin-4-one (CM1), with high affinity and selectivity for iron(III). The results obtained revealed that CM1 is orally active, nontoxic and has higher efficacy to remove iron than DFP, in rats [188].

Hexadentate chelators based on 3,4-HPO chelating units have been also proposed for iron removal [189-191] (reviewed in [10]). The structure of hexadentate ligands includes three bidentate 3,4-HPO chelating units linked by a tripodal anchor. These ligands have high affinity for iron(III) although their size and HLB may compromise *in vivo* applications.
Several other chelators designed by "Raymond's laboratory" have been investigated and these molecules include HPOs as well as hydroxamate and catecholate derived ligands. Among others, Pr(Me-3,2-HOPO) and TREN-(Me-3,2-HOPO), have been investigated as active compounds in the treatment of iron overload disorders [192].
The design of hexadentate HPOs including the three chelating units attached by a tripodal anchor arrangement may favour iron(III) binding. The complex formed adopts a cyclic structure and these tripodal hexadentate ligands exhibite higher chelating capacity in comparison with linear analogues [168, 193].
To enhance iron chelating capacities, Santos and co-workers developed a series of hexadentate tris-(3,4-HP) [169, 181, 194].
Other tripodal hexadentate chelators, namely a CP254 [195], CP262 [180] and CP256 [3] have been described in the work performed by Hider and co-workers.

Other examples of the HPO iron(III) chelators have been described. The 3,4-HPO, maltosine, is derived from the aminoacid lysine and is suggested as an alternative to DFP [196]. Copolymers composed by hexadentate 3,4-HPO monomers, namely CP254, have been synthesized and the macromolecule has shown high affinity and selectivity for iron(III), thus favoring its utilization for decrease iron absorption in the gastrointestinal tract [195].
Recently, in order to improve the permeation capacity of DFP, namely the ability to cross the BBB, other modified 3,4-HPOs have been described. These molecules are fluoro- and amido-disubstituted 3,4-HPOs in order to vary the HLB of the ligands [197].

The combined use of HPOs with other chelators has also been described, in particular for DFO and DFP, in order to improve the metal mobilization, namely in transfused iron-overload patients (reviewed in [10]). Furthermore, the utilization of different HPOs concomitantly is also described [172].

As reviewed in [15], numerous other iron chelators have shown an effect in treatment of iron overload associated disorders. Amongst others, pyridoxal isonicotinoyl hydrazone (PIH) possesses affinity for iron(III) in the same magnitude of the determined for DFO. Other ligands, such as 2-pyridinecarbaldehyde isonicotinoyl hydrazone (HPCIH), curcumin (a polyphenol) and other polyphenol compounds present in green tea (e.g. ECGg) have been also investigated for potential use in chelation therapy [15, 198].
HBED is another chelator described in the literature, although its selectivity towards iron(III) is limited and the ligand also has high affinity for zinc(II) [199].

EDTA and DTPA have been used in patients who are intolerant of DFO, although these chelators are not orally active and also they have low selectivity towards iron(III), namely by competition with zinc(II) ions [200].

Desferrithiocin (DFT), a tridentate bacterial siderophore, has also been reported as a potential orally effective iron(III) chelator, however the ligand has shown nephrotoxicity. An analogue chelator, Deferitrin, was proposed as a more effective and nontoxic alternative for the treatment for β-thalassemia by oral administration [201].

The tridentate chelator Deferitazole (formerly FBS0701) is a new orally active chelator possessing high affinity for iron(III). The ligand has shown efficacy in the treatment of patients suffering of transfusional iron overload and phase 2 trials revealed that the safety and tolerability profiles at therapeutic doses are comparable favorably to other oral chelators [202-204]. This molecule is an alternative candidate to overcome the drawbacks of the two other parent ligands, desferrithiocin and deferitrin, a natural siderophore and its synthetic analogue, respectively, which have demonstrated to induce toxicity in the kidneys [205].

Due to the relevance of increased iron levels in the development of neurodegenerative diseases, as previously discussed in this chapter, a plausible therapeutic approach may consist in decreasing the toxic levels of iron by administration of chelators.

Several studies describe the use of iron(III) chelators in the treatment of neurodegenerative diseases as reviewed in [42]. DFO was the first compound used in the treatment of AD to remove the excess of iron in the central nervous system [206]. Another chelator derived from a neuroprotective peptide has also been suggested as a potential active drug for the treatment of PD and AD [207]. Other iron ligands, such as M30 and HLA20, have shown efficacy in in the treatment of AD [208].

As discussed in the previous section, iron overload is also associated to the development and the progression of cancer (see [209] for a review). As high cell division rate is a characteristic of cancer, the relationship between iron and cancer is mainly due to the requirement of this metal for the activity of the enzyme ribonucleotide reductase, involved in DNA synthesis, as this metabolic process is exacerbated in cancer [10].

According to this fact, chelation therapy is also considered for cancer treatment. Natural siderophores, as amamistatins A and B or carboxymycobactins, isolated from different microorganisms have been tested and the results have shown anticancer activity [100].
Thiosemicarbazone (Dp44mT) is an iron chelator that has demonstrated positive results in the treatment of cancer [210]. DFO has also been effective as iron chelator agent in neuroblastoma cells [211].

Recently, HPO chelators conjugated with 5-aminolaevulinic acid have been synthesized and tested as potential agents for photodynamic therapy [212].
In addition to the described applications of iron chelators, these ligands can also be utilized for disorders related with the generation of ROS, as iron potentiates these reactions. Therefore, the administration of chelators may lead to the formation of iron complexes, sequestering the metal ion and thus preventing ROS production in cells.

Several chelators have been synthesized and tested in the treatment of ROS associated diseases. The PIH structural related ligand, salicylaldehyde isonicotinoyl hydrazone (SIH) has shown capacity to prevent iron-mediated hydroxyl radical formation [198, 213].
HPOs have also been described as iron chelators that have a protective effect against oxidative stress [214], namely CP94 and CP20 [215].

In summary, several efforts have been done in order to develop new molecules capable to remove iron(III) in excess in the organisms and the administration of these ligands led to the development of relevant therapies to control iron overload associated diseases.

1.3.3 Iron deprivation as a tool in the treatment of microbial infections

Bacterial resistance to traditional antibiotics has increased enormously [216, 217] and thus the development of new antimicrobial agents, with novel modes of action and/or different cellular targets becomes imperative.
Innumerous reports of the use of iron chelators to control infections [48] caused by different pathogens have been described and several representative examples will be reviewed in

this section, with particular highlight for the use of iron chelation therapy to control mycobacterial infections.

Removal of iron by chelation showed to improve the clinical outcome in a number of infectious diseases, namely malaria [218-220].
The iron chelator DFO has been reported to be effective in the elimination of the malaria causative pathogen, *Plasmodium falciparum*, in humans [221]. A catechol iron chelator, FR160, has shown *in vitro* activity against the same protozoa [222]. The chelator Deferitazole (FBS0701) was also effective in controlling *Plasmodium falciparum* infection in a murine malaria model [223].

The anti-malaria activity of the 3,4-HPO ligand, DFP, has been proved [224] and the antiplasmodial activity of HPO - chloroquine conjugates has also been investigated [225, 226].

Iron chelators have also been used in the treatment of infections caused by other parasites, namely *Trypanosoma cruzi*, the causative agent of Chagas disease. DFO has been administered to mice infected with this pathogen and results have shown that the level of parasitemia was reduced in the presence of the chelator [227-229]. DFP - chloroquine conjugates have shown activity against two trypanosome species *Trypanosoma brucei* and *Trypanosoma cruzi [220]*.
The effect of iron chelators was also investigated against infections caused by leishmania. DFO showed activity in the control of the growth of *Leishmania chagasi* in infected mice [230]. However, the relevance of iron in leishmanial infections is not well stablished. Several studies described that iron may be toxic for leismania and therefore a possible strategy to combat these infection may include iron supplementation in spite of deprivation of the pathogens from this metal ion (see [44] for a review).
The administration of iron chelators in the treatment of viral infections such as hepatitis C [231] and AIDS [232] is also reported in the literature. Different HPOs have shown relevant anti-influenza virus [233] and anti-herpes simplex viruses activity (HSV-1 and -2) [234, 235].

Several investigations have been reported concerning the use of iron chelators to treat infections caused by fungal pathogens, such as *Aspergillus fumigatus* and *Fusarium oxysporum* [236]. DFX showed antifungal activity, namely in treating experimental mucormycosis and aspergillosis [67, 237, 238].

The effect of iron chelators in the treatment of bacterial infections has been extensively investigated and the first molecules studied were 8-Hydroxyquinoline and its related ligands

[239]. Some chelators as EDHPA, EDTA and DTPA have shown activity against Gram-positive and Gram-negative bacteria (reviewed in [240, 241].
The antibacterial effect of iron chelators to control the growth of *Pseudomonas aeruginosa* has been reported [242, 243] and the conjugation of those molecules with the antibiotic aminopenicillin has also shown positive effects [244].

The effect of iron chelators against bacterial biofilms has also been shown, for instance in the biofilms produced by *Pseudomonas aeruginosa* [243, 245-247] or *Staphylococcus aureus* [248].

The extensively used DFO and DFX iron chelators have demonstrated antibacterial effect in a numerous range of bacterial pathogens [249-252]. However, these ligands offer some drawbacks. DFX is a tridentate ligand and consequently has lower iron affinity than hexadentate ligands. DFO is a hexadentate natural siderophore, but bacteria possess specific receptors for capturing the iron loaded chelator and use the metal ion for their own growth [251, 253, 254].

Thus, in the rational design of antimicrobial chelators, this aspect must be taken into consideration. The structure of antimicrobial agent must be differs from that of common siderophores in order to prevent the recognition of the iron–chelator complex by the pathogens and the subsequent use of the metal ion.
To overcome these disadvantages, the antimicrobial activity of chelator types, which are not present in natural siderophores, such as 3,4-HPOs and namely DFP, has been evaluated. This chelator has shown efficacy against several bacteria, such as *S. aureus* and *P. aeruginosa* [251, 254-256].

Other 3,4-HPO, have shown *in vitro* inhibitory activity against several Gram-positive and Gram-negative bacterial species, including *S. aureus*, *P. aeruginosa* and *Escherichia coli* [68, 257-262].

1.3.3.1 Iron chelators and mycobacterial infections

The development of new drugs to combat the infections caused by mycobacteria remains crucial. As iron is essential for mycobacterial growth and survival [44] the use of iron chelators to remove the iron available for mycobacteria, as a strategy to control mycobacterial infection, is worth considering and several ligands have already been tested (reviewed in [123, 263]).

DFO has been used to inhibit *Mycobacterium aurum* growth [264] and another study suggested that DFO in combination with silybin, an iron-chelating agent from plants, reduced the extracellular growth of *M. tuberculosis.* Although both of these chelators induced slightly effects on the reduction of in intracellular growth of the pathogen [150].
DFO also inhibited biofilm formation by *M. smegmatis* and *M. bovis* BCG [265].

Other ligands, namely spiro pyridopyrrolizines, pyrrolidines [266] and 4*H*-pyrano[3,2-*c*]pyridine derivatives [267], have been tested and the results have shown that the compounds are effective to inhibit the *in vitro* growth of *M. tuberculosis.* Spiro-piperidin-4-ones derivatives also inhibited the growth of *M. tuberculosis*, both *in vitro* and *in vivo* [268]. 2-hydrazino-pyrimidin-4(3*H*)-one derivatives, have been tested against *M. tuberculosis* and several molecules have shown antimycobacterial activity [269].

Gomes *et al*. investigated the antimycobacterial activity of different chelators, namely DFO, HBED, dDFT and VUF-8514. The authors verified that DFO, HBED e VUF8514 inhibit mycobacterial growth in axenic conditions and HBED and DFO also inhibit *M. avium* intramacrophagic growth [123]. *In vivo*, the administration of DFO or HBED had small effect on the growth of the pathogen. Later studies performed by the authors have also demonstrated that the use of iron chelators in *M. avium* infected mice decreases the growth of the pathogen [126].

Douvas *et al*. studied the effect of DFP and other 3,4-HPOs, namely L1Net, L1NPr and L1NAll *In vitro* studies revealed that the influence of the chelators in the replication of *M. avium* may depend on the tested concentration. Chelators enhanced intracellular and extracellular growth of *M. avium* at low concentrations. However, at high concentrations, they are effective in the control of *M. avium* infections [270].

Functionalized tetrahydro-4(1H)-pyridinones have been synthesized and tested revealing *in vitro* activity against M*. tuberculosis* [271].

Our research group has developed several functionalized 3,4-HPO with lipophilic fluorescent moieties attached to the HPO chelating unit and their activity against *M. avium* infection has been evaluated [1, 3, 4].
In the first study, several non-fluorescent bidentate chelators have been tested and none of the ligands significantly inhibited the growth of *M. avium* inside bone marrow derived macrophages (BMM). Different hexadentate ligands bearing different anchors linking the bidentate units (CP262, CP252, CP256 and **MRH7**) (referred as CP777 in [1] and as chelator 4 in [3]) have been synthesized and tested against *M. avium* infection, in axenic

medium and inside BMM. The most active chelator includes in its structure the tripoidal anchor and a rhodamine B isothiocyanate fragment (**MRH7**).
The antimicrobial activity is associated with the chelating properties of **MRH7** but this property *per se* is not sufficient since the non-functionalized chelating unit (CP256) is not effective.
Among the fluorescent chelators functionalized with different fluorophores such as fluorescein or rhodamine, the rhodamine B isothiocyanate labelled chelator exhibited the strongest inhibitory activity and was identified as a lead compound [1].

In addition, comparative studies of the partition and distribution of fluorescein or rhodamine derived chelators have been performed in liposomes and macrophages and the more biologically active compounds are those that interact strongly with lipid phases and cross cell membranes [3].

In the subsequent studies, various rhodamine derived fluorescent chelators have been synthesized and their antimycobacterial activity has been evaluated. All rhodamine derived fluorescent chelators tested were capable of restricting the intramacrophagic growth of *M. avium* and their activity was strongly dependent on the type of fluorophore on the molecular framework. In particular, the most relevant inhibitory effect was obtained with the rhodamine B isothiocyanate labelled compounds, **MRH7** and **MRB7**, whose activity is superior to that observed for the other two chelators (**MRH8** and **MRB8**) [4] (Figure 1.11).

Recently, our group performed NMR and MD simulation studies (Chapter 4) [272] and the results obtained have shown that a strong affinity for lipid bilayers is crucial for the biological activity and that chelators interact with the lipid phases at different levels of the bilayer. The interaction seems to be strengthened for the rhodamine B isothiocyanate labelled compounds, which are those exhibiting the highest biological activity [4]. For a complete understanding of the mechanism of action and the importance of the different functional groups in the diverse rhodamine frameworks tested, further studies are crucial to get insight on the structure-activity relationships of these molecules.

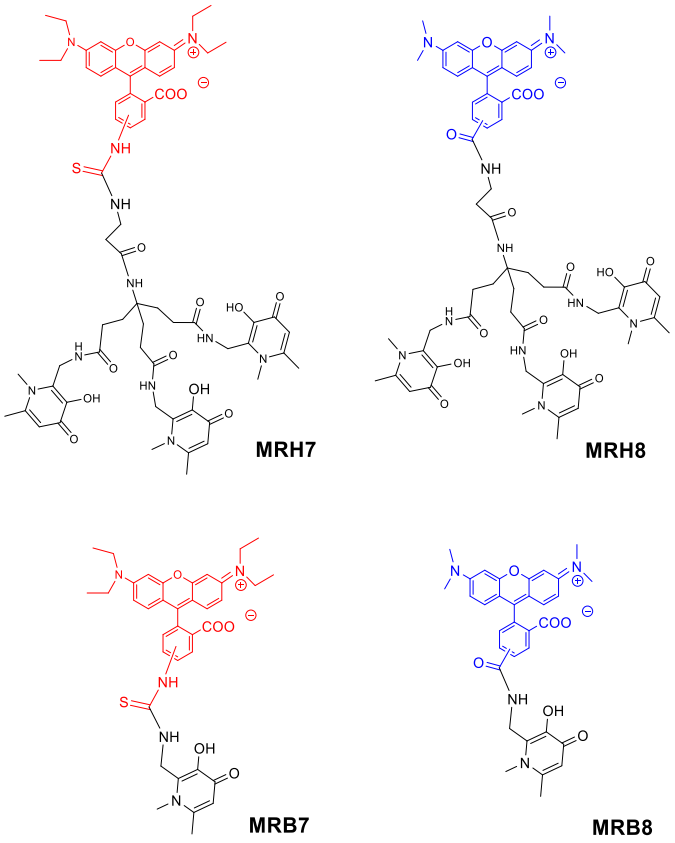

Figure 1.11 – Formulae and numbering of fluorescent bidentate (**MRB7** and **MRB8**) and hexadentate (**MRH7** and **MRH8**) chelators used in this study. In previous works the compound **MRH7** was abbreviated as **CP777** [1] and **4** [3].

Despite of the advantageous use of iron chelators in the treatment of infections caused by several pathogens, the use of chelation therapies also have drawbacks. In particular, the use of iron chelators as antimicrobial drugs may remove the iron required for the generation of ROS, compromising one of the innate defence mechanisms performed by phagocytes [259].

In conclusion, iron metabolism appears to be a plausible target for development of new drugs to treat infections, due to the ability of iron chelators to remove the available metal ion and consequently decrease microbial growth. The knowledge of the structure of natural siderophores produced by bacteria and other organisms may contribute to a better rational design of new iron chelators, thus conducing to the production of chelators with high affinity and selectivity for iron(III) and therefore improving the biological activity of the ligands against the infection.

2 | SYNTHESIS AND CHARACTERIZATION OF 3,4-HPO CHELATORS

2. SYNTHESIS AND CHARACTERIZATION OF 3,4-HPO CHELATORS

2.1 Introduction

As iron is a key factor for the growth of all bacteria, fungi and protozoa [59] and taking into account the concept of iron deprivation as a means to fight infection, systematic work has been performed by our group in order to design and synthesize 3,4-HPO iron (III) chelators that (may) have application in the development of new strategies to reduce iron sources and fight infection [1, 3, 4]. Examples of the use of iron chelation therapies and improvement in infection susceptibility of several microorganisms upon administration of chelators have been reported in the literature and summarized in Chapter 1 [18, 59, 75, 164, 251, 258-261, 273].

The work developed by our research group on the design of 3,4-HPO ligands to be used in several applications is illustrated in references [159, 173, 174, 176, 274]. Bidentate 3,4-HPOs were used as chelating units to obtained ligands with different denticity, by combining one or more of these bidentate frameworks in the structure of the ligand. For the synthesis of hexadentate chelators, the bidentate units were linked by a tripodal anchor which includes a tetrahedral carbon atom. The use of this type of anchor is advantageous in the design of these ligands as it allows further functionalization of the chelator's structure with different functional groups or molecular frameworks, such as fluorophores [3].

Several chelators have been synthesized by our research groups comprising ligands with different denticity, such as bidentate, tetradentate and hexadentate molecules, and the chelating units have also been functionalizing the with several fluorophores [3, 170, 177], namely rhodamine [3, 4, 178, 179]. Several types of linkers between the fluorophore may also be considered in the design of fluorescent chelators. The different components in the structure of the fluorescent chelators are depicted in Figure 2.1.

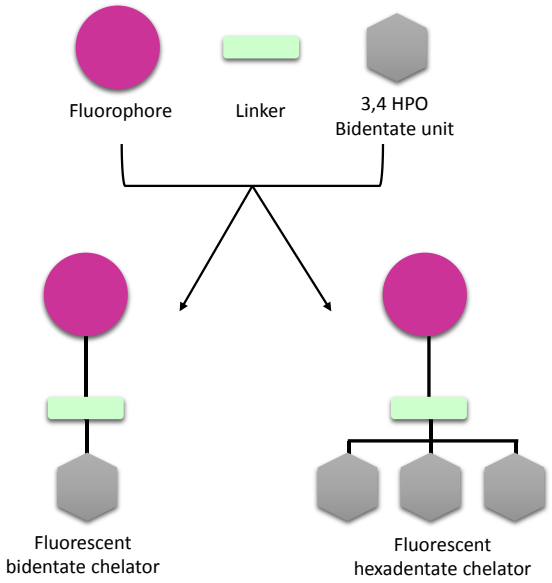

Figure 2.1 –Graphical representation of the structure of fluorescent 3,4-HPO chelators. The fluorophore is represent by a circle, the linker by a rectangle and the bidentate 3,4-HPO chelating unit by a hexagon.

Our results are indicative that all the prepared rhodamine derived fluorescent chelators were capable of restricting the intramacrophagic growth of *M. avium* and their activity is strongly dependent on the presence of the fluorophore on the molecular framework. Both bidentate and hexadentate chelators have been tested and their antimycobacterial activity are similar for the chelators with the same fluorophore in their structure, if the appropriate amount of bidentate and hexadentate ligands are given, thus reinforcing the importance of the fluorophore.

In order to get insight about the relevance of the fluorophore's structure we designed a new set of chelators to evaluate (Appendix, Figure A.1):

a) The importance of Sulphur either as an element per se or as a thiourea group: the rhodamine moiety the ethyl groups linked to nitrogen atoms was maintained. A different linkage, sulfonamide, was considered (**F2**) - Ligand **MRB2** (Figure 2.2 and Figure A.1, in Appendix);

b) The relevance of the thiourea group in association with a rhodamine or associated with other fluorophores: ligand **MRB4** was designed to include a different type of fluorophore, a naphthalene unit (**F4**). We maintained the thiourea connecting the fluorophore and the chelating unit (Figure 2.2 and Figure A.1, in Appendix);

c) The importance of the charge of the chelator: the rhodamine-like moiety is maintained in ligand **MRB20** (Figure 2.2) in whose structure there is no substituent in the position 2' of the phenyl ring (**F20**), leading to a rosamine derived chelator and the positive charge at physiological pH, according to the literature [3, 179, 275] (Figure 2.2 and Figure A.1, in Appendix);

d) The contribution of the rhodamine B isothiocyanate fragment and variation in global lipophilicity: we designed chelators labelled with other rhodamine fragments: tetramethylrhodamine isothiocyanate (**F10**) (chelator **MRH10**) and 5(6)-carboxytetraethylrhodamine (**F9**) (chelator **MRB9**). In the structure of **MRH10**, the thiourea group was maintained (as in rhodamine **F7**) but the ethyl groups linked to the nitrogen in the rhodamine ring were substituted by methyl groups, as present in chelators derived from rhodamine **F8** [4]. In the structure of **MRB9**, the isothiocyanate linkage was changed to the same linkage present in rhodamine **F8** derived ligands but the ethyl groups linked to the nitrogen atom in the rhodamine rings was considered as in ligands with rhodamine **F7** in their structure (Figure 2.2 and Figure A.1, in Appendix).

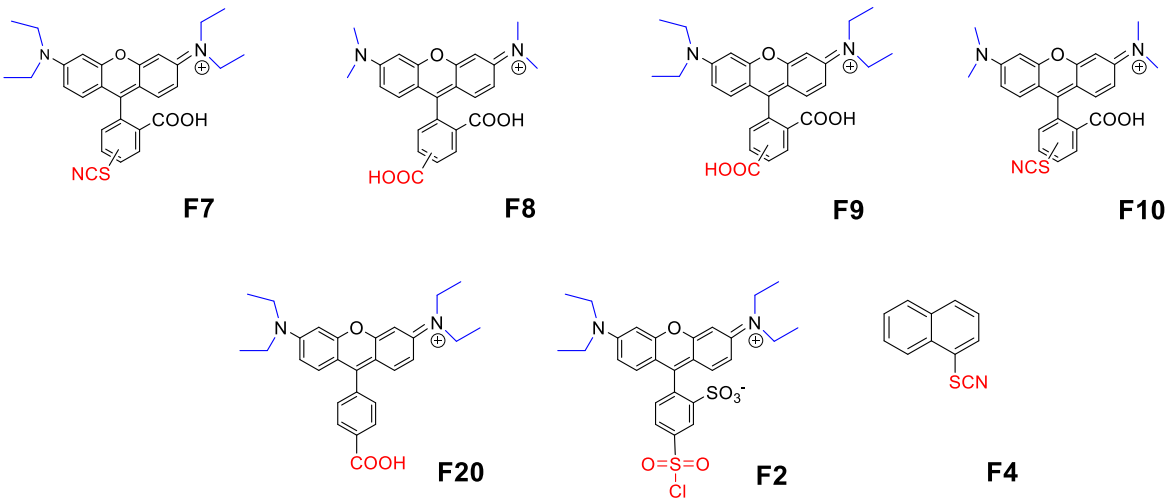

Figure 2.2 –Formulae of fluorophores used for the synthesis of fluorescent 3,4-HPO chelators.

In this chapter we report the synthesis and the structural characterization of the new molecules obtained using several methodologies, such as NMR, mass spectrometry, elemental analysis, UV-Vis and Fluorescence spectroscopies and Single Crystal X-Ray Diffraction, for the ligands which it was possible to obtain crystals suitable for this technique. To the best of our knowledge, this is the first report in which a crystal structure of a rhodamine labelled 3,4-HPO chelator is reported.

The synthesis and characterization of chelators **MRH10** and **MRB9** is published in:

[276] **Moniz, T.**, Silva, D., Silva, T., Gomes, M.S. and Rangel, M., *Antimycobacterial activity of rhodamine 3,4-HPO iron chelators against Mycobacterium avium: analysis of the contribution of functional groups and of chelator´s combination with ethambutol.* MedChemComm, 2015, **6**, 2194-2203.

The synthesis and characterization of chelators **MRB2** and **MRB4** is published in:

Moniz, **T.**, Coimbra, J.T.S., Brás, N.F., Cunha-Silva, L., Ramos, M.J., Fernandes, P.A., de Castro, B. and Rangel M., *Synthesis and structural characterization, by spectroscopic and computational methods, of two fluorescent 3-hydroxy-4-pyridinone chelators bearing sulphorhodamine B and naphthalene*, RSC Advances, **2016**, 6, 4200-4211.

2.2 Methods

2.2.1 Chemicals and instrumentation

Chemicals were obtained from Sigma–Aldrich (grade puriss, p.a.) or Fluka (p.a.) and were used as received unless otherwise specified.

Nuclear Magnetic Resonance (NMR) spectra (^{1}H and ^{13}C NMR) were measured on a Bruker Avance III 400 spectrometer operating at 400.15 MHz and 100.62 MHz for ^{1}H and ^{13}C spectra, respectively. Two-dimensional ^{1}H/^{1}H correlation spectra (COSY), gradient selected ^{1}H/^{13}C heteronuclear single quantum coherence (HSQC) and ^{1}H/^{13}C heteronuclear multiple bond coherence (HMBC) spectra were acquired using the standard Bruker software.

Mass spectrometry (MS), NMR and Electronic Paramangnetic Resonance (EPR) analyses were performed at “Laboratório de Análise Estrutural, Centro de Estudos e Materiais da Universidade do Porto” (CEMUP) (Portugal). Elemental analysis was performed at the analytical services of the “Unidad De Análisis Elemental” of Santiago de Compostela, University of Santiago (Spain).

Absorption spectra were acquired in a Shimadzu spectrophotometer equipped with a constant-temperature cell holder equipped with a constant-temperature cell holder, at 25°C, in 1 cm cuvettes.

Fluorescence measurements for photochemical characterization of the new chelators were performed with a Varian Cary Elipse Spectrofluorometer equipped with a constant-temperature multicell cell holder, at 25°C, in 1 cm cuvettes. To minimize reabsorption effects, the absorbance’s sample values were kept below 0.1.

Flash chromatography was carried out using silica gel Merck (230-400 mesh).

2.2.2 Synthesis of fluorescent 3-hydroxy-4-pyridinone ligands

The formulae of the bidentate and hexadentate chelators used in the present study (Chapters 2, 3, 4 and 5) are shown in Figure A.1, in Appendix. The rhodamine derivatives (**F7** or **F8**) were linked to i) a protected 3,4-HPO bidentate ligand or ii) to a protected 3,4-HPO hexadentate chelator, in order to yield protected forms of fluorescent bidentate and hexadentate chelators, respectively. The final chelators were obtained by deprotection under BCl_3 of the protected forms according to experimental procedures described elsewhere [3, 4]. All the chelators **MRH7**, **MRH8**, **MRB7** and **MRB8** used were synthesized previously and are in stock in our laboratory and their synthesis and characterization is described in the literature [4].

Sulphorhodamine B acid chloride, 1-naphthyl isothiocyanate, and tetramethylrhodamine isothiocyanate are commercially available fluorophores. Carboxyrosamine [275], 5(6)-carboxytetraethylrhodamine [277, 278] and the protected bidentate and hexadentate 3,4-HPO chelating units used [2, 3, 4, 22] are available in stock in our laboratory and produced by our research group accordingly to the methods described in the literature.

*Compound **1***

To a solution of sulphorhodamine B acid chloride (**F2**) (0.107 g, 1.86x10^{-4} mol) in anhydrous DMF (0.7 mL), the protected 3,4-HPO bidentate ligand (2-aminomethyl-3-benzyloxy-1,6-dimethyl-1*H*-pyridin-4-one) (0.040 g, 1.54x10^{-4} mol) was added and the mixture was stirred at room temperature in the dark and under argon atmosphere, for 24 h. The product was purified by gradient flash column chromatography, eluting with chloroform/methanol (9:1) and increasing polarity until chloroform/methanol (6:4) to afford **1** (0.030 g; 24%) as a purple solid (Figure 2.3).

MS: calculated for $C_{42}H_{47}N_4O_8S_2^+$: MS: 799.28: [M$^+$], found: matrix-assisted laser desorption/ionization time of flight MS: 799.27 [M$^+$]. ^{1}H NMR (400.15 MHz, MeOD-d4, ppm): δ 1.31 (t, *J* 7.2 Hz, 12H, $NCH_2C\underline{H}_3$); 2.42 (s, 3H, 6''-$C\underline{H}_3$); 3.69 (m, 8H, $NC\underline{H}_2CH_3$); 3.76 (s, 3H, NCH_3); 4.24 (s, 2H, $C\underline{H}_2NH$); 5.12 (s, 2H, $C\underline{H}_2C_6H_5$); 6.44 (s, 1H, H-5''); 6.94 (d, *J* 2.2 Hz, 2H, H4+ H5); 7.01-7.04 (dd, *J* 2.2, 10.4 Hz, 2H, H2+H7); 7.06 and 7.08 (d, *J* 10.4 Hz, 2H, H1+H8); 7.25-7.32 (m,3H, *m*-+*p*- $CH_2C_6\underline{H}_5$); 7.35-7.38 (m, 2H, *o*- $CH_2C_6\underline{H}_5$ + 1H, H6'); 8.02 (dd, *J* 5.0,1.6 Hz, 1H, H5'); 8.58 (d, *J* 1.6 Hz, H3'); ^{13}C NMR (100.62 MHz, MeOD-d4, ppm): δ 12.8 ($NCH_2\underline{C}H_3$); 21.0 (6''-$\underline{C}H_3$); 37.3 ($N\underline{C}H_3$); 39.5 ($\underline{C}H_2NH$); 46.8 ($N\underline{C}H_2CH_3$); 74.6 (-$\underline{C}H_2C_6H_5$); 97.0 (C4 + C5); 115.1 (C2+ C7); 119.1 (C5"); 127.6 (C3'); 129.5 (C5'); 129.6 (*m*-, *p*- $\underline{C}_6H_5$); 130.2(C6'); 133.5(*o*-$\underline{C}_6H_5$); 133.8 (C1 + C8); 135.8 (C4'); 138.2 (Cq, -$\underline{C}_6H_5$); 142.0 (C2"); 143.0 (C1'); 147.4 (C3"); 151.5 (C6"); 157.2 (C3+C6); 159.4 (C1a + C8a); 174.6 (C4'').

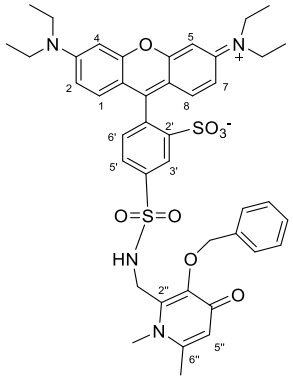

1

Figure 2.3 – Formulae and numbering of compound **1**.

*Compound **MRB2***

Compound **1** (0.029 g, $3.63x10^{-5}$ mol) was dissolved in anhydrous dichloromethane (20 mL), under argon and cooled to 0ºC. BCl_3 (1 mL) was added dropwise and the reaction mixture was kept overnight with stirring at room temperature. Methanol (50 mL) was added and the mixture was stirred for 1 h. The solvent was removed under reduced pressure to afford the crude product. Recrystallization of the product from methanol/diethyl ether (2:8) afforded the hydrochloride salt **MRB2** (0.0244g, 90%) as a purple solid (Figure 2.4).

Elemental analysis for ($C_{35}H_{40}N_4O_8S_2.1.5C_3H_7NO.3.5H_2O.2CHCl_3.3HCl$): Calculated C 40.54; H 5.12; N 6.27. Found: C 40.41; H 4.78; N 6.25. MS: calculated for $C_{35}H_{41}N_4O_8S_2^+$: MS: 709.23: [M^+], found: matrix-assisted laser desorption/ionization time of flight MS: 709.13 [M^+]. ^{1}H NMR (400.15 MHz, MeOD-d4, ppm): δ 1.30 (m, 12H, $NCH_2C\underline{H}_3$); 2.67 (s, 1.5H, 6''-$C\underline{H}_3$, stereoisomer A); 2.70 (s, 1.5H, 6''-$C\underline{H}_3$, stereoisomer B); 3.68 (q, *J* 10.8, 7.2 Hz, 8H, $NC\underline{H}_2CH_3$); 4.13 (s, 3H, NCH_3); 4.66 (s, 2H, $C\underline{H}_2NH$); 6.95 (d, *J* 2.4 Hz, 2H, H4+ H5); 7.00-7.03 (dd, *J* 2.4, 11.6 Hz, 2H, H2+H7); 7.08-7.11 (d, *J* 11.6 Hz, 2H, H1 + H8); 7.09 (s, 1H, H-5''); 7.54 (d, *J* 8.00 Hz, 1H, H6'); 8.02 (dd, *J* 5.0, 3.0 Hz, 1H, H5'); 8.56 (d, *J* 1.6 Hz, H3'); ^{13}C NMR (100.62 MHz, MeOD-d4, ppm): δ 12.3 ($NCH_2\underline{C}H_3$); 21.7 (6''-$\underline{C}H_3$, stereoisomer A); 34.9 (6''-$\underline{C}H_3$, stereoisomer B); 38.2 ($\underline{C}H_2NH$); 39.3 ($N\underline{C}H_3$); 46.3 ($N\underline{C}H_2CH_3$); 96.5 (C4 + C5); 113.5 (C5"); 114.6, 114.8 (C2+ C7); 127.2 (C3'); 129.1 (C5'); 132.1 (C6'); 133.1 (C1 + C8); 135.5 (C4');139.0 (C2"); 142.3 (C1', stereoisomer A); 144.5 (C3"); 146.8 (C1', stereoisomer B); 150.5 (C6"); 156.7 (C3+C6); 157.0 (C9); 158.9(C4a + C5a); 160.0 (C1a + C8a).

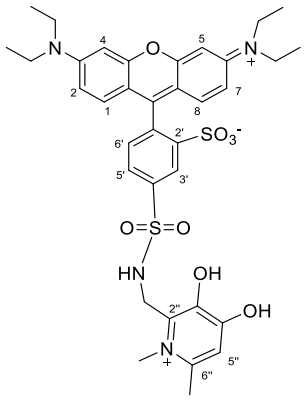

MRB2

Figure 2.4 – Formulae and numbering of compound **MRB2**.

*Compound **3***

To a solution of 1-naphthyl isothiocyanate (**F4**) (0.034 g, 1.85x10^{-4} mol) in anhydrous DMF (0.6 mL) and triethylamine (0.01 mL), protected 3,4-HPO bidentate ligand (2-aminomethyl-3-benzyloxy-1,6-dimethyl-1*H*-pyridin-4-one) (0.040g, 1.8x10^{-4} mol) was added and the mixture was stirred at room temperature in the dark and under argon atmosphere, for 24 h. The product was purified by gradient flash column chromatography, eluting with chloroform/methanol (9:1) to afford **3** (0.052 g; 76%) as a white solid (Figure 2.5).

MS: calculated for $C_{26}H_{26}N_3O_2S^+$: MS: 444.17: [M^+], found: matrix-assisted laser desorption/ionization time of flight MS: 444.19 [M^+]. ^{1}H NMR (400.15 MHz, $CDCl_3$, ppm): δ 2.25 (s, 3H, 6'-C<u>H</u>$_3$); 3.66 (s, 3H, NC<u>H</u>$_3$); 4.90 (d, *J* 5.6 Hz, 2H, C<u>H</u>$_2$NH); 4.99 (s, 2H, C<u>H</u>$_2$C$_6$H$_5$); 6.30 (s, 1H, H-5'); 7.16-7.18 (m,3H, *m*-+*p*- CH$_2$C$_6$<u>H</u>$_5$); 7.22-7.26 (m, 2H, *o*-CH$_2$C$_6$<u>H</u>$_5$); 7.47 (t, *J* 7.8 Hz, 1H, H3); 7.50-7.55 (m, 2H, H6+H7); 7.59 (d, *J* 7.2 Hz, 1H, H2); 7.80 (d, *J* 8.4 Hz, 1H, H4); 7.88-7.91 (m, 1H, H5); 8.07 (d, *J* 9.2 Hz, 1H, H8); ^{13}C NMR (100.62 MHz, $CDCl_3$, ppm): δ 21.9 (6'-<u>C</u>H$_3$); 38.2 (N<u>C</u>H$_3$); 41.9 (<u>C</u>H$_2$NH); 74.2 (-<u>C</u>H$_2$C$_6$H$_5$); 119.8 (C5'); 123.3 (C8); 125.9 (C4); 126.5 (C3); 127.4 (C6); 127.7 (C7); 128.8 (C2); 129.0 (*m*-+*p*- <u>C</u>$_6$H$_5$); 129.3 (*o*- <u>C</u>$_6$H$_5$); 129.5 (C5); 130.8 (C8a); 135.4 (C4a); 137.8 (Cq, -<u>C</u>$_6$H$_5$); 141.7 (C2'); 147.6 (C3'); 148.3 (C6'); 173.9 (C4'); 183.5 (N<u>C</u>S).

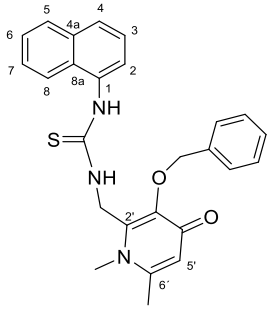

3

Figure 2.5 – Formulae and numbering of compound **3**.

*Compound **MRB4***

Compound **3** (0.052 g, 1.17x10^{-5} mol). was dissolved in anhydrous dichloromethane (20 mL) under argon and cooled to 0ºC. BCl_3 (1 mL) was added dropwise and the reaction mixture was kept overnight with stirring at room temperature. Methanol (50 mL) was added and the mixture was stirred for 1 h. The solvent was removed under reduced pressure to afford the solid product. Recrystallization of the product from chloroform/*n*-hexane (2:8) afforded the hydrochloride salt **MRB4** (0.044g, 96%) as a light brown solid (Figure 2.6).
Elemental analysis for ($C_{19}H_{20}N_3O_2S.0.33CH_3OH.1.33HCl$): Calculated C 56.13; H 5.52; N 10.16. Found: C 56.18; H 5.40; N 9.78. MS: calculated for $C_{19}H_{20}N_3O_2S^+$: MS: 354.13: [M^+], found: matrix-assisted laser desorption/ionization time of flight MS: 354.16 [M^+]. ^{1}H NMR (400.15 MHz, MeOD-d_4, ppm): δ 2.58 (s, 3H, 6'-C<u>H</u>$_3$); 4.00 (s, 3H, NC<u>H</u>$_3$); 5.16 (s, 2H, C<u>H</u>$_2$NH); 6.96 (s, 1H, H-5'); 7.49 (dd, *J* 1.2, 4.2 Hz, 1H, H2); 7.54 (t, *J* 8.4 Hz, 1H, H3); 7.54-7.66 (m, 2H, H6+H7); 7.91 (d, *J* 7.6 Hz, 1H, H4); 7.93-7.96 (m, 2H, H5+H8); ^{13}C NMR (100.62 MHz, MeOD-d_4, ppm): δ 20.6 (6'-<u>C</u>H$_3$); 39.6 (N<u>C</u>H$_3$); 41.3 (<u>C</u>H$_2$NH); 113.3 (C5'); 123.1 (C4); 126.1 (C2); 126.4 (C3); 127.1 (C6); 127.4 (C7); 128.9 (C5); 129.0 (C8); 131.1 (C8a); 134.1 (C1); 135.7 (C4a); 140.5 (C2'); 144.4 (C3'); 149.6 (C6'); 160.6 (C4'); 183.4 (N<u>C</u>S).

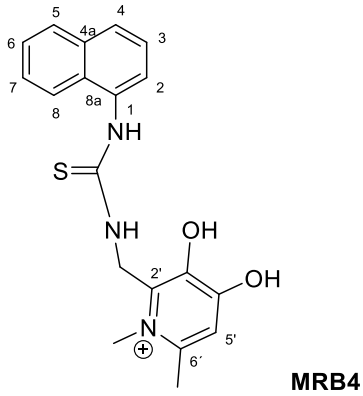

MRB4

Figure 2.6 – Formulae and numbering of compound **MRB4**.

*Compound **MRB20p***

To a solution of carboxyrosamine (**F20**) (97.0 mg, 2.20 x10^{-4} mol) in anhydrous DMF (1 mL), protected 3,4-HPO bidentate ligand (2-aminomethyl-3-benzyloxy-1,6-dimethyl-1*H*-pyridin-4-one) (47.4 mg; 1.83 x10^{-4} mol), DCC (45.8 mg, 2.20 x10^{-4} mol) and *N*-hydroxysuccinimide (NHS) (25.5 mg, 2.20 x10^{-4} mol) were added and the mixture was stirred at room temperature in the dark and under an argon atmosphere, for 2 days. Subsequently, the formed *N*, *N*-dicyclohexylurea (DCU) precipitate was filtered off and the solvent removed under reduced pressure. The product was purified by gradient flash column chromatography, eluting with methanol/chloroform (9:1 followed by an increased gradient until 8:2) to afford **MRB20p** (0.0627 g; 49%) as a purple solid (Figure 2.7).

400.15 MHz ^{1}H NMR (MeOD-d_4, ppm): δ 1.31 (t, *J* 7.2 Hz, 12H, $NCH_2C\underline{H}_3$); 2.45 (s, 3H, 6''-$C\underline{H}_3$); 3.69 (m, 8H, $NC\underline{H}_2CH_3$); 3.72 (s, 3H, NCH_3); 4.73 (s, 2H, $C\underline{H}_2NH$); 5.22 (s, 2H, $C\underline{H}_2C_6H_5$); 6.50 (s, 1H, H-5''); 6.99 (d, *J* 2.5 Hz, 2H, H4+ H5); 7.06-7.09 (dd, *J* 2.5; *J* 12.0 Hz, 2H, H2+H7); 7.27-7.36 (m,5H, $CH_2C_6\underline{H}_5$); 7.45-7.48 (d, *J* 12.0 Hz, 2H, H1+H8); 7.58 (d, *J* 8.5 Hz, 2H, H2' + H6'); 8.08 (d, *J* 8.5 Hz, 1H, H3' + H5'); 100.62 MHz ^{13}C NMR (MeOD-d_4, ppm): δ 12.8 ($NCH_2\underline{C}H_3$); 20.9 (6''-$\underline{C}H_3$); 37.2 ($\underline{C}H_2NH$); 37.5 ($N\underline{C}H_3$); 46.9 ($N\underline{C}H_2CH_3$); 74.8 (-$\underline{C}H_2C_6H_5$); 97.5 (C4 + C5); 115.7 (C2+ C7); 119.2 (C5''); 129.1 (C3' + C5'); 129.4 (*o* - $\underline{C}_6H_5$); 129.5 (*p* - $\underline{C}_6H_5$); 130.1 (C1 + C8); 131.0 (C2' + C6'); 132.8 (*m*-$\underline{C}_6H_5$); 136.6 (C1'); 136.9 (C4'); 138.5 (Cq, -$\underline{C}_6H_5$); 143.2 (C2''); 147.7 (C3''); 151.1 (C6''); 157.2 (C3+C6); 157.5 (C1a + C8a); 159.5 (C4a + C5a); 169.0 (HNCO); 175.0 (C4'').

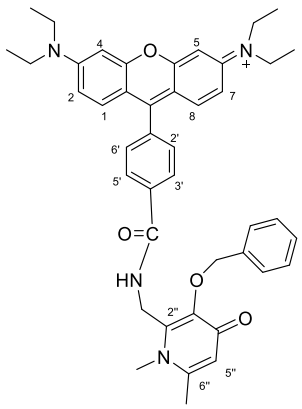

MRB20p

Figure 2.7 – Formulae and numbering of compound **MRB20p**.

*Compound **MRB20***

Compound **MRB20p** (0.0627g, $9.19x10^{-5}$ mol). was dissolved in anhydrous dichloromethane (15 mL), under argon and cooled to 0ºC. BCl_3 (1 mL) was added dropwise and the reaction mixture was kept overnight with stirring at room temperature. Methanol (50 mL) was added and the mixture was stirred for 1 h. The solvent was removed under reduced pressure to afford the crude product. Recrystallization of the crude product from methanol/ diethylether (1:9) afforded one first solid that was rejected after NMR analysis and the organic phase was then concentrated. A second recrystallization was performed, yielding the hydrochloride salt **MRB20** (0.0343 g, 56%) as a purple solid (Figure 2.8).

Elemental analysis for ($C_{36}H_{42}N_4O_4^{2+}.2Cl^-.2HCl.0.5CH_2Cl_2.0.5H_2O$): Calculated (found): C 55.49 (55.71); H 5.87 (5.61); N 7.09 (7.36). MS: calculated for $C_{36}H_{41}N_4O_4^+$: 593.31 [M^+]; found: ESI - MS: 593.31 [M^+]; 297.15820 [$M^+/2$]. 400.15 MHz ^{1}H NMR (MeOD-d_4, ppm): δ 1.32 (t, *J* 7.2 Hz, 12H, $NCH_2C\underline{H}_3$); 2.64 (s, 3H, 6''-$C\underline{H}_3$); 3.70 (m, 8H, $NC\underline{H}_2CH_3$); 4.09 (s, 3H, NCH_3); 5.02 (s, 2H, $C\underline{H}_2NH$); 7.01 (d, *J* 2.5 Hz, 2H, H4+ H5 and s, 1H, H-5''); 7.08-7.11 (dd, *J* 2.5; 10.8 Hz, 2H, H2+H7); 7.31-7.34 (d, *J* 10.8 Hz, 2H, H1+H8); 7.61 (d, *J* 8.4 Hz, 2H, H2' + H6'); 8.16 (d, *J* 8.3 Hz, 1H, H3' + H5'); 100.62 MHz ^{13}C NMR (MeOD-d_4, ppm): δ 12.8 ($NCH_2\underline{C}H_3$); 21.2 (6''-$\underline{C}H_3$); 37.2 ($\underline{C}H_2NH$); 39.4 ($N\underline{C}H_3$); 46.9 ($N\underline{C}H_2CH_3$); 97.5 (C5"); 114.2 (C4 + C5); 114.3 (C2+ C7); 129.2 (C3' + C5'); 131.1 (C2' + C6'); 132.8 (C1 + C8); 136.2 (C6); 137.3 (C3); 139.4 (C2"); 145.6 (C3"); 150.4 (C2");157.3 (C1a + C8a); 159.5 (C4a + C5a); 169.7 (HNCO).

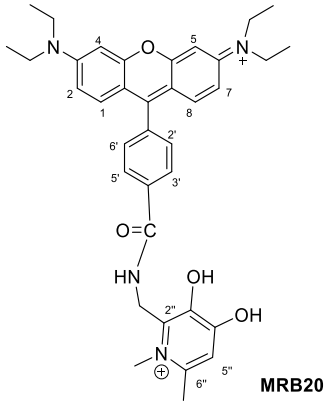

MRB20

Figure 2.8 – Formulae and numbering of compound **MRB20**.

*Compound **MRH10p***

To a solution of tetramethylrhodamine isothiocyanate (**F10**) (0.0319 g, $7.19x10^{-5}$ mol) in anhydrous DMF (0.5 mL) and triethylamine (0.01 mL) was added the protected 3,4-HPO hexadentate ligand (0.0622g, $5.99x10^{-5}$ mol) and the mixture was stirred at room temperature in the dark and under argon atmosphere, for 48 hours. The product was purified by gradient flash column chromatography, eluting with chloroform/methanol (7:3) and increasing polarity until chloroform/methanol (4:6) and ammonia. The sample was then purified by TLC eluting with acetonitrile/water/ammonia (3:2:0.05) to afford **MRH10p** (0.0430 g; 48%) as a purple solid. Only 5'-isomer was obtained as determined through NMR spectra analysis (Figure 2.9).

^{1}H NMR (400.15 MHz, MeOD-d_4, ppm): δ 1.87 (m, 6H, CC$\underline{H}_2$CH$_2$); 2.08 (m, 6H, CCH$_2$C$\underline{H}_2$); 2.33 (s, 9H, 6''-CH$_3$); 2.45 (t, *J* 6,2 Hz, 2H, NCH$_2$C$\underline{H}_2$CO); 3.19 (s, 12H, C$\underline{H}_3$-rhodamine); 3.49 (s, 9H, NCH$_3$); 3.76 (bs, 2H, NC$\underline{H}_2$CH$_2$CO); 4.45 (s, 6H, C$\underline{H}_2$NH); 5.07 (s, 6H, C$\underline{H}_2$C$_6$H$_5$); 6.40 (s, 3H, H-5''); 6.77 (bs, 2H, H4, H5); 6.88-6.90 (d, *J* 9.6 Hz, 2H, H2, H7); 7.23-7.44 (m, 15H, - CH$_2$C$_6$$\underline{H}_5$ and 2H, H1, H8); 7.71 (bs, 2H, H4', H6'); 8.07 (d, *J* 9.5 Hz,1H, H3'). ^{13}C NMR (100.62 MHz, MeOD-d_4, ppm): δ 20.9 (6''-CH$_3$); 30.9 (CCH$_2$$\underline{C}H_2$); 31.3 (C$\underline{C}H_2CH_2$); 36.3 ($\underline{C}H_2$NH); 37.4 (NCH$_3$); 40.9 (CH$_3$-rhodamine); 74.8 ($\underline{C}H_2C_6H_5$); 97.2 (C4, C5); 114.7 (C1, C8); 115.0 (C2, C7); 119.4 (C5''); 124.0 (C4', 6'); 129.4 – 130.1 (C- CH$_2$$\underline{C}$$_6H_5$); 132.5 (C3'); 138.4 ($\underline{C}$q-C$_6H_5$); 143.3 (C2''); 147.4 (C3''); 150.9 (C6''); 158.4 (C4"); 158.8 (C4a, C5a); 160.8 (C1a, C8a); 175.3 ($\underline{C}$ONHCH$_2$).

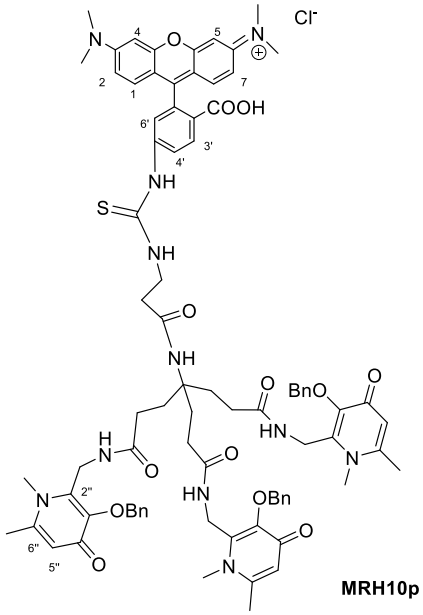

Figure 2.9 – Formulae and numbering of compound **MRH10p**.

*Compound **MRH10***

Compound **MRH10p** (0.0400g, $2.67x10^{-5}$ mol). was dissolved in anhydrous dichloromethane (20 mL), under argon and cooled to 0ºC. BCl_3 (1 mL) was added dropwise and the reaction mixture was kept overnight with stirring at room temperature. Methanol (50 mL) was added and the mixture was stirred for 1 h. The solvent was removed under reduced pressure to afford the crude product. Recrystallization of the crude product from methanol/acetone (1:9) afforded the hydrochloride salt **MRH10** (0.0224g, 61%) as a purple solid (Figure 2.10).

Elemental analysis for ($C_{62}H_{77}N_{11}O_{13}S^{4+}.4Cl^{-}.11HCl.6H_2O$): Calculated (found): C 39.88 (39.71); H 5.40 (5.10); N 8.25 (8.21). MS: calculated for $C_{62}H_{74}N_{11}O_{13}S^{+}.K^{+}$: 1251.48 [$M^{+}.K^{+}$]; found: matrix-assisted laser desorption/ionization time of flight MS: 1251.40 [$M^{+}.K^{+}$]. ^{1}H NMR (400.15 MHz, MeOD-d_4, ppm): δ 1.95 (m, 6H, CC<u>H</u>$_2$CH$_2$); 2.22 (m, 6H, CCH$_2$C<u>H</u>$_2$); 2.63 (s, 9H, 6''-CH$_3$); 3.02 (m, 2H, NCH$_2$C<u>H</u>$_2$CO); 3.31 (s, 12H, CH$_3$-rhodamine); 3.97 (s, 9H, NCH$_3$); 4.52 m, 2H, NC<u>H</u>$_2$CH$_2$CO); 4.65 (s, 6H, C<u>H</u>$_2$NH); 7.01 (s, 3H, H5''); 6.86-7.38 (m, 6H, H1, H2, H4, H5, H7, H8); 7.64-8.49 (m, 3H, H3'- H6'). ^{13}C NMR (100.62 MHz, MeOD-d_4, ppm): δ 21.3 (2''-CH$_3$); 30.6 (CCH$_2$<u>C</u>H$_2$); 31.0 (<u>C</u>CH$_2$CH$_2$); 35.7 (NCH$_2$<u>C</u>H$_2$CO); 36.3 (<u>C</u>H$_2$NH); 40.0 (N<u>C</u>H$_3$); 41.1 (CH$_3$-rhodamine); 44.5 (N<u>C</u>H$_2$CH$_2$CO); 97.5 (C4, C5); 114.2 (C5"); 117.9, 123.8, 124.2, 129.2, 132.0 (C1 – C8); 132.5, 133.5, 134.8 (C3'- C6'); 140.8 (C2''); 144.8 (C3'');150.9 (C4''); 159.0 (C4a, C5a); 161.2 (C6"); 176.3 (CH$_2$<u>C</u>ONHCH$_2$).

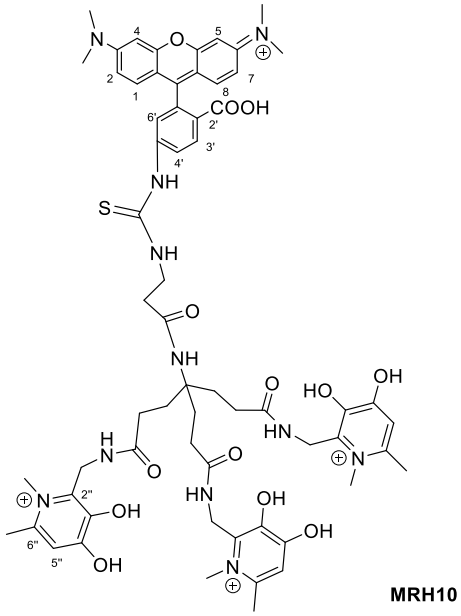

Figure 2.10 – Formulae and numbering of compound **MRH10**.

*Compound **MRB9p***

To a solution of 5(6)-carboxytetraethyl-rhodamine (**F9**) (168.6 mg, 3.46×10^{-4} mol) in anhydrous DMF (10 mL), protected 3,4-HPO bidentate ligand (2-aminomethyl-3-benzyloxy-1,6-dimethyl-1*H*-pyridin-4-one) (73.3 mg; 2.84×10^{-4} mol), DCC (73.0 mg, 3.50×10^{-4} mol) and *N*-hydroxysuccinimide (NHS) (47.7 mg, 40.2×10^{-4} mol) were added and the mixture was stirred at room temperature in the dark and under an argon atmosphere, for 2 days. Subsequently, the formed (DCU) precipitate was filtered off and the solvent removed under reduced pressure. The product was purified by gradient flash column chromatography, eluting with chloroform/methanol (8:2) to afford **MRB9p** (52.5 mg; 25%) as a purple solid. Compound **MRB9p** was obtained as a 1.1:1 ratio mixture of 4'- and 5'- isomers as determined through NMR spectra analysis (Figure 2.11).

^{1}H NMR (400.15 MHz, MeOD-d_4, ppm): δ 1.28 (t, *J* 6.9, 24H, $CH_2C\underline{H}_3$-rhodamine); 2.39 (s, 3H, 6''-CH_3, 5'-isomer); 2.45 (s, 3H, 6''-CH_3, 4'-isomer); 3.65 (m, 3H, NCH_3, 5' isomer + 16H, $C\underline{H}_2CH_3$-rhodamine); 3.72 (s, 3H, NCH_3, 4'-isomer); 4.66 (s, 2H, $C\underline{H}_2NH$, 5'-isomer); 4.74 (s, 2H, $C\underline{H}_2NH$, 4'-isomer); 5.15 (s, 2H, $C\underline{H}_2C_6H_5$, 5'-isomer); 5.23 (s, 2H, $C\underline{H}_2C_6H_5$, 4'-isomer); 6.45 (s, 1H, H5'', 5'-isomer); 6.51 (s, 1H, H5'', 4'-isomer); 6.90 (d, *J* 2.5 Hz, 4H, H4 + H5); 6.99 (br s, 4H, H2 + H7); 7.21-7.40 (m, 10H, H1 + H8; H6', 4'-isomer; *m-, p*- C_6H_5 ; *o*- C_6H_5, 5'-isomer); 7.46-7.48 (m, 1H, *o*- C_6H_5, 4'-isomer); 7.64 (d, *J* 1.7, 1H, H6', 5'-isomer); 7.99 (dd, *J* 1.7; 8.1, 1H, H5', 4'-isomer); 8.03 (dd, *J* 1.7; 8.1, 1H, H4', 5'-isomer); 8.10 (br d, *J* 8.1, 1H, H3', 5'-isomer); 8.43 (d, *J* 1.7, 1H, H3', 4'-isomer); ^{13}C NMR (100.62 MHz, MeOD-d_4, ppm): δ 12.8 ($CH_2\underline{C}H_3$-rhodamine); 20.8 (2''-CH_3, 5'-isomer); 20.9 (6''-CH_3, 4'-isomer); 37.1 (CH_2NH, 5'-isomer); 37.2 (CH_2NH, 4'-isomer); 37.4 (NCH_3, 5'-isomer); 37.5 (NCH_3, 4'-isomer); 46.7 ($\underline{C}H_2CH_3$-rhodamine); 74.7 ($\underline{C}H_2C_6H_5$, 5'-isomer); 74.9 ($\underline{C}H_2C_6H_5$, 4'-isomer); 97.1 (C4 + C5); 114.8 (CH); 114.9 (C2 + C7); 119.2 (C5''); 129.4 (CH); 129.5 (C6', 5'-isomer); 129.6 (C5', 4'-isomer); 129.7 (CH); 129.8 (C4', 5'-isomer); 130.0 (CH *o*-C_6H_5); 130.2 (C3', 4´-isomer); 131.0 (C3', 5'-isomer); 132.9 (C1 + C8, 5'-isomer, 4'-isomer); 133.1 (CH); 133.7 (C_q, 5'-isomer); 135.6 (C_q); 136.4 (C_q); 136.8 (C4', 4'-isomer); 138.4 (C_q C_6H_5, 5'-isomer); 138.5 (C_q C_6H_5, 4'-isomer); 142.3 (C_q); 143.1 (C2'' 5'-isomer); 143.3 (C2'' 4'-isomer); 145.0 (C5', 5'-isomer); 147.6 (C5'', 5'-isomer); 147.7 (C3'', 4'-isomer); 151.0 (C2'', 5'-isomer); 151.1 (C6'', 4'-isomer); 156.9 (C9); 159.3 (C4a, 4'-isomer); 159.4 (C4a, 5'-isomer); 162.0 (C1', 5'-isomer); 162.2 (C1', 4'-isomer); 168.6 (CONH, 5'-isomer); 169.1 (CONH, 4'-isomer); 172.3 (2'-CO_2H, 5'-isomer); 172.5 (2'- CO_2H, 4'-isomer);175.0 (C4'', 5'-isomer); 175.1 (C4'', 4'-isomer).

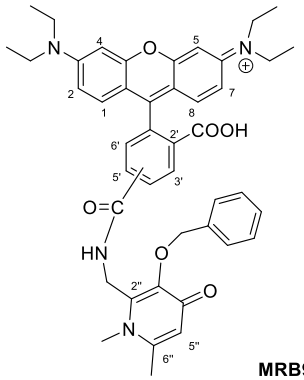

MRB9p

Figure 2.11 – Formulae and numbering of compound **MRB9p**.

*Compound **MRB9***

Compound **MRB9p** (37.7 mg, 5.50×10^{-4} mol) was dissolved in anhydrous dichloromethane (8 mL), under argon and cooled to 0ºC. BCl_3 (0.8 mL) was added dropwise and the reaction mixture was kept overnight with stirring at room temperature. Methanol (30 mL) was added and the mixture was stirred for 1 h. The solvent was removed under reduced pressure to afford the crude product. Recrystallization of the crude product from methanol/acetone (4:6) afforded the hydrochloride salt **MRB9** (37.1 mg, 82%) as a purple solid (Figure 2.12).
Elemental analysis for ($C_{38}H_{46}N_4O_6^{2+}.2Cl^-.CHCl_3$): Calculated (found): C 55.43 (55.03); H 5.61 (5.07); N 6.63 (6.52). MS: calculated for $C_{38}H_{45}N_4O_6^+$: 653.33 [M^+]; found: ESI - MS: 653.2952 [M^+]. ^{1}H NMR (400.15 MHz, MeOD-d_4, ppm): δ 1.31 (t, *J* 6.7, 24 H, $CH_2C\underline{H}_3$-rhodamine); 2.63 (s, 3H, 6'' -CH_3, 5'-isomer); 2.68 (s, 3H, 6'' -CH_3, 4'-isomer); 3.68 (q, *J* 6.7, 16H, $C\underline{H}_2CH_3$-rhodamine); 4.08 (s, 3H, NCH_3, 5'-isomer); 4.15 (s, 3H, NCH_3, 4'-isomer); 4.97 (s, 2H, CH_2NH, 5'-isomer); 5.06 (s, 2H, CH_2NH, 4'-isomer); 7.02-7.11 (m, 14H, H5'', 5'-isomer, 4'-isomer + H1, H2, H4, H5, H7, H8); 7.55 (d, *J* 5.7 Hz, 1H, H6', 4'-isomer); 7.88 (br s, 1H, H6', 5'-isomer); 8.27 (br s, 1H, H4', 5'-isomer); 8.33 (br s, 1H, H5', 4'-isomer); 8.41 (br s, 1H, H3', 5'-isomer); 8.82 (s, 1H, H3', 4'-isomer).^{13}C NMR (100.62 MHz, MeOD-d_4, ppm): δ 12.8 ($CH_2\underline{C}H_3$-rhodamine); 21.3 (6''-CH_3); 37.2 (CH_2NH, 5'-isomer); 37.3 (CH_2NH, 4'-isomer); 40.0 (NCH_3); 46.9 ($\underline{C}H_2CH_3$-rhodamine); 97.3 (C5''); 114.2 (C4); 114.6 (C5); 114.7 (C2); 115.5 (C7); 130.4 (C4', 5'-isomer); 130.6 (C6', 5'-isomer); 131.6 (C3', 4'-isomer); 132.1(C1); 132.2 (C6', 4'-isomer); 132.4 (C8); 132.6 (C5', 4'-isomer); 132.9 (C3', 5'-isomer); 135.3 (C2', 5'-isomer); 135.6 (C5', 5'-isomer); 136.4 (C2', 4-isomer); 138.2 (C1', 5'-isomer); 138.6 (C1', 4'-isomer); 140.6 (C2'' 5'-isomer); 140.8 (C2'', 4'-isomer); 145.2 (C3''); 150.7 (C6''); 157.2 (C3+C6); 159.3 (C9); 159.6 (C_q); 159.7 (C_q); 161.3 (C4a + C5a); 167.3 (2'- CO_2H); 168.6 (C_q); 168.8 (CONH).

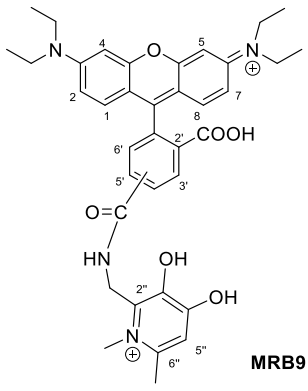

MRB9

Figure 2.12 – Formulae and numbering of compound **MRB9**.

2.2.3 Electronic spectroscopy: absorption and fluorescence properties

Electronic absorption measurements were performed using the conditions T= 25ºC, l=1cm cuvettes and wavelength range 225-700 nm.

Fluorescence measurements were performed using the conditions T= 25ºC, l=1cm cuvettes. Spectra were recorded at: a) λ_{exc} = 568 nm, λ_{em} from 570-700 nm, 600 V, 5 nm slits, for ligand **MRB2**; b) λ_{exc} = 290 nm, λ_{em} from 300-550 nm, 600 V, 10 nm slits for ligand **MRB4**. c) λ_{exc}=562 nm and λ_{em} from 566 to 700 nm, 650 V, 5 nm slits, for **MRB20**; d) λ_{exc}=553 nm and λ_{em} from 560 to 700 nm, 650 V, 5 nm slits, for **MRH10**; e) λ_{exc}=560 nm and λ_{em} from 561 to 700 nm, 650 V, 5 nm slits, for **MRB9.**

Stock solutions of the different compounds were obtained by preparing a concentrated solution of the compound in DMSO. Samples for absorption and fluorescence measurements were prepared by dilution of a known volume of the DMSO stock solution in 3-(*N*-morpholino)propanesulfonic acid (MOPS) buffer solution (pH 7.4, I=0.1 M NaCl). The percentage of the DMSO stock solution was always less than 1% in the final volume.

2.2.4 Single-crystal X-ray diffraction

Crystalline material of the compounds **1**, **MRB2**, **3** and **MRB4**, were manually harvested and an appropriate crystal of each compound mounted on cryoloops using appropriate inert oil [279]. Diffraction data were collected at 180.0(2)K on a Bruker X8 Kappa APEX II Charge-Coupled Device (CCD) area-detector diffractometer controlled by the APEX2 software package [280] (MoK_α graphite-monochromated radiation, λ = 0.71073Å), and equipped with an Oxford Cryosystems Series 700 cryostream monitored remotely with the software interface Cryopad [281]. Images were processed with the software SAINT+,[282] and absorption effects corrected with the multi-scan method implemented in SADABS.[283] The structures were solved by direct or Patterson methods employed in SHELXS-97 [284, 285] allowing the immediate location of the Sulphur atoms. Remaining non-H-atoms of the compounds were located from difference Fourier maps calculated by successive full-matrix least-squares refinement cycles on F^2 using SHELXL-97 [285, 286] and have been successfully refined with anisotropic displacement parameters.

Hydrogens attached to Carbon atoms of were placed at their geometrical positions using appropriate *HFIX* instructions in SHELXL and incorporated in subsequent refinement cycles in riding-motion approximation with isotropic thermal displacements parameters (U_{iso}) fixed at 1.2 or 1.5 × U_{eq} of the parent atom. Furthermore, the Hydrogen atoms of the hydroxyl, sulfonamide and water molecules (in **MRB2**) were clearly visible in the difference Fourier

maps, and included in subsequent refinement stages with the distances adequately restrained. In the structure of **1,** a considerable some electron density, mainly due to disordered solvent molecules, was not possible to modulate and refine properly. Searches for the total potential solvent area using the software package *PLATON* [287, 288] revealed the existence of cavities with a potential solvent accessible voids. The original data sets were then treated with the *SQUEEZE* [289] routine to remove the contribution of these disordered molecules in the solvent-accessible volume, and the calculated solvent-free reflection list was consequently used for the final structure refinement.
The crystallographic characterization was performed by a member of our research group (Luís Cunha-Silva).

Table 2.1 - Crystal and structure data for compounds **1**, **MRB2**, **3** and **MRB4**.

	1	**MRB2**	**3**	**MRB4**
Formula	$C_{42}H_{46}N_4O_8S_2$	$C_{35}H_{51}N_4O_{13}S_2$	$C_{26}H_{25}N_3O_2S$	$C_{19}H_{19}N_3O_2S$
Mr	798.95	835.36	443.55	353.43
Crystal morphology	pink prism	pink prism	Colourless plate	Colourless needle
Crystal size /mm	0.35 × 0.21 × 0.15	0.16 × 0.11 × 0.04	0.22 × 0.06 × 0.01	0.20 × 0.03 × 0.02
Crystal system	Triclinic	Triclinic	Monoclinic	Triclinic
Space group	*P*-1	*P*-1	$P2_1/n$	*P*-1

2.3 Results and Discussion

2.3.1 Synthesis

The new fluorescent ligands **MRB2**, **MRB4**, **MRB20**, **MRH10** and **MRB9** were prepared using straightforward synthetic protocols [3, 4, 22] involving the coupling of the fluorophores, sulphorhodamine B acid chloride (**F2**), 1-naphthyl isothiocyanate (**F4**), carboxyrosamine (**F20**), tetramethylrhodamine isothiocyanate (**F10**) and 5(6)-carboxytetraethylrhodamine (**F9**), respectively, to the protected 3,4-HPO chelating units.
The last step is the deprotection reaction for the removal of the protecting group with under BCl_3.

To prepare the protected compounds **1** or **3**, the protected 3,4-HPO bidentate ligands were added to the fluorophores (sulphorhodamine B acid chloride or 1-naphthyl isothiocyanate) and the reactions were performed in the presence of anhydrous DMF (and triethylamine (Et_3N) for ligand **3**). The deproteced fluorescent 3,4-HPO ligands, **MRB2** and **MRB4,** were obtained by deprotection with BCl_3 (Figure 2.13 and 2.14).

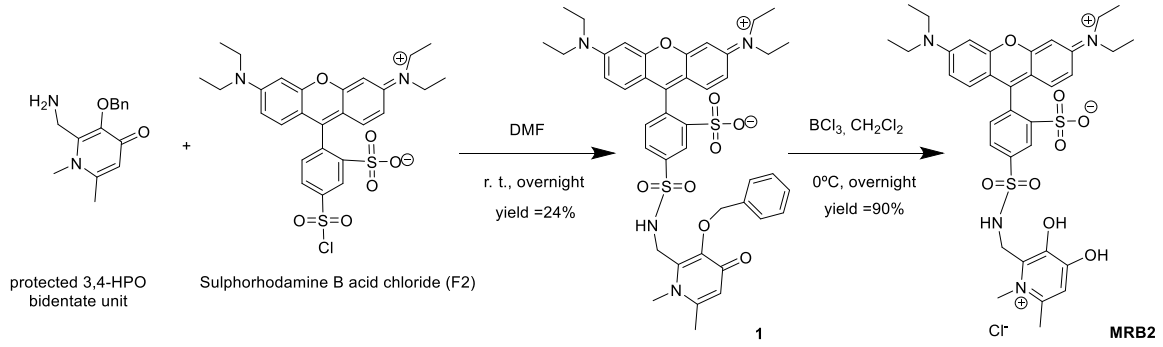

Figure 2.13 –Reaction scheme of the synthetic route for the preparation of compound **MRB2**.

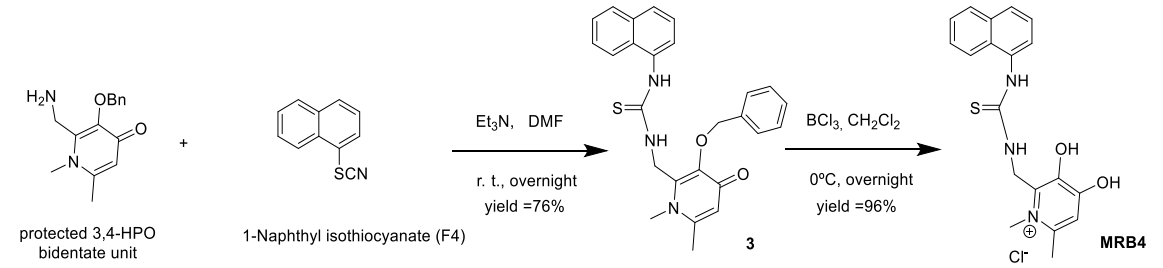

Figure 2.14 –Reaction scheme of the synthetic route for the preparation of compound **MRB4**.

MRB20p was obtained by reaction of carboxyrosamine (**F20**) in the presence of anhydrous DMF, DCC and NHS in order to generate the activated ester form of the rhodamine derivate. The protected compound was subsequently deprotected with BCl_3 to yield the carboxyrosamine - labelled bidentate 3,4-HPO (**MRB20**), as summarized in Figure 2.15.

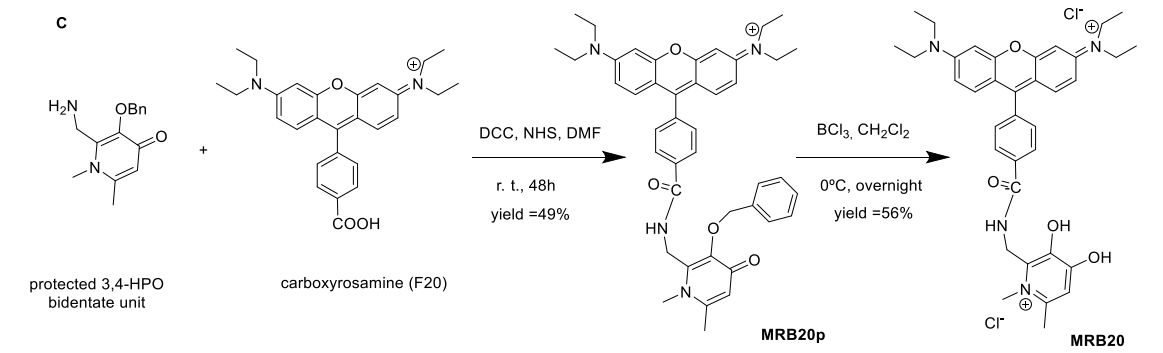

Figure 2.15 –Reaction scheme of the synthetic route for the preparation of compound **MRB20**.

For the synthesis of **MRH10p**, the 3,4-HPO hexadentate unit was coupled to tetramethylrhodamine isothiocyanate (**F10**) in the presence of anhydrous DMF and Et_3N to produce the protected ligand, followed by deprotection with BCl_3 to yield the **MRH10**.

MRB9p was obtained by reaction of 3,4-HPO bidentate unit with 5(6)-carboxytetraethylrhodamine (**F9**) in the presence of anhydrous DMF, DCC and NHS in order to generate the activated ester form of the rhodamine derivate. The protected compound was subsequently deprotected with BCl_3 to yield the rhodamine **MRB9**. The 3,4-HPO units and fluorophores used to obtain **MRH10** and **MRB9** ligands synthesized in this work and the synthetic procedures are outlined in Figures 2.16 and 2.17.

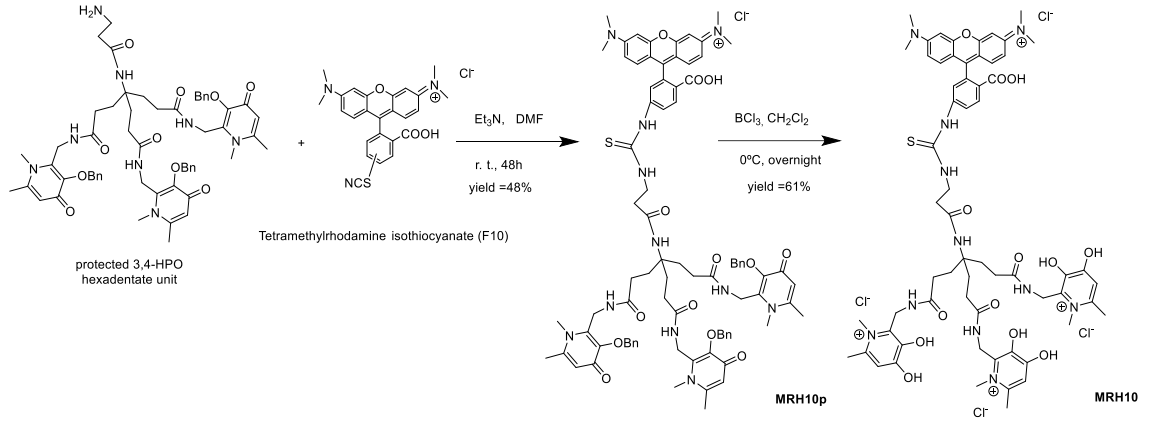

Figure 2.16 –Reaction scheme of the synthetic route for the preparation of compound **MRH10**.

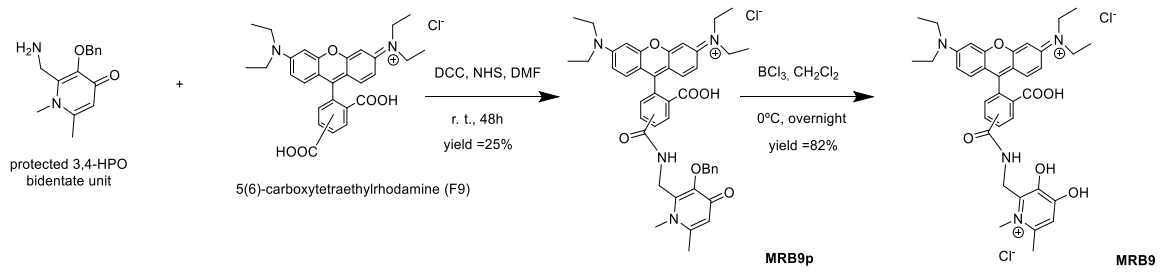

Figure 2.17 –Reaction scheme of the synthetic route for the preparation of compound **MRB9**.

Although the synthetic procedures are very similar to those described in previous work [4], differences in the yield of the reactions (see Figures 2.13 - 2.17) were verified. These differences may be related with the different functional groups of the fluorophores that react with the amine group pf the protected 3,4-HPO units. The HLB of the protected ligands obtained may also influences the purification process and contribute the yield of the reaction.

The comparison of the results obtained for the coupling reactions to synthesize the protected ligands shows that ligand **1** was obtained in the lowest yield probably due to the lower stability of the functional group of sulphorhodamine B acid chloride that should react with the amine group of the protected 3,4-HPO bidentate ligand.

In the reaction of 1-naphthyl isothiocyanate with the same bidentate unit, we obtained ligand **3** in 76 % yield. This value is significantly higher than those obtained for naphthalene derived 3,4-HPO [170] and higher than the yield obtained in the synthesis of previously prepared compounds **MRB7** and **MRB8** [4].

Considering ligand **MRB20p**, the yield of this reaction is higher than those described previously for similar reactions [4] and for the value obtained for the reaction performed to produce **MRB9p.** This fact could be related with the inexistence of the possibility of formation of positional isomers leading only to the reaction in the position 4' of the phenyl ring of the rosamine. This is a plausible since the rosamine has the functional group only in this position of the ring.

The yield of the reactions to produce **MRH10p** and **MRB9p** is of the same order of magnitude of that obtained for similar reactions [4]. The reaction for the synthesis of **MRH10p** has revealed isomer selectivity, since only the 5'-isomer was obtained.

Despite the fact that the methodologies for the synthesis of **MRH10p** and for ligand **3** are similar, the yields of reaction obtained are significantly different. This fact may be due to the requirement of additional processes of purification to the usual flash chromatography, such as the TLC purification, necessary to purify **MRH10p**.

In the deprotection reactions, no major differences are observed and ligands **MRB2**, **MRB4** and **MRB9** were successfully synthesized and the yield of reactions are respectively 90, 96 and 96%. In the deprotection reaction to obtain the ligands **MRB20** and **MRH10**, both chelators were successfully synthesized although the yield of these reactions is slightly lower, 56 and 61%, respectively, than those described for the other ligands synthesized in this work or in studies [4]. The lower yield in the case of **MRB20** may be justified by the requirement of a second recrystallization process to obtain the pure deprotected ligand.

Based on previous results [4], and as it will be discussed later in Chapter 3, we expect to get insight on the structure activity relationships (SAR) of the rhodamine labelled chelators, as they are the ligands with higher antimycobacterial activity. In particular, we aim to be able understand the importance of the hydro-lipophilic balance of the ligand and the type of linker between the fluorophore and the chelating unit, for the biological effect.

As the amount of hexadentate chelator to reach similar effect is three times lower than measured for bidentate chelators, in the synthesis of **MRB9,** we first tried to synthesize the chelator by functionalization of the protected hexadentate unit with the desired rhodamine. Unfortunately, the reaction of 5(6)-carboxytetraethyl-rhodamine (**F9**) with the hexadentate unit have shown several problems in the synthesis and purification processes and we couldn't obtain the expected ligand. When we tried the reaction of the same **F9** with the bidentate unit, **MRB9** was successfully obtained.
As described in our previous results [4], and taking into consideration the denticity of the chelators, we tested the bidentate chelator **MRB9** using threefold concentrations relative to those of hexadentate chelators (**MRH7** and **MRH10**) in order to allow chelation of an equal amount of iron. According to this fact , we expect, as reported previously [4], to be able to compare the new chelators with each other, in terms of their antimycobacterial effect.

The synthesis of **MRB9** was performed in collaboration with a member of our laboratorial team (Daniel Silva) and is reported in this work, as the chelator was tested against *M. avium* (and other bacterial species) in comparison to the other ligands prepared.

2.3.2 NMR spectroscopy

The structures of the protected and deprotected ligands in solution were established by NMR analysis (^{1}H and ^{13}C, 1D and 2D experiments, including COSY, HSQC and HMBC spectra for unequivocal assignment of the most characteristic proton and carbon chemical shifts). The assignment of the resonance signals in ^{13}C NMR spectra of the protected and de-protected compounds was achieved by analysis of $^{1}H/^{13}C$ HSQC and $^{1}H/^{13}C$ HMBC spectra, which provide one and multiple bond ^{1}H-^{13}C connectivity. The formulae and numbering of the chelators are depicted in Figures 2.3 - 2.12.

The ^{1}H and ^{13}C NMR spectra of ligand **1** revealed that the resonance signals of the methyl and methylene protons of the rhodamine residue appear at 1.31 and 3.69 ppm and those of H1 - H8 protons in the spectra are between 6.94 and 7.08 ppm. The protons of the methyl group of the pyridinone ring appear at 2.42 ppm and the protons of the methyl linked to the nitrogen of the ring appear at 3.76 ppm. The signal at 4.24 ppm is attributed to the $C\underline{H}_2NH$ protons and shows HMBC correlation with a carbon at 142.0 ppm assigned as C2''and C3'' that appears at 147.4 ppm. The protons of di-substituted aromatic ring of rhodamine, H3', H5' and H6', appear respectively at 8.58, 8.02 and 7.35-7.38 ppm.
The signals related with the protecting group are the singlet at 5.12 ppm that corresponds to the $-C\underline{H}_2C_6H_5$ protons and the protons of the ring ($-CH_2C_6\underline{H}_5$) in the protecting group

appearing between 7.25-7.38 ppm. The carbon -$\underline{C}H_2C_6H_5$ is at 74.6 ppm, the quaternary carbon appears at 138.2 ppm and the other carbons (-$CH_2\underline{C}_6H_5$) of the protecting group appear between 129.6 - 133.5 ppm.

After the deprotection (ligand **MRB2**), significant differences in the ^1H and ^{13}C spectra are detected as for example the shift of the protons of methyl group linked to the nitrogen of the pyridinone from 3.76 to 4.13 ppm as also the shift in the protons of the ethyl group of the linkage ($C\underline{H}_2NH$) from 4.24 to 4.66 ppm. Their respective carbons are also dislocated, namely $N\underline{C}H_3$ from 37.3 in the protected ligand to 39.3 in the deprotected form and the shift from 39.5 to 38.2 ppm for the carbon of the linkage ($C\underline{H}_2NH$).

In the ^1H and ^{13}C NMR spectra of ligand **3**, the characteristic protons of methyl groups of pyridinone ring (6'-CH_3 and NCH_3) appear, respectively, at 2.25 and 3.66 ppm. The signal at 4.90 is attributed to $C\underline{H}_2NH$ group of the linkage between the 3,4-HPO and the naphthalene.

Signals related with the protecting group are the singlet at 4.99 ppm that corresponds to the protons -$C\underline{H}_2C_6H_5$ and the other protons (-$CH_2C_6\underline{H}_5$) of the protecting group appear between 7.16-7.26 ppm. The carbon -$\underline{C}H_2C_6H_5$ appears at 74.2 ppm, the quaternary carbon at 137.8 ppm and the other carbons (-$CH_2\underline{C}_6H_5$) appear at 129.0 and 129.3 ppm. The carbons of the naphthalene ring appear between 123.3 and 129.5 ppm and the quaternary carbons, C8a and C4a, appear at 130.8 and 135.4 ppm, respectively. The signal at 183.5 ppm is attributed to the carbon of S$\underline{C}$N group and it shows long range couplings in HMBC with the $C\underline{H}_2NH$ protons of the linkage, appearing at 4.90 ppm in the ^1H spectrum. The protons $C\underline{H}_2NH$ are also correlated with carbons C6' and C5' (141.7 and 147.6 ppm).

The deprotection reaction was successfully achieved as confirmed by the changes of the chemical shift of characteristics protons and carbons of the ligand **MRB4**. In the ^1H spectrum of ligand **MRB4**, the characteristic protons of methyl groups of pyridinone ring (6'-CH_3 and NCH_3) appear, respectively, at 2.58 and 4.00 ppm. The resonance signals attributed to $C\underline{H}_2NH$ protons of the linkage between the 3,4-HPO and the naphthalene are shifted to the low field region at 5.16 ppm. The carbons of the pyridinone ring that were most directly affected by de deprotection, C3', C4' and C5', are also shifted from 119.8, 173.9 and 147.6 to 113.3, 160.6 and 144.4 ppm, respectively.

The ^1H and ^{13}C NMR spectra of protected ligand **MRB20p** revealed that the resonance signals of the methyl and methylene protons of the rhodamine moiety appear at 1.31 and 3.69 ppm. The H4/H5, H2/H7 and H1/H8 protons of rhodamine framework appear at 6.99,

7.08 and 7.46 ppm, respectively. The protons of the substituted aromatic ring, H2'/H6' and H3'/H5'appear in low field region, respectively, at 7.58 and 8.08 ppm.

The protons of the methyl group of the pyridinone ring appear at 2.45 ppm and the protons of the methyl linked to the nitrogen of the ring appear at 3.72 ppm. The signal at 4.73 ppm is attributed to the C$\underline{H}_2$NH protons and shows HSQC correlation with carbons assigned as $\underline{C}H_2$NH (37.22 ppm). This signal has also HMBC correlation with carbons at 143.2, 147.7, 169.0 ppm, assigned respectively as C2'', C3'' and HNCO.

The signals related with the protecting groups are the singlet at 5.22 ppm that corresponds to the -C$\underline{H}_2C_6H_5$ protons and the -$CH_2C_6\underline{H}_5$ protons of the protecting group appear between 7.27-7.36 ppm. The carbon -$\underline{C}H_2C_6H_5$ is at 74.8 ppm, the quaternary carbon appears at 138.5 ppm and the other carbons of the protecting group (-$CH_2\underline{C}_6H_5$) appear at 129.4, 129.5 and 132.8 ppm.

Signals at 143.2 and 147.7 ppm were attributed as carbons C2'' and C3'' due to their HMBC correlations with H3'', C$\underline{H}_2$NH, NC$\underline{H}_3$ and with H5'', C$\underline{H}_2$NH, C$\underline{H}_2C_6H_5$, respectively. The carbon at 151.1 ppm shows HMBC correlation with H5'', NC$\underline{H}_3$ and 6''-C$\underline{H}_3$ protons and was attributed to C6''. The carbon that appears at higher value of chemical shift (175.0 ppm) was attributed to C4''and shows HMBC correlation with H5'' proton.

The carbon of the carbonyl group (HNCO) of the linkage between the rhodamine and pyridinone appears at 169.0 ppm and was attributed based on their HMBC connectivity with C$\underline{H}_2$NH, H2'/H6' and H3'/H5' protons of the substituted aromatic ring.

After the deprotection (**MRB20**), significant differences in the ^{1}H and ^{13}C spectra are detected as for example the shift of the protons of the methyl group of the pyridinone ring from 2.45 to 2.64 ppm and also the protons of methyl group linked to the nitrogen of the pyridinone from 3.72 to 4.09 ppm. There was verified a shift in the C$\underline{H}_2$NH protons of the linkage from 4.84 to 5.02 ppm. Their respective carbons are also dislocated, namely N$\underline{C}H_3$ from 37.5 ppm in the protected ligand and 39.4 ppm in the deprotected form and the shift from 119.2 to 97.5 ppm for the C5''.

The carbon at 139.4 ppm shows HMBC correlation with C$\underline{H}_2$NH and 6''-C$\underline{H}_3$ protons and was attributed to C2''. The carbon at 145.6 ppm shows HMBC correlation with H3''and C$\underline{H}_2$NH protons and was attributed to C3''. Signal at 150.4 ppm was attributed as carbon C6'' due to their HMBC correlations with H5'', NC$\underline{H}_3$ and 6''C$\underline{H}_3$.

The resonance signal at 169.7 ppm was found to give long range coupling to C$\underline{H}_2$NH protons and was attributed to carbonyl carbon of the amide group in the linkage between the rhodamine and the pyridinone (HNCO).

The NMR spectra of ligand **MRH10p** revealed that the resonance signals of the methyl protons of the rhodamine residue appear at 3.19 ppm and those of H1 - H8 protons in the spectral are between 6.77 and 7.44 ppm. The two multiplets at high field (1.87-2.08 ppm) were assigned to -C(CH_2CH_2)$_3$ protons. The resonance signals of NCH_2CH_2CO protons appear as triplets or broad singlets at 2.45 and 3.76 ppm. The protons of the methyl group of the pyridinone ring appear at 2.33 ppm and the protons of the methyl linked to the nitrogen of the ring appear at 3.49 ppm. The resonance signal at 6.40 ppm was assigned to proton H5'' of the pyridinone residue and shows HMBC correlation with a carbon at 20.9 ppm assigned as 6''-$\underline{C}H_3$. The set observed in the low field spectral region (7.7-8.1 ppm) was assigned to the protons of di-substituted aromatic ring of rhodamine framework. Due to the characteristic chemical shift of carbon C3', the reaction was isomeric selective and only 5' isomer was obtained.

The signals related with the protecting groups are the singlet at 5.07 ppm that corresponds to the -$C\underline{H}_2C_6H_5$ protons and the protons -$CH_2C_6\underline{H}_5$ of the protecting group appearing between 7.23-7.44 ppm. The carbon -$\underline{C}H_2C_6H_5$ is at 74.8 ppm, the quaternary carbon appears at 138.4 ppm and the other carbons of the protecting group (-$CH_2\underline{C}_6H_5$) appear between 129.4 and 130.1 ppm. The resonance signal at 175.3 ppm was found to give long range coupling to the resonance signal of -C(CH_2CH_2)$_3$ and - $C\underline{H}_2NH$ protons and was attributed to carbonyl carbons of the three amide groups.

After the deprotection (**MRH10**), the expected differences in the ^1H and ^{13}C spectra are detected such as the shift of the protons of methyl group linked to the nitrogen of the pyridinone from 3.49 to 3.97 ppm as also the shift in the protons of the methylene group of the linkage ($C\underline{H}_2NH$) from 4.45 to 4.65 ppm. Their respective carbons are also dislocated to low field region, namely $N\underline{C}H_3$ from 37.4 in the protected ligand and 40.0 in the deprotected form and the shift from 119.4 to 114.2 ppm for the carbon C5''.

The carbon at 140.8 shows HMBC correlation with H5'', $C\underline{H}_2NH$ and 6''-$C\underline{H}_3$ protons and was attributed to C2''. The carbon at 144.8 shows HMBC correlation with H5'and $C\underline{H}_2NH$ protons and was attributed to C3''. Signals at 150.9 and 161.2 were attributed as carbons C4'' and C6'' due to their HMBC correlations with H5'', $NC\underline{H}_3$, 6''$C\underline{H}_3$ and H5'', $NC\underline{H}_3$, respectively. The resonance signal at 176.3 ppm was found to give long range coupling to the resonance signal of -C(CH_2CH_2)$_3$ and - $C\underline{H}_2NH$ protons and was attributed to carbonyl carbons of the three amide groups.

In which concerned to the NMR spectra of the protected ligand **MRB9p**, the resonance signals of the methyl and methylene protons of the rhodamine residue appear at 1.28 ppm

and 3.65 ppm, respectively. The signals of H4/H5 appear as a doublet at 6.90 ppm while H2/H7 appear as a broad singlet at 6.99 ppm.

The protons of the methyl group of the 3,4-HPO group appear at 2.39 ppm for the 5'-isomer and at 2.45 ppm for 4'-isomer. The proportion between the intensities of these was used to determine the ratio of both isomers in the mixture (1:1.1 of the 5'- and 4'- isomers), being this result coherent with the one found for other analogous signals of both isomers. The protons of $C\underline{H}_2NH$ of the linkage appear at 3.49 ppm.

The resonance signal at 6.45 ppm was assigned to the aromatic proton (H5") of the 5'-isomer of the 3,4-HPO and shows a HMBC correlation with a carbon at 20.8 ppm of the carbon 6''-CH_3 of the 5'-isomer), while the signal at 6.51 was attributed to the H5" of the 4'-isomer correlated to the carbon 6''-CH_3 of the 4'-isomer at 20.9 ppm.

The aromatic signals (6.9-7.4 ppm) were assigned to the protons of di-substituted aromatic ring of rhodamine moiety.

The signals related to the protecting group are the singlets at 5.17 ppm (5'-isomer) and 5.23 ppm (4'isomer) (-$C\underline{H}_2C_6H_5$). The aromatic protons (-$CH_2C_6\underline{H}_5$) appear as two sets of multiplets comprised between 7.21-7.40 ppm and 7.46-7.48 ppm. The carbon -$\underline{C}H_2C_6H_5$ is found at 74.7 ppm for the 5'-isomer and at 74.9 ppm for the 4'-isomer.

The quaternary carbons in ^{13}C NMR were assigned resorting to HMBC correlation, namely the signals assigned to 2'-COOH at 172.3 and 172.5 ppm for 5'- and 4'-isomers respectively due to correlation with the respective H3' proton signals at 8.10 ppm (5'-isomer) and 8.43 ppm (4'-isomer). The signal at 168.6 ppm was identified as belonging to the carbon of CONH of 5'- isomer, due to correlation with the corresponding signals at 4.66 ppm ($C\underline{H}_2NH_2$) and with 7.64 ppm (H6') both associated to 5'-isomer. Similarly, the signal at 169.1 ppm was assigned to carbon of CONH of 4'- isomer because of the observed correlation with the signals at 4.74 ppm ($C\underline{H}_2NH_2$) and 8.43 ppm (H3') associated to 4'- isomer. The resonance signals at 175.0 and 175.1 were assigned to C4'' of 5'- and 4'-isomers respectively, due to correlation with respective H5'' proton signals of 6.45 and 6.51 ppm of both isomers. The carbons at 151.0 and 151.1 ppm were assigned to C6'' of 5'and 4'- -isomers respectively, based on correlations with the respective H5'', $C\underline{H}_2NH$ and 6''-$C\underline{H}_3$ signals. C3'' signals were assigned to 147.6 ppm (5'-isomer) and 147.7 ppm (4'-isomer) based on correlation with the corresponding H3'and $C\underline{H}_2NH$ protons. Signals at 143.1 ppm (5'-isomer) and 143.3 ppm (4'-isomer) were attributed to C2'' based on the correlations with corresponding H5'', NCH_3 and $C\underline{H}_2NH$ protons.

In the spectra of **MRB9** the signals for the 4'- and 5'-isomers show the same chemical shifts for analogous atoms while in their precursor (compound **MRB9p**) these appear often fully

resolved with distinct chemical shifts, being the peaks of 5'-isomer at higher field than the corresponding ones for 4'-isomer. **MRB9** also shows observable increase for chemical shifts of the protons and carbons in the ^{1}H and ^{13}C spectra respectively, to higher field in comparison to compound **MRB9p**. Among others, it is quite noticeable the change observed for the NCH_3 protons of the pyridinone from 3.65 ppm in compound **MRB9p** to 4.08 ppm in **MRB9** (5'-isomer) and from 3.72 to 4.15 ppm (4'-isomer). A similar observation can be made for the $C\underline{H}_2NH$ protons of the linkage, varying from 4.66 ppm in **MRB9p** to 4.97 ppm (5'-isomer), and from 4.74 ppm to 5.06 ppm (4'-isomer). Their respective carbon signals are also dislocated to lower field region, namely $N\underline{C}H_3$ 37.4 ppm (5'-isomer) and 37.5 ppm (4'-isomer) to 40.0 ppm for both isomers.

The observed differences in the chemical shifts of ^{1}H and ^{13}C nucleus in the spectra of the protected and deprotected compounds is primarily due to the deprotection of the hydroxyl group and the acidic pH of the deprotection reaction that lead to isolate the final ligands in the enol form [4, 170].

2.3.3 Photophysical properties in aqueous solution

The absorption UV-Vis spectra of the ligands studied **MRB2**, **MRB4**, **MRB20**, **MRH10** and **MRB9** show two sets of bands in different regions of the spectra, which correspond to $\pi \rightarrow \pi^*$ transitions of the π systems of 3,4-HPO and of the fluorophores (rhodamines, rosamine or naphthalene) that constitute the ligand structure. Transitions in the range 281-290 nm are associated with ethylene and benzene bonds of the aromatic ring of the 3,4-HPO. The other set of transitions in the range of 450-650 nm are signed to π system of rhodamines of ligands **MRB2, MRH10** and **MRB9** or to the rosamine in the case of ligand **MRB20**. In the case of ligand **MRB4**, a shoulder at ca. 312 nm is discernible and is assigned to π system of 1-naphthyl isothiocyanate. The molar absorptivity values obtained are in the magnitude (10^4) close to those reported in previous results for similar rhodamine or naphtalene derived chelators [3, 4, 170].

The fluorescence spectra of ligands **MRB2**, **MRB4**, **MRB20**, **MRH10** and **MRB9** show bands in different regions of the spectra that are characteristic for the fluorophore included in the structure of each ligand. In the case of ligands **MRB2, MRB20**, **MRH10** and **MRB9** the band is in the range of 560-670 nm and for ligand **MRB4** the band is in the range of 335-525 nm (Table 2.2). The values obtained are in agreement with those reported in the literature for similar ligands [3, 4, 170].

Confirmation of the predominance of the keto form at pH 7.4 is particularly evident for compound **MRB4** by observation of the characteristic λ_{max} of fluorescence emission at 385

nm as previously described by our research group for other naphthalene labelled 3,4-HPO ligands [170].

The spectral parameters of the new fluorescent chelators are summarized in Table 2.2.

Table 2.2 – Spectral parameters of the fluorescent chelators **MRB2**, **MRB4**, **MRB20**, **MRH10** and **MRB9** (25ºC, MOPS buffer, I=0.1 M, pH=7.4). Fluorescence spectra were recorded at: a) λ_{exc} = 568 nm, λ_{em} from 570-700 nm, 600 V, 5 nm slits, for ligand **MRB2**; b) λ_{exc} = 290 nm, λ_{em} from 300-550 nm, 600 V, 10 nm slits for ligand **MRB4**. c) λ_{exc}=562 nm and λ_{em} from 566 to 700 nm, 650 V, 5 nm slits, for **MRB20**; d) λ_{exc}=553 nm and λ_{em} from 560 to 700 nm, 650 V, 5 nm slits, for **MRH10**; e) λ_{exc}=560 nm and λ_{em} from 561 to 700 nm, 650 V, 5 nm slits, for **MRB9.**

Ligand	Absorption	Fluorescence		
	ε / mol^{-1} dm^3 cm^{-1}	λ_{max} / nm		
		fluorophore	excitation	emission
MRB2	$3.8x10^4$	566	568	586
MRB4	$1.5x10^4$	312	290	385
MRB20	5.9×10^4	561	562	587
MRH10	3.2×10^4	552	560	575
MRB9	5.4×10^4	559	561	583

2.3.4 X-Ray Crystallography

Single-crystals of the rhodamine derivative compounds **1** and **MRB2** suitable for X-ray diffraction analyses were obtained by controlled recrystallization from MeOH/$CHCl_3$ and MeOH/Et_2O solvent mixtures, respectively. The two solid-state crystalline structures were determined in the triclinic space group P-1, confirming the synthesis of the protected and unprotected forms of the desired ligand (Figure 2.18). The asymmetric unit (asu) of **1** reveals only a neutral organic molecule while the asu of **MRB2** contains one cationic organic molecule, one chloride anion and five water molecules of crystallization. The structural arrangement of ligand **MRB2** shows the xanthene group almost perpendicular with the adjacent phenyl ring and the pyridinone ring [dihedral angle between the average planes defined by these aromatic groups is 84.66(2)º and 75.49(2)º, respectively].

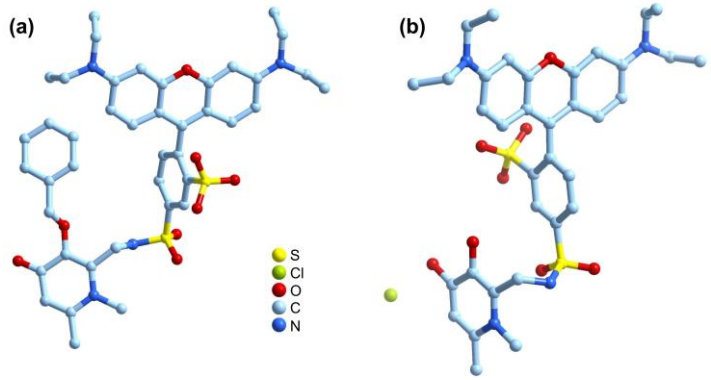

Figure 2.18 - Crystal structures of the rhodamine derivative molecules: protected ligand **1** (**a**) and **MRB2** (**b**) represented in the ball-and-stick model. Hydrogen atoms were omitted for clarity reasons.

The contiguous ligands **MRB2** closely interact by a strong N−H···O hydrogen bond involving the sulfonamide and sulfonate groups of adjacent molecules leading to the formation of one-dimensional supramolecular structures (Figure 2.19 a). The extended packing of these supramolecular entities leads to an overall porous structure with one-dimensional tunnels along the direction of the unit cell (Figures 2.19 b). The porous are entirely occupied by the crystallization water molecules and the charge-balancing chloride anions, which are also involved in an extensive inter-molecular hydrogen bonding network, namely O−H···O, O−H···Cl and N−H···O interactions (not represented).

To the best of our knowledge, this is the first report of an X-ray crystal structure of a rhodamine derivative 3,4-HPO.

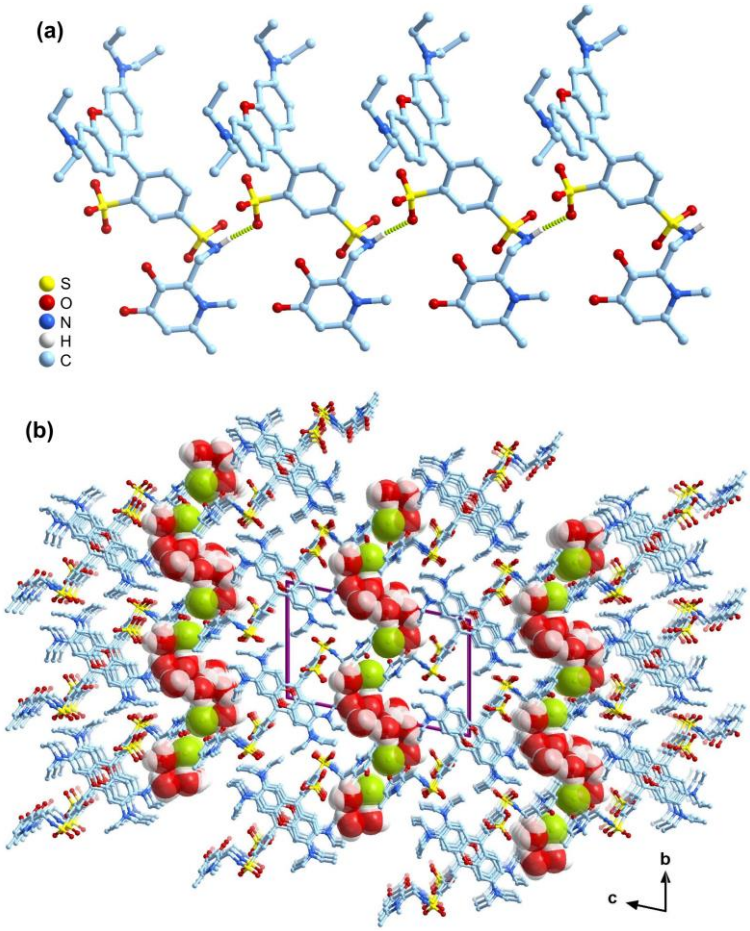

Figure2.19 - Structural features of the crystal structure of the ligand **MRB2**: (**a**) one-dimensional supramolecular structure with the N–H···O interactions represented as green dashed lines; **(b)** crystal packing viewed in the [1 0 0] direction of the unit cell with the Cl^- anions and crystallization water molecules occupying the channels.

Crystalline materials of the naphthalene derivatives molecules **3** and **MRB4** with quality for single-crystal X-ray diffraction analyses were isolated by recrystallization from solution of MeOH/$CHCl_3$ and $CHCl_3$/*n*-hexane, respectively. The crystal structure of compound **3** was determined in monoclinic space group $P2_1/n$, while the structure of ligand **MRB4** was unveiled in the triclinic space group P-1, confirming unequivocally the preparation of the protected and unprotected forms of the desired ligand (Figure 2.20). The asu of the two crystal structures comprises only the respective neutral organic molecule. The structural arrangement of ligand **MRB4** reveals the xanthene group practically in the same plane of the pyridinone ring [dihedral angle between the average planes defined by the two aromatic groups is 8.62(1)º].

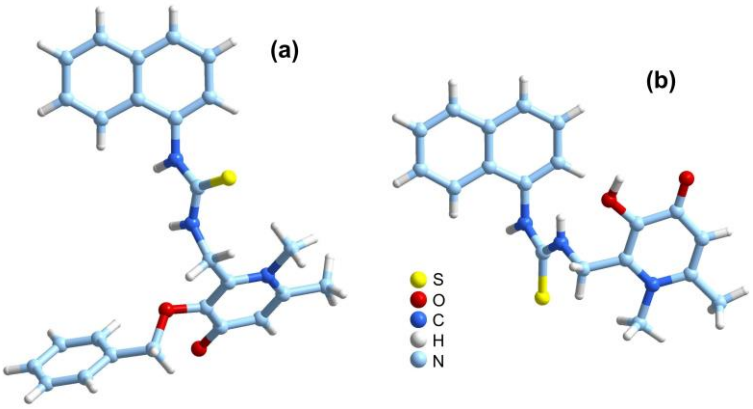

Figure 2.20 - Crystal structures of the naphthalene derivatives ligand: protected **3** (**a**) and unprotected form **MRB4** (**b**) represented in the ball-and-stick model.

In the crystalline material, the deprotected ligand **MRB4** was obtained in the keto form.
A pair of O−H···O hydrogen bonds involving the hydroxypyridinone groups of two adjacent molecules leads to the formation of dimeric entities with the two molecules positioned in anti-parallel mode (Figure 2.21 a). Furthermore, the organic molecules **MRB4** also interact by an extensive network of weak non-covalent interactions (not shown), such as C−H···O, C−H···S, C−H···π and long π···π stacking which further strengthen the cohesion of the crystalline packing (Figure 2.21 b).

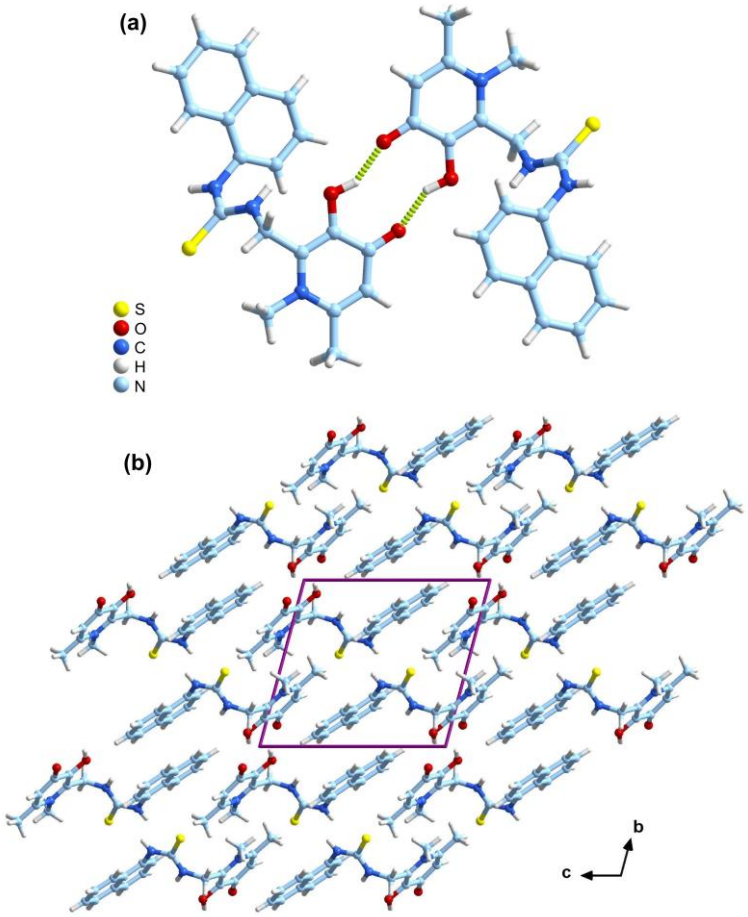

Figure 2.21 - Structural features of the crystalline structure of the ligand **MRB4**: (**a**) dimeric supramolecular structure with the O–H···O interactions represented as green dashed lines; **(b)** crystal packing viewed in the [1 0 0] direction of the unit.

2.4 Conclusions

Novel fluorescent ligands **MRB2**, **MRB4**, **MRB20**, **MRH10** and **MRB9** derived from distinct fluorescent units, rhodamines, rosamine or naphthalene, were successfully synthesized and the yields of the reactions were satisfactory according to the previous work performed by our research group. All structures of the synthesized chelators were fully characterized by several technics, namely NMR, mass spectrometry, elemental analysis, UV-Vis, Fluorescence and Single Crystal X-Ray Diffraction in the case of the ligands for which we could obtain a crystal.

The analysis of the data obtained from the crystalline structure of the compounds revealed that molecules **1**, **3** and **MRB4** have neutral charge while compound **MRB2** is mono cationic. The results also demonstrate that the deprotected ligand **MRB2** remains in the enol form as described for other fluorescent pyridinone ligands [170] but chelator **MRB4** crystallized in the keto form. In the single crystal structure of ligand **MRB2**, the xanthene moiety of the rhodamine is almost perpendicular to the adjacent phenyl ring and the pyridinone ring whereas in ligand **MRB4** the xanthene group of the naphthalene framework is almost coplanar with the pyridinone ring.

The potential antibacterial activity of these new fluorescent chelators against several bacteria, namely *M. avium*, will be explored in Chapter 3. The results of antibacterial studies will be compared with those obtained previously [1, 4] in order to get insight on the SAR of the 3,4-HPO fluorescent iron(III) chelators.

3 | ANTIBACTERIAL ACTIVITY OF 3,4-HPO CHELATORS

3. ANTIBACTERIAL ACTIVITY OF 3,4-HPO CHELATORS

3.1 Introduction

Bacterial resistance to currently available antibiotics is a rising global problem and therefore efforts should be done in order to develop new pharmacologic alternatives targeting different mechanisms and pathways [216, 217, 290]. Iron is an essential element for the growth of all living organisms [59] and it has been demonstrated that limiting the amount of available iron for the growth of pathogenic microorganisms can be considered as a strategy to control infections [10, 67, 68, 102, 164, 168, 291]. Several reports suggesting the application of chelation therapies for the control of infections caused by several microorganisms have been described [18, 59, 75, 164, 251, 258-261, 273].
The use of iron chelators to restrict the iron available for mycobacterial growth has been reported [101] , namely for *M. tuberculosis* [292, 293] and *M. avium* [1, 3, 4, 123].

In our previous studies we reported that the inhibitory effect of fluorescent chelators on the intramacrophagic growth of *M. avium* was dependent on the presence and type of fluorophore. The results are consistent for both bidentate and hexadentate fluorescent ligands.
Interestingly, the non-fluorescent hexadentate (CP256) and bidentate (Hdmpp) chelators were not effective in the control of *M. avium* infection revealing that the chelation of iron is a required but not sufficient property for the antimycobacterial effect.
When both bidentate and hexadentate chelators were tested, regarding the activity of fluorescent chelators, we found that the antimycobacterial activity was similar for the bidentate and hexadentate chelators with the same fluorophore, if the appropriate amount of ligands were administered. Moreover, the inhibitory effect of the rhodamine B isothiocyanate labelled compounds (**MRH7** and **MRB7**) was significantly higher than that observed for the carboxytetramethylrhodamine derived chelators (**MRH8** and **MRB8**), thus pointing out the significance of the rhodamine B isothiocyanate molecular fragment but also the potential importance of the HLB and the presence of sulphur atom (or even thiourea group) [1, 4].

One of the aims in this chapter is the study of the potential of the synthesized molecules (described in Chapter 2) for the control of the growth of *M. avium* inside macrophages.

We also expect to improve our knowledge on the importance of the different functional groups of the chelator for the final biological effect. The formulae of the studied chelators are depicted in Figures 3.1, 3.3 and A.1, in Appendix.

Drug combinations of new molecules with classic antibiotics is an emerging and promising strategy to overcome bacterial antibiotic-resistance mechanisms and to restore antibiotic effectiveness [294]. Accordingly, the most active iron chelator against *M. avium* growth, was also tested in combination with a classic antimycobacterial antibiotic.
The clinical potential of the combination of iron chelators with other antibiotics has been demonstrated to treat bacterial [67, 68, 101, 249, 250, 262], fungal [238] and protozoal [220] infections.
To the best of our knowledge, no reports were found of the use of combination therapies involving iron chelators and classic antimycobacterial antibiotics used in the clinics.

To achieve this goal, we performed studies in which the most active chelator was tested in combination with ethambutol. This drug, [(S,S)-2,20-(ethylenediimino)-di-1-butanol], was first reported in the early 1960s [295] and is one of the few well-known and reliable antimycobacterial used in clinical [81, 95, 220, 296]. Ethambutol acts by inhibiting mycobacterial arabinofuranosyl transferases which are responsible for glycosylation steps in the biosynthesis of LAM and AG, both constituents of the mycobacterial cell wall [111-113]. Ethambutol is active against *M. avium* pathogens but high doses and combinations therapies are needed to achieve an effect and also antibiotic resistance has been reported [81, 95, 96, 297-300]. Moreover, there is some evidence that combined therapies using ethambutol have advantages due to the ability of this drug to increase cell wall permeability in *M. avium* and consequently favour the influx of other drugs tested in combination [301, 302]. In addition, there are some reports of the ability of ethambutol to chelate metals ions, namely iron and copper, therefore contributing to a better control of the infection [301, 303-305].

In this chapter we report the results of the *in vitro* effect of compounds **MRB2**, **MRB4**, **MRH10** and **MRB9** and the *in vitro* inhibitory effect of **MRH7** when used alone and in combination with ethambutol against *M. avium.*

The studies of the antimycobacterial effect of the chelators against *M. avium* in macrophages were performed in collaboration with Professor Maria Salomé Gomes, in the III – Iron and Innate Immunity group at IBMC.

We also report the results, obtained by our research group, related with the evaluation of the potential of the chelators to control extracellular bacterial growth, including Gram-positive and Gram-negative bacteria. These data are discussed in the present chapter, as they are useful for comparison with those performed in this work with *M. avium*. These experiments were performed by Maria José Feio.

The results of the antibacterial activity of chelators **MRB9**, **MRH10** and **MRH7** in combination with ETH, against *M. avium,* are published in:

[276] **Moniz, T.**, Silva, D., Silva, T., Gomes, M.S. and Rangel, M., *Antimycobacterial activity of rhodamine 3,4-HPO iron chelators against Mycobacterium avium: analysis of the contribution of functional groups and of chelator´s combination with ethambutol.* MedChemComm, 2015, **6**, 2194-2203.

3.2 Methods

3.2.1 Bacteria

M. avium strain 2447, smooth transparent variant (SmT) was isolated from an AIDS patient and provided by F. Portaels (Institute of Tropical Medicine, Antwerp, Belgium). Mycobacteria were grown to mid-log phase in Middlebrook 7H9 medium (Difco, Sparks, MD) containing 0.04% V/V of Tween 80 (Sigma, St. Louis, MO) at 37ºC.

Bacteria were harvested by centrifugation, suspended in a small volume of saline containing 0.04% V/V of Tween 80 (Sigma) and briefly sonicated in order to disrupt bacterial clumps. The suspension was diluted and stored in aliquots at -80ºC until use.

3.2.2 Bone marrow derived macrophages (BMM)

Macrophages were derived from the bone marrow of BALB/c mice. Each femur was flushed with 5 mL of Hanks' balanced salt solution (HBSS, Life Technologies, Paisley, U.K.). The resulting cell suspension was centrifuged and the cells re-suspended in DMEM (Life Technologies, Paisley, U.K.) supplemented with 10 mM glutamine, 10 mM HEPES, 1 mM sodium pyruvate, 10% FBS (Fetal Bovine Serum) (Life Technologies), and 10% of L929 cell conditioned medium (LCCM) as a source of Macrophage Colony Stimulating Factor (M-CSF). According to manufacturer's information, the iron content of DMEM is 0.25 mM. The added FBS contributes an additional 3 mM of iron. In order to remove fibroblasts, the cells were cultured overnight, at 37ºC in a 7% CO_2 atmosphere, on a cell culture dish. The non-adherent cells were collected with warm HBSS medium, washed and resuspended in

DMEM with 10% LCCM at a cell density of $4x10^5$ cells/ml. One ml of this cell suspension was distributed per well in 24-well plates which were incubated at 37ºC in a 7% CO_2 atmosphere. Three days later, 0.1 mL of LCCM was added. On the 7th day of culture, the medium was renewed.

3.2.3 Infection and treatments of BMM

On the tenth day of culture, the macrophages of each well were incubated with 0.2 mL of DMEM containing 10^6 *M. avium* colony forming units (CFU) for 4 h at 37ºC in a 7% CO_2 atmosphere. The cells were washed with warm HBSS to remove extracellular mycobacteria and reincubated in DMEM with 10% FBS and 10% LCCM with or without the addition of compounds. To quantify the number of intracellular mycobacteria at time zero of infection, macrophages from three wells were immediately lysed with 0.1% of saponin.

The iron chelator solutions were obtained by preparing concentrated solutions of the different compounds in DMSO followed by dilution of a known volume of the DMSO stock solution in DMEM. The percentage of the DMSO stock solution was always less than 1% in the final volume.

Chelators were added to the culture medium at the concentrations indicated in each figure (Figures 3.2. 3.4 and 3.5) (ranging from 1 to 120 μM). **MRH7** was tested alone and in combination with ethambutol (ETH) at 2 μg/ mL. Ethambutol was also tested alone at the same concentration used in combination with chelators. Each concentration was tested in triplicates. All the results were confirmed in at least three independent assays. The formulae of the bidentate and hexadentate ligands used in the present study are shown in Figures 3.1, 3.3 and A.1, in Appendix.

3.2.4 Quantification of *M. avium* inside BMM

After 5 days of infection, the growth of *M. avium* 2447 SmT was evaluated by counting the colony forming units. Macrophages were lysed using 0.1% saponin and the resulting bacterial suspension was diluted in water containing 0.04% Tween 80. The dilutions were plated in Middlebrook 7H10 agar (Difco) and the number of colonies was counted after 8 days at 37ºC. The difference, in terms of $\log_{10}$ CFU/well, between time zero of infection and the last day in culture (day 5), is abbreviated as ‘‘$\log_{10}$ increase’’.

3.2.5 Statistical analysis

All the experimental data are expressed as mean values ± standard deviation (SD) for the number of experiments (one animal per experiment) indicated in the legends of the figures.

Data obtained were analysed using the software Graph Pad Prism version 6.0. For compounds **MRB2**, **MRB4** and **MRB20**, statistical analysis was performed using *t-Student* test to compare the bacterial growth in the absence of chelator with that of chelator-treated cells and according to previous work [1, 4].
For multiple comparison of the effect of **MRH7**, **MRH10** and **MRB9** and for studies of combined therapies (**MRH7** and ETH), multiple comparisons were performed using one-way analysis of variance (ANOVA) followed by Bonferroni multiple comparison posthoc test. Significance was accepted when p value < 0.05 was obtained.

3.3 Results and Discussion

3.3.1 Evaluation of antimycobacterial activity

*3.3.1.1 Effect of chelator **MRB2**, **MRB4** and **MRB20** on the intramacrophagic growth of M. avium 2447 SmT*

As described in Chapter 2, we designed a set of chelators to investigate, the importance of the presence of sulphur either as an element *per se* or as a thiourea group and also if this group is important in association with a rhodamine or if it is relevant even associated with other fluorophores.
In Ligand **MRB2** the rhodamine moiety was maintained with the ethyl groups linked to nitrogen atoms (Figure 3.1, in blue) and a sulfonamide linker was considered (Figure 3.1, in red).
Ligand **MRB4** was designed to include in its structure a different type of fluorophore, a naphthalene unit. The thiourea linkage was maintained between the fluorophore and the chelating unit (Figure 3.1, in red).
To evaluate the relevance of the global charge of the chelator, in ligand **MRB20**, the rhodamine-like moiety was maintained. In its structure there is no substituent in the position 2' of the phenyl ring, leading to a rosamine derived chelator and the global charge balance is positive (+1) at physiological pH, according to the literature [3, 179, 275].

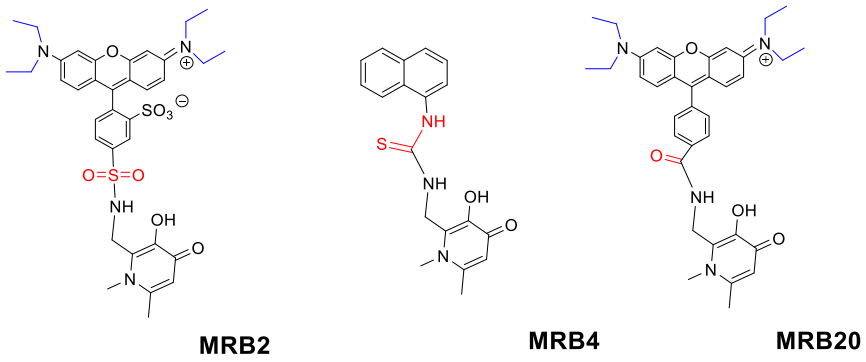

Figure 3.1 – Formulae of **MRB2**, **MRB4** and **MRB20** chelators. The linkers are highlighted in red and the substituents on the nitrogen of the xanthene ring are highlighted in blue.

M. avium growth inside macrophages was measured, as CFU, after five days in culture in the absence (control = ctrl) or in the presence of the chelators. The biological activity of each chelator was calculated as the difference in $\log_{10}$ CFU/well between day 0 and day 5 and the results obtained are represented in Figure 3.2.

The concentrations of chelators chosen to be administered to the macrophages were based on the previous results [4]. The lower concentrations were maintained (1 and 10 μM for hexadentate and 3 and 30 μM for bidentate chelators) and the highest concentration was changed to 20 or 40 μM for hexadentate and to 60 and 120 μM for bidentate ligands.

In comparison with the control, none of the tested ligands, **MRB2**, **MRB4** and **MRB20** induced a statistically significant decrease on *M. avium* growth at any of the tested concentrations.

For compound **MRB4** we started to test the same concentrations chosen for rhodamine and rosamine derived 3,4-HPOs. However, we verified, by the routine observation of the cells on the microscope during the time of the experiment, that these concentration values were lethal for the macrophages. Thus, we gradually decreased these values and even at lower concentration values as 10 μM, **MRB4** was toxic. Then, we reduced again the concentration of the chelator to 7 μM and apparently no toxicity was observed on the microscope visualization of the macrophages. A similar scenario was verified for the treatment with **MRB20**. The latter chelator, at 30 and 60 μM, was toxic and lead to the death of the macrophages. However at the lowest concentration (3 μM), the cells seemed healthy on the microscope visualization of the cultures.

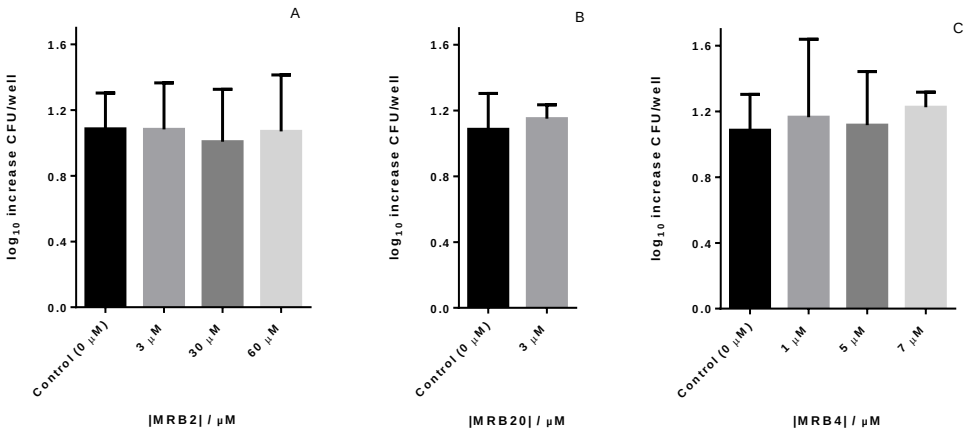

Figure 3.2 - Effect of **MRB2** (A), **MRB20** (B) and **MRB4** (C) on intramacrophagic growth of *M. avium.* BMM were infected with *M. avium* 2447 (SmT). Each chelator was added, just after infection, at a concentration of 3, 30 and 60 μM for **MRB2**, at 3 μM for **MRB20** and 1, 5 and 7 μM for **MRB4**. Infected BMM were incubated for 5 days to measure the intracellular growth of the bacteria. The difference, in terms of log_{10} CFU/well, between days 0 and 5 was designated ''log_{10} increase''. The graphs show the geometric mean ± SD of the log_{10} increase per well obtained from three wells for each condition from three independent experiments. Statistical analysis was performed using *t-Student* test to compare the bacterial growth in the absence (ctrl) or presence of each of the chelators.

*3.3.1.2 Effect of **MRH10** and **MRB9** chelators on the intramacrophagic growth of M. avium 2447 SmT in comparison with **MRH7***

To get insight on the importance of the thiourea group and the HLB of the chelator for the biological effect, we designed:

a) **MRH10** in which thiourea group was maintained (Figure 3.3, in red) but the ethyl groups linked to the nitrogen in the rhodamine ring were substituted by methyl groups (Figure 3.3, in blue).

b) **MRB9** in which the thiourea linkage was changed by an amide linker (Figure 3.3, in red) and the ethyl groups linked to the nitrogen in the rhodamine rings were maintained (Figure 3.3, in blue).

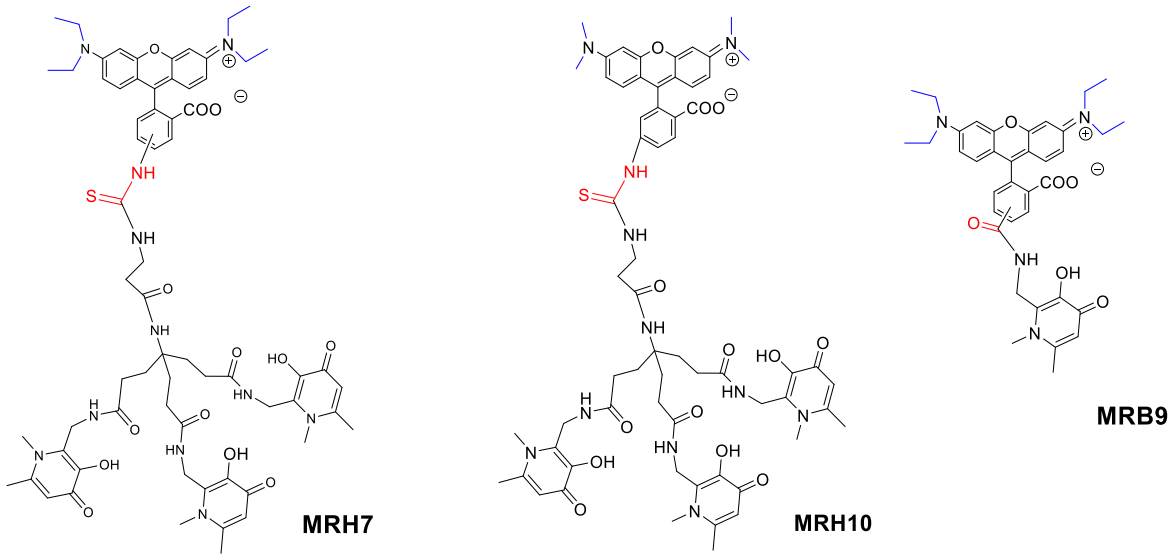

Figure 3.3 – Formulae of **MRH7, MRH10** and **MRB9** chelators. The linkers are highlighted in red and the substituents on the nitrogen of the xanthene ring are highlighted in blue.

Intramacrophagic growth of the bacteria was measured (as CFUs) after five days in culture in the absence or in the presence of the chelators. The effect of each compound in the intramacrophagic growth of *M. avium* was calculated as described before in 3.3.1.1..
The antimycobacterial effect of the new chelators **MRH10** vs **MRB9** was tested and compared with the effect of chelator **MRH7**, used herein as a second control, for the same comparable concentrations: (a), (b), (c) and (d). All compounds were tested in at least three independent assays and the results are represented in Figure 3.4.

The results are indicative that all the fluorescent chelators exhibit antimycobacterial effect and this activity seems to be dose-dependent. In comparison with the control, **MRH7** has a significant effect at lower concentrations such as 10 µM while the new chelator **MRH10** only induces a reproducible inhibitory effect leading to a significant decrease on *M. avium* growth at a concentrations equal or above 20 µM. Moreover, **MRB9** is only effective at the highest concentration tested (120 µM).

Comparison of the effect of the three chelators shows that:

i) at the lowest concentration (concentration a), Figure 3.4), no significant differences are observed for the activity of **MHR10** and **MRH7** and the effect of the latter is significantly higher than the obtained for **MRB9**.

ii) at intermediate concentrations (concentrations b) and c), Figure 3.4) **MRH7** exhibits the highest activity and its effect is significantly greater than that obtained for **MRB9**. No

significant differences on the inhibition of bacterial growth is apparent between **MHR10** and **MRB9.**

iii) at the highest concentration tested (concentration d), Figure 3.4), all ligands induce a significant decrease on the intramacrophagic growth of *M. avium* and the effect is not significantly different between them.

The results obtained show that **MRH7** seems to remain the most active chelator in inhibiting *M. avium* growth, being effective in concentration equal or above 10 μM. Chelator **MRH10** as a similar activity than **MRH7** and its effect is significantly better than that of **MRB9.**
The present results point out the relevance of the concomitant presence of the two functional groups, *N*-ethyl groups in the xanthene structure and the thiourea link, for the antimycobacterial effect.

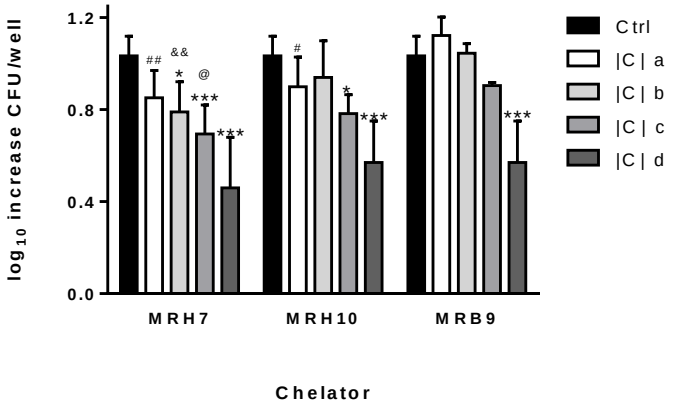

Figure 3.4 - Effect of **MRH7**, **MRH10** and **MRB9** on intramacrophagic growth of *M. avium*. BMM were infected with *M. avium* 2447 (SmT). Each chelator was added, just after infection, at a concentration of 5 (a), 10 (b), 20 (c) and 40 (d) μM for **MRH7** and **MRH10** and 15 (a), 30 (b), 60 (c) and 120 (d) μM for **MRB9**. Infected BMM were incubated for 5 days to measure the intracellular growth of bacteria. The difference, in terms of $\log_{10}$ CFU/well, between days 0 and 5 was designated ''$\log_{10}$ increase''. The graphs show the geometric mean ± SD of the $\log_{10}$ increase per well obtained from three wells for each condition from three of five independent experiments. Statistical analysis was performed using ANOVA test to compare the bacterial growth: i) in the absence or presence of each the chelators and ii) in the presence **MRH7** vs **MRH10** vs **MRB9**, for the same concentrations, (a), (b), (c) and (d). Statistical significance: * $p<0.05$ and *** $p<0.001$ when compared with control (no chelator); $^{\#}$ $p<0.05$ for **MRH10** vs **MRB9** or $^{\#\#}$ $p< 0.01$ for **MRH7** vs **MRB9**, at concentration (a); $^{\&\&}$ $p< 0.01$ for **MRH7** vs **MRB9**, at concentration (b); $^{@}$ $p<0.05$ for **MRH7** vs **MRB9**, at concentration (c).

*3.3.1.3 Effect of **MRH7** in combination with ethambutol (ETH) on the intramacrophagic growth of M. avium 2447 SmT*

The effects of the chelator **MRH7** and of the classic antimycobacterial antibiotic, ETH, were evaluated *per se* and in combination. Different concentrations of ETH were tested in preliminary studies and the chosen value 7.2 μM (2 μg/ mL) represents the concentration for which the effect of the antibiotic alone is virtually null. The experiments were performed using a fixed concentration of the antibiotic combined with **MRH7** in the concentrations of 5, 10 and 20 μM. The antimycobacterial activity of **MRH7**, ETH and their combination was compared with the control (no treatment) and all the conditions were compared between them. The results obtained are represented in Figure 3.5.

The results of the combination of **MRH7** with ETH reveal that the effect is significantly different from the control for all the concentration range, even at the lowest concentration (5 μM) of **MRH7**. Also, the effect of the combination of **MRH7** with ETH at 10 and 20 μM is significantly higher than the effect obtained with ETH *per se*.
Considering the combination of **MRH7** with ETH at the highest concentration of chelator (20 μM), the effect is also significantly higher than that obtained for **MRH7** *per se*, at the same concentration.
These data reinforce our hypothesis of the advantageous use of the combination of iron(III) chelators and the clinically used antimycobacterial antibiotic, ETH, as a strategy to fight *M. avium* infections. This approach may be useful as two different targets are simultaneously considered, the effect of chelators on the iron deprivation and the activity of ETH in the disruption of mycobacterial cell wall.

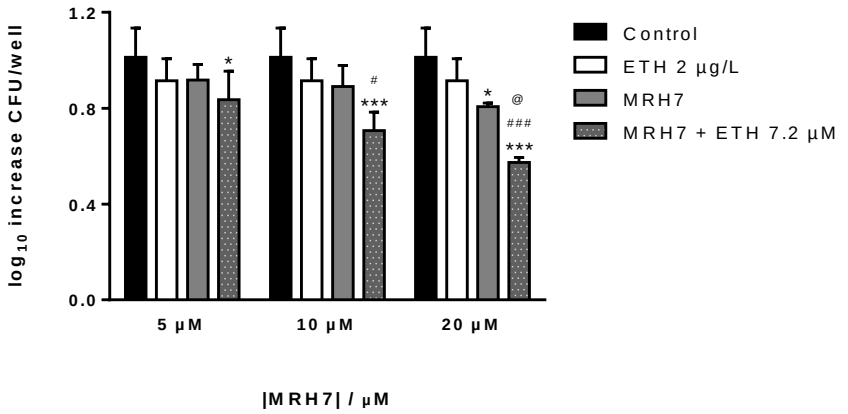

Figure 3.5 - Effect of **MRH7**, ETH and their combination on intramacrophagic growth of *M. avium*. BMM were infected with *M. avium* 2447 (SmT). Each compound was added, just after infection, at a concentration of 5, 10 and 20 µM for **MRH7** and 7.2 µM for ETH. Infected BMM were incubated for 5 days to measure the intracellular growth of bacteria. The difference, in terms of log_{10} CFU/well, between days 0 and 5 was designated ''log_{10} increase''. The graphs show the geometric mean ± SD of the log_{10} increase per well obtained from three wells for each condition from four independent experiments. Statistical analysis was performed using ANOVA test to compare the bacterial growth in the absence or presence of **MRH7**, ETH or their combination and in the presence of **MRH7**, with or without combination of ETH. Statistical significance: * $p<0.05$ and *** $p<0.001$ when compared with control (no compound); # $p<0.05$ or ### $p< 0.001$ when compared with ETH 2 µM; $^{@}$ $p<0.05$ when compared with **MRH7** (without ETH).

3.4 Conclusions

Our previous results demonstrated that rhodamine-labelled iron chelators are able to restrict *M. avium* growth inside macrophages due to their ability to chelate the iron available for the bacterial survival [1, 3, 4]. These results have also shown that the non-fluorescent ligand is not active against intramacrophagic growth of the bacteria and also that the inhibitory effect is strongly dependent on the fluorophore. In particular, the more active chelators are those conjugated with rhodamine B isothiocyanate, emphasizing the importance of the isothiocyanate group but also the relevance of the lipophilicity which seems to favour the membrane interaction and consequently the antibacterial activity [4, 272]. *M. avium* is an intracellular pathogen that survives in the phagosome and that has the capacity to prolong its life by blocking phagosome maturation thus maintaining the access to extracellular and endosomal iron sources [306]. Consequently, the ability of the chelator to enter inside the host cell, cross membranes and reach the infection target is an additional requirement for an efficient iron-depriving effect of the ligand.

Several aspects of the structure activity relationships were investigated, namely the importance of the isothiocyanate group, or even the thiourea group, and the importance of global lipophilicity and charge of the chelators in study.

Isothiocyanates (ITCs) that are naturally present in cruciferous vegetables (such as broccoli and cabbage) are released by mechanical disruption of cruciferous plant tissues. Several examples of the antibacterial activity against Gram-positive and Gram-negative bacteria are described for ITCs. The mechanism of action of ITCs is based on disturbing the bacterial membrane and is also described an effect on the inactivation of extracellular enzymes through oxidative cleavage of disulphide bonds, which was proposed to be mediated by the formation of reactive thiocyanate radicals [307-313].
As the more efficient chelators contain a thiourea group, we consider plausible that this group may also be important for antimycobacterial effect and we hypothesise that the presence of thiourea group in the structure of the chelators may allow the targeting of the bacterial cell wall, and this effect although not enhancing the ironing out effect but could also help to control the survival of the pathogen.

The introduction of the thiourea group in the molecular framework of the first rhodamine labelled chelator synthesized by our research group, **MRH7**, was not deliberate but it was a consequence of the rhodamine framework that was used in the synthesis [3]. In the condensation reaction to link the fluorophore to the chelating unit, the reaction of the thiocyanate group with the amine conduces to the formation of a thiourea linkage. Several studies reported the antibacterial activity of molecules with this functional group [314, 315] and namely against mycobacterial species such as *M. tuberculosis* and *M. avium* [316-323].

The relevance of the charge of the chelator was also investigated and, for this propose, the ligand **MRB20** was synthesized. This topic has particular interest due to existence of reports in the literature of the targeting of mitochondria by compounds with charged rhodamines in their structure, which could be related with some toxicity for the host cells [324, 325]. Moreover, we are interested in study if a positive charge of the chelators, in comparison to the zwitterionic chelators tested in our previous studies [1, 4], influences their interaction with biological membranes, such as reported for other molecules, namely antimicrobial peptides (reviewed in [326, 327]).
The contribution of the different lipophilicity of rhodamine fragment was evaluated by comparing structurally related chelators, **MRH10** and **MRB9,** in which the functional groups of the linkage or linked to the nitrogen atom in the xanthene ring were changed, in comparison with **MRH7**.

The present results show that:

i) Ligands **MRB2**, **MRB4** and **MRB20** do not significantly decrease *M. avium* growth at any of the tested concentration (from 1 to 60 μM);

ii) Ligands **MRB4** (10 μM) and **MRB20** (30 and 60 μM) were toxic and lead to the death of the macrophages cultures;

iii) The inhibitory effect of the rhodamine B isothiocyanate derivatives (**MRH7** and **MRH10**) is superior to the one observed for carboxytetraethylrhodamine chelator (**MRB9**).

iv) The highest inhibitory effect was obtained for the chelator labelled with rhodamine B isothiocyanate, **MRH7**, with ethyl groups linked to the nitrogen atom in the xanthene ring.

The inefficiency of ligand **MRB2** corroborates the importance of the thiourea linkage and the results seems to demonstrate that the presence of the sulphur atom, namely in other functional groups, is not a sufficient property to reach the final biological activity.
Ligand **MRB4** includes a naphthalene fragment as a fluorophore moiety. This framework seemed promising to include on the structure of our ligands, however revealed toxicity for the macrophages cultures. We reduced the concentration range tested for ligand **MRB4**, comparing to the concentrations tested for rhodamine derived ligands to allow the execution of the experiments. This apparent toxicity could be justified by several reports in the literature concerning on the ability of ITCs and naphthalene derived molecules to interfere with the cell stability and act as chemotherapeutic agents in cancer therapies [328-334].
The toxicity verified for the cultures of macrophages to which the ligand **MRB20** was administered (at 30 and 60 μM), could probably be related with the targeting of the positively charged ligand to the mitochondria and the associated destabilization in the metabolism of the cell, leading at least on the death of the macrophages.

The present results substantiate that the inhibitory effect of rhodamine labelled 3,4-HPO chelators is strongly dependent on the fluorophore and confirm the importance of the a zwitterionic global charge, the thiourea linkage, the ethyl substituents on the amino groups of the xanthene ring and the advantage of their associated inclusion in the rhodamine molecular framework. As hexadentate chelators are more effective than the bidentate for lower doses, the ligand that comprises all these characteristics is **MRH7**.

Moreover, the combined administration of chelator **MRH7** with the antibiotic ethambutol proved to be advantageous to achieve a higher antimycobacterial effect when compared

with the activity of the chelator and the antibiotic *per se*. The results imply that it is possible to reduce the amount of chelator used to obtain a significant biological effect while simultaneously improving the activity of ETH.
To the best of our knowledge the present work is the first report revealing the advantageous combination of iron chelators and classic antibiotics in the treatment of intracellular infections such as *M. avium* infections.

These results reinforce our hypothesis in which compounds including the thiourea group in their structure and high lipophilicity (*N*-ethyl substituents in xanthene ring) seem to be the most promising approach for designing this class of molecules and also their combination with classic antibiotics used in clinics.

Several 3,4-HPO chelators have also been tested as antibacterial agents against other bacterial pathogens. Since there is no report in the literature concerning the effect of fluorescent 3,4-HPO iron(III) chelators against other bacterial species, namely against extracellular bacteria, we considered the investigation of the effect of the fluorescent chelators in study in the present work against other bacterial pathogens.

The rhodamine derived chelators have also been tested against extracellular bacteria. The potential effect of the iron(III) chelators was evaluated by determining the minimum inhibitory concentration (MIC) of the compounds that can limit the bacterial growth, after the incubation time of 24h. All the compounds were tested in at least three independent assays and the results are summarized in Table 3.1.

Table 3.1 - Antibacterial activity of chelators (MIC). MICs for bacteria were determined in Iso-Sensitest broth after 24 h of incubation at 37ºC, according to the standard micro-dilution technique and with visual inspection of bacterial growth [335].

	Gram-negative bacteria			**Gram-positive bacteria**	
Tested compound	***E. coli* ATCC 25922**	***Klebsiela pneumoniae ATCC 13883***	***P. aeruginosa***	***S. aureus* ATCC 25923**	***S. epidermis ATCC 12228***
MRB7	> 0.133	> 0.126	> 0.147	0.133	> 0.171
MRB8	> 0.130	> 0.130	> 0.147	0.130	0.171
MRB9	> 0.125	> 0.125	> 0.125	0.125	0.063
MRB2	> 0.126	-	-	> 0.126	-
MRB20	0.034	-	-	0.016	-
MRH7	0.063	> 0.127	> 0.147	0.016	0.086
MRH8	> 0.136	> 0.136	> 0.147	0.068	0.147
MRH10	> 0.126	> 0.126	> 0.126	0.063	0.016
Hdmpp	> 0.255	> 0.255	> 0.255	> 0.255	> 0.255
CP256	> 0.130	> 0.130	> 0.130	> 0.130	0.130

The antibacterial effect of the chelators **MRH7**, **MRH8**, **MRH10**, **MRB7**, **MRB8**, **MRB9** and **MRB20** was tested and compared with the effect with the non-functionalized hexadentate and bidentate chelating units, **CP256** and **Hdmpp**, respectively.

The results have shown that the majority the fluorescent hexadentate chelators have higher activity against Gram-positive bacteria than against Gram-negative bacteria, with the exception of **MRH7** and **MRB20**, which were effective against both Gram-negative (*E. coli*) and positive bacteria.

Amongst the bidentate chelators, only **MRB20** has shown antibacterial activity against extracellular bacteria, for both Gram-negative and positive bacterial types. However, this chelator seems to be more active against Gram-positive bacteria, namely *S. aureus*. As this ligand differs from the other bidentate ligands tested in the global charge (positive for **MRB20**), we hypothesize that the presence of charge contributes to the toxicity of this chelator for BMM (as discussed in Chapter 3 and 5) although this property seems to be

relevant for the activity against extracellular Gram-positive bacteria, probably by the higher ability to cross or to interact with the bacterial membrane.

Comparing the fluorescent hexadentate ligands (**MRH7**, **MRH8** and **MRH10**), the most active hexadentate chelator against *S. aureus* was **MRH7** and the effect of the other two hexadentate fluorescent ligands is similar against this bacteria.
The present results have also demonstrated that the chelator **MRH10** showed highest activity against *S. epidermidis,* followed by **MRH7** and **MRH8**.
MRH8 (not containing thiourea group) have shown the lowest activity against the bacteria in study.

Most important, the relevance of the presence of the thiourea linkage in the structure of the chelators for their activity against extracellular bacteria has also been confirmed.

As previously found in experiments with *M. avium*, the non-functionalized chelating units, **CP256** and **Hdmpp**, were not active against the extracellular bacteria studied, suggesting that the chelating property *per se* is not sufficient, reinforcing the importance of the contribution of a lipophilic component, namely the rhodamine moiety, in the entire structure of the chelator.

The higher antibacterial effect demonstrated for Gram-positive bacteria may be related with the differences in the organization of the bacterial cell wall and the different ability of the chelators to interact with the bacterial membranes.
In one hand, Gram-negative bacteria may be less accessible for the penetration of the chelators as this type of bacteria possesses an inner cytoplasmic cell membrane, a cell wall with a thin peptidoglycan layer and a more complex external membrane, limiting the permeation of the drugs. On the other hand, the composition of the cell envelope in Gram-positive bacteria are less complex and is constituted by a cytoplasmic membrane and a thick peptidoglycan layer in the cell wall, leading to an easier barrier to cross and thus facilitating the permeation of the chelators.

More insights about this effect was obtained with studies concerning on the correlation of the presence of diverse functional groups in the structure of the chelators and their interaction with membrane models (as referred in Chapter 4 and reference [272]). Those results indicative that the presence of a thiourea link and ethyl groups in the structure of the chelators seem to improve the interaction of these ligands with the liposome surface and their ability to penetrate deeper into the non-polar region of the lipid bilayer.

These results reinforce the importance the rhodamine framework and the advantage of the presence of the thiourea linkage in the structure of the chelators for their activity against extracellular bacteria, as verified in the investigations about the effect of these ligands to fight *M. avium* intramacrophagic infection [4, 276].
The importance of the lipophilicity seems to be not as relevant as for the activity of the ligands against *M. avium*, as the chelators with the thiourea link (even with *N*-ethyl groups or *N*-methyl groups, **MRH7** and **MRH10**, respectively) seem to be more effective as antibacterial agents than those with amide linkage.

As a final remark, we would like to highlight that the present results improve our knowledge about SAR and are relevant for the design of novel molecular architectures to be considered as promising drugs to fight infections caused by these families of bacterial species.

4 | INTERACTION OF 3,4-HPO CHELATORS WITH BIOLOGICAL MEMBRANES

4. INTERACTION OF 3,4-HPO CHELATORS WITH BIOLOGICAL MEMBRANES

4.1 Introduction

Drug-membrane interactions have enormous importance in drug design processes and the understanding of these interactions at a molecular level allows the development of more effective antibiotics with higher intrinsic activity and higher capacity to reach their targets [327, 336, 337]. Even when the drug's target is not the lipid bilayer of the cell membrane or is not located in a membrane structure, such as receptors or transporters, drugs have to interact or cross the cellular membrane in order to reach their targets [338]. In the context of *M. avium* infection, the ability of drugs to interact with and cross barriers is particularly important because *M. avium* is a facultative intracellular pathogen that resides in mammalian cells, such as macrophages, where bacteria are confined inside phagosomes. Moreover, the complex composition of the cell wall of these pathogens is an additional obstacle to the permeation of antibiotics (referred in [89]). Thus, it is of extreme importance the study of the interaction of parental chelators with the membrane and how this phenomenon is related with antimycobacterial effect.

Several examples are reported in the literature, in which membrane interactions are suggested as part of the activity of different antimicrobials such as anti-parasite, antifungal and antibacterial drugs, namely fluoroquinolones and macrolides (see [336] for a review). Distinctive interactions of fluoroquinolones with membranes are correlated with their efflux from bacteria. In the case of macrolides, their toxicity seems to be associated with the effects that macrolides produce in the membrane. Other examples of the importance of drug membrane interactions are also reported for other classes of drugs such as anti-inflammatory, cardiovascular, antipsychotic, anticancer, anticonvulsive and anaesthetics, as reviewed in [336].

The studies referred above have shown how the interactions between the drug and the membrane of the cell (or membrane models) can change different membrane properties and that these interactions can favour the pharmaceutical activity of the drug itself.

In studies regarding the inhibitory effect of several 3,4-HPO chelators on intracellular growth of *M. avium*, the results have shown that the chelation of iron is a determinant although not sufficient property for antimicrobial activity [1]. Also, the biological activity seems to be

related with the fluorophore structure, where **MRH7**/ **MRB7** are more effective than **MRH8**/ **MRB8**, pointing out the importance of the HLB in the final structure of the chelators [4].
Together with other reports in the literature [339, 340] where the authors demonstrated the importance of the fluorophore in the structure of rhodamine B conjugated peptides for their interaction with the membrane, we hypothesized that rhodamine B potentiates the effect of the iron chelators by enhancing their ability to cross the membranes and reach the phagosome.

Comparative studies of the partition and distribution of fluorescein or rhodamine derived chelators have been previously performed by our research group, in liposomes and macrophages. The latter have provided evidence that compounds with higher biological activity interact strongly with lipid phases and cross cell membranes while the less-active do not [3].

Considering that the knowledge about permeation of drugs across a lipid bilayer is crucial to understand the mechanism of action of drugs and is a significant contribution to the development of new bioactive molecules, we further explored the interaction of the chelators with model membranes. We selected a set of four chelators, **MRH7**, **MRB7**, **MRH8** and **MRB8** to be studied.

Drug membrane interactions were assessed through spectroscopic technics such as Fluorescence, NMR and EPR spectroscopies. Fluorescence confocal microscopy was also used to map the cellular distribution of fluorescent chelators inside bone marrow derived macrophages and its compartments. To get insight on the chelators's uptake by the cells, fluorescence confocal microscopy studies were also performed with peripheral blood mononuclear cells (PBMCs).
The combined use of several methodologies allows correlation of the structure of the chelators with their different affinity for lipid phases and their distribution inside the cells. This knowledge is crucial to understand if these properties are relevant for the access of chelators to their targets and to the future design of novel iron chelators with improved antibacterial activity.

The experiments concerning the intracellular distribution studies of fluorescent chelators in BMM and PBMCs were performed at "IBMC - Instituto de Biologia Molecular e Celular". The studies with macrophages were part of the collaboration with the group of Professor Maria Salomé Gomes, III - Iron and Innate Immunity. The experiments with PBMCs were

performed in the group of Professor Graça Porto, BCRIB - Basic & Clinical Research on Iron Biology.

As a complementary approach to investigate the interaction of the chelators with model membranes, Molecular Dynamics (MD) simulations were performed and the results obtained in the studies for chelators **MRB7**, **MRB8** and **MRH7** are also discussed in the conclusions of this chapter (Chapter 4.4).
Computational studies were performed by Theoretical Biochemistry group of Professor Maria João Ramos and Professor Pedro Fernandes.

The computational and NMR studies performed are published in:

[272] Coimbra, J.T.S.[#], **Moniz, T.**[#], Brás, N.F.[#], Ivanova, G.[#], Fernandes, P.A., Ramos, M.J. and Rangel, M., *Relevant Interactions of Antimicrobial Iron Chelators and Membrane Models Revealed by Nuclear Magnetic Resonance and Molecular Dynamics Simulations*, The Journal of Physical Chemistry B, **2014**, *118*, 14590−14601. ([#]These authors contributed the same.)

Moniz, T., de Castro, B., Rangel, M. and Ivanova**,** G., *NMR study of the interaction of fluorescent 3-hydroxy-4-pyridinone chelators with DMPC liposomes*, Physical Chemistry Chemical Physics, **2016**, accepted manuscript.

4.2 Methods

4.2.1 Chemicals and instrumentation

Chemicals were obtained from Sigma–Aldrich (grade puriss, p.a.) or Fluka (p.a.) and were used as received unless otherwise specified.
The lipids 1,2-dimyristoyl-*sn*-glycero-3-phosphocholine (DMPC) and 1,2-dimyristoyl-*sn*-glycero-3-phospho-(1'-rac-glycerol) (sodium salt) (DMPG) were purchased from Avanti Polar Lipids (Alabaster, AL, USA). 1,6-Diphenyl-1,3,5-hexatriene (DPH) and trimethylammoniumdiphenylhexatriene (TMA-DPH) were purchased from Sigma and Fluka, respectively. 5- doxyl-stearic acid (5-DSA, free radical) and 16-doxyl-stearic acid (16-DSA, free radical) were all purchased from Sigma.
NMR experiments were recorded on a Bruker Avance III 600 HD spectrometer, operating at 600.13 MHz for ^{1}H, equipped with 5 mm CryoProbe Prodigy and pulse gradient units,

capable of producing magnetic field pulsed gradients in the z-direction of 50 G cm^{-1}. Electron paramagnetic resonance (EPR) spectra were measured on a Bruker ELEXSYS E 500 equipped with a variable temperature unit controller ER 4B1 VT.
Fluorescence measurements were performed in a Varian Cary Eclipse spectrofluorometer, equipped with a constant temperature cell holder (Peltier Multicell Holder, Cary Temperature Probe series II). To minimize reabsorption effects, the absorbance's sample values were kept below 0.1.

4.2.2 Liposome preparation

As membrane models, we used DMPC, which is a zwitterionic phospholipid, as mammalian cell membrane model and DMPG, an anionic phospholipid, was selected due to its abundance in bacterial cell membranes [341, 342].

Liposomes were prepared by evaporation to dryness with a stream of nitrogen of a lipid solution in chloroform in case of DMPC or in mixture of chloroform/ methanol (1:1) for DMPG [3]. The films were maintained under a vacuum, for a minimum of 4 h to remove all traces of organic solvents. The resulting dried lipid films were dispersed with MOPS buffer and the mixture was vortexed above the phase-transition temperature (37 ± 0.1ºC) to produce multilamellar liposomes (MLVs). The multilamellar liposomes were then subjected five times to the following procedure: freeze vesicles in liquid nitrogen and then warm in a water bath at 37 ± 0.1 ºC. Lipid suspensions were equilibrated at 37 ± 0.1 ºC for 30 min and extruded ten times through polycarbonate filters (100 nm) to produce large unilamellar vesicles (LUVs). Extrusion of liposomes was performed with a Lipex Biomembranes (Vancouver, Canada) extruder attached to a circulating water bath. The size distribution of extruded DMPC or DMPG liposomes was determined by dynamic light scattering (DLS) analysis using a Malvern Instruments Zetasizer nano ZS.

For steady state anisotropy studies, stock solutions of DPH or TMA-DPH (in methanol) were codissolved in the lipids solution and mixed. Then, the mixture was dried to form the lipid films. The molar ratios of DPH:lipid and TMA-DPH:lipid were 1:300 (mol:mol) [343-345].

For NMR studies, liposomes were prepared as described above in general protocol, although the resulting dried lipid film was dispersed with D_2O (≈ 20 mM), instead of using MOPS buffer.

For EPR studies, spin-labelled liposomes were also prepared as described for fluorescence studies with a slightly difference in the initial step, where the lipid was codissolved with the

spin labels (5-DSA or 16-DSA) (from a stock solution in methanol) in the ratio 1:100 (mol:mol) of spin label:lipid [343].

4.2.3 Fluorescence spectroscopy

4.2.3.1 Partition constants (Kp)

The effect of the liposomes on the fluorescence intensity of the chelators was different according to the type of fluorophore used. A fluorescence enhancement was observed for chelators **MRH7** and **MRB7** while a fluorescence quenching was found for chelators **MRH8** and **MRB8**. As a consequence, two different equations were used to calculate the values of the corresponding Partition Constants (*K*p).
For **MRH7** and **MRB7**, *K*p values for the liposome distribution of chelators were determined using the equation:

$$\Delta I = \frac{\Delta I_{max}\,[lipid]}{\frac{1}{K_p \gamma} + [lipid]}$$

in which *I* is the fluorescence intensity of the fluorophore in the presence of lipid vesicles and I_0 is the fluorescence intensity in its absence, $\Delta I = I - I_0$, $\Delta I_{max} = I_\infty - I_0$ is the maximum difference in fluorescence intensity, I_∞ represents the limiting value of *I*, and γ is the molar volume of the lipid [337].

For **MRH8** and **MRB8** data were analysed considering the Stern–Volmer equation [337, 346]:

$$\frac{I_0}{I} = 1 + K_{SV}\,[Q]$$

In this equation, I_0 and *I* are the fluorescence intensities in the absence and presence of the liposome suspension (the quencher), respectively; K_{SV} is the the Stern–Volmer constant; [Q] is the concentration of the liposome suspension.
Fluorescent chelators were added to suspensions with increasing concentrations of these liposomes, by dilution of the appropriate amount of DMSO stock solutions of chelators in the liposome suspensions to give a final concentration of 3 μM of chelator.
Samples were prepared by adding a known volume of chelator, a suitable aliquot of vesicle suspension (LUVs) and MOPS, whereas the corresponding references were prepared in an

identical manner but without the chelator (final volume of 1.5 ml). All suspensions were then vortexed for 2 min and incubated at 37 °C for 2h. Three sets of samples were used in each experiment. Experiments were performed according to the methods described [3, 345].

4.2.3.2 Steady state anisotropy

The structural order of a lipid membrane system in interaction with fluorescent chelators was investigated by measuring, as a function of temperature, the steady-state fluorescence anisotropy (r_s) of DPH and TMA-DPH incorporated into DMPC or DMPG liposomes. Fluorescent chelators were added to these liposomes by dilution of the appropriate amount of DMSO stock solutions of chelators in the liposome suspensions (2mM) to give a final concentration of 3 μM of chelator. MOPS buffer 0.1M NaCl, pH 7.4 was used to adjust the samples to the final volume (1.5 ml). After addition of chelators into the liposome suspension, the mixtures were vortexed. The suspensions of liposomes were mixed with TMA-DPH or DPH for 30 min. The corresponding references were prepared in an identical manner but without the chelator.
The steady-state fluorescent anisotropy was recorded at 2 - 4 ºC intervals for all studied systems, using both probes, in the range of temperature from 0 to 40 ºC. Samples were left to stabilize during five minutes at each temperature. The excitation and emission wavelengths used were 355/426 and 336/427 nm for TMA-DPH and DPH, respectively. Three independent experiments, for each system, were made. Fluorescence anisotropy experiments were performed according to the methods described [344, 345].

The steady state fluorescence anisotropy (r_s) [347] is defined by the following equation:

$$r_s = \frac{I_{VV} - I_{VH}G}{I_{VV} + 2I_{VH}G}$$

where I_{VV} and I_{VH} are the intensities measured in directions parallel and perpendicular to the excitation beam, respectively. The correction factor G is the ratio of the detection system sensitivity for vertically and horizontally polarized light, which is given by the ratio of vertical to horizontal components when the excitation light is polarized in the horizontal direction [347]:

$$G = I_{HV} / I_{HH}$$

The following equation was fitted to the anisotropy versus temperature data:

$$r_s = r_{s2} + \frac{r_{s1} - r_{s2}}{1 + 10^{B'\left(\frac{T}{T_m} - 1\right)}}$$

where T is the absolute temperature; T_m is the midpoint phase transition; and r_{s1} and r_{s2} are the upper and lower values of r_s. B' is the slope factor which is correlated with the extent of cooperativity (B) by B = [1 1/(1 + B')]; the introduction of B yields a convenient scale of cooperativity ranging from 0 to 1 [348].

4.2.4 Magnetic resonance spectroscopy

4.2.4.1 NMR studies

Chelator/Liposome Mixtures for NMR studies

Stock solutions of compounds **MRB7** and **MRB8** were obtained by preparing a solution of the compound in dimethylsulfoxide (DMSO-d_6). For the preparation of NMR samples, 15µL of the chelator stock solution was added to the DMPC liposome suspension (2×10^{-2} M) to lead to a final concentration in the samples of 3×10^{-3} or 3×10^{-5} M, respectively for the studies at high (*) and low concentration conditions. The choice of this concentration and molecular ratio for the “low concentration conditions” was based on the concentration of chelator used for studies with other techniques, namely fluorescence and EPR studies. Higher concentration conditions have been also studied in order to follow the NMR parameters of the chelators.

After addition of the chelator solution to the liposome suspension, the mixtures were mixed for 5 min producing the samples labelled as DMPC-MRB7*(2×10^{-2} M : 3×10^{-3} M), DPMC-MRB8*(2×10^{-2} M : 3×10^{-3} M), DMPC-MRB7(2×10^{-2} M : 3×10^{-5} M) and DMPC-MRB8(2×10^{-2} M : 3×10^{-5} M).

In **MRB8** experiments, at 60h, a small amount of $SmCl_3$ (~1 mg) was added to the mixture in order to induce significant chemical shift on choline signals.

NMR spectroscopy measurements

Before starting the NMR experiments, the temperature was stabilized and kept at 310 K, as measured using the spectrometer thermocouple system.

The NMR measurements were carried out in deuterium oxide (D_2O), at 310 K and spectral width of 10000 Hz. ^{1}H NMR experiments were performed with water suppression using

excitation sculpting with gradients [349]. Chemical shifts of the ^{1}H NMR signals were obtained by referring to the absorption frequency of the deuterated solvent monitored as the lock signal and further scaled to the resonance frequency of DMSO- d_6 added in equal amount (15 μL) to all samples.
Typically, in each experiment a number of 16 spectra of 16K data points and 64 scans were collected. The pulse gradient (g) was incremented from 2 to 98% of the maximum gradient strength in a linear ramp. The spectra were processed with the Bruker Topspin software package (version 3.2). For each sample at least two independent assays were performed, using freshly prepared liposomes.

4.2.4.2 EPR studies

Chelator/Liposome Mixtures for EPR studies

To the lipid suspension (1.5 mL, 2 mM), the appropriated amount of chelator was added in order to get a 3 μM concentration. The mixtures were incubated for 2h at 37 °C in order to allow the chelator–vesicle interaction, before recording the spectra [343].

Spectra were acquired at 37 °C (310K) using a central field of 3360 G, a sweep width of 100 G and a modulation frequency of 100k Hz. A microwave power of 5 mW was used and 5 or 10 scans recorded for 16-DSA or 5-DSA probe, respectively, with a modulation amplitude of 4 G, 60dB of gain and a time constant of 100 s or 200s for 16-DSA or 5-DSA probe, respectively. Three independent experiments, for each system, were performed.

In the EPR spectrum of 5-DSA incorporated into the lipid membranes, the fluidity of the membrane can be estimated from the outermost separation between the spectral extremes, the maximum hyperfine splitting ($2A_{max}$) (Figure 4.1). This value reflects the rotational motion freedom of the phospholipids close to the polar head group in the bilayer, which increases with the decrease in fluidity [350].

The rotation correlation time (τ) is the parameter that can be obtained from the EPR spectrum of the 16-DSA incorporated in the lipid bilayer and reflects the motion of the probe, which is also an indication of the fluidity of the membrane. This parameter is calculated using the equation:

$$\tau(s) = 6.5 \times 10^{-10}\, W_0 \left[\left(\frac{h_0}{h_{-1}} \right)^{0.5} - 1 \right]$$

where W_0 is the midfield line width and h_0 and h_{-1} are the mid- and high-field line amplitudes (Figure 4.1), and τ increases with the decrease in fluidity [343, 350].

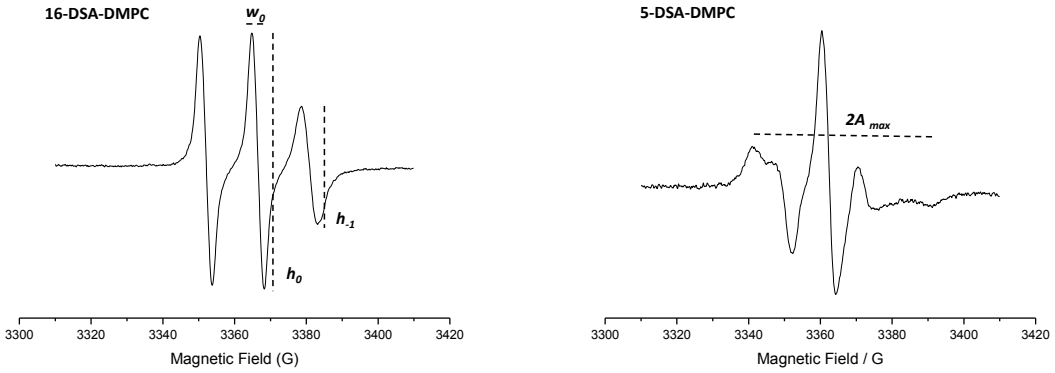

Figure 4.1 – Representation of W_0, h_0 e h_{-1} (left) and $2A_{max}$, in representative EPR spectra of 16-DSA and 5-DSA in DMPC liposomes, respectively. Adapted from [343].

4.2.5 Intracellular distribution of fluorescent chelators in BMM and PBMCs

4.2.5.1. Bacteria

M. avium 104:pMV306 (hsp60/gfp) expressing green fluorescent protein (*M. avium*-GFP) was used in confocal microscopy experiments [351]. Mycobacteria were grown to mid-log phase in Middlebrook 7H9 medium (Difco, Sparks, MD) containing 0.04% V/V of Tween 80 (Sigma, St. Louis, MO) at 37ºC. Bacteria were harvested by centrifugation, suspended in a small volume of saline containing 0.04% V/V of Tween 80 (Sigma) and briefly sonicated in order to disrupt bacterial clumps. The suspension was diluted and stored in aliquots at -80ºC until use.

4.2.5.2 Bone marrow derived macrophages (BMM)

Macrophages were derived from the bone marrow of BALB/c mice. Each femur was flushed with 5 mL of HBSS (Life Technologies, Paisley, U.K.). The resulting cell suspension was centrifuged and the cells re-suspended in DMEM (Life Technologies, Paisley, U.K.) supplemented with 10 mM glutamine, 10 mM HEPES, 1 mM sodium pyruvate, 10% FBS (Fetal Bovine Serum) (Life Technologies), and 10% of LCCM as a source of Macrophage colony stimulating factor (M-CSF). According to manufacturer's information, the iron (Fe(III)) content of DMEM is 0.25 mM. The added FBS contributes an additional 3 mM of iron. In

order to remove fibroblasts, the cells were cultured overnight, at 37ºC in a 7% CO_2 atmosphere, on a cell culture dish. The non-adherent cells were collected with warm HBSS medium, washed and resuspended in DMEM with 10% LCCM at a cell density of 10^5 cells/ml. 300 µL of this cell suspension was distributed per well in µ-Slide 8 well plates (IBIDI) which were incubated at 37ºC in a 7% CO_2 atmosphere. Three days later, 30 µL of LCCM was added. On the 7th day of culture, the medium was renewed [4].

4.2.5.3 Isolation of human peripheral blood cells (PBMCs)

PBMCs were obtained from apparently healthy volunteer blood donors, randomly recruited at "Hospital de Santo António" Blood Bank (Porto, Portugal) who gave their consent to participate in this study, approved by the "Hospital de Santo António" Ethical Committee. The blood was diluted (1:2) with PBS and cells were isolated by gradient centrifugation over Lymphoprep (Nycomed). After the first centrifugation, the buffy coat was collected and diluted with PBS. After the lysis of erythrocytes and the remove of the platelets, cells were resuspended in RPMI (GibcoBRL) supplemented with 10% fetal calf serum (FCS; GibcoBRL) and incubated at 37ºC in a 5% CO_2 atmosphere overnight, according to the methods described in the literature [352]. In the next day, cells were resuspended in RPMI (GibcoBRL) for visualization under the microscope.

4.2.5.4 Confocal microscopy of BMM

For live cell imaging of intracellular probe distribution, BMM were plated onto µ-Slide 8 well plates (IBIDI) at 10^5 cells/mL and visualized on the 14^{th} day of culture. For late endosomal labelling, fluorescein-conjugated dextran (10,000 MW) (Invitrogen) was added at 100 µg/ mL for 4 h and subsequently chased overnight with cell medium. For phagosomal labelling, cells were incubated with fluorescein-conjugated Zymosan A *S. cerevisiae* BioParticles (Invitrogen) or fluorescent Latex beads (amine-modified polystyrene, 2µm) (Sigma) (30 particles/cell) for 20 min or 3h, respectively, subsequently washed with PBS and the cell medium was replaced.

For imaging mycobacteria, BMM were infected on the 10^{th} day of culture (4 days before imaging) with *M. avium*-GFP (10^6 CFU/mL) for 4h and then the cells were washed with HBSS and the medium was replaced with DMEM 10% LCCM, according to the protocol described in previous work [4]. As a control group, other BMM were infected with *M. avium* 2447 (10^6 CFU/mL) in the same experimental conditions and no differences were obtained in the distribution of chelators in non-infected BMM (data not shown). For golgi labelling, CellLight Golgi-GFP, BacMam 2.0 (Invitrogen) was added (20 particles/cell) and incubated

overnight. All chelators tested were incubated for 20 min (5 µM of **MRH7** or **MRB7** or 30 µM of **MRH8** or **MRB8**) in the BMM culture. Simultaneously to the addition of the chelators, fluorescein-conjugated dextran (100 µg/ mL), MitoTracker Green FM (Invitrogen) (100 nM) or ER-Tracker Green (Invitrogen) (1 µM) were added for early endosome, mitochondria or endoplasmic reticulum (ER) labelling, respectively. Cells were washed with cold PBS and resuspended in RPMI medium (no phenol red) (Life Technologies, Paisley, U.K.). Macrophages were observed and photographed in a Laser Scanning Confocal Microscope Leica TCS SP5II (Laser Microsystems, Germany) with the 40x water objective.

4.2.5.5 Confocal microscopy of PBMCs

The number of cells were estimated and the cells were plated onto 15 mL falcons at 10^5 cells/mL, in RPMI medium. All chelators tested were added and incubated for 20 min (5 µM of **MRH7** or **MRB7** or 30 µM of **MRH8** or **MRB8**) in cell culture medium, based on the concentrations optimized in the experiments with BMM. Cells were washed with cold PBS and resuspended in RPMI medium (no phenol red). For live cell imaging of intracellular distribution of the chelators, PBMCs were transferred to µ-Slide 8 well plates (IBIDI) and cells were observed and photographed in a Laser Scanning Confocal Microscope Leica TCS SP5II (Laser Microsystems, Germany) with the 40x water objective.

4.3 Results and Discussion

4.3.1 Fluorescence spectroscopy

4.3.1.1 Partition constants (K_p)

In order to investigate the relation between the antimycobacterial activity and the affinity for (liposome) membranes, partition studies were performed using, liposome suspensions of DMPC and DMPG lipids (Figure 4.2) as membrane models.

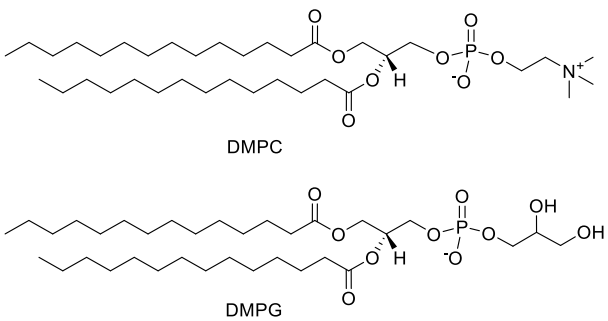

Figure 4.2 – Formulae of DMPC and DMPG lipids used for the preparation of liposomes.

The value of K_p is an indication of the interaction of the compound with the membranes and reflects the preference of the ligands for the lipid or the aqueous phase. The values are obtained by measuring and analysing the changes in the fluorescence intensity of the fluorescent molecule (chelators) upon being incubated with liposome suspensions of increasing concentrations.

The partition constants (Table 4.1) of chelators **MRB7**, **MRH8**, **MRB8** in DMPC and DMPG suspensions were determined as described previously for **MRH7** [3, 345]. In Figure 4.3 a representative fluorescent intensity spectra and a fitting of fluorescence intensity parameters are shown for **MRB7** in the presence of DMPG and for **MRB8** in the presence of DMPC.

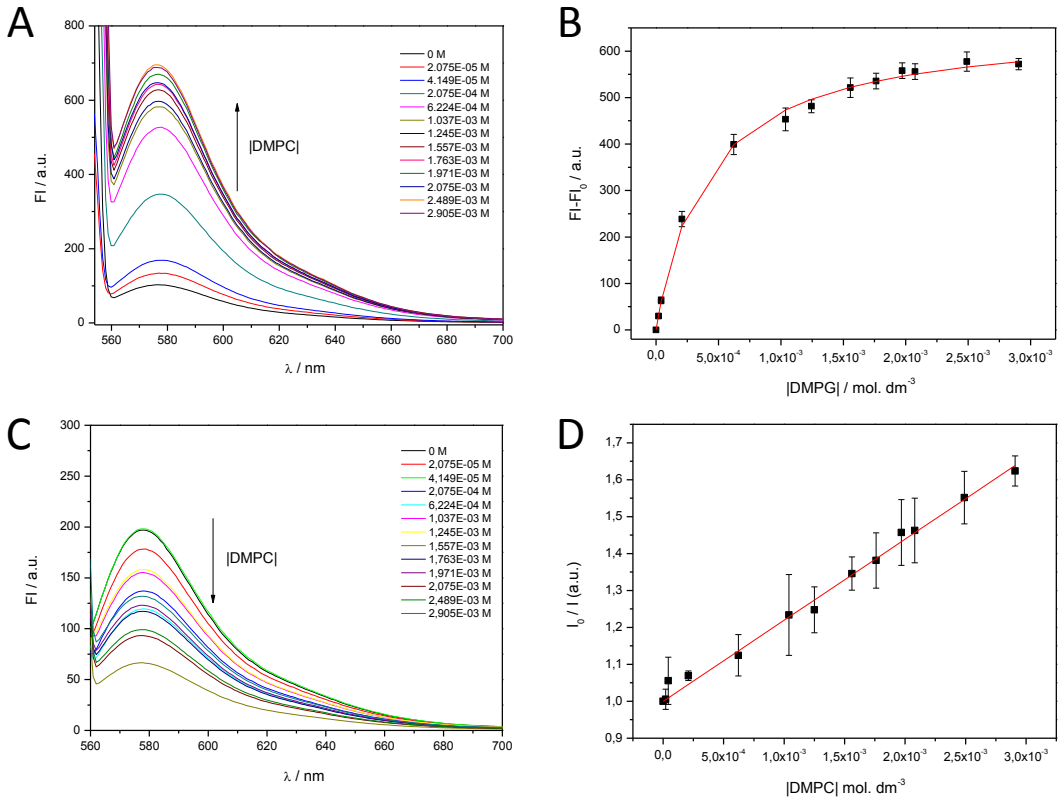

Figure 4.3 – Representative spectra of the fluorescence intensity (FI) observed for chelators **MRB7** (A) and **MRB8** (C) in the presence of suspensions of DMPG and DMPC liposomes, respectively, prepared with lipid concentrations described in the figures; Fitting of fluorescence intensity parameters of chelators **MRB7** (B) and **MRB8** (D) in the presence of suspensions of DMPG and DMPC liposomes, respectively, at the different concentrations indicated. *I* and I_0 are the fluorescence intensity (*F*) of the chelator in the presence or absence of liposomes, respectively.

Table 4.1 – *K*p and K_{SV} calculated for the fluorescent chelators **MRH7**, **MRB7**, **MRH8**, and **MRB8** in DMPC and DMPG liposomes suspensions.

		MRH7	**MRB7**		**MRH8**	**MRB8**
DMPC	K_p	5848 ± 906 [3]	2586 ± 300	K_p	268 ± 8	327 ± 5
				K_{SV}	177 ± 8	216 ± 5
DMPG	K_p	6144 ± 316 [3]	4784 ± 322	K_p	225 ± 10	1231 ± 34
				K_{SV}	117 ± 10	639 ± 34

For the rhodamine isothiocyanate labelled chelator (**MRB7**) the fluorescence intensity is enhanced with the increase of liposome concentration, in the presence of DMPC and DMPG liposomes. The fluorescence intensity enhancement is related with the interaction of **MRB7** with the phospholipid membrane of the liposomes.

The values of K_p obtained for **MRB7** are lower than those obtained for **MRH7** [3] nonetheless those values are in the same magnitude, in both DMPC and DMPG suspensions. Comparing the K_p values obtained for DMPC *vs* DMPG, the value was higher for the latter liposome suspension and this evidence was also verified for **MRH7** [3].
In studies concerning the interaction of carboxy-rhodamine derived chelators (**MRH8** and **MRB8**) with membranes, the fluorescence intensity is quenched by increasing the liposome concentration, in both DMPC and DMPG suspensions (Fig. 4.3 B and D).
This result is consistent with that described for the interaction of rhodamine B with cyclodextrins, in which an enhancement or a quenching of the fluorescence intensity is observed, according to the different part of the rhodamine B moiety that is included in the cyclodextrins [353].

Due to the different data obtained for **MRB7** vs **MRH8** and **MRB8**, the equation used for **MRB7** (the same used for **MRH7**) is not the adequate for fitting the results obtained for these chelators, and thus other equation was used to calculate the K_p values. As a quenching of the fluorescence intensity is observed and the data fit a linear equation, to calculate the partition constant for **MRH8** and **MRB8,** the Stern–Volmer equation was considered and a K_{SV} was determined.

However, in order to compare the values obtained for all chelators studied, the contribution of the volume fraction of membrane phase has to considered by correcting the value of K_{SV} with the molar volume (γ) of the lipid, according to the following equations:

$$\Delta I = \Delta I_{\infty} \cdot \frac{P \cdot [lipid]}{\frac{1}{\gamma_{lipid}} + P \cdot [lipid]} \quad \text{and} \quad \Delta I = \Delta I_{\infty} \cdot \frac{P'' \cdot [lipid]}{1 + P'' \cdot [lipid]}$$

If,

$$\Delta I_{\infty} \cdot \frac{P \cdot [lipid]}{\frac{1}{\gamma_{lipid}} + P \cdot [lipid]} = \Delta I_{\infty} \cdot \frac{P'' \cdot [lipid]}{1 + P'' \cdot [lipid]} \Leftrightarrow \frac{P \cdot [lipid]}{\frac{1}{\gamma_{lipid}} + P \cdot [lipid]} = \frac{P'' \cdot [lipid]}{1 + P'' \cdot [lipid]} \Leftrightarrow$$

$$\Leftrightarrow P \cdot [lipid] + P \cdot [lipid] * P'' \cdot [lipid] = \frac{1}{\gamma_{lipid}} * P'' \cdot [lipid] + P \cdot [lipid] * P'' \cdot [lipid] \Leftrightarrow$$

$$\Leftrightarrow P \cdot [lipid] = \frac{1}{\gamma_{lipid}} * P'' \cdot [lipid] \Leftrightarrow P'' \cdot [lipid] = \frac{1}{\gamma_{lipid}} * P \cdot [lipid]$$

Considering:

$P \cdot [lipid] = K_p$ and $P'' \cdot [lipid] = K_{SV}$:

$$K_p = \frac{K_{SV}}{\gamma}$$

The values obtained for chelators **MRH8** and **MRB8** were significantly lower than those obtained for rhodamine isothiocyanate derived chelators and these results evidence the relevance of the functional groups, namely the *N*-ethyl groups and the thiourea linkage, of the rhodamine moiety for the interaction with lipidic components.

4.3.1.2 Steady state anisotropy

In the steady state fluorescence anisotropy studies, two different fluorescent probes DPH (localized deeply in the bilayer) and TMA-DPH (localized near the lipid head groups) (Figure 4.4) were incorporated in DMPC or DMPG liposomes, according to the studies already performed for **MRH7** in previous work [345] and which will also be discussed in this section, for comparison with the results obtained.

The fluorescent chelators **MRB7**, **MRH8**, **MRB8** were incubated in liposome suspensions to allow ligand/liposome interactions (Table 4.2).

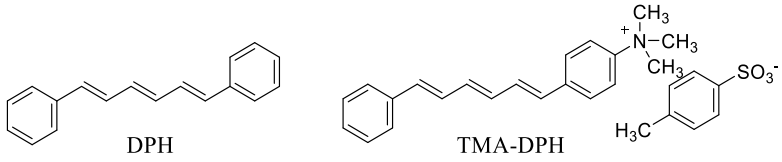

Figure 4.4 - Fluorescent probes used in steady state anisotropy studies.

Table 4.2 – T_m calculated for DMPC and DMPG liposomes suspensions in the presence and absence of the chelators.

		DPH	TMA-DPH
DMPC	**No chelator**	23.77 ± 0.19	24.01 ± 0.20
	MRH7	24.14± 0.19 [345]	23.84 ± 0.20 [345]
	MRB7	22.76 ± 0.25	23.43 ± 0.21
	MRH8	23.60 ± 0.28	23.57 ± 0.20
	MRB8	23.64 ± 0.21	23.56 ± 0.25
DMPG	**No chelator**	23.35 ± 0.19	23.91 ± 0.20
	MRH7	23.18 ± 0.19 [345]	26.91 ± 0.18 [345]
	MRB7	22.62 ± 0.20	22.42 ± 0.25
	MRH8	22.49 ± 0.21	22.39 ± 0.24
	MRB8	22.47 ± 0.20	22.51 ± 0.28

Considering the results obtained for the probe DPH incorporated in DMPC, there is no significant change in the T_m. The same results are obtained for the same liposome incorporated with TMA-DPH probe.

The results obtained for DMPG liposomes incorporated with DPH probe showed that the T_m remains the same in the presence of each chelator. The studies of DMPG liposomes labelled with TMA-DPH probe showed that in the presence of **MRB7**, **MRH8** and **MRB8** the T_m is not altered. However, in presence of **MRH7,** a slight increase in the value of T_m was verified and this fact can be related with the fluidity of the membrane induced by the interaction with the chelator.

According to the results obtained by this technique, only discrete interactions were verified which are justified by the existence of electrostatic interactions of **MRH7** with the polar heads of the lipids, as described for other drug-membrane interactions [343, 344, 354].

4.3.2 Magnetic resonance spectroscopy

4.3.2.1 NMR Studies

The affinity of **MRB7** and **MBR8** for the phospholipid bilayer of DMPC liposomes and the chelators permeation properties through the vesicles were estimated with basis on the induced alterations of a number of NMR parameters, such as chemical shifts and line shape, of the lipids and the liposomes.
For experimental reasons, the bidentate **MRB7** and **MRB8** were chosen to be studied by NMR. For NMR studies, DMPC liposomes were selected as a representative membrane model due to our previous knowledge obtained in previous work [344].

Two lipid:chelator molar ratios were used to study the dynamics and interaction of **MRB7** and **MRB8** with DMPC liposomes. Analyses have been performed for samples with the different molar ratios, as described in section 4.2.4.1. The molar ratio DMPC-chelator (2×10^{-2} M: 3×10^{-5} M) has been used for consistency with the concentrations used in the studies of the interaction with membranes performed with other techniques and also with the concentrations tested in the microbiology experiments. The higher molar ratio was used in order to allow for the minimum amount of chelator to generate NMR signals with appropriate intensity for measurements based on the chelators NMR spectra.

NMR studies were first carried out on “pure” DMPC liposome samples as a control and afterwards on samples prepared by incubation of **MRB7** or **MBR8** with DMPC liposomes, thus allowing the analysis of the changes in the chemical shifts induced by the presence of compounds **MRB7** or **MBR8**. NMR spectral analysis was carried out in the time range from 30 minutes to 48 or 60 hours after incubation of liposomes with the chelators.
The formulae and numbering of the fluorescent chelators under study in this work and of the lipid DMPC are depicted in Figure 4.5.

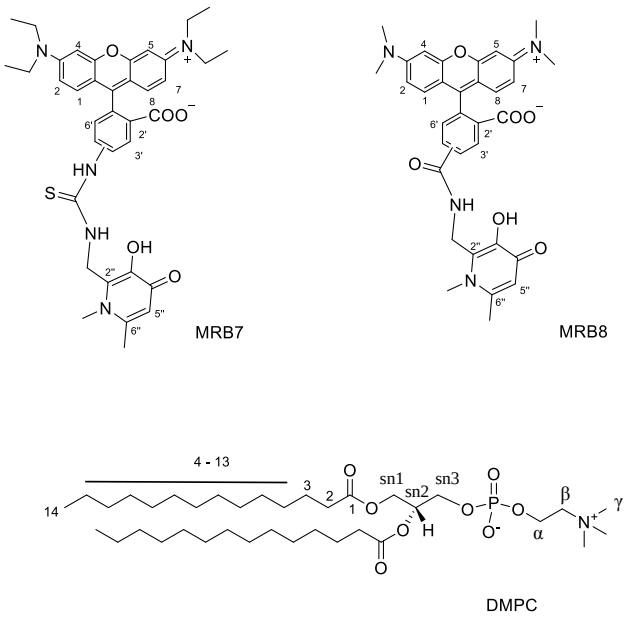

Figure 4.5 - Formulae and numbering of **MRB7** and **MRB8** chelators and of the lipid 1,2-dimyristoyl-*sn*-glycero-3-phosphocholine (DMPC).

Resonance signals belonging to **MRB7** and **MRB8** were registered only in the NMR spectra of DMPC-MRB7* and DMPC-MRB8* model systems due to their low concentrations in the diluted samples. Representative ^{1}H NMR spectra of DMPC-MRB7*, DMPC-MRB8* and DMPC liposomes in D_2O recorded at 37 °C are shown in Figure 4.6 with the assignment of characteristic resonance signals in the molecules.

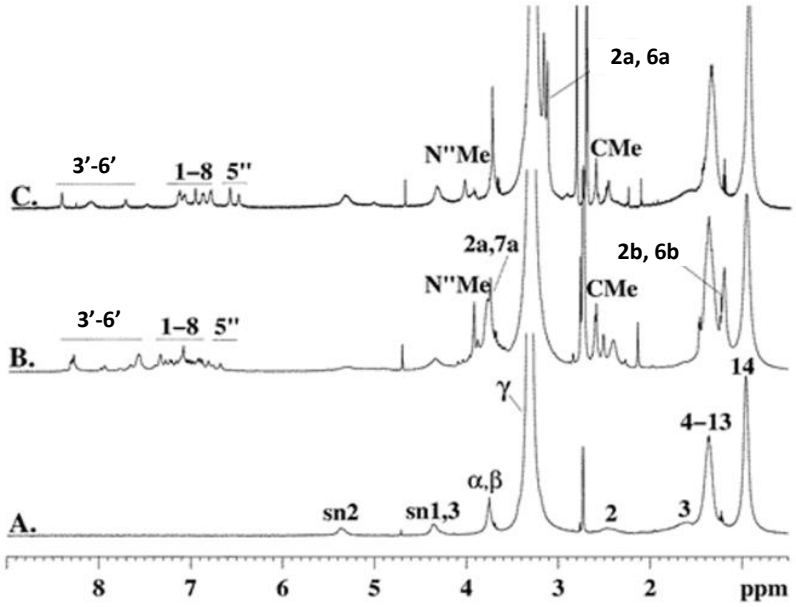

Figure 4.6 - 600.13 MHz 1H NMR spectra in D2O at 37 ºC of: A. DMPC liposomes; B. DMPC-MRB7* and C. DMPC-MRB8*.

For the studies performed at low concentration conditions, the chemical shift changes of the lipid resonances of protons (-CH_3 Choline (γ), -NCH_2 Choline (β), -CH_2 (4-13); -CH_3 (14) -OCH_2 (sn_1, sn_3), and -OCH (sn_2)) were observed and registered upon addition of **MRB7** and **MBR8**, for the time interval from 30 minutes to 48 hours. The values are summarized in the graphics in Figure 4.7 (A-F).

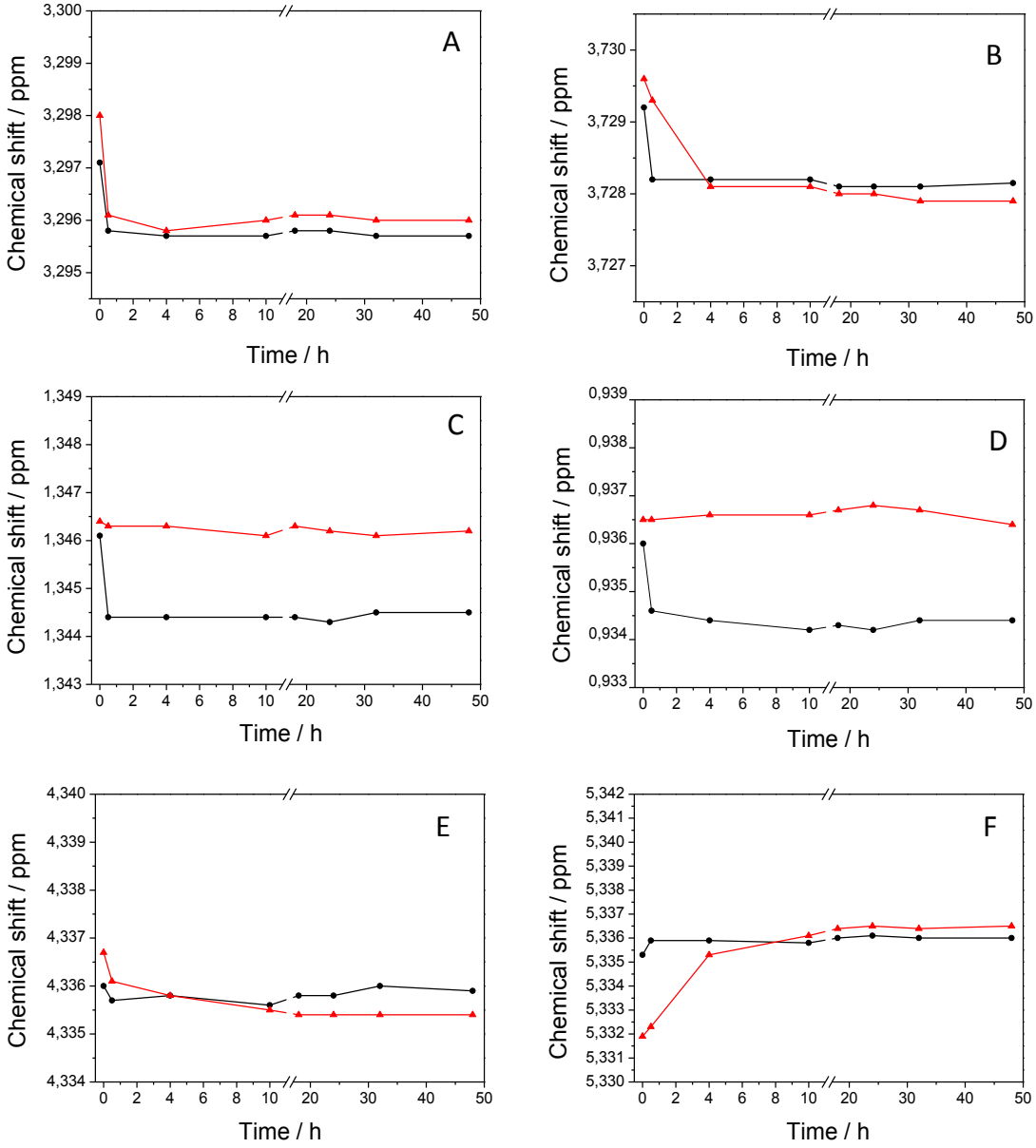

Figure 4.7 - Variation along time of the chemical shift values of protons of different groups in the lipid structure in the presence of **MRB7** (black circles) or **MRB8** (red triangles): (A) -CH_3 Choline (γ); (B) -NCH_2 Choline (β); (C) -CH_2 acyl chain (4-13); -CH_3 acyl chain (14); (E) – OCH_2 (sn 1, sn 3); and (F) -OCH (sn 2).

Upon 30 minutes of incubation of the liposomes with the chelators, the resonances of *N*-methyl (γ) and *N*-methylene (β) protons of the choline groups located at the liposome surface are up-field shifted in both DMPC-MRB7 and DMPC-MRB8 samples, in comparison with the spectra of the liposomes without chelators (Figure 4.7 - A and B). These chemical shift changes have shown the ability of both **MRB7** and **MBR8** molecules to interact with the hydrophilic surface of phospholipid bilayer. A significant drop is observed after 30 minutes upon incubation and the chemical shift value is not further altered in the time interval of the experiment. We believe that the electrostatic interactions between the local charges of the neutral **MRB7** or **MRB8** molecules and lipids at lipid-water interface play a dominant role in the molecular association to liposomes.

The changes in the resonances of the terminal protons of the acyl chains -CH_2 (4-13) and -CH_3 (14) (Figure 4.7- C and D) provide the most important difference between the permeation ability of chelators **MRB7** and **MRB8**. The addition of **MRB7** to the DMPC vesicles induces significant up-field shift of the resonance signals of the methyl and methylene protons of the hydrophobic chain region of the phospholipid bilayer in contrast with the addition of **MRB8** upon which no significant changes are observed in the chemical shifts of the protons -CH_2 (13) and -CH_3 (14). Again, a significant drop in the chemical shift value is observed after 30 minutes upon incubation and no further change was registered in the time interval of the experiment.
The chemical shift values of protons of the glycerol framework, -OCH_2 (sn_1, sn_3), -OCH (sn_2) suffer very small or no changes upon incubation of the liposomes with the chelators (Figure 4.7 - E and F).

The chemical shift changes observed for the protons associated with the different functional groups of the phospholipid can be related with a different distribution and location of **MRB7** and **MRB8** in the bilayer of DMPC liposome. The results suggest that chelator **MRB7** strongly interacts with the choline head groups at the surface of the liposome sphere and is able to permeate deeper and reach the centre of hydrophobic area of the phospholipid bilayer as demonstrated by the significant perturbations of the proton resonances induced on the terminal protons of the acyl chains located in that area, -CH_3 (14). In contrast, **MRB8** molecules strongly interact with the polar surface of liposomes and seem to be preferably trapped between the polar interface and ester groups of the lipid bilayer thus justifying the non-perturbation of the proton resonances belonging to the lipid acyl chains.

The above results obtained along a period of 48 hours suggest a bimodal distribution of **MRB7** in DMPC liposomes with some **MRB7** molecules located at the choline and some at the lipid acyl chains region while most **MRB8** molecules preferably occupy the surface of the liposome. Additionally, the induced chemical shift changes in ^{1}H NMR spectra of liposomes were found to occur in a shorter time interval in the presence of **MRB7** than **MRB8** and thus, the results also suggest a quicker intensity of **MRB7** to interact with the phospholipid bilayer of the DMPC liposomes.
The presence of *N*-ethyl groups in the xanthene framework and the thiourea linkage in the structure of **MRB7**, as opposed to *N*-methyl groups in the xanthene and an amide linkage in the structure of **MRB8**, seems to facilitate the interaction of **MRB7** molecules to the liposome surface and their ability to penetrate deeper into the hydrophobic interior of lipid bilayer. No further changes in ^{1}H NMR spectra of (DMPC-MRB7 and DMPC-MRB8) were registered up to 48 hours after incubation.

In the studies performed at high concentration conditions, the variation on the chemical shift, induced by the interaction with the chelators, was registered for the *N*-methyl (γ) choline, -CH_2 (4-13) and -CH_3 (14) protons of the lipid chains of liposomes and compared with the values for “pure” liposomes, measured at the same experimental conditions (time 0 h). The results obtained for are summarized in Figure 4.8.

The results demonstrate that the induced chemical shift alterations of liposome proton resonances depend not only on the presence of the chelator but also on the concentration. In the ^{1}H NMR spectra of DMPC-MRB7 (Figure 4.7, A, C, D) and DMPC-MRB7* (Figure 4.8, A*, B*, C*) up-field shift of the resonance signals of *N*-methyl (γ) choline, -CH_2 (4-13) and -CH_3 (14) protons of phospholipid chains was observed, where the effect was much stronger at higher **MRB7** concentration. A significant drop of the *N*-methyl (γ) choline chemical shift was observed instantly upon adding of **MRB7** with a further increase along the period between 6 and 12 hours and maintenance of the attained values up to 48 hours, as also verified for low concentration.

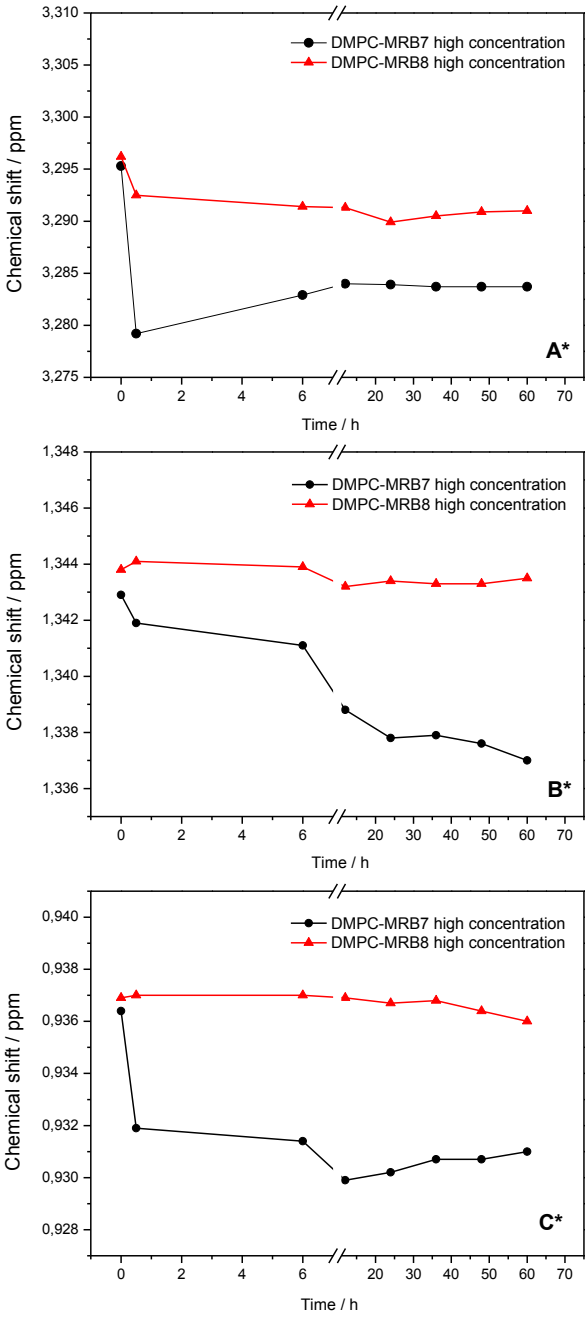

Figure 4.8 - Chemical shift of protons of the -CH_3 Choline (γ) (A*), -CH_2- acyl chain (4-13) (B*) and -CH_3 acyl chain (14) (C*) groups in DMPC structure in the presence of **MRB7** (black circles) or **MRB8** (red triangles), at high concentrations conditions.

The main alterations of -CH_2 (4-13) and -CH_3 (14) resonances registered in the experiments performed at low concentration conditions (Figure 4.7, C and D) was also verified for the high concentration conditions (Figure 4.8, B* and C*), corroborating the occurrence of an interaction of **MRB7** molecules with the choline head groups from the outer leaflet shortly after adding of the chelator and further penetration and interaction with the lipid acyl chains

from the interior of liposomes. In agreement with the results obtained for low concentration studies, through the time of the experiment, no change in the spectral line shape of the choline resonance was observed as a result of a preferred accumulation of **MRB7** molecules at the surface of liposomes. This could be an indication for the transport and crossing of **MRB7** molecules through the membrane, and ability for an interaction with the choline head groups from the inner layer of liposomes.

The analysis of the more concentrated samples provided additional information regarding the interaction of the chelator. In the ^{1}H NMR spectra of DMPC-MRB7* recorded in 36 hours, we observed in the region of the choline protons, the appearance of a narrow signal, slightly shifted towards higher magnetic field values (at 3.246 ppm), with a gradually increasing intensity along the time (Figure 4.9, left). A resonance signal with the same NMR characteristics was registered in NMR spectra of DMPC liposomes recorded before performing an extrusion procedure (Figure 4.10). Considering the specific line shape and chemical shift, the resonance signal at 3.246 ppm in the ^{1}H NMR spectra of DMPC-MRB7* was assigned to *N*-methyl (γ) choline protons of lipid acyl chains generated in the process of destruction of part of the DMPC vesicles in the presence of **MRB7** at high concentration [355, 356].

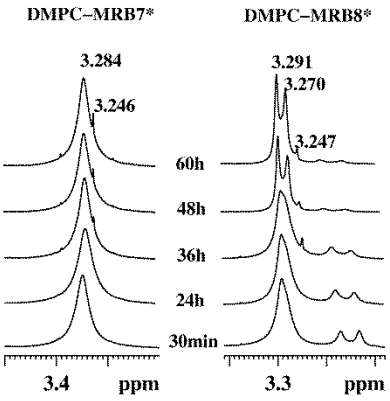

Figure 4.9 - Choline resonance signals in 600.13 MHz ^{1}H NMR spectra of DMPC-MRB7* (left) and DMPC-MRB8*(right), along the time of incubation with chelators.

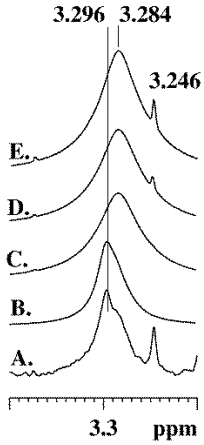

Figure 4.10 - Choline resonance signals in 600 MHz ^{1}H NMR spectra of DMPC liposomes before (A) and after extrusion, along the time of incubation with chelators (B-E).

The results obtained for **MRB8** at high concentration conditions are similar to those obtained in the experiments with low concentration of chelator and described above.

Additionally, the higher **MRB8** concentration used in these studies allow us to register, in the ^{1}H NMR spectra of DMPC-MRB8*, a broadening (in 36 h) and further splitting (in 48 h) of the choline resonance signal (Figure 4.9, right). This splitting can be related to the accumulation of **MRB8** molecules associated to the polar outer leaflet of DMPC liposomes, which allows the resonance signals of protons from the phospholipid head groups of the outer and inner layers to be distinguished. Our assumption was verified by analysis of ^{1}H NMR spectra of DMPC-MRB8* recorded in the presence of $SmCl_3$. The addition of samarium ions (Sm^{3+}) induced significant chemical shift (Figure 4.11) of the choline resonance signal at 3.291 ppm and this signal was assigned to protons from the phospholipid head groups of the outer layer of liposomes. The observed chemical shift changes are due to the pseudo contact shifts produced by shift reagents from the group of lanthanides, such as samarium ions [357].

In the ^{1}H NMR spectra of DMPC-MRB8* recorded in 36 hours, we observed the appearance of weak signal at 3.246 ppm related to the generation of lipid acyl chains under the influence of **MRB8** (Figure 4.9, right).

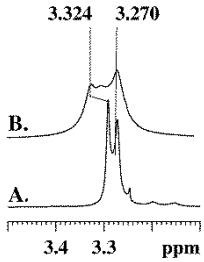

Figure 4.11 - Choline resonance signals in 600 MHz ^{1}H NMR spectra of DMPC-MRB8* (in 60 h; in D_2O; at 310 K) before (A) and after (B) addition of $SmCl_3$.

The overall results obtained for high concentration studies are in agreement with those obtained with lower chelator concentration indicating that **MRB7** and **MRB8** interact with liposomes but exhibit quite different permeation properties and binding affinity and also that this interaction is the same at the different concentration tested for the chelators.

The deep penetration of **MRB7** could be a reason for a distortion of the well-organized structure of liposomes, resulting in a generation of a certain amount of lipid acyl chains [355]. The same effect but much less displayed was observed for the chelator **MRB8** added at high concentration (Figure 4.9).

4.3.2.2 EPR studies

EPR spectroscopy was used to complement the study of the interaction of the chelators with liposomes by checking the molecular dynamics of the lipids using 5-DSA and 16-doxyl-stearic acid 16-DSA as spin probes Figure 4.12, to supplement the fluorescence and NMR studies.

The structure of 5-DSA and 16-DSA is determinant for the localization of the radical in the lipid bilayer and the radical is located near to the carbon 5 or 16 of the alkyl chain, respectively. The localization of the probe is related with the local motion profiles in the two main regions of the bilayer. 5-DSA is near the polar head group and 16-DSA is located at the end of the nonpolar chain of the lipid (Figure 4.13) [343, 350].

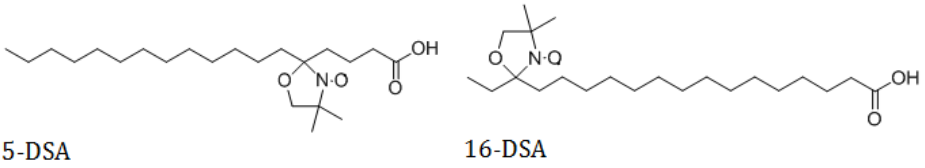

Figure 4.12 – Spin probes used for EPR studies.

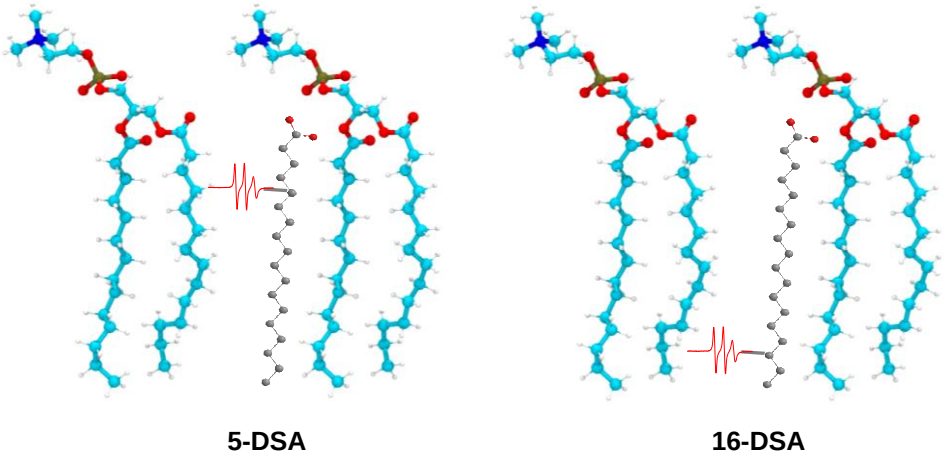

Figure 4.13 – Schematic representation of the localization of the spin probes 15- and 5-DSA within liposomes.

All the compounds were tested in at least three independent experiments and the data are expressed as mean values ± standard deviation (SD) (Tables 4.3 and 4.4). In Figure 4.14, are shown representative EPR spectra of the16-DSA and 5-DSA probes incorporated in DMPC and DMPG, in the presence or absence of a chelator, **MRB7**.

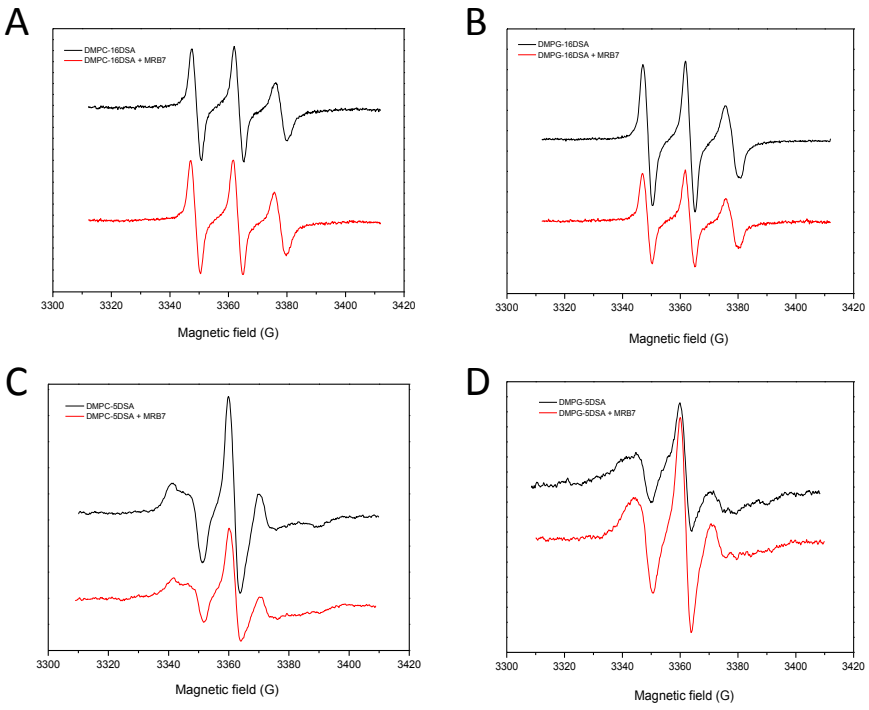

Figure 4.14– Representative EPR spectra of the16-DSA (A, B) and 5-DSA (C, D) probes incorporated in DMPC (A, C) and DMPG (B, D), in the presence (red line) or absence (black line) of chelator **MRB7**.

For “pure” DMPC and DMPG liposomes labelled with the 16-DSA and 5-DSA spin probes, the EPR spectra obtained are in agreement with the literature for similar experimental conditions [343].

From the analysis of the information collected from the EPR spectra, for the 16-DSA probe incorporated in DMPC or DMPG liposomes and in the presence or absence of each chelator, the values obtained for the rotation correlation times (τ) were calculated (Table 4.3).

The values of rotation correlation times (τ) are similar for both “pure” liposomes and in the presence of the fluorescent ligands. According to these results, the presence of chelators did not influence this experimental parameter and chelators seem not to penetrate deeply into the membrane.

Table 4.3 – Correlation time (T) calculated for 16-DSA probe in DMPC and DMPG liposomes suspensions in the presence or absence of chelators.

Sample		Average T ± SD (s)
16-DSA / DMPC	**No chelator**	$1.059 \times 10^{-9} \pm 6.538 \times 10^{-11}$
	MRH7	$9.582 \times 10^{-10} \pm 8.371 \times 10^{-11}$
	MRB7	$9.949 \times 10^{-10} \pm 6.473 \times 10^{-11}$
	MRH8	$9.892 \times 10^{-10} \pm 6.086 \times 10^{-11}$
	MRB8	$1.014 \times 10^{-9} \pm 4.7977 \times 10^{-11}$
16-DSA / DMPG	**No chelator**	$1.126 \times 10^{-9} \pm 1.235 \times 10^{-10}$
	MRH7	$1.109 \times 10^{-9} \pm 9.066 \times 10^{-11}$
	MRB7	$1.141 \times 10^{-9} \pm 1.208 \times 10^{-10}$
	MRH8	$1.152 \times 10^{-9} \pm 1.040 \times 10^{-10}$
	MRB8	$1.218 \times 10^{-9} \pm 8.182 \times 10^{-11}$

The interaction of each chelator with both liposomes was also investigated by measuring the variation the in the $2A_{max}$ parameter on the EPR spectra, with and without chelator. In the studies with DMPC, the $2A_{max}$ values in the presence or absence of each chelator were similar and for DMPG, only slightly differences were obtained for isothiocyanate derived chelators, **MRH7** and **MRB7** (Table 4.4).

Likewise the results obtained by fluorescence anisotropy, only discrete interactions were verified which may be governed mainly by the electrostatic interactions of **MRH7** and **MRB7** chelators with the headgroup of the lipids, inducing changes in the orientation of the phosphoryl group.

Table 4.4 – $2A_{max}$ calculated for 5-DSA probe in DMPC and DMPG liposomes suspensions in the presence or absence of chelators.

Sample		Average $2A_{max}$ ± SD (G)
5-DSA / DMPC	**No chelator**	49.18 ± 0.91
	MRH7	49.10 ± 0.87
	MRB7	49.58 ± 1.00
	MRH8	50.07 ± 0.83
	MRB8	49.31 ± 0.43
5-DSA / DMPG	**No chelator**	45.02 ± 0.85
	MRH7	46.81 ± 0.98
	MRB7	46.62 ± 0.59
	MRH8	45.10 ± 0.59
	MRB8	45.25 ± 0.37

4.3.3 Intracellular distribution of fluorescent chelators in BMM and PBMCs

4.3.3.1 Intracellular distribution of fluorescent chelators in BMM

In order to access the intracellular distribution of chelators, compounds **MRH7**, **MRB7**, **MRH8** and **MRB8** were incubated in BMM derived from BALB/c mice and the cells were observed by fluorescence confocal microscopy. Preliminary experiments, using variable concentration of the 4 chelators, were performed to establish the ideal concentration for observation of the cellular distribution. To obtain similar fluorescence intensity, a concentration of 5 μM was selected for **MRH7** and **MRB7** and a concentration 30 μM was used for **MRH8** and **MRB8**.
Upon incubation of chelators in macrophages, in DMEM at 37ºC for 20 min, the cells were washed with cold PBS and the intracellular distribution was visualized. The images obtained are depicted in (Figure 4.15) and show that upon 20 min of incubation, all the chelators were internalized by macrophages and the distribution pattern seems similar for all the ligands, nonetheless the differences in the fluorescence intensity.

In previous work, we perceived that fluorescein and rhodamine labelled chelators, which have different antimycobacterial activity, exhibit distinctive cellular distribution and reach different cellular targets [3]. In order to characterize the intracellular compartments targeted by the chelators **MRH7**, **MRB7**, **MRH8** and **MRB8**, we performed co-localization studies using the appropriate markers. Specific compartment markers such as fluorescein-labelled zymosan, latex beads and *M. avium*-GFP were used as phagosome markers, due to their ability to induce phagocytosis. Fluorescein-conjugated dextran was used for early and late endosomes labelling, MitoTracker Green FM as mitochondrial marker and or ER-Tracker Green for endoplasmic reticulum (ER) labelling.

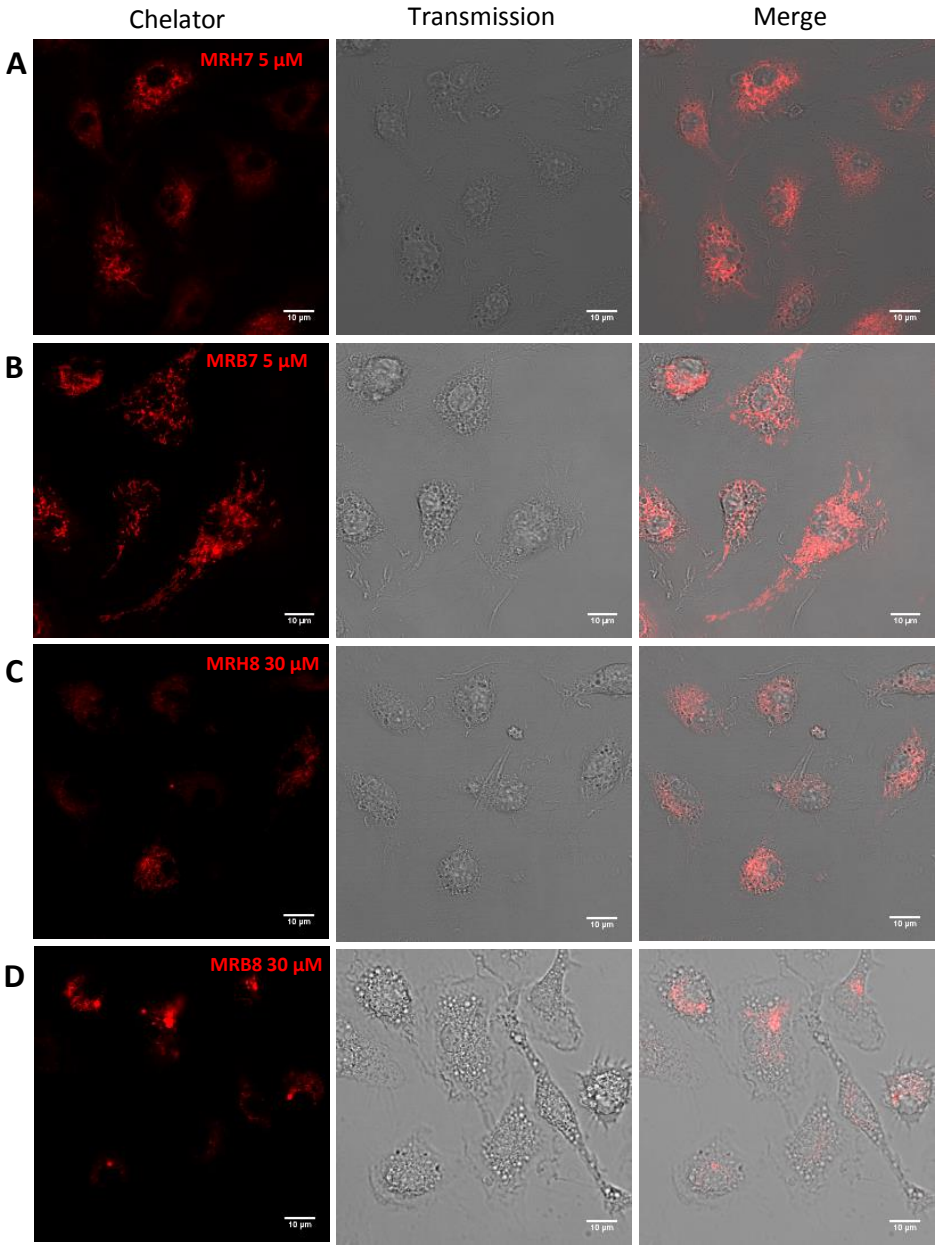

Figure 4.15 – Representative confocal microscopy images of intracellular distribution of chelators **MRH7** and **MRB7** (5 µM), **MRH8** and **MRB8** (30 µM) in bone marrow-derived macrophages (BMM).

To display the visualization of the co-localization of chelators with different markers we use a figure for each compound (Figure 4.16 for **MRH7**, Figure 4.17 for **MRB7**, Figure 4.18 for **MRH8**, Figure 4.19 for **MRB8**). In each figure different letters were used to designate different compartments/markers (A-early endosomes, B-late endosomes, C-mitochondria, D-phagosome-zymosan, E-phagosome-latex beads, F-phagosome-*M.avium*, G-endoplasmic reticulum).

The results are indicative that all fluorescent chelators seem to have access to the phagosomes formed by phagocytosis of zymosan or latex beads, after 20 min or 3h incubation, respectively. For chelator **MRH7** we also performed a study with green coloured *M. avium*-GFP. On the 4th day of infection, **MRH7** was added (5 μM) to BMM infected with *M. avium*-GFP and cells were visualized. Apparently, the fluorescent chelator does not colocalize with the *M. avium*-GFP containg phagosome, a result which is in agreement with previous work with fixed cells. **MRH7** could sequester the cytosolic iron and/or generate a concentration gradient from the phagosome to the cytosol. Moreover, as the fluorescence intensity of **MRH7** is quenched in the presence of iron [3] we have to consider that **MRH7** could interact with the *M. avium*-GFP containing phagosome, but could not be detected due to loss of its fluorescence.

Simultaneous incubation of macrophages with **MRH7**, **MRB7**, **MRH8**, **MRB8** and the mitochondria marker MitoTracker Green FM for 20 min, showed that all chelators were able to accesses mitochondria (Figures 4.16 - 4.18, C).

Incubation of fluorescent chelators in macrophages that contain the endosomal probe fluorescein-labelled dextran, for 20 min or overnight, revealed that the chelators tested do not co-localize with early or late endosomes, respectively (Figures 4.16 - 4.19, A and B).

Due to the similar distribution pattern of all chelators and the great interest in **MRH7** only the latter chelator was studied as a representative ligand for co-localization studies with endoplasmic reticulum (ER) and Golgi complex. Unfortunately, the Golgi marker seems to induce some toxicity for macrophages and consequently we could not acquire images. The experiments performed with ER-Tracker Green for endoplasmic reticulum (ER) labelling revealed that **MRH7** seems to access ER compartments (Figure 4.16, G).

For all the fluorescent ligands studied, the cellular distribution seems similar due to the analogous co-localization patterns. However, both the amount of chelator internalized and the “velocity” of uptake seems to be significantly higher for chelators **MRH7** and **MRB7** than those observed for **MRH8** and **MRB8**. Considering the distinct interaction of the two groups of chelators with liposomes, these results suggest that, despite its higher initial concentration, a smaller amount of **MRH8** and **MRB8** is internalized by BMM and the reminiscent amount is lost in the washing procedures.

In all confocal studies, we have to keep in mind that all of the chelators exhibit identical affinity for iron(III) and are *turn-off* ligands in the presence of iron [3, 4] thus implying that its fluorescence is quenched upon iron chelation. Consequently, as these molecules are chelating iron contained in BMM, the fluorescence signal observed in the microscope corresponds to that of the free ligand.

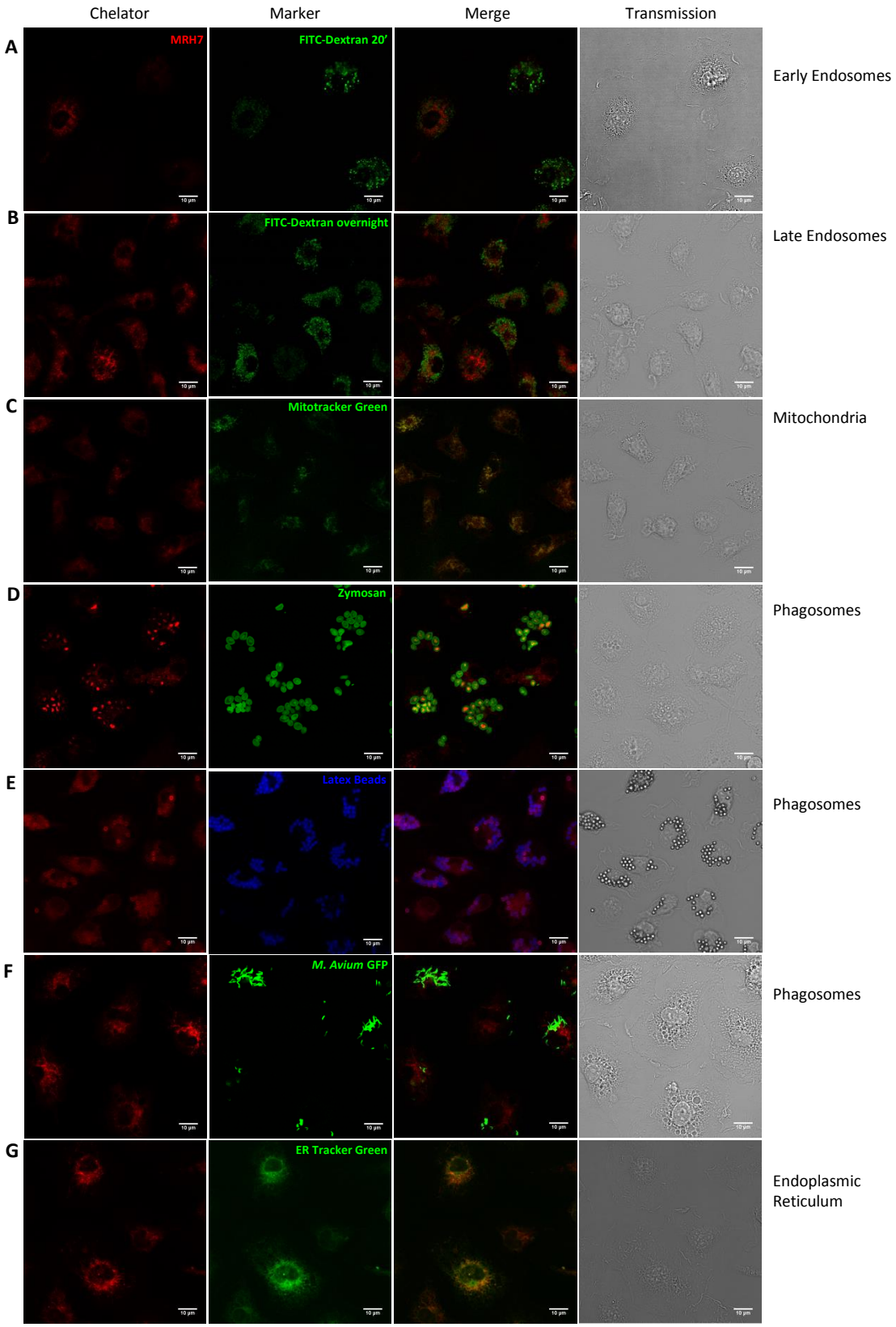

Figure 4.16 - Representative confocal microscopy images of intracellular distribution and colocalization studies of chelator **MRH7** in bone marrow-derived macrophages (BMM). (A-early endosomes, B-late endosomes, C-mitochondria, D-phagosome-zymosan, E-phagosome-latex beads, F-phagosome-*M.avium*, G-endoplasmic reticulum).

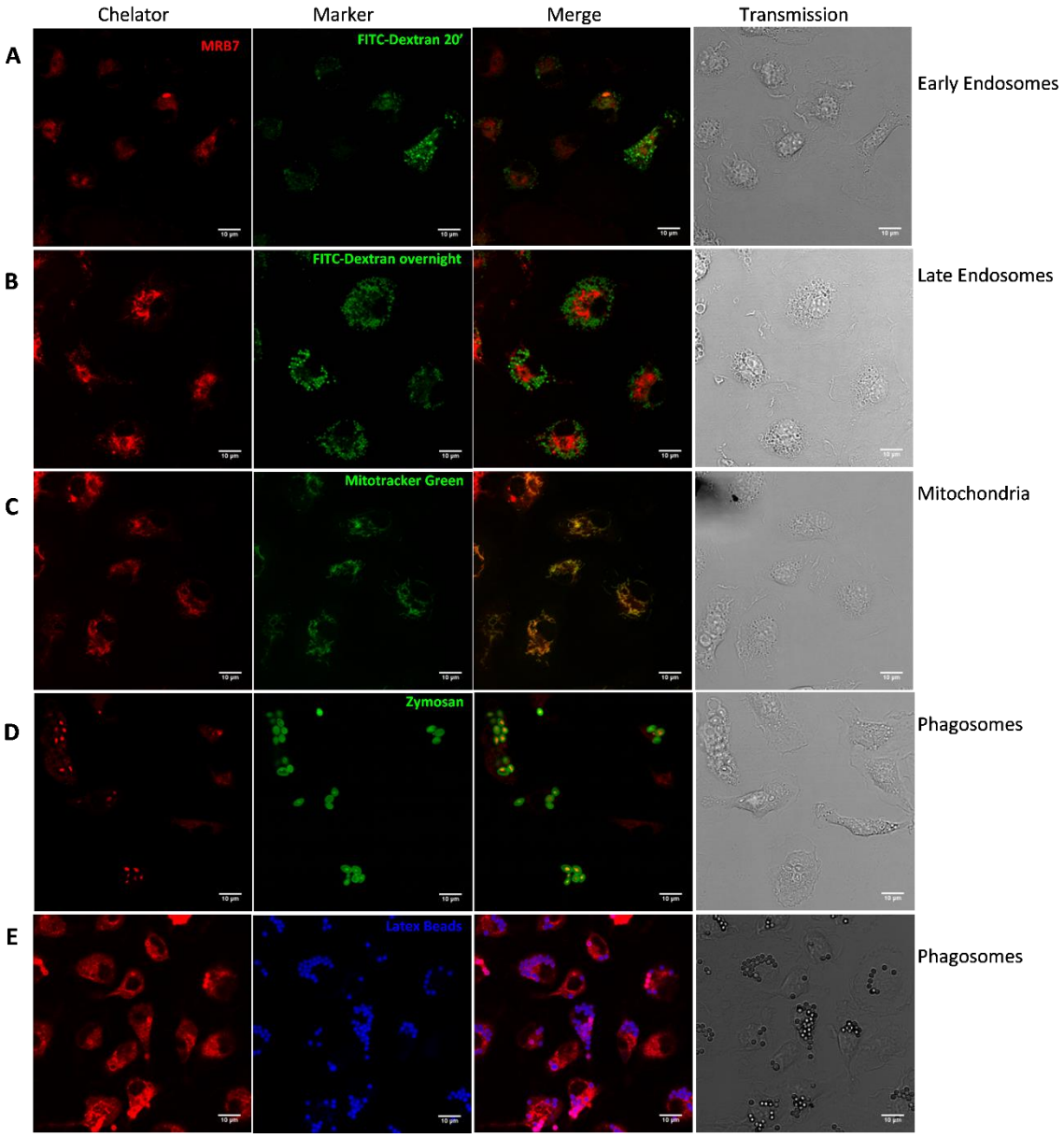

Figure 4.17 - Representative confocal microscopy images of intracellular distribution and colocalization studies of chelator **MRB7** in bone marrow-derived macrophages (BMM). (A-early endosomes, B-late endosomes, C-mitochondria, D-phagosome-zymosan, E-phagosome-latex beads).

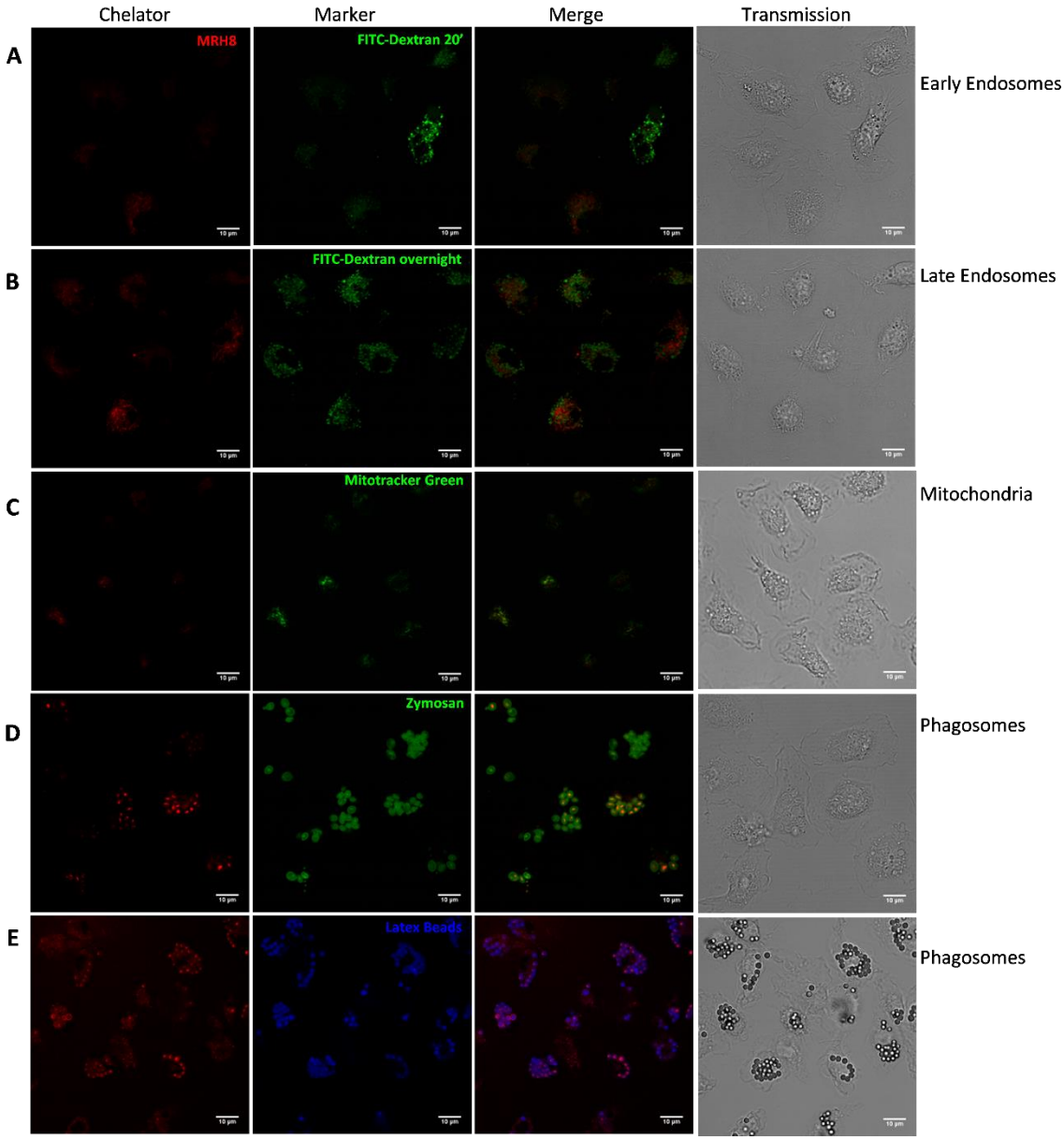

Figure 4.18 - Representative confocal microscopy images of intracellular distribution and colocalization studies of chelator **MRH8** in bone marrow-derived macrophages (BMM). (A-early endosomes, B-late endosomes, C-mitochondria, D-phagosome-zymosan, E-phagosome-latex beads).

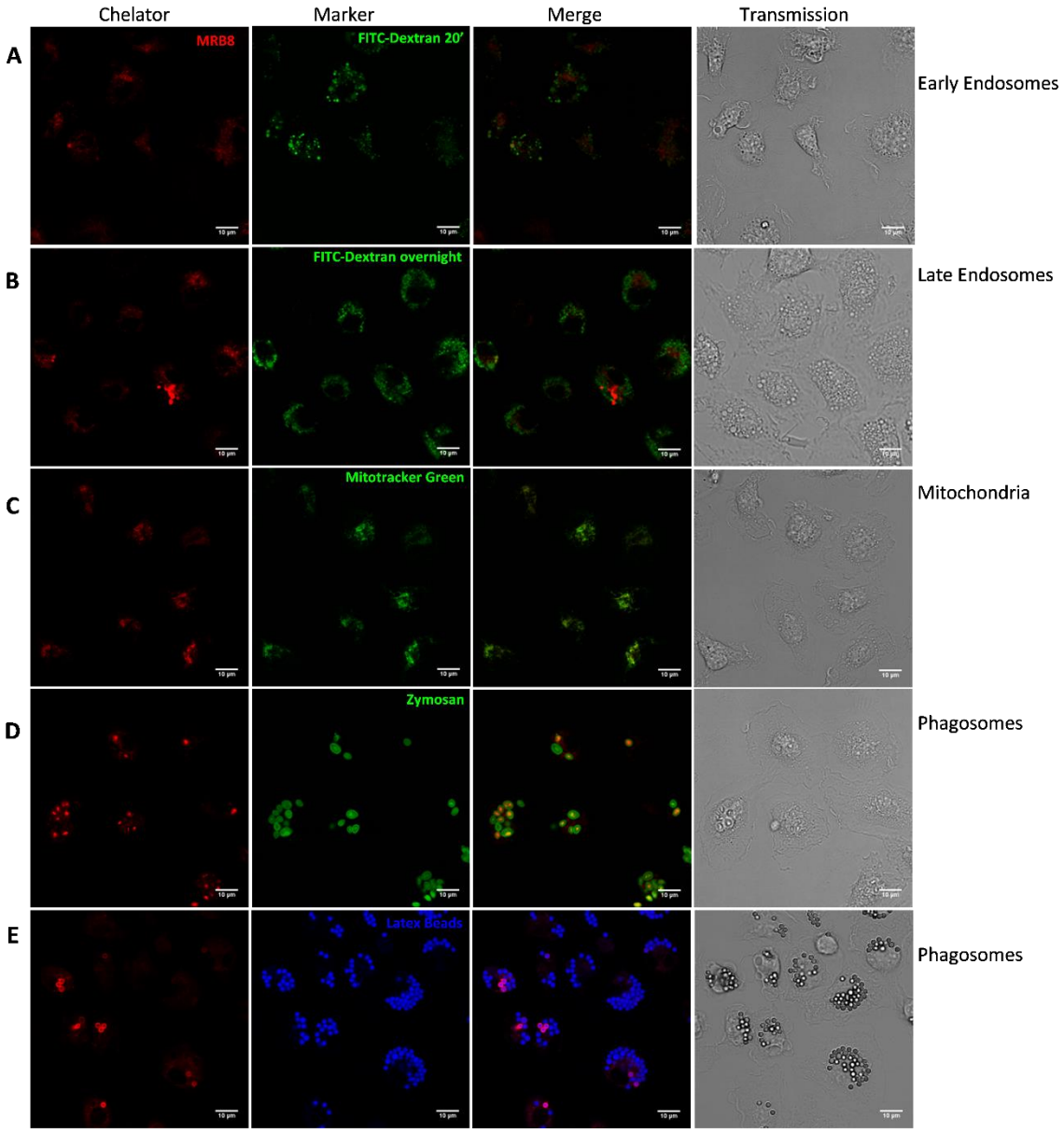

Figure 4.19 - Representative confocal microscopy images of intracellular distribution and colocalization studies of chelator **MRB8** in bone marrow-derived macrophages (BMM). (A-early endosomes, B-late endosomes, C-mitochondria, D-phagosome-zymosan, E-phagosome-latex beads).

4.3.3.2 Intracellular distribution of fluorescent chelators in PBMCs

Fluorescent chelators **MRH7**, **MRB7**, **MRH8**, **MRB8** were incubated with PBMCs to try to get insight on the uptake of these ligands by the cells. Despite the fact that macrophages are able to do endocytosis, the results described in the section above (section 4.3.3.1) suggest that the uptake of the chelators was not achieved by endocytic processes in BMM.

As PBMCs are also cells from the immune system but with less capacity for endocytosis, these cells were used to confirm if the uptake of the chelators may occur by non-endocytic mechanisms.

After 20 min of incubation, all the chelators were internalized by the PBMCs and the distribution pattern seems similar for all tested ligands nonetheless the differences in the fluorescence intensity that were verified between the **MRH7** / **MRB7** and **MRH8** / **MRB8** (Figure 4.20). These results suggest that although these type of molecules may enter by endocytosis, in different cell types, such as BMM and PBMCs, they can cross the membrane and access the cytoplasm by other mechanisms, such as mediated transport by receptors or diffusion through the cellular membrane.

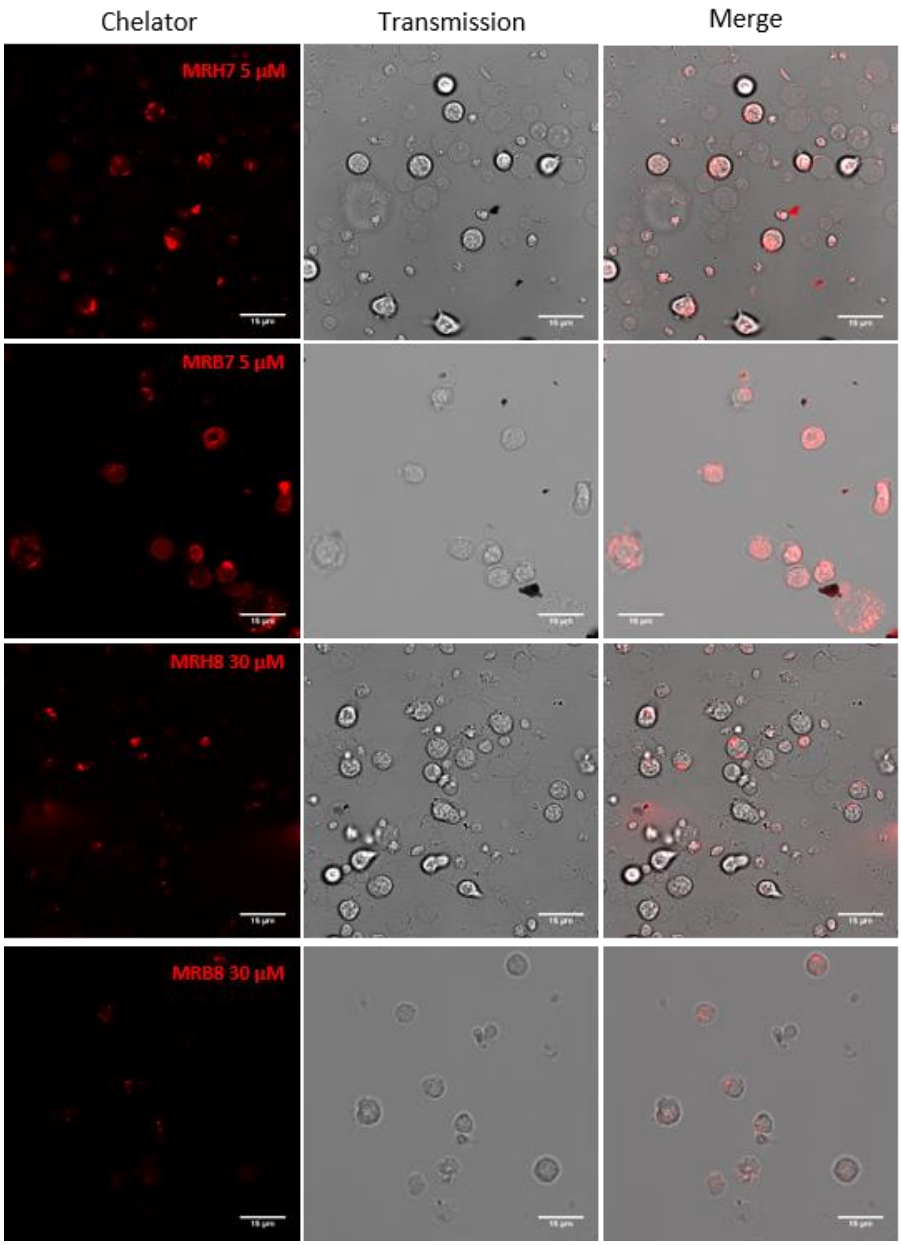

Figure 4.20 - Representative confocal microscopy images of intracellular distribution of chelators **MRH7** and **MRB7** (5 µM), **MRH8** and **MRB8** (30 µM) in peripheral blood mononuclear cells (PBMCs).

4.4 Conclusions

In this chapter, we performed experiments to evaluate the influence of the structural modifications included in the parent chelators, in comparison with previous results [3], for the chelators interaction with membranes, either in liposomes or cell membranes of macrophages and PBMCs.

Computational studies of the interaction of a set of fluorescent 3,4-HPOs chelators with DMPC liposome membrane models [272] were also used as a complementary technique to complement the results described above. The results obtained for **MRB7**, **MRB8** and **MRH7** chelators will also be discussed in this chapter section, as the results are relevant for comparison with those obtained by other technics.

The results suggest that **MRB7** seems to have the higher insertion and residence time in the hydrophobic region of the bilayer, in comparison with **MRB8** (Figure 4.21, A and B). This result is consistent with the partition constants determined by fluorescence spectroscopy and mainly with NMR. **MRB8** also interacts with the hydrophobic phase but and does not seem to go as deep as the **MRB7** compound; nor the number of interacting chelators is comparable with **MRB7**.

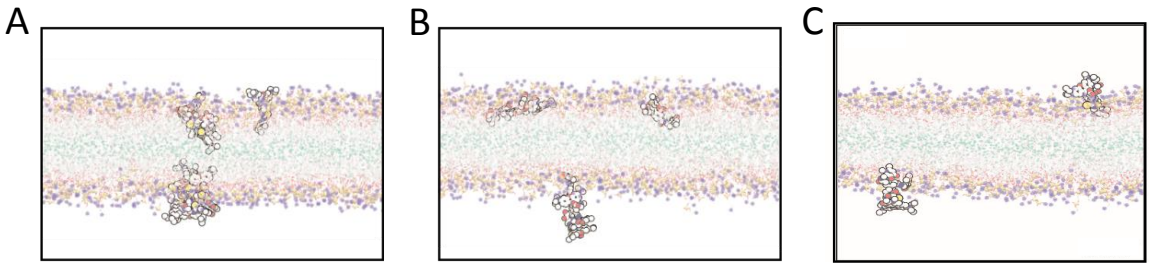

Figure 4.21 - Graphical representation of the interaction of the bidentate compounds, **MRB7** (A), **MRB8** (B) and **MRH7** (C), with the DMPC bilayer model, obtained in MD simulations.

We have also observed the type of interaction with the membrane bilayer and, the results show that the compounds are able to indiscriminately interact by the rhodamine or chelating group. However, it appears that only through the rhodamine group they are able to penetrate deeper in the bilayer. **MRB7** and **MRB8** can go as deep in the bilayer as to surpass the plane defined by the ester oxygen atoms (these represent the end of the polar region, and the beginning of the non-polar one).

Based on the results obtained for the hexadentate chelator **MRH7**, we observe that this ligand is able to interact with the bilayer, but at a more superficial level than the analogous bidentate ligand **MRB7** (Figure 4.21, C). In addition, the chelator interacts with the bilayer through the polar chelating units, which could prevent their higher insertion in the bilayer.

As we observed that there is an apparent higher interaction of all these compounds with lipid phases, several efforts have been done to understand the uptake of these compounds through the bilayer because it is less usual that ionic large molecules would cross the bilayer through diffusion.
As it has been proposed in the literature that rhodamine123 could cross cells through protein-mediated mechanisms in Caco-2 cells [358], we have tested a possible transport hypothesis through docking and MD calculations, taking into consideration an endocytic receptor (DC-SIGN). In these experiments, we studied the interaction of **MRB7** and **MRB8** chelators and of the non-fluorescent bidentate unit (**CHELu**) with this receptor (See formulae in Figure A.1, in Appendix).
In the MD simulation, **CHELu** initially interacts with the receptor but, after 4 ns, the molecule begins to detach from the receptor. These results reinforce our premise that the fluorophore framework in the chelator's structure is essential for an efficient binding, thus providing a possible explanation for the inactivity of the non-fluorescent 3,4-HPO chelating units in the *M. avium* infection model [1]. The results also demonstrate that **MRB7** chelator (with *N*-ethyl group and thiourea link) exhibits a stronger binding to this receptor.

The results of the combined studies substantiate our premise that a strong affinity for lipid bilayers is crucial for the biological activity, as suggested in previous work [4].

In summary, our present results show that:

i) The distribution of rhodamine labelled chelators in liposomes is higher for the rhodamine B isothiocyanate derivatives (**MRH7** and **MRB7)** than for carboxytetramethylrhodamine chelators, **MRH8** and **MRB8**;

ii) Both NMR and MD simulation show that chelators interact with the lipid phases at different levels of the bilayer and that the interaction seems to be strengthened for the compounds that contain *N*-ethyl groups and a thiourea linkage (**MRB7** and **MRH7**) which are those exhibiting the highest biological activity [4]; these studies also show that this interaction comprises the hydrophobic region of the membrane models employed;

iii) Confocal microscopy studies have shown that the distribution and the interaction with different cellular compartments in BMM is similar for all tested chelators;

iv) Experiments performed with PBMCs corroborated that endocytosis is not the preferred pathway for the chelator's cellular uptake;

v) Confocal microscopy studies revealed that, for the same experimental conditions, an amount six times greater than that used for **MRH7** and **MRB7** is needed for carboxytetramethylrhodamine chelators (**MRH8**, **MRB8)** visualization;

vi) No significant results were obtained, using steady state fluorescent anisotropy studies or EPR spectroscopy. This fact may be explained bearing in mind that in both methods, the evaluation of the interaction is obtained by considering reporter probes in spite of the fluorescent chelators in study.

According to the data obtained we suggest that the "strength" of the interaction of each chelator with the membranes is determinant for the final biological effect and therefore rhodamine B isothiocyanate labelled chelators, **MRH7** and **MRB7**, are better candidates for controlling intramacrophagic growth of *M. avium* than those derived from carboxytetramethylrhodamine (**MRH8** and **MRB8**).

As a final remark, we outline in Figure 4.22 the hypothetical mode of interaction with and progress of the rhodamine B isothiocyanate labelled chelators (**MRH7**, **MRB7)** and of the carboxytetramethylrhodamine (**MRH8**, **MRB8**) with biological membranes.

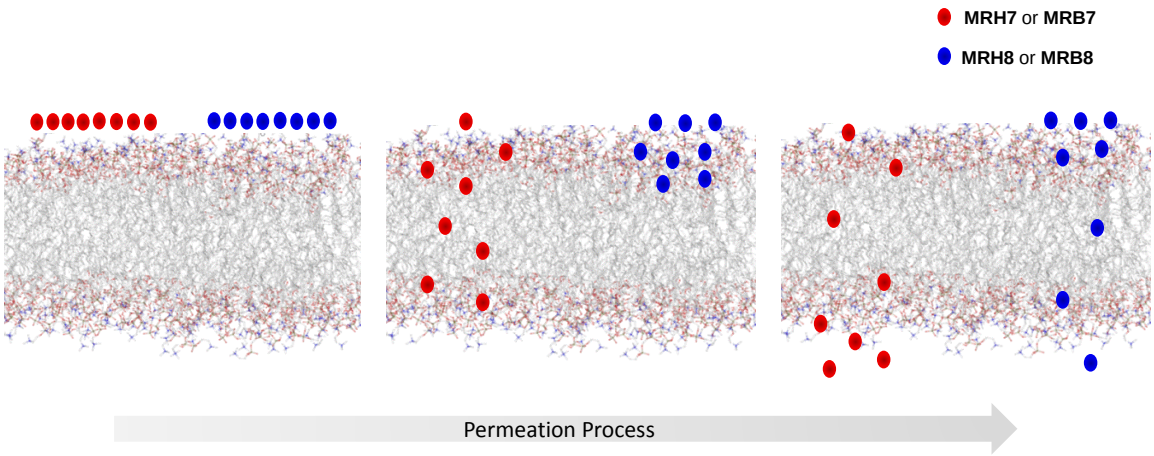

Figure 4.22 - Outline of a hypothetical mode of interaction and progress of the rhodamine labelled 3,4-HPO chelators, **MRH7** and **MRB7** (red) and **MRH8** and **MRB8** (blue) through the biological membranes, along the time.

5 | *IN VITRO* SAFETY STUDIES IN HEPATOCYTES

5. *IN VITRO* SAFETY STUDIES IN HEPATOCYTES

5.1 Introduction

The evaluation of the toxic profile of new compounds is of great importance in the process of developing new therapeutic agents, parallel to the assessment of their efficacy, as their eventual toxicity may compromise clinical applications.

In order to evaluate the toxicity of the rhodamine derived chelators, we investigated the detrimental effects of the ligands in the human hepatoma cell line HepG2, which is commonly used as an *in vitro* model for the liver cells [359-361]. HepG2 cells preserve the morphological and functional differentiation of the *in vivo* hepatocyte. These cells are highly polarized, i.e. they display cell asymmetry resultant from the presence of basolateral and apical poles. Additionally to phenotypical features, this cell line also expresses several enzymes involved in the metabolism and detoxification of xenobiotics *in vivo*, justifying the suitability of this cellular model for the toxicological screening of new drugs [362-367].

To evaluate the toxicity of the newly synthesized drugs in HepG2 cells, two viability assays were performed: i) the 3-[4,5-dimethylthiazol-2-yl]-2,5 diphenyl tetrazolium bromide (MTT) reduction assay and ii) the lactate dehydrogenase (LDH) leakage assay.

The MTT assay is a colorimetric test based on the indirect measurement of the activity of the mitochondrial enzymes that reduce the soluble yellow MTT into purple insoluble crystals of formazan (Figure 5.1). As the mitochondrial activity is correlated with cell viability, the cytotoxicity of the drug is estimated considering the rate of MTT reduction [368]. The amount of purple formazan produced by cells treated with the drugs is compared with the amount of formazan produced by untreated control cells. Therefore, the ability of the drug to cause death or change the normal metabolism of cells can be easily assessed.

In order to measure the insoluble formazan that is produced, crystals are dissolved in a solubilisation agent (usually DMSO) and the absorbance of the purple solution is measured at the maximum wavelength of absorbance (λ = 550 nm).

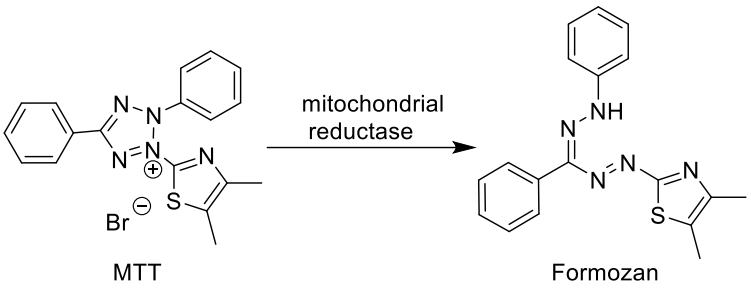

Figure 5.1 - MTT reduction reaction by action of mitochondrial reductases.

Despite the fact that viability assays, such as the MTT assay, are often used for primary screening [369, 370], we have to consider some drawbacks. Different results might be obtained by other viability tests, as several different conditions may increase or decrease metabolic activity of the cell. Consequently, higher or lower MTT reduction rates may be attained, while keeping the number of viable cells constant [370]. Moreover, in a MTT assay it is not possible to distinguish between a scenario of a cell cycle inhibition or cell death [371-373].

In our particular system, the MTT assay may present additional limitations as the formazan formed has maximal absorbance in the same wavelength range of the rhodamine derived chelators, as described in Chapter 2. Moreover, as the MTT assay is a destructive test and we are interested in evaluating the toxicity of the chelators along the time of the experiment (5 days), it restricts the possibility of performing the assay in intermediate time points.

In the safety studies here reported, the time of incubation of chelators with the HepG2 cells was 5 days in order to be the same time of incubation considered in the studies of antimycobacterial effect of these chelators inside macrophages (Chapter 3).

To overcome these limitations, the LDH leakage assay was also performed to access the viability of the cells in the presence of the chelators.

In this method, the effect of the chelators on cell viability is indirectly evaluated through the measurement of the activity of the LDH enzyme. As LDH is a cytoplasmic enzyme, its presence in the extracellular medium is indicative of alterations in cytoplasmic membrane permeability and cell integrity. This assay is one of the most accepted for the determination of the toxicity of drugs *in vitro* [369, 373-375].

LDH is an oxidoreductase enzyme that catalyses the reversible conversion of pyruvate to lactate, in the presence of NADH, which in turn is oxidized to NAD^+ (Figure 5.2). The evolution of the oxidation of NADH to NAD^+ is followed by measuring the absorbance (λ = 340 nm) [376].

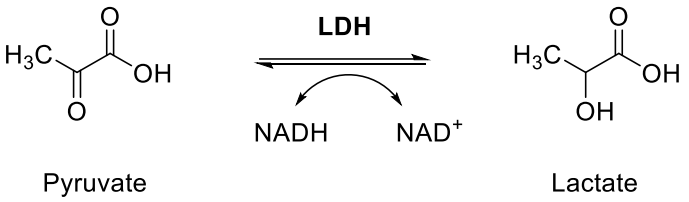

Figure 5.2 - Conversion of pyruvate into lactate by action of LDH enzyme.

Despite the advantages of this assay, such as its reliability, quickness [373, 377] and the non-destructive nature, the method may as well present some disadvantages. The method has limited sensitivity and LDH has relatively short half-life in the medium [378, 379]. For these reasons, and taking into account the advantages and disadvantages of both methods, the cytotoxicity results after exposure of HepG2 cells to rhodamine derived chelators, obtained both in the MTT reduction and in the LDH leakage assays were compared.

The safety studies were performed in collaboration with the group of Professor Maria de Lourdes Bastos at “Laboratório de Toxicologia” in “Faculdade de Farmácia da Universidade do Porto”.

5.2 Methods

5.2.1 HepG2 cell culture routine

The human hepatoma HepG2 cell line was gently given by Doctor Ricardo Dinis-Oliveira (CESPU, Instituto Superior de Ciências da Saúde – Norte, Gandra, Portugal). HepG2 cells were routinely maintained in 75 cm^2 canted-neck tissue culture flasks (Sigma-Aldrich) and cultured as monolayer in cell culture medium, i.e. DMEM, high glucose, GlutaMAX™ (Life Technologies, Paisley, U.K.) supplemented with 10% fetal bovine serum (FBS), 1% antibiotic (Penicillin 5000 U/mL + Streptomycin 10000 µg/mL) (Life Technologies, Paisley, U.K.), 0.5% fungizone (250 mg/mL amphotericin B), (Life Technologies, Paisley, U.K.) in a humidified incubator, with a 5% CO_2 atmosphere, at 37 ^oC. Cells were subcultured at approximately 70-80% confluence over a maximum of 10 passages. Each passage was performed by medium removal, cells were then washed with Hank’s balanced salt solution (HBSS)) (GIBCO, Invitrogen Corporations, Paisley, UK). To promote cells detachment, 2 ml of 0.25% trypsin/1 mM EDTA solution was added and the flask was placed in the incubator for 5 minutes. The cells were re-suspend in 10 mL of cell culture medium and split into new flasks.

For the MTT and LDH assays, cells were planted onto 96-well plates (Falcon, BD Biosciences, Oxford, UK) at a density of 5×10^4 per well (100 µL of suspension to each well) and placed in the incubator at 37 ºC, for 24 h prior to the addition of the treatments. Peripheral wells on the plate were left empty to prevent evaporation and concentration of test solutions [380].

5.2.2 Cell Treatments

On the day of the experiments, the medium was removed and the HepG2 cells were exposed to a set of concentrations of each rhodamine derived chelators (ranging from 1 to 40 µM or 3 to 120 µM, for hexadentate or bidentate ligands, respectively). To prepare the serial dilutions to be tested, the appropriated volume of stock solution of each chelator was diluted in cell culture medium. The stocks were set at a concentration of 0.5 mM, prepared in sterilized water with 4% DMSO (V/V)). Each condition was tested in triplicates by adding 250 µL of testing solution to each well of the 96-well plate. A positive control, consisting of 1% Triton X-100 (V/V) (Sigma-Aldrich, Co.), and a negative control (cell in culture medium without treatments) were also included. In all experiments, a solvent control (cells treated with 1% DMSO (V/V)) was included to mimic the maximum concentration of DMSO present in the treatments. Cells were incubated at 37 °C for 5 days. No significant differences were observed between solvent and negative control (cells in culture medium) (data not showed).

5.2.3 Cell viability by the MTT reduction assay

After 5 days of incubation at 37 °C, the medium was removed and to the attached cells were added of 100 µL of 0.5mg/mL MTT solution (Sigma-Aldrich, Co.), in HBSS. The plates were incubated at 37ºC. After 90 min, the cell culture medium was aspirated and the formed intracellular formazan crystals were dissolved with DMSO. The plates were placed in a shaker for 15 minutes, protected from light. The absorbance was recorded at 550 nm, using a multi-well plate reader (Labsystems Multiskan, Basingstoke, UK) [380, 381].

5.2.4 Cell viability by the LDH leakage assay

After 1 day, 3 days, and 5 days of cell treatments, an aliquot (10 µL) of the supernatants of each well was removed and placed in new 96-well plates. Then 40 µL of 0.05 M potassium phosphate buffer (pH 7.4) (KH_2PO_4, Merck) and 200 µL of 0.15 mg/mL β-nicotinamide adenine dinucleotide (β-NADH, Sigma-Aldrich, Co.) were added. Immediately before the absorbance reading, 25 µL of 2.5 mg/mL sodium pyruvate (Sigma-Aldrich, Co.) were

pipetted into each well to start the reaction. The β-NADH and sodium pyruvate solutions were freshly prepared each day in buffer solution. The absorbance was read every 16 seconds for 2.40 minutes, at 340nm on an automatic plate reader (BioTek Instruments, VT, USA) in a kinetic photometric assay. Results are presented as % cell death, as compared to negative control (culture medium) [382].

5.2.5 Statistical analysis

The cytotoxicity data from the MTT reduction and LDH leakage assays were obtained from four independent experiments, with each test plate containing three replicates of eight increasing concentrations of each tested chelator. To reduce variability between experiments, data was normalized plate-by-plate by negative and positive controls, as previously described [380, 381, 383].

The results are presented as mean standard error (SEM) of the mean. Normality of data distribution was assessed by the Kolmogorov–Smirnov, D'Agostino & Pearson omnibus, and Shapiro-Wilk normality tests. Statistical comparisons were performed by one-way analysis of variance (ANOVA) followed by Holm-Sidak's multiple comparison test. The solvent and negative control values (raw data) were compared by the Student's unpaired t-test. Data obtained were analysed using the software Graph Pad Prism version 6.0. Significance was accepted when p value < 0.05 was obtained.

5.3 Results and discussion

5.3.1 Cell viability by the MTT reduction assay

The toxicity of 3,4-HPO chelators was investigated by evaluating cellular viability after exposing HepG2 cells to the drugs, for five days. The percentage of MTT reduced by cells was measured and the values are correlated with the mitochondrial activity, which is an indication of cell viability.

Chelators were tested in a range of concentrations comprising the minimum and the maximum concentration administered to the macrophages (1-40 μM and 3-120 μM for hexadentate and bidentate chelators, respectively), in the studies of the antimycobacterial activity. All the compounds were tested in four independent experiments and the results are presented in Figures 5.3 and 5.4, for bidentate and hexadentate chelators, respectively.

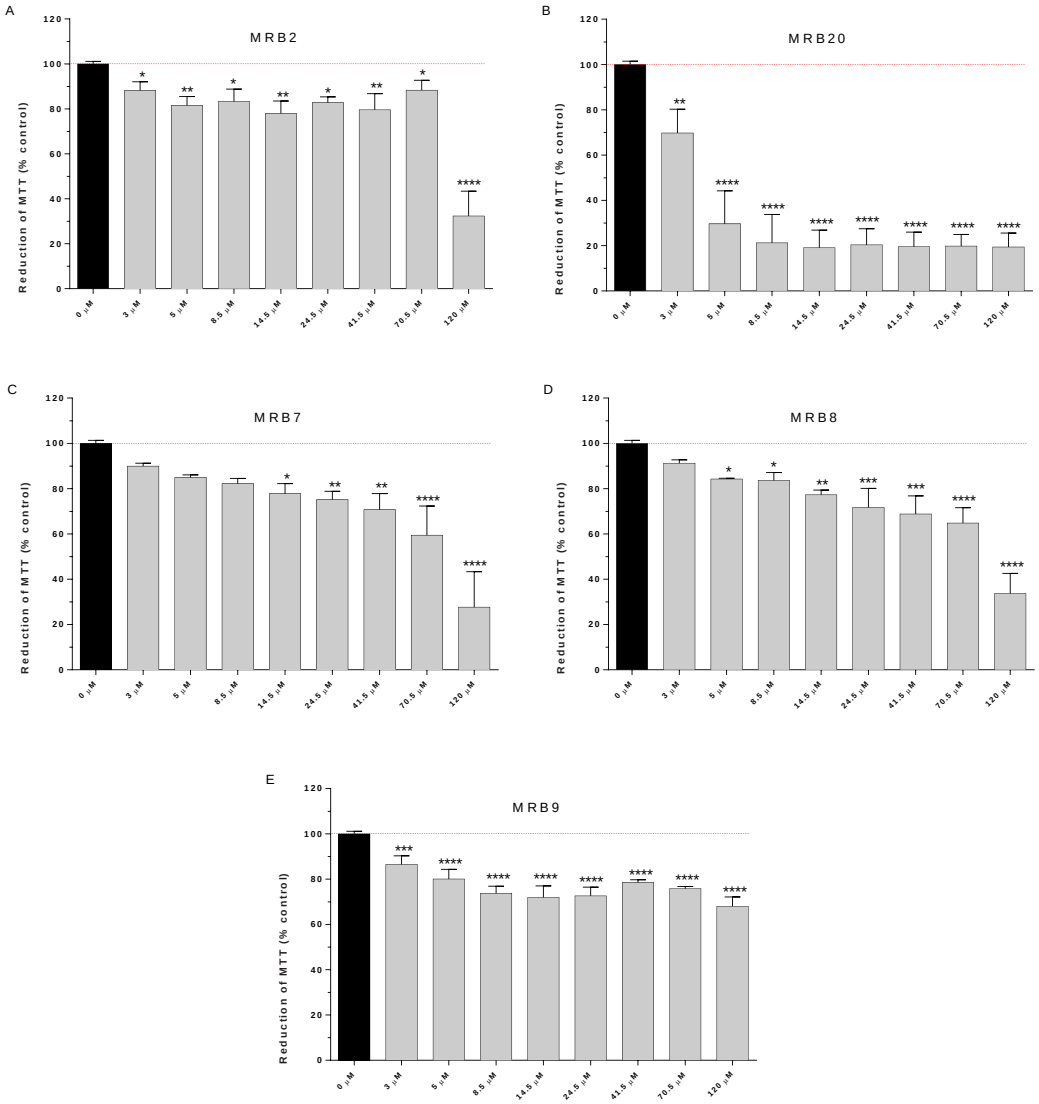

Figure 5.3 - MTT reduction cytotoxicity assay for bidentate chelators, i.e. **MRB2** (A), **MRB20** (B), **MRB7** (C), **MRB8** (D) and **MRB9** (E) in Hep G2 cells, after 5 day-incubation at 37ºC. Each chelator was tested at a concentration range of 3 to 120 µM. The graphs show the geometric mean ± SEM of reduction of MTT (percentage of control) obtained from four independent experiments. Each condition was tested in triplicates. Statistical analysis was performed using ANOVA followed by Holm-Sidak's multiple comparison test. Statistical significance: * p<0.05, ** p<0.01, *** p<0.001 and **** p<0.0001, when compared with control (0 µM).

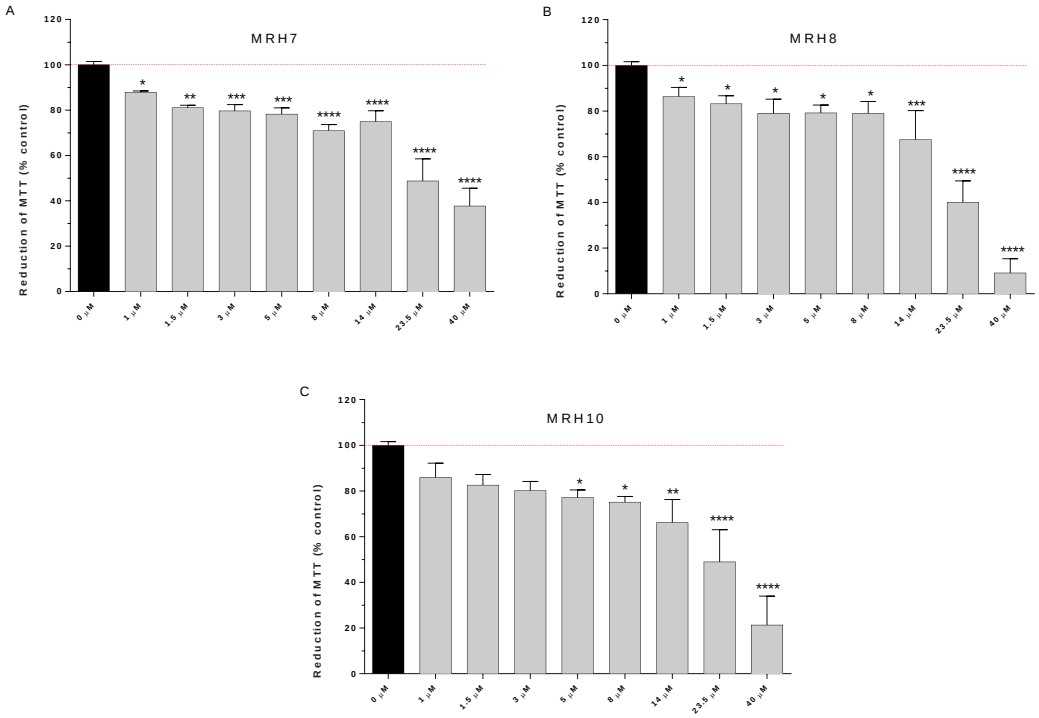

Figure 5.4 - MTT reduction cytotoxicity assay for hexadentate chelators, i.e. **MRH7** (A), **MRH8** (B) and **MRH10** (C) in Hep G2 cells, after 5 day-incubation at 37ºC. Each chelator was tested at a concentration range of 1 to 40 μM. The graphs show the geometric mean ± SEM of reduction of MTT (percentage of control) obtained from four independent experiments. Each condition was tested in triplicates. Statistical analysis was performed using ANOVA followed by Holm-Sidak's multiple comparison test. Statistical significance: * p<0.05, ** p<0.01, *** p<0.001 and **** p<0.0001, when compared with control (0 μM).

Considering the data obtained for all the fluorescent chelators, a direct correlation between concentration and cytotoxicity seems to exist.

Chelators **MRB8** and **MRH10** have shown significant cytotoxicity from concentrations as low as 5 μM, while **MRB7** presented toxicity at concentrations higher than 14.5 μM. All the other chelators have shown considerable differences to controls at the entire range of tested concentrations.

Of particular interest, the bidentate **MRB20** was the most cytotoxic drug, since from 3 μM and at all tested concentrations. This chelator induced, at concentration equal or superior to 5 μM, a decrease in the cell viability to levels lower than 29.65 ± 14.56%.

For the bidentate chelators, **MRB2**, **MRB7** and **MRB8**, a similar profile was verified, between each other. For these chelators, although significantly different from the control, the cell viability was between 60-80%, for concentration values until 70.5 μM. Only at the highest concentration value (120 μM), the percentage of viable cells decreases to values around 30-35%.

The chelator **MRB9** was relatively less toxic than the other bidentate ligands as it was the only drug that did not induce a decrease cell viability higher than 30%. Either at the highest concentration tested, i.e. 120 μM, the cell viability was 67.98 ± 4.14%.

The cytotoxic profile obtained for hexadentate chelators is similar for between each other and for concentrations inferior or equal to 14 μM, the hepatocytes's viability was approximately 70%. All hexadentate chelators, when tested at 23.5 μM and 40 μM, effectively killing HepG2 cells (cell viability was below 48.94 ± 14.10%).

Regarding the MTT assay, a couple of aspects should be considered. First, the results obtained in the current assay were achieved after 5 day-drug exposures. It is well established that long incubation periods largely reduce cellular viability. The cell culture medium was not changed during exposures and the cells were not split to provide room to grow, therefore some level of basal stress is naturally expected. Second, as the maximum wavelengths of absorptions of reduced MTT and of rhodamine derived chelators occur at the same wavelength region, the existence of interferences during the absorbance measurement may be verified. Given this, the absorbance recorded may be overestimated, wrongly indicating higher cellular viability. Nevertheless, during the experiments, no macroscopic evidence of this fact was verified.

5.3.2 Cell viability by the LDH leakage assay

A complementary method, the LDH leakage assay, was used to investigate the toxicity of 3,4-HPO chelators. According to this assay, the deleterious effect provoked by the chelators on cell viability was indirectly evaluated through the measurement of the activity of LDH. The presence of this cytoplasmic enzyme in the extracellular medium is indicative of alterations on the permeability of the cytoplasmic membrane and in the integrity of the cells. Thus, the higher the amount of enzyme released, the higher the cell integrity impairment triggered by chelators.

The activity of the enzyme was measured in the culture medium after exposing HepG2 cells for 1, 3 and 5 days. All the compounds were tested in four independent experiments and the results are presented in Figures 5.5 and 5.6 (bidentate and hexadentate chelators, respectively).

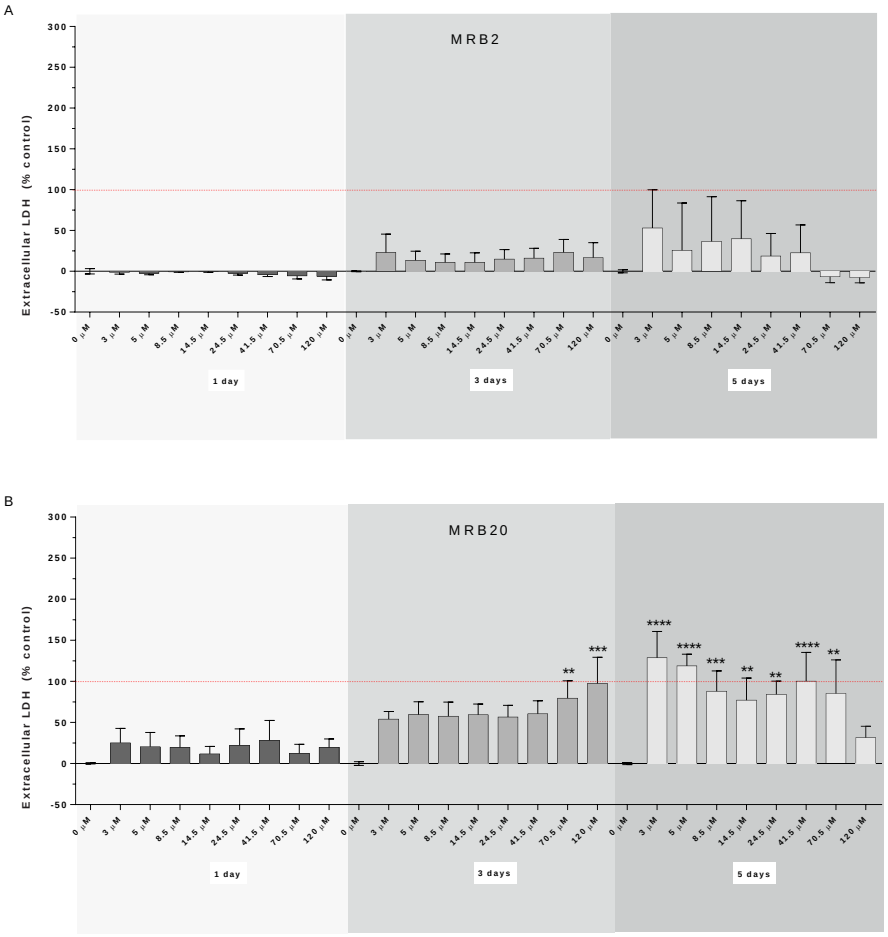

Figure 5.5 (A, B) - LDH leakage cytotoxicity assay for bidentate chelators, i.e. **MRB2** (A), **MRB20** (B), **MRB7** (C), **MRB8** (D) and **MRB9** (E) in Hep G2 cells, after 1, 2, or 5 day-incubation at 37ºC. Each chelator was tested at a concentration range of 3 to 120 μM. The graphs show the geometric mean ± SEM of extracellular LDH (percentage of control) obtained from four independent experiments. Each condition was tested in triplicates. The dashed line represent the percentage of LDH leakage obtained for the positive control (cell treated with triton). Statistical analysis was performed using ANOVA followed by Holm-Sidak's multiple comparison test. Statistical significance: * p<0.05, ** p<0.01, *** p<0.001 and **** p<0.0001, when compared with control (0 μM) of the respective time-point.

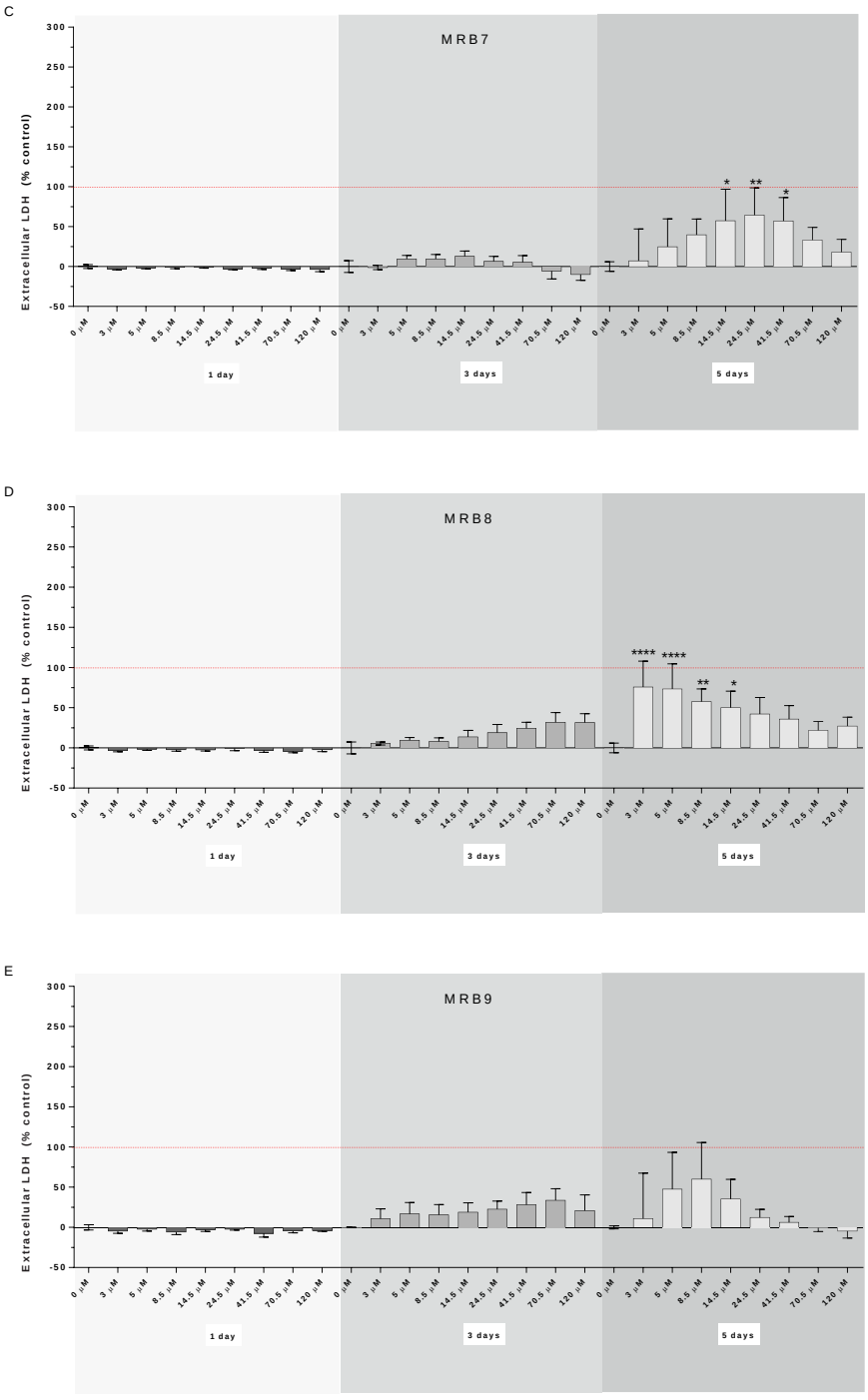

Figure 5.5 (C, D, E) - LDH leakage cytotoxicity assay for bidentate chelators, i.e. **MRB2** (A), **MRB20** (B), **MRB7** (C), **MRB8** (D) and **MRB9** (E) in Hep G2 cells, after 1, 2, or 5 day-incubation at 37ºC. Each chelator was tested at a concentration range of 3 to 120 μM. The graphs show the geometric mean ± SEM of extracellular LDH (percentage of control) obtained from four independent experiments. Each condition was tested in triplicates. The dashed line represent the percentage of LDH leakage obtained for the positive control (cell treated with triton). Statistical analysis was performed using ANOVA followed by Holm-Sidak's multiple comparison test. Statistical significance: * $p<0.05$, ** $p<0.01$, *** $p<0.001$ and **** $p<0.0001$, when compared with control (0 μM) of the respective time-point.

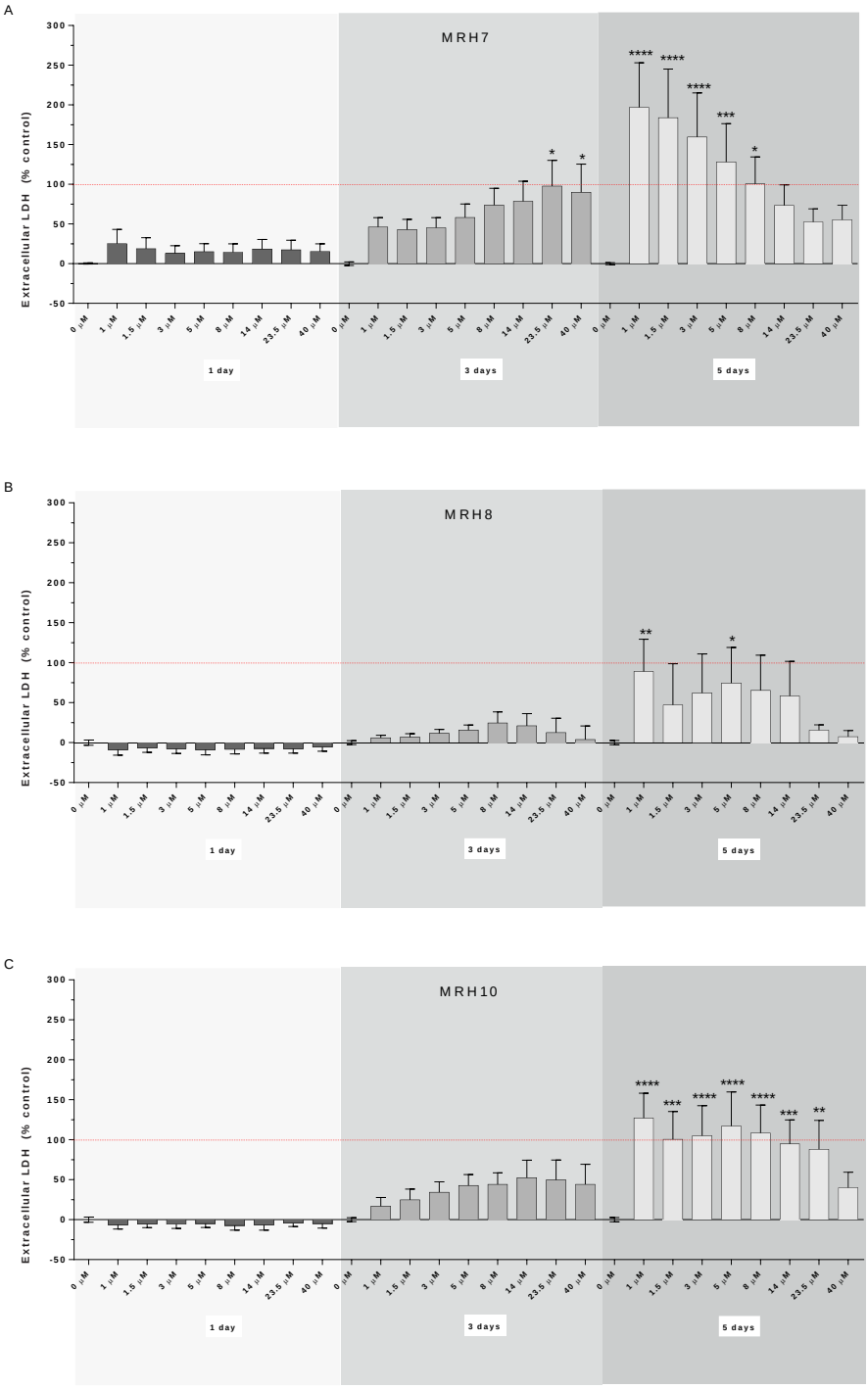

Figure 5.6 - LDH leakage cytotoxicity assay for hexadentate chelators, i.e. **MRH7** (A), **MRH8** (B) and **MRH10** (C) in Hep G2 cells, after 1, 2, or 5 day-incubation at 37ºC. Each chelator was tested at a concentration range of 3 to 120 μM. The graphs show the geometric mean ± SEM of extracellular LDH (percentage of control) obtained from four independent experiments. The dashed line represent the percentage of LDH leakage obtained for the positive control (cell treated with triton). Statistical analysis was performed using ANOVA followed by Holm-Sidak's multiple comparison test. Statistical significance: * $p<0.05$, ** $p<0.01$, *** $p<0.001$ and **** $p<0.0001$, when compared with control (0 μM) of the respective time-point.

The results show that the cytotoxicity of all tested chelators appears to increase over incubation time.

After 24h of incubation, no significant toxicity was observed for all the chelators. However, ligand **MRB20** seems to show some tendency to induce LDH release at this stage (the lowest concentration tested, i.e. 3 μM, promoted 25.24 ± 17.59% of response).

At the third day of incubation, ligands **MRB20** and **MRH7** have shown to produce significant toxicity for the cells at the two highest concentrations tested.
The bidentate ligand **MRB20** induces a leakage of enzyme up to 79.53 ± 21.10% for concentrations equal to or superior than 70.5 μM. Although not significantly different from control, lower concentrations increased cell death up to 60.63 ± 15.69%.
The hexadentate ligand **MRH7** promoted the enzyme leakage up to 97.5 ± 32.54% at concentrations equal to or superior than 23.5 μM. The percentage of extracellular LDH ranged from 43.05 ± 12.85 to 78.60 ± 25.17% for concentrations between 1 and 14 μM, although these values are not significantly different from control.

At the last day of incubation (day 5), all chelators induced toxicity on HepG2 cells, with the exception of the bidentate ligands **MRB9** and **MRB2**. For the latter chelators, although not statistically different from control, the values of extracellular LDH were higher than those attained for shorter incubation periods (24h and 72h).

Considering the positive control, i.e. 1% Triton X-100, the leakage of the intracellular content of LDH is expected to occur at the beginning of the experiment (~0h).
In the case of experiments with long drug exposures, this fact may introduce some artefacts on the obtained results, as the LDH activity will be lower due to an eventual degradation of the released enzyme in the course of time.
Accordingly, at day 5, some concentrations of the chelators **MRB20**, **MRH7** and **MRH10**, produced levels of extracellular LDH were higher than 100%. Contrary to the initial leakage of the total content of intracellular enzyme (that occurs for positive control), when cells are exposed to chelators, the enzyme appears to be released latter originating higher levels of LDH for treatments (when compared to positive control).

5.4 Conclusions

Comparing both methods used for the evaluation of the cytotoxic profile of chelators, MTT and LDH assays, the results obtained by the first method seem to indicate that, after 5 days of incubation, the compounds induce significant toxicity for the majority of tested concentrations. Nevertheless, in general, only the highest concentrations tested were above the half maximal effective concentration (EC50) (i.e. the concentration of a drug required to produce 50% of the drug's maximal effect as depicted by a graded dose-response curve [384]).The unique exception was the chelator **MRB20** that, from 5 μM, highly reduced the viability of hepatocytes to levels lower than 50%.

The results obtained by LDH assay showed that the rhodamine chelators induce toxicity to HepG2 cells particularly during longer periods of incubation, i.e. 5 days. For earlier time-points, the toxicity was inexistent or low.
Once again, **MRB20** was the molecule that induced higher toxicity for HepG2 cells. Evidence of the toxicity of this compound was previously reported in the experiments performed with macrophages (at concentrations up to 3 μM) for the evaluation of the antimycobacterial effect of the drug (Chapter 3.3.1.1).
Altogether, this molecule seems to be the most toxic chelator for HepG2 cells (and macrophages) and this property may be explained by its charge, as this chelator is the sole of this set of molecules that has a positive charge at physiological pH (as discussed previously in Chapter 3).

Amongst the hexadentate ligands, **MRH7** and **MRH10** were the most toxic chelators and induced higher toxicity at day 5. However, in the results obtained by the MTT assay, the cytotoxic profile of all the hexadentate chelators are similar.
Curiously, **MRH10** and mainly **MRH7** are the most active chelators in terms of its antibacterial effect (*M. avium* and extracellular bacteria). In particular, **MRH7** is also the hexadentate chelator that presents higher interaction with membranes (liposomes, macrophages and PBMC's, as discussed in chapter 4).
This fact may suggest that the chelator(s) has clearly higher ability to interact with membranes than the other hexadentate ligands, namely those derived from carboxyrhodamines (**MRH8**, **MRB8** and **MRB9**). This increased ability to "disturb" the membranes may be useful for the antibiotic activity.

However, for long exposures, it may cause some degree of toxicity, as corroborated by alterations on the membrane permeability and mitochondrial competence that ultimately led to the impairment the cellular viability.

The overall results also suggest that hexadentate chelators seem to show more toxicity than bidentate ligands. This fact may be explained, bearing in mind, and as mentioned before, that three molecules of a bidentate ligand are needed to chelate the amount of iron(III) as opposed to one molecule of a hexadentate ligand. Therefore the concentrations of hexadentate chelators tested were three times lower than those selected for bidentate ligands.

These results also put forward that an incubation time of 5 days seems to be excessively long. As the chelators are less toxic at 24h of incubations, the applicability of the chelators as antibiotics may be more relevant to fight fast growth bacteria, such as *M. smegmatis* or some extracellular bacteria, as *E.coli* or *S. aureus*.

To the best of our knowledge, the work described in this chapter is the first report concerning the *in vitro* cytotoxic profile of rhodamine derived 3,4-HPO chelators, which gain particular relevance as the chelators are expected to be used as antibacterial agents.

6 | 3,4-HPO CHELATORS WITH ENHANCED WATER SOLUBILITY FOR ANALYTICAL APPLICATIONS

6. 3,4-HPO CHELATORS WITH ENHANCED WATER SOLUBILITY FOR ANALYTICAL APPLICATIONS

6.1 Introduction

Our research group has a well stablished collaboration with the colleagues from the analytical chemistry field [174, 175] in order to produce ligands for detection of metal ions, namely iron, in water, with improved analytical properties and lower toxicity. Most of the used reagents currently available are toxic [385] and, in a recent work, low toxicity 3,4-HPO ligands were tested and successfully applied to the determination of iron in bathing waters [174]. However, its efficiency was limited by the ligand solubility as the sensitivity for the determination of iron increased with the increase of ligand concentration in solution [174].

In this scenario, we designed a 3,4-HPO with improved water solubility. This possibility is feasible as the structure of 3,4-HPO allows tailoring of their hydrophilic/lipophilic balance without significantly changing its chelating properties. The variation in this balance can be achieved by simply introducing appropriate substituents on the nitrogen atom of the pyridinone ring. As referred in the literature [168], the effect of the insertion of different substituent groups, such as alkyl and alkyl-amine, -carboxylic, -amide, and hydroxyalkyl groups in the nitrogen atom on the hydrolipophilic character and in *in vivo* iron mobilization was investigated [386]. The corresponding logarithmic distribution coefficient values (log D_{ligand}; 1-octanol/ water, MOPS buffer, pH = 7.4) were calculated. The authors verified that there is a relationship between the lipophilicity of the ligands (log D_{ligand}) and that of the corresponding iron complexes (log $D_{complex}$) and they put forward that for lipophilic ligands (log $D_{ligand} > -1$), the complex can be approximately 3-fold more lipophilic than the corresponding ligand but for more hydrophilic compounds (log $D_{ligand} < -1$) the lipophilicity of the complexes accompanies more closely that of the ligands suggesting identical solvation effects for the ligands and complexes.

Consequently, a more hydrophilic ligand is expected to form a iron(III) complex that provides a more sensitive method with lower detection limit than the previously used 3,4-HPO ligands [174].

In this chapter, the synthesis of a more water soluble 3,4-HPO is reported. The compound was obtained by introducing a polyethylene glycol (PEG) chain in the nitrogen atom of the pyridinone ring. The aim was to increase the sensitivity and decrease the detection limit for

the spectrophotometric determination of iron, which was limited by the low solubility of the ligand used in the previous work [174].

The synthesis and solution properties of 3,4-HPO ligands and their complexes with M(II) and M(III) metal ions is a central interest in our research group [159, 174, 175, 177]. In order to improve the water solubility of ligans and complexes we considered the inclusion pf PEGylated substituents on the nitrogen of the 3,4-HPO ring. Oligo(ethylene glycol)s (OEGs) have been reported in the literature as compounds with high water solubility [387]. Herein we report the synthesis of an amine-terminated OEGs with a methyl group in the end of the chain and of the corresponding 3,4-HPO ligand, PEG-HPO (Figure 6.1) obtained through reaction of the amine with protected for of 2-methyl-3-hydroxy-4-pyrone (maltol).

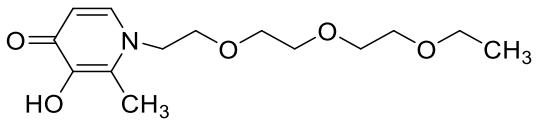

PEG-HPO
or
(MRB12)

Figure 6.1 - Formula of 3,4-HPO functionalized with a hydrophilic ethylene glycol chain (PEG-HPO or **MRB12**).

The conjugation of these amino-PEGylated chains with 3,4-HPO will improve the hydrophilicity of these ligands and their metal ion complexes allowing their wider use in biological and analytical applications.

The efficiency of this new compound as a novel iron chelator was tested in a sequential injection system. The complexation reaction of the synthesized ligand and iron(III) was studied in-line and applied to two certified waters samples. The results obtained in terms of sensitivity, selectivity and limit of detection were critically compared with those previously described using the less hydrophilic 3,4-HPO ligand [174]. The choice of sequential injection (SI) analysis, as flow analysis technique, was based not only on its extensive use as an efficient tool for water analysis [388] but also to attain an appropriate comparison with the previously developed method. In the end, a SI method for the determination of iron is proposed, based on a newly synthesized hydrophilic 3,4-HPO ligand as an alternative reagent for iron determination.

The PEGylated chain was synthesized in collaboration with Professor Enrique Borges and his group researchers. The mass spectrometry experiments for the characterization of the Iron(III) complex of PEGylated 3,4-HPO were performed by a member of our group, André Silva. The analytical studies were performed by the group of Professor António Rangel at “CBQF - Centro de Biotecnologia e Química Fina - Laboratório Associado, Escola Superior

de Biotecnologia, Universidade Católica Portuguesa/Porto". The results obtained in these studies will be discussed in the present chapter as they describe an application of the molecule synthesized in the analytical field.

The synthesis and characterization of the new 3,4-HPO discussed in this chapter. Further details for analytical methods and results and discussion were published in:

[389] Mesquita, R.B.R. [#], **Moniz, T.**[#], Miranda, J.L.A.[#], Gomes, V.[#], Silva, A.M.N., Rodriguez-Borges, J.E., Rangel, A.O.S.S. and Rangel, M.*, Synthesis and characterization of a 3-hydroxy-4-pyridinone chelator functionalized with a polyethylene glycol (PEG) chain aimed at sequential injection determination of iron in natural waters*, Polyhedron, **2015**, 101, 171-178. DOI: 10.1016/j.poly.2015.09.015. ([#] These authors contributed the same)

6.2 Methods

6.2.1 Synthetic procedures

6.2.1.1. Synthesis of the PEGylated chain

The PEGylated chain was synthesized and characterized according to procedures described in the literature [387].
Microwave-assisted reactions were carried out in a CEM Discovery Labmate circular single-mode cavity instrument (300 W max magnetron power output) from CEM Corporation.

*6.2.1.2 Synthesis of the protected PEGylated 3,4-HPO (**3**)*

The protected PEGylated 3,4-HPO was obtained using the typical procedure utilized to prepare 3,4-HPOs in which a protected 3-hydroxy-4-pyrone reacts with a primary amine [390, 391] (Figure 6.4).

A mixture of amine **1** (2.1459g, 0.01832 mol) dissolved in dried ethanol (6 mL) was placed in a 10 mL reaction vial, which was then closed under argon atmosphere and placed in the cavity of a CEM microwave reactor. The reaction vial was irradiated: 1 min ramp to 160ºC and 120 min hold at 160ºC, using 100 W maximum power. The reaction solvent was evaporated and the crude oil resultant was dissolved in 50 mL of water. The product was separated from the starting material 2 by liquid/liquid extraction with 3 x 30 mL of diethyl ether. The organic phase was rejected and the aqueous phase was concentrated and then

purified by chromatography, using a mixture of chloroform/methanol (9:1), affording 1.7520 g of conjugate **3** (49% yield) (Figures 6.2 and 6.4).

^{1}H NMR (400.15 MHz, MeOD-d_4, ppm): δ 1.55 (t, J= 7.1 Hz, 3H, -$CH_2C\underline{H}_3$); 2.22 (s, 3H, 2-$C\underline{H}_3$); 3.46-3.61 (m, 10H, H3'-H7'); 3.68 (t, J= 4.6 Hz, 2H, 2'-$C\underline{H}_2$); 4.13 (t, J= 4.6 Hz, 2H, 1'-$C\underline{H}_2$); 5.07 (s, 2H, -$C\underline{H}_2C_6H_5$); 6.48 (d, J= 7.4 Hz, 1H, H5); 7.27-7.42 (m, 5H,- $CH_2C_6\underline{H}_5$); 7.69 (d, J= 7.4 Hz, 1H, H6). ^{13}C NMR (100.62 MHz, MeOD-d_4, ppm): δ 12.9 (2-$\underline{C}H_3$); 15.2 (-$CH_2\underline{C}H_3$); 54.4 (C1'); 70.5 (C2'); 71.0-71.3 (C3'- C7'); 74.1 (-$\underline{C}H_2C_6H_5$); 116.4 (C5); 128.9-129.1 (-$\underline{C}_6H_5$); 129.8 (Cq, -$\underline{C}_6H_5$); 138.1 (C6); 141.9 (C2); 145.1 (C3); 174.1 (C4).

6.2.1.3 Synthesis of the PEGylated 3,4-HPO (PEG-HPO)

A solution of ligand **3** (2.0117 g, 0.00536 mol) in methanol (40 mL) and HCl (0.01 mL) was placed into a hydrogenation vessel. The air was removed with N_2, a catalytic amount of 10% Pd/C (w/w) was added and the mixture was stirred at room temperature, with H_2 at 40 PSi for 6 h. The reaction mixture was filtered, washed with methanol and CH_2Cl_2 and the solvent evaporated in vacuum to give the brown oil product. The resulting residue was dried under vaccum to give 1.6378 g of PEG-HPO (95% yield) (Figures 6.2 and 6.4).

^{1}H NMR (400.15 MHz, MeOD-d_4, ppm): δ 1.04 (t, J= 7.1 Hz, 3H, -$CH_2C\underline{H}_3$); 2.54 (s, 3H, 2-$C\underline{H}_3$); 3.37-3.56 (m, 10H, H3'-H7'); 3.79 (t, J= 4.8 Hz, 2H, 2'-$C\underline{H}_2$); 4.48 (t, J= 4.8 Hz, 2H, 1'-$C\underline{H}_2$); 7.03 (d, J= 7.4 Hz, 1H, H5); 8.04 (d, J= 7.4 Hz, 1H, H6). ^{13}C NMR (100.62 MHz, MeOD-d_4, ppm): δ 13.2 (2-$\underline{C}H_3$); 15.4 (-$CH_2\underline{C}H_3$); 57.0 (C1'); 67.5 (C7'); 70.1 (C2'); 70.5-71.5 (C3'- C6'); 111.4 (C5); 140.0 (C6); 143.2 (C2); 144.6 (C3); 160.3 (C4). MS: calculated for $C_{14}H_{24}NO_5^+$: 286.16 (monoisotopic molecular weight M^+), found: MS: 286.16261.

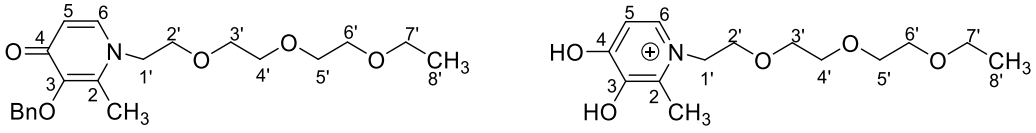

3 **PEG-HPO**

Figure 6.2 - Formulae and numbering of compound **3** and chelator PEG-HPO.

6.2.1.4 Iron(III) complex of PEGylated 3,4-HPO ($Fe(PEG\text{-}HPO)_3$)

FeL_3 complex was prepared by dissolving stoichiometric amounts of $Fe(NO_3)_3$. $9H_2O$ (0.283 g, 0.7 mmol) and ligand PEG-HPO (0.60 g, 0.0021 mol) in water, adjusting the pH to 8 with a diluted solution of NaOH. The reaction mixture was kept with stirring, for 3 days at room

temperature. A precipitate was formed, collected by filtration and washed with water and a red power was isolated (quantitative yield).

MS: $[H_2L]^+$ ($C_{14}H_{24}NO_5^+$), *m/z* = 286.16499 (Δm = 0.3 ppm); $[NaHL]^+$ ($NaC_{14}H_{23}NO_5^+$), *m/z* = 308.14664 (Δm = -0.7 ppm); $[Fe(L)_2]^+$ ($FeC_{28}H_{44}N_2O_{10}^+$), *m/z* = 624.23363 (Δm = -0.6 ppm); $[H(Fe(L)_3)]^+$ ($FeC_{42}H_{67}N_3O_{15}^+$), *m/z* = 909.39250 (Δm = 1 ppm); $[Na(Fe(L)_3)]^+$ ($NaFeC_{42}H_{66}N_3O_{15}^+$), *m/z* = 931.37393 (Δm = 0.4 ppm).

6.3 Results and discussion

6.3.1 Synthesis of the new iron chelator

Ligands of the 3,4-HPO type are usually synthesized through the reaction of a 3-hydroxy-4-pyrone and a primary amine as depicted in Figure 6.4 [171].

Figure 6.3 - Generic reaction of the synthesis of pyridinones from pyrones.

The above reaction (Figure 6.3) allows the introduction of different R^2 substituents on the heterocyclic nitrogen atom by selection of the appropriate amine. The use of amines with different R^2 substituents allows the synthesis of 3,4-HPOs with variable physicochemical properties, such as water solubility. Moreover, and as shown in previous studies [159, 171, 173, 391], such alterations on the substituents of the nitrogen atom of the heterocyclic ring of 3,4-HPOs do not significantly change the chelating properties of the 3,4-HPO ligands.

Aiming to increase the water solubility of the 3,4-HPOs used in the previous study and considering the water solubility of Oligo(ethylene glycol) chains. We used an amino-PEGylated chain with a methyl group in the end of the chain and the corresponding 3,4-HPO ligand as shown in Figure 6.4.

*6.3.1.1 Optimization of the experimental procedures the synthesis of the protected PEGylated 3,4-HPO (**6.3**)*

The synthesized amine functionalized with an OGE chain (**6.1**) reacts with the protected 3-hydroxy-4-pyrone (**6.2**) leading to the displacement of the oxygen atom of the ring and its further replacement by the nitrogen of the anime group of the chain producing a protected 3,4-HPO (Figure 6.4). Compound **6.2** was synthesized in our laboratory following the procedures described in the literature [390].

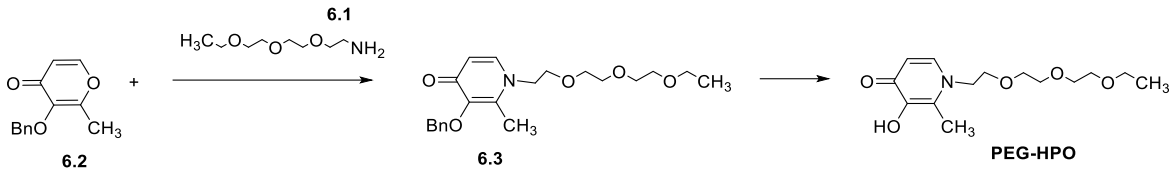

Figure 6.4 - Synthesis of: A, the PEGylated chain; and B, the functionalized 3,4-HPO.

The synthesis of **6.3** was performed by adding **6.1** to **6.2** in ethanol under reflux (oil-bath) for 72 h yielding **6.3** in 27% yield (a, Table 6.1). In order to improve the reaction outcome to synthesize **6.3**, some modifications were performed on the synthetic procedure.

Microwave-assisted organic chemistry was used instead of the traditional oil bath in order to obtain the desired compound **6.3** in a good yield, decreasing the reaction time and consequently promoting a more efficient synthetic protocol. Therefore, in a monomode reactor, under closed-vessel conditions the reaction was performed using an excess of 1.5 eq of the amine **6.1** and 100 mg of **6.2**, during 2h. Then, the reacting mixture was analysed by NMR and the conversion of **6.2** into **6.3** was calculated and 38% of the limiting reagent **6.2** was converted in **6.3** (b, Table 6.2). The same conditions was performed but with acidification of the medium with HCl and the percentage of conversion was determined and 24% occurred (c, Table 6.1). This result have shown that the reaction occurs with higher percentage of conversion of **6.2** into **6.3** in non-acidified medium and we tested the same excess of 1.5 eq of the amine **6.1** during 2h but scaling up the amount of reagents to 500 mg of **6.2** (d, Table 6.1) and the conversion obtained was 59%. In the next condition tested (e, Table 6.1), we increased the excess of the amine **6.1** to 2 eq and we maintained 500 mg of **6.2**, and 2h of reaction leading us to obtain a percentage of conversion of 84%.

This modification allowed formation of a higher amount of the ligand **6.3** and concomitantly we obtained our desired product with lower reaction time. All the experimental conditions performed for the synthesis of **6.3** are summarized in Table 6.2.

Table 6.1 - Experimental conditions of the synthesis of modified 3,4-HPO (**3**). *yield obtained by product isolation after purification.

Entry	Method	Fold excess of (6.1)	Amount of (6.2)	Time	% of conversion in (6.3) (calculated by NMR)
a	Oil bath	1.5	500 mg	72 h	27*
b	MW	1.5	100 mg	2 h	38
c	MW	1.5	100 mg (+ HCl)	2 h	24
d	MW	1.5	500 mg	2h	59
e	MW	2	500 mg	2 h	84

In order to obtain the final 3,4-HPO ligand, the protecting group of **6.3** was removed under a hydrogen atmosphere in the presence of Pd/C (10%) and HCl, to obtain the hydrochloride salt of ligand PEG-HPO.

The derivatization of 3,4-HPO ligands with amino-PEGylated chains was successfully achieved and a new 3,4-HPO ligand with an enhanced solubility in water was obtained. The new type of 3,4-HPO ligands will significantly enhance the water solubility of the ligands and its metal ion complexes and for that reason will allow to enlarge the field of application of this class of ligands.

6.3.1.2 NMR spectroscopy

The structures of the ligands **6.3** and PEG-HPO in solution were established by NMR analysis (^{1}H and ^{13}C, 1D and 2D experiments, including COSY, HSQC and HMBC spectra for unequivocal assignment of the most characteristic proton and carbon chemical shifts). The assignment of the resonance signals in ^{13}C NMR spectra of the protected and de-protected compounds was achieved by analysis of $^{1}H/^{13}C$ HSQC and $^{1}H/^{13}C$ HMBC spectra, which provide one and multiple bond ^{1}H-^{13}C connectivity.

The ^{1}H NMR spectra of ligand **6.3** revealed that the resonance signals of the methyl protons from the terminal group (8'-C$\underline{H}_3$) appear at 1.15 ppm and the correspondent carbon (C8'), with HSQC correlation, appear at 15.17 ppm. The singlet at 2.22 ppm was attributed to the methyl substituent in the pyridinone ring (2-C$\underline{H}_3$) and HSQC correlation with resonance signal at 12.85 ppm allow us to attribute this pick to 2-$\underline{C}H_3$ carbon. The multiplet in the aliphatic region of the spectra (3.46 – 3.61 ppm) was assigned to protons of –CH_2 groups (3'-C$\underline{H}_2$ - 7'-C$\underline{H}_2$) of the ethoxyl tail and their respective carbons appear between 71.04 – 71.33 ppm. Signals at 3.68 and 4.13 ppm were assigned as the protons of the –CH_2 groups

linked to the nitrogen atom of the pyridinone ring (2'-C$\underline{H}_2$ and 1'-C$\underline{H}_2$) and their respective carbons appear at 70.5 and 54.4 ppm. For carbon C1', HMBC correlation with carbon 2-$\underline{C}H_3$ was found, allowing the assignment performed.

The resonance singlets at 6.48 and 7.69 ppm were assigned to the aromatic CH protons (H5 and H6, respectively) of the pyridinone residue and show HSQC and HMBC correlations with carbons at 116.4 and 138.1 ppm, assigned as C5 and C6, respectively. The signals related with the protecting group are the singlet at 5.07 ppm that corresponds -C$\underline{H}_2C_6H_5$ and the -$CH_2C_6\underline{H}_5$ protons of the protecting group appear as a multiplet between 7.27-7.42 ppm. The carbon -$\underline{C}H_2C_6H_5$ is at 74.1 ppm and the other carbons of the protecting group (-$CH_2\underline{C}_6H_5$) appear between 128.9 and 129.0 ppm. The resonance signal at 129.8 ppm was found to give long range coupling to the resonance signals of the protons -C$\underline{H}_2C_6H_5$ and the CH protons of the protecting group and was attributed to the quaternary carbon of the protecting group. The last quaternary carbons at 141.9, 145.1 and 174.1 ppm were attributed C2, C3 and C4 due to their correlations in HMBC with the protons of the pyridinone ring and with C1' for carbon C2.

After the deprotection (PEG-HPO), significant differences in the ^{1}H and ^{13}C spectra were detected as for example the shift of the protons of methyl substituent in the position 2 of the pyridinone ring (2-C$\underline{H}_3$) that moved from 2.22 to 2.54 ppm and the respective carbon signal, 2-$\underline{C}H_3$, was shifted from 12.85 to 13.21 ppm. The protons of -CH_2 groups near to the nitrogen of the pyridinone are also shifted, namely 2'-C$\underline{H}_2$ and 1'-C$\underline{H}_2$, that moved to 3.79 and 4.48 ppm as well as their respective carbons from 70.5 to 70.1 ppm and namely from 54.4 to 57.0 ppm, respectively.

The resonance signals attributed to the -CH protons H5 and H6 revealed a shift from 6.48 to 7.03 ppm and from 7.69 to 8.04 ppm, respectively. Their respective carbons are also dislocated to low field region, namely from 116.4 and 138.0 ppm in the protected ligand, to 111.4 and 140.0 ppm in the deprotected form, respectively for C5 and C6 carbons.

The resonance signal at 143.2 ppm has shown HMBC correlation with H6, 1''-C$\underline{H}_2$ and 2-C$\underline{H}_3$ protons and was attributed to C2. The carbon at 144.6 ppm shows HMBC correlation with H5, H6 and protons and 2-C$\underline{H}_3$ and was attributed to C3. The pick at 160.3 ppm was attributed as carbons C4 due to its HMBC correlations with H5 and H6.

The observed differences in the chemical shifts of ^{1}H and ^{13}C nucleus in the spectra of the protected and deprotected compounds are primarily due to the deprotection of the hydroxyl group and the acidic pH of the deprotection reaction that lead to isolate the final ligands in the enol form [170].

6.3.1.3 Synthesis and characterization of the Iron(III) complex of Ligand PEG-HPO

The complex $Fe(L)_3$ was synthesized by mixing the iron salt, $Fe(NO_3)_3 \cdot 9H_2O$, and the ligand in water at pH = 8. Upon precipitation, the complex was isolated and its composition was determined by ESI-MS. The mass spectrum of the isolated complex shows the free ligand (*m/z* = 286.16499 $[H_2L]^+$ and *m/z* = 308.14664 $[NaHL]^+$) and two charged iron complexes, $[Fe(L)_2]^+$ (*m/z* = 624.23363) and $Fe(L)_3$ (m/z = 909.39250 $[H(Fe(L)_3)]^+$ and *m/z* = 931.37393 $[Na(Fe(L)_3)]^+$), as observed for the alkylpyridinone iron(III) complexes [171]. The high accuracy mass determination together with the observed isotopic patterns allowed to unequivocally assign the chemical composition of the ions. As revealed by solution speciation studies, the presence of both iron complexes is to be expected at acidic pH values (pH ≤ 6), which can be provided by the electrospray plume acidification occurring in positive ionization mode [392, 393]. In addition, it should be noted that the $Fe(L)_3$ complex is a neutral species and its ionization requires protonation or sodium adduct formation. However, these reactions are likely to promote ligand dissociation, leading to the detection of the more stable $[Fe(L)_2]^+$ cation and the free ligand in its fully protonated ($[H_2L]^+$) and sodiated ($[NaHL]^+$) forms. Altogether, MS data provides further evidence for the ability of L to bind ferric ions, forming FeL_2 and FeL_3 complexes, as expected for a 3,4-HPO bidentate ligand.

6.3.2 Analytical procedure - sequential injection method

The advantageous characteristics of sequential injection (SI) analysis concept namely versatility, extent of automation and low reagent consumption, made it an appropriate choice for automation of the analytical application of 3,4-HPO ligands for iron determination. In this context, it was important to confirm that the complexation reaction was as fast as evidenced in the previous work involving other 3,4-HPO ligands, as this would strongly influence the SI protocol to be designed. To do so, the absorbance of a mixture, placed in a conventional cell, of 1 mL ligand solution 178.5 mg/L, 0.1 mL carbonate buffer 0.25 M and 0.5 mL of 10 mg/L iron(III) standard was measured for 1 minute. According to the work of Mesquita et al. [174], the absorbance was monitored at 460 nm, corresponding to the maximum absorbance of the FeL_3 complex. The colour was observed almost immediately after mixing, indicating the complex formation. After the observed initial reaction, there was no significant absorbance increase, ≤ 9%, during the measured time (1 min).

As described in the previous study with other 3,4-HPO ligands [174], the carbonate buffer was needed to adjust the pH of the solution, obtained by mixing sample/standard, ligand solution and buffer, to about seven. Considering that the standard solutions were acidified to pH ≈ 2, the buffer solution was used at a pH ≈ 9.5.

After the detailed studies for the determination of iron based on the coloured complex formed with the PEG-HPO bidentate ligand, the characteristics of the developed method were summarized (Table 6.2).

Table 6.2 - Features of the developed methodologies for iron(III) determination in water samples using PEG-HPO ligand as a colorimetric reagent.

Dynamic range (mg/L)	Typical calibration curve[a] A = m.[Fe^{3+}] + b	LOD (µg/L)	Quantification rate (h^{-1})	Reagent/sample consumption	Effluent production (µL)
0.10 - 1.00	y = 0.0392 (±0.0017) [Fe^{3+}] + 0.008 (±0.002) R^2 = 0.996 ± 0.005	48	72	44.3 ug 3,4-HPO 0.71 mg $NaHCO_3$ 0.92 mg HNO_3 500 µL	1860

[a] n=5

The limit of detection, LOD, was calculated according to IUPAC recommendations [394], three times the standard deviation of ten blank signals. A typical calibration curve corresponds to the mean of five calibration curves obtained in consecutive days (with the standard deviation values in brackets). The determination rate was calculated based on the time spent per cycle; a complete analytical cycle took about 0.83 min. An analytical cycle is the sum of the time needed for each step plus the time necessary for the port selection in the selection valve. The presented consumption values, for reagents and sample, and the effluent production were calculated per determination.

The repeatability was assessed by calculation of the relative standard deviation (RSD) obtained by the mean of ten consecutive injections of sample. The calculated RSD was 3.1% (0.225 ± 0.007 mg Fe /L).

6.4 Conclusions

In this work, the synthesis of new highly soluble 3,4-HPO chelator functionalized with a hydrophilic polyethylene glycol chain (PEG-HPO) was successfully achieved and is reported together with that of its iron(III) complex. The improved hydrophilic balance of the PEGylated 3,4-HPO ligand was fully explored in an analytical application with the development of an alternative flow analysis method. The new molecule especially designed to present a higher water solubility, proved to meet the aim of improving the detection limit and sensitivity in the determination of iron.

In fact, the sensitivity (calibration curve slope) obtained with the developed SI method, using the new ligand, showed an increase close to 60% when compared to the previously described method [174] and a decrease of the detection limit to about half (Table 6.3).

Table 6.3 - Comparison of the developed SI method, using the newly synthesized ligand, PEG-HPO, with the previously described less soluble form of the 3,4-HPO.

Ligand formula	|Ligand|	Sensitivity (L/mg)	LOD (µg Fe/L)	Sample consumption/ determination	Ref.
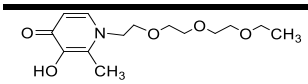 PEG-HPO	178 mg/L	S = 0.0392	48	500 µL	This work
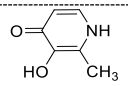 Hmpp	20 mg/L	S = 0.0251	83	300 µL	[174]

The choice of sequential injection as a flow technique proved to be highly appropriated, enabling the detailed study of the complexation reaction with a fast and automatic method. For a flow analysis effective application, contributed the excellent characteristic of the complex formation being almost immediate. Furthermore, the good results obtained with the certified water samples (data not shown), reinforced the successful application to the determination of iron in natural waters.

Finally, and from the point of view of synthesis of new compounds, the newly synthesized ligand is not only important for this particular work but also opens new perspectives for the synthesis of other metal ion complexes with improved water solubility. The design of new 3,4-HPO functionalized with different PEGylated chains, varying the length of the chain, of will be considered as future work in order to develop molecules with different HLB, according to the desired application.

CONCLUDING REMARKS

CONCLUDING REMARKS

The present work is part of an on-going long term project in our research group regarding the development of new antibiotics based on the concept of iron deprivation, a novel drug target. In order to answer the questions raised in previous work, we designed new 3,4-HPO fluorescent chelators in which several structural modifications have been introduced.
Different types of fluorophores have been used for functionalization of the chelating units. For the rhodamine labelled chelators, different functional groups were considered in the fluorophore moiety. The set of newly synthesized compounds was studied in what concerns to their potential antimycobacterial effect. Biophysical studies were performed to get insight on chelator's interaction with membranes.

As the rhodamine framework of chelators has shown seems to be determinant for the antimycobacterial effect, the properties of the rhodamine labelled 3,4-HPO chelators, such as the HLB and charge, have been modified. With this purpose we changed the linker, between the fluorophore and chelating unit, and varied the functional groups bound to the nitrogen atom in the fluorophore structure. Chelators **MRB2**, **MRB4**, **MRB20**, **MRH10** and **MRB9** were designed in order to evaluate the influence of the functional groups *per se* and the establishment of the best conjunction of fluorophore substituents and type of linkage to improve antimycobacterial activity.
The effect of these new chelators in the control of the intramacrophagic growth of *M. avium* has been studied and the overall results reinforce our previous hypothesis. Chelators that include the thiourea group and have high lipophilicity, provided by the *N*-ethyl substituents in the xanthene ring, appear to be the most active ligands in terms of their antimycobacterial effect.
We previously assumed a possible correlation between the different functional groups in the structure of rhodamine labelled 3,4-HPO chelators and their interaction with biological membranes. Moreover, it seems that this interaction may ultimately be related with the observed antimycobacterial effect.
Several experiments regarding the study of the interaction of the rhodamine labelled 3,4-HPO chelators with biological membranes were performed, using different methods such as Fluorescence, NMR and EPR spectroscopies and MD. The results have shown that the distribution of these ligands in liposomes is better achieved for chelators labelled with

rhodamine B isothiocyanate (**MRH7** and **MRB7**) than for those functionalized with carboxytetramethylrhodamine, **MRH8** and **MRB8**. The results also revealed that the interaction of the ligands with the lipid phases comprises the hydrophobic region of the membrane models at different levels of the bilayer.

Cellular studies performed, using fluorescence confocal microscopy as a tool to explore the distribution of the rhodamine labelled chelators inside the cells (BMM and PBMC's), have shown that ligands can access the cytoplasm of both cell types. Results also pointed out the fact that the uptake of the more active compounds seems to be facilitated, as a higher amount of ligand was able to reach the cytosol. The studies of co-localization demonstrated that, once inside the BMM, the fluorescent ligands were able to access their targets, namely the phagosome.

Bearing in mind the overall results, we speculate that the mode of action of the different rhodamine labelled chelators seems to be similar due to the identical distribution patterns obtained in cellular studies and the subcellular compartments that these chelators can reach. In fact, **MRH7** and **MRB7** appear to have a higher ability to interact with biological membranes, as confirmed by the studies with liposomes. This property allows them to cross through the several barriers that exist in the cell. Once inside the host cell, chelators can accomplish their chelating function and combat the infection, decreasing the amount of iron available for *M. avium* survival. In contrast, **MRH8** and **MRB8** seem to have more affinity for aqueous environment and consequently they tend to stay outside the membrane, even in liposome suspensions or cells, thus being less effective ligands to chelate iron in the infection scenario. In Figure CR.1 a hypothetical mechanism is presented, showing that rhodamine framework potentiates the effect of the chelators.

As referred previously [4], we hypothesized that the fluorescent chelators are uptake and diffuse within macrophages. In our hypothesis we suggest that the rhodamine labelled 3,4-HPO chelators are targeting the phagosome and that the phagosomal membrane is one possible place where the fluorophore framework may tether the ligands, allowing the removal of iron from the interior of the phagosome.

Together with the results obtained in previous work [3], the present results illustrate the importance of small changes in the structure of the molecules with biological relevance and the influence of these modifications in drug membrane interaction, which is at least correlated with the final biological activity.

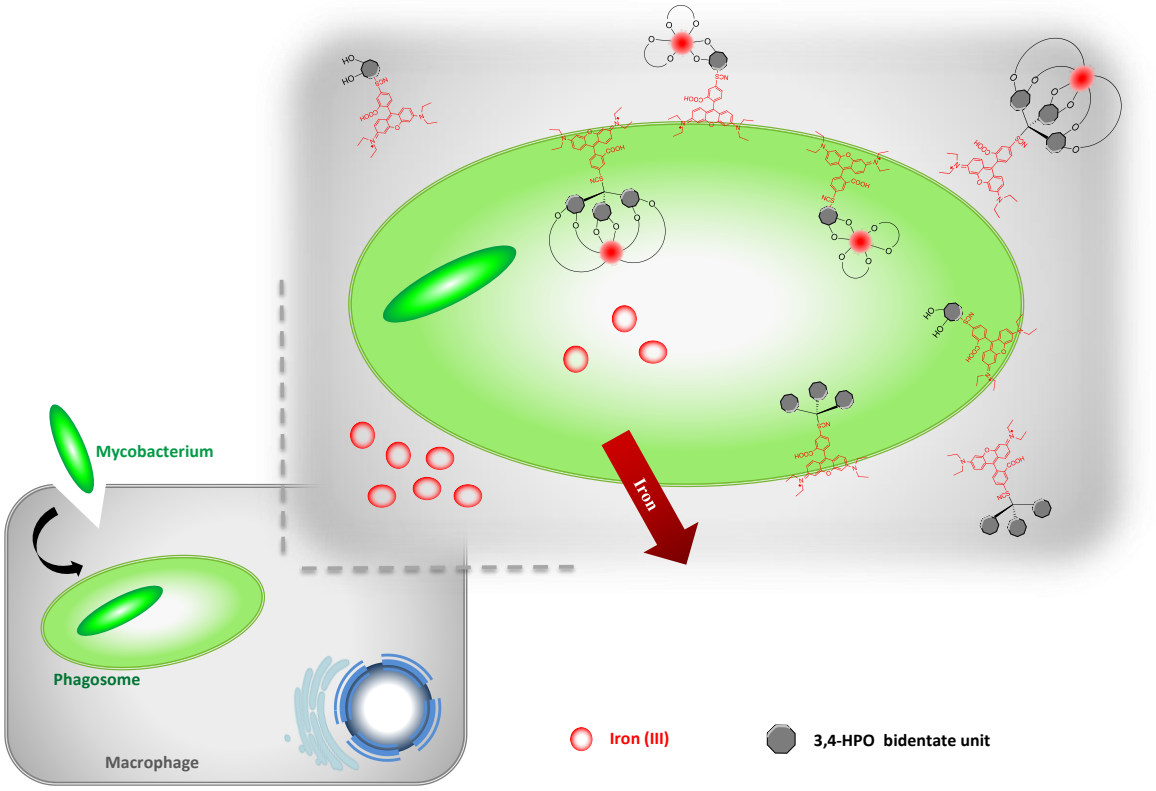

Figure CR.1 Outline of a hypothetical mechanism for the ironing-out effect produced by the rhodamine labelled 3,4-HPO chelators.

In vitro safety studies of rhodamine derived 3,4-HPO chelators were also performed. The viability of HepG2 cells was evaluated by MTT reduction and LDH leakage assays and the results obtained by both protocols were compared, providing evidence that hexadentate chelators seem to be more toxic than the bidentate related ligands.

Chelators induced toxicity to HepG2 cells particularly during longer periods of incubation (5 days), however, for earlier time-points, the toxicity was inexistent or low.

The results obtained suggest an eventual correlation between the toxicity of the chelators and their ability to interact with biological membranes.

Chelator **MRB20** was the most toxic molecule for HepG2 cells (Chapter 5) and at concentrations superior than 3 μM, the ligand reduced cellular viability to levels lower than 50%. The toxicity of **MRB20** was also observed in BMM in which the ligand induced the cell death at concentrations up to 3 μM (Chapter 3). These results may be explained by the fact that **MRB20** is a positively charged ligand (at physiological pH) and as it has been described, rhodamines with positive charge interact with the mitochondrial membrane [324, 325], destabilization in the cellular metabolism may occur, leading at last to the cell death.

Ligands **MRH7** and **MRH10** have also shown some toxicity at day 5 for HepG2 cells (in LDH leakage assay).

MRH7 was the hexadentate chelator that presents higher interaction with membranes (liposomes, macrophages and PBMC's, as discussed in Chapter 4). Curiously, both molecules are hexadentate ligands possessing a thiourea linkage. The relevance of the thiourea group for the interaction with bacterial surface has been reported [314]. It has also been described that the presence of a thiourea group may contribute for the inhibition of cell wall biosynthesis in *M. tuberculosis* [320]. The thiourea functional group is derived from an isothiocyanate (ITC) group present in the fluorophore moiety and it has also been described that the mechanism of action of ITCs may be related with the disturbing of biological membranes [309, 311, 312].

The relative antibacterial activity of the several chelators studied, their ability to interact with biological membranes and toxicity are summarized in Table CR.1.

Table CR.1 – Comparative table of chelator's antibacterial activity, their interaction with biological membranes and toxicity. 0 – no effect; + - low; ++ moderate; +++ - high; ++++ very high effect; *nd* – not determined.

Chelator	Structural features				Antibacterial activity	Toxicity	Membrane interaction
	Fluorophore	*N*-substituents	Linker	Charge (at pH = 7.4)			
MRH7	Rhodamine	*N*-ethyl	Thiourea	Neutral	++++	++	+++
MRH8	Rhodamine	*N*-methyl	Amide	Neutral	++	+	+
MRH10	Rhodamine	*N*-methyl	Thiourea	Neutral	+++	++	*nd*
MRB7	Rhodamine	*N*-ethyl	Thiourea	Neutral	++++	+	++
MRB8	Rhodamine	*N*-methyl	Amide	Neutral	++	+	+
MRB9	Rhodamine	*N*-ethyl	Amide	Neutral	++	+	*nd*
MRB2	Rhodamine	*N*-ethyl	Sulfonamide	Neutral	0	+	*nd*
MRB4	Naphthalene	---	Thiourea	Neutral	0	*nd*	*nd*
MRB20	Rosamine	*N*-ethyl	Amide	Positive	+	++++	*nd*

The most relevant conclusions are:

i) The antibacterial activity seems to be the conjugation of thiourea group and *N*-ethyl substituents in xanthene ring;

ii) The toxicity appear to be a result of several factors, mainly charge, but also the thiourea linker and higher denticity;

iii) The interaction with biological membranes may be the presence of *N*-ethyl substituents in xanthene ring and/ or thiourea group.

These facts suggest that the chelators that revealed higher capacity to interact with biological membranes may also have increased ability to "disturb" membranes. This property may contribute to a greater antibacterial effect but simultaneously may lead to a higher toxicity of the ligands.

In the field of medicinal chemistry and drug design, the overall results put in evidence that molecules can be optimized in terms of their structure in order to design iron(III) chelators with improved antibacterial effect and ability to interact (or to pass), through the barrier of the cell membrane(s) and reach the site of action, consequently enhancing their therapeutic effect.

The results discussed in this thesis have clarified some assumptions and answered the raised questions. However, other questions emerged and remain to be answered.
Thus, as future lines to investigate, some topics are proposed.
We are interested in the evaluation of the combination of most active chelator(s) with other antibiotics used for the treatment of mycobacterial infection.
We identified the finest combination of rhodamine labelled 3,4-HPO chelators a classic antibiotic to achieve higher biological activity. The results obtained have shown that the co-administration of the most active chelator, **MRH7**, with one of the currently used antibiotic in the treatment of mycobacterial infections, ethambutol, is a promising approach to fight *M. avium* infections.
As future work in the field of designing chelators to ironing out bacteria, we also intend to investigate the effect of ethambutol, in combination with other chelators, namely the non-fluorescent chelating units (Hdmpp and CP256), which were not effective in the control of intramacrophagic growth of *M. avium* and may gain advantage in their co-administration with other antibiotics.

In this thesis, another topic of research was also reported concerning on the synthesis of a new chelator (**PEG-HPO** or **MRB12**) specially conceived to improve the water solubility of the 3,4-HPO chelator and its complexes. The design of this new compound was performed bearing in mind that several modifications can be included in the 3,4-HPO moiety in order to change properties of these ligands, namely the HLB, without altering their chelating capacity. According to this, we introduced a PEGylated chain in the nitrogen atom of the 3,4-HPO ring. This new molecule has provided better sensitivity and lower LOD for the determination of iron in aqueous samples.
In this field, as future perspectives, we aim to design a set of new ligands with improved water solubility, based on PEGylated chains. Different chains with different length and terminal functional groups will be considered. We expect to be able to prepare ligands with an adequate HLB in order to produce water soluble molecules with simultaneous ability to interact with biological membranes.

As a final comment, the current results are relevant for the design of novel molecular architectures with application in varied fields and corroborate the versatility of the 3,4-HPO family of ligands. In 3,4-HPO structures, several modifications may be considered to tune the properties of the ligands according to the desired application in the different fields of research.

REFERENCES

REFERENCES

[1] Fernandes, S.S., Nunes, A., Gomes, A.R., de Castro, B., Hider, R.C., Rangel, M., Appelberg, R. and Gomes, M.S., *Identification of a new hexadentate iron chelator capable of restricting the intramacrophagic growth of Mycobacterium avium.* Microbes and Infection, 2010, **12**, 287-294.

[2] Moniz, T., *Novas Arquitecturas Moleculares para Combater Processos Infecciosos.* Tese de Mestrado em Bioquímica, Departamento de Química e Bioquímica, Faculdade de Ciências da Universidade do Porto, Porto, **2009**.

[3] Nunes, A., Podinovskaia, M., Leite, A., Gameiro, P., Zhou, T., Ma, Y., Kong, X., Schaible, U.E., Hider, R.C. and Rangel, M., *Fluorescent 3-hydroxy-4-pyridinone hexadentate iron chelators: intracellular distribution and the relevance to antimycobacterial properties.* Journal of Biological Inorganic Chemistry, 2010, **15**, 861–877.

[4] Moniz, T., Nunes, A., Silva, A.M.G., Queirós, C., Ivanova, G., Gomes, M.S. and Rangel, M., *Rhodamine labeling of 3-hydroxy-4-pyridinone iron chelators is an important contribution to target Mycobacterium avium infection.* Journal of Inorganic Biochemistry, 2013, **121**, 156-166.

[5] Latunde-Dada, G.O., *Iron metabolism: microbes, mouse, and man.* Bioessays, 2009, **31**, 1309-1317.

[6] Oliveira, F., Rocha, S. and Fernandes, R., *Iron metabolism: from health to disease.* Journal of Clinical Laboratory Analysis, 2014, **28**, 210-218.

[7] Miethke, M. and Marahiel, M.A., *Siderophore-based iron acquisition and pathogen control.* Microbiology and Molecular Biology Reviews, 2007, **71**, 413-451.

[8] Kim, S. and Ponka, P., *Role of nitric oxide in cellular iron metabolism.* Biometals, 2003, **16**, 125-135.

[9] Spellberg, B. and Ibrahim, A.S., *Recent advances in the treatment of mucormycosis.* Current Infectious Disease Reports, 2010, **12**, 423-429.

[10] Kalinowski, D.S. and Richardson, D.R., *The Evolution of Iron Chelators for the Treatment of Iron Overload Disease and Cancer.* Pharmacological Reviews, 2005, **57**, 547-583.

[11] Cowart, R.E., *Reduction of iron by extracellular iron reductases: implications for microbial iron acquisition.* Archives of Biochemistry and Biophysics, 2002, **400**, 273-281.

[12] Roosenberg, J.M., II, Lin, Y.M., Lu, Y. and Miller, M.J., *Studies and syntheses of siderophores, microbial iron chelators, and analogs as potential drug delivery agents.* Current Medicinal Chemistry, 2000, **7**, 159-197.

[13] Crichton, R., *Iron Metabolism: From Molecular Mechanisms to Clinical Consequences*, 2009, 3rd Edition, Wiley, United Kingdom.

[14] Nevitt, T., *War-Fe-re: iron at the core of fungal virulence and host immunity.* Biometals, 2011, **24**, 547-558.

[15] Sharpe, P.C., Richardson, D.R., Kalinowski, D.S. and Bernhardt, P.V., *Synthetic and natural products as iron chelators.* Current Topics in Medicinal Chemistry, 2011, **11**, 591-607.

[16] Kohgo, Y., Ikuta, K., Ohtake, T., Torimoto, Y. and Kato, J., *Body iron metabolism and pathophysiology of iron overload.* International Journal of Hematology, 2008, **88**, 7-15.

[17] Sun, H.Q., Lu, X.M. and Gao, P.J., *The exploration of the antibacterial mechanism of Fe3+ against bacteria.* Brazilian Journal of Microbiology, 2011, **42**, 410-414.

[18] Ratledge, C. and Dover, L.G., *Iron Metabolism in Pathogenic Bacteria.* Annual Review of Microbiology, 2000, **54**, 881–941.

[19] Kang, J.H., *Oxidative damage of DNA induced by ferritin and hydrogen peroxide.* Bulletin of the Korean Chemical Society, 2010, **31**, 2873-2876.

[20] Wang, X. and Zhao, X., *Contribution of oxidative damage to antimicrobial lethality.* Antimicrobial Agents and Chemotherapy, 2009, **53**, 1395-1402.

[21] Valko, M., Morris, H. and Cronin, M.T., *Metals, toxicity and oxidative stress.* Current Medicinal Chemistry, 2005, **12**, 1161-1208.

[22] Fakih, S., Podinovskaia, M., Kong, X., Collins, H.L., Schaible, U.E. and Hider, R.C., *Targeting the Lysosome: Fluorescent Iron(III) Chelators To Selectively Monitor Endosomal/Lysosomal Labile Iron Pools.* Journal of Medicinal Chemistry, 2008, **51**, 4539-4552.

[23] Munoz, M., Garcia-Erce, J.A. and Remacha, A.F., *Disorders of iron metabolism. Part 1: molecular basis of iron homoeostasis.* Journal of Clinical Pathology, 2011, **64**, 281-286.

[24] Gkouvatsos, K., Papanikolaou, G. and Pantopoulos, K., *Regulation of iron transport and the role of transferrin.* Biochimica et Biophysica Acta, 2012, **1820**, 188-202.

[25] Winter, W.E., Bazydlo, L.A. and Harris, N.S., *The molecular biology of human iron metabolism.* LabMedicine, 2014, **45**, 92-102.

[26] Cherayil, B.J., *The role of iron in the immune response to bacterial infection.* Immunologic Research, 2011, **50**, 1-9.

[27] Grotto, H.Z.W., *Iron physiology and metabolism.* Revista Brasileira de Hematologia e Hemoterapia, 2010, **32**, 8-17.

[28] Andrews, N.C. and Schmidt, P.J., *Iron homeostasis.* Annual Review of Physiology, 2007, **69**, 69-85.

[29] Wessling-Resnick, M., *Iron homeostasis and the inflammatory response.* Annual Review of Nutrition, 2010, **30**, 105-122.

[30] Gunshin, H., Fujiwara, Y., Custodio, A.O., Direnzo, C., Robine, S. and Andrews, N.C., *Slc11a2 is required for intestinal iron absorption and erythropoiesis but dispensable in placenta and liver.* Journal of Clinical Investigation, 2005, **115**, 1258-1266.

[31] Sebastiani, G. and Pantopoulos, K., *Disorders associated with systemic or local iron overload: from pathophysiology to clinical practice.* Metallomics, 2011, **3**, 971-986.

[32] Cassat, J.E. and Skaar, E.P., *Iron in Infection and Immunity.* Cell Host & Microbe, 2013, **13**, 509-519.

[33] Levi, S. and Arosio, P., *Mitochondrial ferritin.* The International Journal of Biochemistry & Cell Biology, 2004, **36**, 1887-1889.

[34] Hentze, M.W., Muckenthaler, M.U., Galy, B. and Camaschella, C., *Two to tango: regulation of Mammalian iron metabolism.* Cell, 2010, **142**, 24-38.

[35] Cherayil, B.J., *Iron and immunity: immunological consequences of iron deficiency and overload.* Archivum Immunologiae et Therapia Experimentalis, 2010, **58**, 407-415.

[36] Viatte, L., Lesbordes-Brion, J.C., Lou, D.Q., Bennoun, M., Nicolas, G., Kahn, A., Canonne-Hergaux, F. and Vaulont, S., *Deregulation of proteins involved in iron metabolism in hepcidin-deficient mice.* Blood, 2005, **105**, 4861-4864.

[37] Singh, B., Arora, S., Agrawal, P. and Gupta, S.K., *Hepcidin: A novel peptide hormone regulating iron metabolism.* Clinica Chimica Acta, 2011, **412**, 823-830.

[38] Wrighting, D.M. and Andrews, N.C., *Interleukin-6 induces hepcidin expression through STAT3.* Blood, 2006, **108**, 3204-3209.

[39] Lee, P.L. and Beutler, E., *Regulation of hepcidin and iron-overload disease.* Annual Review of Pathology, 2009, **4**, 489-515.

[40] Babitt, J.L., Huang, F.W., Wrighting, D.M., Xia, Y., Sidis, Y., Samad, T.A., Campagna, J.A., Chung, R.T., Schneyer, A.L., Woolf, C.J., Andrews, N.C. and Lin, H.Y., *Bone morphogenetic protein signaling by hemojuvelin regulates hepcidin expression.* Nature Genetics, 2006, **38**, 531-539.

[41] Weinberg, E.D., *Iron Out-of-Balance: A Risk Factor for Acute and Chronic Diseases.* Hemoglobin, 2008, **32**, 117-122.

[42] Hider, R.C., Roy, S., Ma, Y.M., Le Kong, X. and Preston, J., *The potential application of iron chelators for the treatment of neurodegenerative diseases.* Metallomics, 2011, **3**, 239-249.

[43] Jonker, F.A.M. and Boele van Hensbroek, M., *Anaemia, iron deficiency and susceptibility to infections.* Journal of Infection, 2014, **69**, Supplement 1, S23-S27.

[44] Silva-Gomes, S., Vale-Costa, S., Appelberg, R. and Gomes, M.S., *Iron in intracellular infection: to provide or to deprive?* Frontiers in Cellular and Infection Microbiology, 2013, **3**, Article 96, 1-11.

[45] Hood, M.I. and Skaar, E.P., *Nutritional immunity: transition metals at the pathogen-host interface.* Nature Reviews Microbiology, 2012, **10**, 525-537.

[46] Becker, K.W. and Skaar, E.P., *Metal limitation and toxicity at the interface between host and pathogen.* FEMS Microbiology Reviews, 2014, **38**, 1235-1249.

[47] Barber, M.F. and Elde, N.C., *Escape from bacterial iron piracy through rapid evolution of transferrin.* Science, 2014, **346**, 1362-1366.

[48] Zhou, T., Ma, Y., Kong, X. and Hider, R.C., *Design of iron chelators with therapeutic application.* Dalton Transactions, 2012, **41**, 6371-6389.

[49] Hider, R.C. and Kong, X., *Chemistry and biology of siderophores.* Natural Product Reports, 2010, **27**, 637-657.

[50] Qiao, C., Gupte, A., Boshoff, H.I., Wilson, D.J., Bennett, E.M., Somu, R.V., Barry, C.E. and Aldrich, C.C., *5'-O-[(N-acyl)sulfamoyl]adenosines as antitubercular agents that inhibit MbtA: an adenylation enzyme required for siderophore biosynthesis of the mycobactins.* Journal of Medicinal Chemistry, 2007, **50**, 6080-6094.

[51] Winkelmann, G., *Microbial siderophore-mediated transport.* Biochemical Society Transactions, 2002, **30**, 691-696.

[52] Foley, T.L. and Simeonov, A., *Targeting iron assimilation to develop new antibacterials.* Expert Opinion on Drug Discovery 2012, **7**, 831-847.

[53] Martinez, J.S. and Butler, A., *Marine amphiphilic siderophores: marinobactin structure, uptake, and microbial partitioning.* Journal of Inorganic Biochemistry, 2007, **101**, 1692-1698.

[54] Mies, K.A., Gebhardt, P., Mollmann, U. and Crumbliss, A.L., *Synthesis, siderophore activity and iron(III) chelation chemistry of a novel mono-hydroxamate, bis-catecholate siderophore mimic: N(alpha),-N(epsilon)-Bis[2,3-dihydroxybenzoyl]-l-lysyl-(gamma-N-methyl-N-hydroxya mido)-L-glutamic acid.* Journal of Inorganic Biochemistry, 2008, **102**, 850-861.

[55] Ji, C., Juárez-Hernández, R.E. and Miller, M.J., *Exploiting bacterial iron acquisition: siderophore conjugates.* Future Medicinal Chemistry, 2012, **4**, 297-313.

[56] Apostol, M., Baret, P., Serratrice, G., Desbrieres, J., Putaux, J.L., Stebe, M.J., Expert, D. and Pierre, J.L., *Self-assembly of an amphiphilic iron(III) chelator: mimicking iron acquisition in marine bacteria.* Angewandte Chemie International Edition, 2005, **44**, 2580-2582.

[57] Miller, M.J., Walz, A.J., Zhu, H., Wu, C., Moraski, G., Möllmann, U., Tristani, E.M., Crumbliss, A.L., Ferdig, M.T., Checkley, L., Edwards, R.L. and Boshoff, H.I., *Design, Synthesis, and Study of a Mycobactin−Artemisinin Conjugate That Has Selective and Potent Activity against Tuberculosis and Malaria.* Journal of the American Chemical Society, 2011, **133**, 2076-2079.

[58] Ganz, T., *Iron in innate immunity: starve the invaders.* Current Opinion in Immunology, 2009, **21**, 63-67.

[59] Marx, J.J.M., *Iron and infection: competition between host and microbes for a precious element.* Best Practice & Research Clinical Haematology, 2002, **15**, 411-426.

[60] M. Höpfner, R.N., A. Rohr, D. Harms, S. Schubert, U. R. Fölsch, *Yersinia enterocolitica Infection with Multiple Liver Abscesses Uncovering a Primary Hemochromatosis.* Scandinavian Journal of Gastroenterology, 2001, **36**, 220-224.

[61] Barton, J.C. and Acton, R.T., *Hemochromatosis and Vibrio vulnificus Wound Infections.* Journal of Clinical Gastroenterology, 2009, **43**, 890-893.

[62] Kabyemela, E.R., Fried, M., Kurtis, J.D., Mutabingwa, T.K. and Duffy, P.E., *Decreased Susceptibility to Plasmodium falciparum Infection in Pregnant Women with Iron Deficiency.* Journal of Infectious Diseases, 2008, **198**, 163-166.

[63] Kortman, G.A., Boleij, A., Swinkels, D.W. and Tjalsma, H., *Iron availability increases the pathogenic potential of Salmonella typhimurium and other enteric pathogens at the intestinal epithelial interface.* PLoS One, 2012, **7**, e29968.

[64] McLaughlin, H.P., Hill, C. and Gahan, C.G., *The impact of iron on Listeria monocytogenes; inside and outside the host.* Current Opinion in Biotechnology, 2011, **22**, 194-199.

[65] Lin, L., Pantapalangkoor, P., Tan, B., Bruhn, K.W., Ho, T., Nielsen, T., Skaar, E.P., Zhang, Y., Bai, R., Wang, A., Doherty, T.M. and Spellberg, B., *Transferrin iron starvation therapy for lethal bacterial and fungal infections.* The Journal of Infectious Diseases, 2014, **210**, 254-264.

[66] Nairz, M., Schroll, A., Sonnweber, T. and Weiss, G., *The struggle for iron - a metal at the host-pathogen interface.* Cell Microbiology, 2010, **12**, 1691-1702.

[67] Luo, G., Spellberg, B., Gebremariam, T., Lee, H., Xiong, Y.Q., French, S.W., Bayer, A. and Ibrahim, A.S., *Combination therapy with iron chelation and vancomycin in treating murine staphylococcemia.* European Journal of Clinical Microbiology & Infectious Diseases, 2014, **33**, 845-851.

[68] Zhu, C.F., Qiu, D.H., Kong, X.L., Hider, R.C. and Zhou, T., *Synthesis and in-vitro antimicrobial evaluation of a high-affinity iron chelator in combination with chloramphenicol.* Journal of Pharmacy and Pharmacology, 2013, **65**, 512-520.

[69] Fritsche, G., Dlaska, M., Barton, H., Theurl, I., Garimorth, K. and Weiss, G., *Nramp1 Functionality Increases Inducible Nitric Oxide Synthase Transcription Via Stimulation of IFN Regulatory Factor 1 Expression.* Journal of Immunology, 2003, **171**, 1994-1998.

[70] Clifton, M.C., Corrent, C. and Strong, R.K., *Siderocalins: siderophore-binding proteins of the innate immune system.* Biometals, 2009, **22**, 557-564.

[71] Philpott, C., *Bioinorganic chemistry: Getting a grip on iron.* Nature Chemical Biology, 2010, **6**, 568-570.

[72] Peyssonnaux, C., Zinkernagel, A.S., Datta, V., Lauth, X., Johnson, R.S. and Nizet, V., *TLR4-dependent hepcidin expression by myeloid cells in response to bacterial pathogens.* Blood, 2006, **107**, 3727-3732.

[73] Arezes, J., Jung, G., Gabayan, V., Valore, E., Ruchala, P., Gulig, P.A., Ganz, T., Nemeth, E. and Bulut, Y., *Hepcidin-Induced Hypoferremia Is a Critical Host Defense Mechanism against the Siderophilic Bacterium Vibrio vulnificus.* Cell Host & Microbe, 2015, **17**, 47-57.

[74] Nairz, M., Schroll, A., Demetz, E., Tancevski, I., Theurl, I. and Weiss, G., *'Ride on the ferrous wheel' – The cycle of iron in macrophages in health and disease.* Immunobiology, 2015, **220**, 280-294.

[75] Ward, R.J., Crichton, R.R., Taylor, D.L., Corte, L.D., Srai, S.K. and Dexter, D.T., *Iron and the immune system.* Journal of Neural Transmission, 2011, **118**, 315-328.

[76] Sow, F.B., Alvarez, G.R., Gross, R.P., Satoskar, A.R., Schlesinger, L.S., Zwilling, B.S. and Lafuse, W.P., *Role of STAT1, NF-κB, and C/EBPβ in the macrophage transcriptional regulation of hepcidin by mycobacterial infection and IFN-γ.* Journal of Leukocyte Biology, 2009, **86**, 1247-1258.

[77] Matzanke, B.F., Bohnke, R., Mollmann, U., Reissbrodt, R., Schunemann, V. and Trautwein, A.X., *Iron uptake and intracellular metal transfer in mycobacteria mediated by xenosiderophores.* Biometals, 1997, **10**, 193-203.

[78] de Monye, C., Karcher, D.S., Boelaert, J.R. and Gordeuk, V.R., *Bone marrow macrophage iron grade and survival of HIV-seropositive patients.* AIDS, 1999, **13**, 375-380.

[79] Dhungana, S., Miller, M.J., Dong, L., Ratledge, C. and Crumbliss, A.L., *Iron Chelation Properties of an Extracellular Siderophore Exochelin MN.* Journal of the American Chemical Society, 2003, **125**, 7654-7663.

[80] David, S., Barros, V., Passos Guerra, K. and Delgado, R., *Exploring Mycobacterium avium inhibition by macrocyclic compounds.* Research in Microbiology, 2005, **156**, 904-910.

[81] Miwa, S., Shirai, M., Toyoshima, M., Shirai, T., Yasuda, K., Yokomura, K., Yamada, T., Masuda, M., Inui, N., Chida, K., Suda, T. and Hayakawa, H., *Efficacy of clarithromycin and ethambutol for Mycobacterium avium complex pulmonary disease. A preliminary study.* Annals of the American Thoracic Society, 2014, **11**, 23-29.

[82] Kim, S.Y., Koh, W.J., Park, H.Y., Jeon, K., Kwon, O.J., Cho, S.N. and Shin, S.J., *Changes in serum immunomolecules during antibiotic therapy for Mycobacterium avium complex lung disease.* Clinical & Experimental Immunology, 2014, **176**, 93-101.

[83] Tortoli, E., *Clinical manifestations of nontuberculous mycobacteria infections.* Clinical Microbiology and Infection, 2009, **15**, 906-910.

[84] Li, Y.J., Danelishvili, L., Wagner, D., Petrofsky, M. and Bermudez, L.E., *Identification of virulence determinants of Mycobacterium avium that impact on the ability to resist host killing mechanisms.* Journal of Medical Microbiology, 2010, **59**, 8-16.

[85] Quesniaux, V., Fremond, C., Jacobs, M., Parida, S., Nicolle, D., Yeremeev, V., Bihl, F., Erard, F., Botha, T., Drennan, M., Soler, M.N., Le Bert, M., Schnyder, B. and Ryffel, B., *Toll-like receptor pathways in the immune responses to mycobacteria.* Microbes and Infection, 2004, **6**, 946-959.

[86] Guenin-Mace, L., Simeone, R. and Demangel, C., *Lipids of pathogenic Mycobacteria: contributions to virulence and host immune suppression.* Transboundary and Emerging Diseases, 2009, **56**, 255-268.

[87] Brennan, P.J., *Structure, function, and biogenesis of the cell wall of Mycobacterium tuberculosis.* Tuberculosis, 2003, **83**, 91-97.

[88] Neyrolles, O., Wolschendorf, F., Mitra, A. and Niederweis, M., *Mycobacteria, metals, and the macrophage.* Immunological Reviews, 2015, **264**, 249-263.

[89] Wagner, D., Maser, J., Moric, I., Vogt, S., Kern, W.V. and Bermudez, L.E., *Elemental analysis of the Mycobacterium avium phagosome in Balb/c mouse macrophages.* Biochemical and Biophysical Research Communications, 2006, **344**, 1346-1351.

[90] Wagner, D., Maser, J., Lai, B., Cai, Z., Barry, C.E., 3rd, Honer Zu Bentrup, K., Russell, D.G. and Bermudez, L.E., *Elemental analysis of Mycobacterium avium-, Mycobacterium tuberculosis-, and Mycobacterium smegmatis-containing phagosomes indicates pathogen-induced microenvironments within the host cell's endosomal system.* Journal of Immunology, 2005, **174**, 1491-1500.

[91] Weiss, G. and Schaible, U.E., *Macrophage defense mechanisms against intracellular bacteria.* Immunological Reviews, 2015, **264**, 182-203.

[92] Gomes, M.S., Paul, S., Moreira, A.L., Appelberg, R., Rabinovitch, M. and Kaplan, G., *Survival of Mycobacterium avium and Mycobacterium tuberculosis in Acidified Vacuoles of Murine Macrophages.* Infection and Immunity, 1999, **67**, 3199-3206.

[93] Sturgill-Koszycki, S., Schlesinger, P.H., Chakraborty, P., Haddix, P.L., Collins, H.L., Fok, A.K., Allen, R.D., Gluck, S.L., Heuser, J. and Russell, D.G., *Lack of acidification in Mycobacterium phagosomes produced by exclusion of the vesicular proton-ATPase.* Science, 1994, **263**, 678-681.

[94] Kelley, V.A. and Schorey, J.S., *Mycobacterium's arrest of phagosome maturation in macrophages requires Rab5 activity and accessibility to iron.* Molecular Biology of the Cell, 2003, **14**, 3366-3377.

[95] Adams, I.B., Schafer, J.J., Roberts, A.L. and Short, W.R., *Mycobacterium avium complex (MAC) Immune Reconstitution Syndrome (IRIS) With Reduced Susceptibility to Ethambutol in an HIV-Infected Patient.* Annals of Pharmacotherapy, 2014, **48**, 1219-1224.

[96] Field, S.K. and Cowie, R.L., *Treatment of mycobacterium avium-intracellulare complex lung disease with a macrolide, ethambutol, and clofazimine.* CHEST Journal, 2003, **124**, 1482-1486.

[97] Kim, P., Zhang, Y.-M., Shenoy, G., Nguyen, Q.-A., Boshoff, H.I., Manjunatha, U.H., Goodwin, M.B., Lonsdale, J., Price, A.C., Miller, D.J., Duncan, K., White, S.W., Rock, C.O., Barry, C.E.

and Dowd, C.S., *Structure−Activity Relationships at the 5-Position of Thiolactomycin: An Intact (5R)-Isoprene Unit Is Required for Activity against the Condensing Enzymes from Mycobacterium tuberculosis and Escherichia coli.* Journal of Medicinal Chemistry, 2006, **49**, 159-171.

[98] Kim, P., Kang, S., Boshoff, H.I., Jiricek, J., Collins, M., Singh, R., Manjunatha, U.H., Niyomrattanakit, P., Zhang, L., Goodwin, M., Dick, T., Keller, T.H., Dowd, C.S. and Barry, C.E., *Structure−Activity Relationships of Antitubercular Nitroimidazoles. 2. Determinants of Aerobic Activity and Quantitative Structure−Activity Relationships.* Journal of Medicinal Chemistry, 2009, **52**, 1329-1344.

[99] Cho, Y., Ioerger, T.R. and Sacchettini, J.C., *Discovery of Novel Nitrobenzothiazole Inhibitors for Mycobacterium tuberculosis ATP Phosphoribosyl Transferase (HisG) through Virtual Screening.* Journal of Medicinal Chemistry, 2008, **51**, 5984-5992.

[100] Miller, M.J., Zhu, H., Xu, Y., Wu, C., Walz, A.J., Vergne, A., Roosenberg, J.M., Moraski, G., Minnick, A.A., McKee-Dolence, J., Hu, J., Fennell, K., Kurt Dolence, E., Dong, L., Franzblau, S., Malouin, F. and Mollmann, U., *Utilization of microbial iron assimilation processes for the development of new antibiotics and inspiration for the design of new anticancer agents.* Biometals, 2009, **22**, 61-75.

[101] Ratledge, C., *Iron, mycobacteria and tuberculosis.* Tuberculosis, 2004, **84**, 110-130.

[102] Neres, J., Labello, N.P., Somu, R.V., Boshoff, H.I., Wilson, D.J., Vannada, J., Chen, L., Barry, C.E., Bennett, E.M. and Aldrich, C.C., *Inhibition of Siderophore Biosynthesis in Mycobacterium tuberculosis with Nucleoside Bisubstrate Analogues: Structure−Activity Relationships of the Nucleobase Domain of 5'-O-[N-(Salicyl)sulfamoyl]adenosine.* Journal of Medicinal Chemistry, 2008, **51**, 5349-5370.

[103] Manjunatha, U.H., S. Rao, S.P., Kondreddi, R.R., Noble, C.G., Camacho, L.R., Tan, B.H., Ng, S.H., Ng, P.S., Ma, N.L., Lakshminarayana, S.B., Herve, M., Barnes, S.W., Yu, W., Kuhen, K., Blasco, F., Beer, D., Walker, J.R., Tonge, P.J., Glynne, R., Smith, P.W. and Diagana, T.T., *Direct inhibitors of InhA are active against Mycobacterium tuberculosis.* Science Translational Medicine, 2015, **7**, 269ra3.

[104] Edwards, D.I., *Nitroimidazole drugs-action and resistance mechanisms I. Mechanism of action.* Journal of Antimicrobial Chemotherapy, 1993, **31**, 9-20.

[105] Edwards, D.I., *Mechanisms of selective toxicity of metronidazole and other nitroimidazole drugs.* British Journal of Venereal Diseases, 1980, **56**, 285-290.

[106] Hooper, D.C., *Mode of action of fluoroquinolones.* Drugs, 1999, **58** Supplement 2, 6-10.

[107] Calvori, C., Frontali, L., Leoni, L. and Tecce, G., *Effect of Rifamycin on Protein Synthesis.* Nature, 1965, **207**, 417-418.

[108] Mingeot-Leclercq, M.-P., Glupczynski, Y. and Tulkens, P.M., *Aminoglycosides: Activity and Resistance.* Antimicrobial Agents and Chemotherapy, 1999, **43**, 727-737.

[109] Corper, H.J. and Cohn, M.L., *The Probable Mechanism of Streptomycin Action in Tuberculosis.* The Yale Journal of Biology and Medicine, 1949, **21**, 181-200.2.

[110] Tenson, T., Lovmar, M. and Ehrenberg, M., *The Mechanism of Action of Macrolides, Lincosamides and Streptogramin B Reveals the Nascent Peptide Exit Path in the Ribosome.* Journal of Molecular Biology, 2003, **330**, 1005-1014.

[111] Lee, R.E., Mikusova, K., Brennan, P.J. and Besra, G.S., *Synthesis of the mycobacterial arabinose donor β-D-arabinofuranosyl-1-monophosphoryldecaprenol, development of a basic arabinosyl-transferase assay, and identification of ethambutol as an arabinosyl transferase inhibitor.* Journal of the American Chemical Society, 1995, **117**, 11829-11832.

[112] Lety, M.A., Nair, S., Berche, P. and Escuyer, V., *A single point mutation in the embB gene is responsible for resistance to ethambutol in Mycobacterium smegmatis.* Antimicrobial Agents and Chemotherapy, 1997, **41**, 2629-2633.

[113] Goude, R., Amin, A.G., Chatterjee, D. and Parish, T., *The arabinosyltransferase EmbC is inhibited by ethambutol in Mycobacterium tuberculosis.* Antimicrobial Agents and Chemotherapy, 2009, **53**, 4138-4146.

[114] Heifets, L.B., Lindholm-Levy, P.J. and Flory, M., *Comparison of bacteriostatic and bactericidal activity of isoniazid and ethionamide against Mycobacterium avium and Mycobacterium tuberculosis.* The American review of respiratory disease, 1991, **143**, 268-270.

[115] Mdluli, K., Swanson, J., Fischer, E., Lee, R.E. and Barry, C.E., 3rd, *Mechanisms involved in the intrinsic isoniazid resistance of Mycobacterium avium.* Molecular Microbiology, 1998, **27**, 1223-1233.

[116] Quémard, A., Lanéelle, G. and Lacave, C., *Mycolic acid synthesis: a target for ethionamide in mycobacteria?* Antimicrobial Agents and Chemotherapy, 1992, **36**, 1316-1321.

[117] Zimhony, O., Cox, J.S., Welch, J.T., Vilcheze, C. and Jacobs, W.R., Jr., *Pyrazinamide inhibits the eukaryotic-like fatty acid synthetase I (FASI) of Mycobacterium tuberculosis.* Nature Medicine, 2000, **6**, 1043-1047.

[118] Prosser, G.A. and de Carvalho, L.P.S., *Kinetic mechanism and inhibition of Mycobacterium tuberculosis d-alanine:d-alanine ligase by the antibiotic d-cycloserine.* FEBS Journal, 2013, **280**, 1150-1166.

[119] Freeland-Graves, J.H., Sanjeevi, N. and Lee, J.J., *Global perspectives on trace element requirements.* Journal of Trace Elements in Medicine and Biology, 2015, **31**, 135-141.

[120] Wolschendorf, F., Ackart, D., Shrestha, T.B., Hascall-Dove, L., Nolan, S., Lamichhane, G., Wang, Y., Bossmann, S.H., Basaraba, R.J. and Niederweis, M., *Copper resistance is essential for virulence of Mycobacterium tuberculosis.* Proceedings of the National Academy of Sciences, 2011, **108**, 1621-1626.

[121] Ratledge, C. and Winder, F.G., *The accumulation of salicylic acid by mycobacteria during growth on an iron-deficient medium.* Biochemical Journal, 1962, **84**, 501-506.

[122] Winder, F.G. and O'Hara, C., *Effects of iron deficiency and of zinc deficiency on the activities of some enzymes in Mycobacterium smegmatis.* Biochemical Journal, 1964, **90**, 122-126.

[123] Gomes, M.S., Dom, G., Pedrosa, J., Boelaert, J.R. and Appelberg, R., *Effects of iron deprivation on Mycobacterium avium growth.* Tubercle and Lung Disease, 1999, **79**, 321-328.

[124] De Voss, J.J., Rutter, K., Schroeder, B.G. and Barry, C.E., III, *Iron Acquisition and Metabolism by Mycobacteria.* The Journal of Bacteriology, 1999, **181**, 4443-4451.

[125] Gomes and Appelberg, *Evidence for a link between iron metabolism and Nramp1 gene function in innate resistance against Mycobacterium avium.* Immunology, 1998, **95**, 165-168.

[126] Gomes, M.S., Boelaert, J.R. and Appelberg, R., *Role of iron in experimental Mycobacterium avium infection.* Journal of Clinical Virology, 2001, **20**, 117-122.

[127] Lounis, N., Maslo, C., Truffot-Pernot, C., Grosset, J. and Boelaert, R.J., *Impact of iron loading on the activity of isoniazid or ethambutol in the treatment of murine tuberculosis.* International Journal of Tuberculosis and Lung Disease, 2003, **7**, 575-579.

[128] Schaible, U.E., Collins, H.L., Priem, F. and Kaufmann, S.H., *Correction of the iron overload defect in beta-2-microglobulin knockout mice by lactoferrin abolishes their increased susceptibility to tuberculosis.* The Journal of Experimental Medicine, 2002, **196**, 1507-1513.

[129] Gangaidzo, I.T., Moyo, V.M., Mvundura, E., Aggrey, G., Murphree, N.L., Khumalo, H., Saungweme, T., Kasvosve, I., Gomo, Z.A., Rouault, T., Boelaert, J.R. and Gordeuk, V.R., *Association of pulmonary tuberculosis with increased dietary iron.* The Journal of Infectious Diseases, 2001, **184**, 936-939.

[130] Gomes-Pereira, S., Rodrigues, P.N., Appelberg, R. and Gomes, M.S., *Increased susceptibility to Mycobacterium avium in hemochromatosis protein HFE-deficient mice.* Infection and Immunity, 2008, **76**, 4713-4719.

[131] McDermid, J.M., Hennig, B.J., van der Sande, M., Hill, A.V., Whittle, H.C., Jaye, A. and Prentice, A.M., *Host iron redistribution as a risk factor for incident tuberculosis in HIV infection: an 11-year retrospective cohort study.* BMC Infectious Diseases, 2013, **13**, Article 48.

[132] Banerjee, S., Farhana, A., Ehtesham, N.Z. and Hasnain, S.E., *Iron acquisition, assimilation and regulation in mycobacteria.* Infection, Genetics and Evolution, 2011, **11**, 825-838.

[133] Dhungana, S., Ratledge, C. and Crumbliss, A.L., *Iron chelation properties of an extracellular siderophore exochelin MS.* Inorganic Chemistry, 2004, **43**, 6274-6283.

[134] De Voss, J.J., Rutter, K., Schroeder, B.G., Su, H., Zhu, Y. and Barry, C.E., *The salicylate-derived mycobactin siderophores of Mycobacterium tuberculosis are essential for growth in macrophages.* Proceedings of the National Academy of Sciences, 2000, **97**, 1252-1257.

[135] Rodriguez, G.M. and Smith, I., *Mechanisms of iron regulation in mycobacteria: role in physiology and virulence.* Molecular Microbiology, 2003, **47**, 1485-1494.

[136] Rodriguez, G.M., *Control of iron metabolism in Mycobacterium tuberculosis.* Trends in Microbiology, 2006, **14**, 320-327.

[137] Rodriguez, G.M. and Smith, I., *Identification of an ABC Transporter Required for Iron Acquisition and Virulence in Mycobacterium tuberculosis.* Journal of Bacteriology, 2006, **188**, 424-430.

[138] Luo, M., Fadeev, E.A. and Groves, J.T., *Mycobactin-mediated iron acquisition within macrophages.* Nature Chemical Biology, 2005, **1**, 149-153.

[139] Wong, D.K., Gobin, J., Horwitz, M.A. and Gibson, B.W., *Characterization of exochelins of Mycobacterium avium: evidence for saturated and unsaturated and for acid and ester forms.* Journal of Bacteriology, 1996, **178**, 6394-6398.

[140] Sritharan, M., *Iron as a candidate in virulence and pathogenesis in mycobacteria and other microorganisms.* World Journal of Microbiology and Biotechnology, 2000, **16**, 769-780.

[141] Appelberg, R., *Macrophage nutriprive antimicrobial mechanisms.* Journal of Leukocyte Biology, 2006, **79**, 1117-1128.

[142] Theurl, I., Fritsche, G., Ludwiczek, S., Garimorth, K., Bellmann-Weiler, R. and Weiss, G., *The macrophage: a cellular factory at the interphase between iron and immunity for the control of infections.* Biometals, 2005, **18**, 359-367.

[143] Bogdan, C., Rollinghoff, M. and Diefenbach, A., *Reactive oxygen and reactive nitrogen intermediates in innate and specific immunity.* Current Opinion in Immunology, 2000, **12**, 64-76.

[144] Nathan, C. and Shiloh, M.U., *Reactive oxygen and nitrogen intermediates in the relationship between mammalian hosts and microbial pathogens.* Proceedings of the National Academy of Sciences, 2000, **97**, 8841-8848.

[145] Gomes, M.S. and Appelberg, R., *NRAMP1- or cytokine-induced bacteriostasis of Mycobacterium avium by mouse macrophages is independent of the respiratory burst.* Microbiology, 2002, **148**, 3155-3160.

[146] Gomes, M.S., Florido, M., Pais, T.F. and Appelberg, R., *Improved clearance of Mycobacterium avium upon disruption of the inducible nitric oxide synthase gene.* Journal of Immunology, 1999, **162**, 6734-6739.

[147] Chan, J., Tanaka, K., Carroll, D., Flynn, J. and Bloom, B.R., *Effects of nitric oxide synthase inhibitors on murine infection with Mycobacterium tuberculosis.* Infection and Immunity, 1995, **63**, 736-740.

[148] MacMicking, J.D., North, R.J., LaCourse, R., Mudgett, J.S., Shah, S.K. and Nathan, C.F., *Identification of nitric oxide synthase as a protective locus against tuberculosis.* Proceedings of the National Academy of Sciences, 1997, **94**, 5243-5248.

[149] Segal, B.H., Doherty, T.M., Wynn, T.A., Cheever, A.W., Sher, A. and Holland, S.M., *The p47(phox-/-) mouse model of chronic granulomatous disease has normal granuloma formation and cytokine responses to Mycobacterium avium and Schistosoma mansoni eggs.* Infection and Immunity, 1999, **67**, 1659-1665.

[150] Cronjé, L., Edmondson, N., Eisenach, K.D. and Bornman, L., *Iron and iron chelating agents modulate Mycobacterium tuberculosis growth and monocyte-macrophage viability and effector functions.* FEMS Immunology and Medical Microbiology, 2005, **45**, 103-112.

[151] North, R.J., LaCourse, R., Ryan, L. and Gros, P., *Consequence of Nramp1 Deletion to Mycobacterium tuberculosis Infection in Mice.* Infection and Immunity, 1999, **67**, 5811-5814.

[152] Silva-Gomes, S., Bouton, C., Silva, T., Santambrogio, P., Rodrigues, P., Appelberg, R. and Gomes, M.S., *Mycobacterium avium Infection Induces H-Ferritin Expression in Mouse Primary Macrophages by Activating Toll-Like Receptor 2.* PLoS One, 2013, **8**, e82874.

[153] Sow, F.B., Florence, W.C., Satoskar, A.R., Schlesinger, L.S., Zwilling, B.S. and Lafuse, W.P., *Expression and localization of hepcidin in macrophages: a role in host defense against tuberculosis.* Journal of Leukocyte Biology, 2007, **82**, 934-945.

[154] Johnson, E.E., Sandgren, A., Cherayil, B.J., Murray, M. and Wessling-Resnick, M., *Role of Ferroportin in Macrophage-Mediated Immunity.* Infection and Immunity, 2010, **78**, 5099-5106.

[155] Zhong, W., Lafuse, W.P. and Zwilling, B.S., *Infection with Mycobacterium aviumDifferentially Regulates the Expression of Iron Transport Protein mRNA in Murine Peritoneal Macrophages.* Infection and Immunity, 2001, **69**, 6618-6624.

[156] Holmes, M.A., Paulsene, W., Jide, X., Ratledge, C. and Strong, R.K., *Siderocalin (Lcn 2) Also Binds Carboxymycobactins, Potentially Defending against Mycobacterial Infections through Iron Sequestration.* Structure, 2005, **13**, 29-41.

[157] Saiga, H., Nishimura, J., Kuwata, H., Okuyama, M., Matsumoto, S., Sato, S., Matsumoto, M., Akira, S., Yoshikai, Y., Honda, K., Yamamoto, M. and Takeda, K., *Lipocalin 2-dependent inhibition of mycobacterial growth in alveolar epithelium.* Journal of Immunology, 2008, **181**, 8521-8527.

[158] Scott, L.E. and Orvig, C., *Medicinal inorganic chemistry approaches to passivation and removal of aberrant metal ions in disease.* Chemical Review, 2009, **109**, 4885-4910.

[159] Moniz, T., Amorim, M.J., Ferreira, R., Nunes, A., Silva, A., Queirós, C., Leite, A., Gameiro, P., Sarmento, B., Remião, F., Yoshikawa, Y., Sakurai, H. and Rangel, M., *Investigation of the insulin-like properties of zinc(II) complexes of 3-hydroxy-4-pyridinones: identification of a compound with glucose lowering effect in STZ-induced type I diabetic animals.* Journal of Inorganic Biochemistry, 2011, **105**, 1675-1682.

[160] Rangel, M., Leite, A., Joao Amorim, M., Garribba, E., Micera, G. and Lodyga-Chruscinska, E., *Spectroscopic and potentiometric characterization of oxovanadium(IV) complexes formed by 3-hydroxy-4-pyridinones. Rationalization of the influence of basicity and electronic structure of the ligand on the properties of V(IV)O species in aqueous solution.* Inorganic Chemistry, 2006, **45**, 8086-8097.

[161] Rangel, M., Tamura, A., Fukushima, C. and Sakurai, H., *In vitro study of the insulin-like action of vanadyl-pyrone and -pyridinone complexes with a VO(O4) coordination mode.* Journal of Biological Inorganic Chemistry, 2001, **6**, 128-132.

[162] Muller, P., *Glossary of terms used in physical organic chemistry (IUPAC Recommendations 1994).* Pure and Applied Chemistry, 1994, **66**, 1077-1184.

[163] Haas, K.L. and Franz, K.J., *Application of metal coordination chemistry to explore and manipulate cell biology.* Chemical Review, 2009, **109**, 4921-4960.

[164] Zhou, T., Winkelmann, G., Dai, Z.-Y. and Hider, R.C., *Design of clinically useful macromolecular iron chelators.* Journal of Pharmacy and Pharmacology, 2011, **63**, 893-903.

[165] Raymond, K., Müller, G. and Matzanke, B., *Complexation of iron by siderophores a review of their solution and structural chemistry and biological function*, Structural Chemistry, 1984, p. 49-102. Springer, Berlin Heidelberg.

[166] Dhungana, S., Harrington, J.M., Gebhardt, P., Mollmann, U. and Crumbliss, A.L., *Iron chelation equilibria, redox, and siderophore activity of a saccharide platform ferrichrome analogue.* Inorganic Chemistry, 2007, **46**, 8362-8371.

[167] Liu, Z.D. and Hider, R.C., *Design of clinically useful iron(III)-selective chelators.* Medicinal Research Reviews, 2002, **22**, 26-64.

[168] Santos, M.A., Marques, S.M. and Chaves, S., *Hydroxypyridinones as "privileged" chelating structures for the design of medicinal drugs.* Coordination Chemistry Reviews, 2012, **256**, 240-259.

[169] Grazina, R., Gano, L., Sebestik, J. and Amelia Santos, M., *New tripodal hydroxypyridinone based chelating agents for Fe(III), Al(III) and Ga(III): Synthesis, physico-chemical properties and bioevaluation.* Journal of Inorganic Biochemistry, 2009, **103**, 262-273.

[170] Silva, A.M.G., Leite, A., Andrade, M., Gameiro, P., Brandão, P., Felix, V., de Castro, B. and Rangel, M., *Microwave-assisted synthesis of 3-hydroxy-4-pyridinone/naphthalene conjugates. Structural characterization and selection of a fluorescent ion sensor.* Tetrahedron, 2010, **66**, 8544-8550.

[171] Burgess, J. and Rangel, M., *Hydroxypyranones, hydroxypyridinones, and their complexes*, Advances in Inorganic Chemistry, 2008, p. 167-243. Elsevier, Academic Press, United Kingdom.

[172] Gama, S., Gil, M., Gano, L., Farkas, E. and Amelia Santos, M., *Combined chelation of bi-functional bis-hydroxypiridinone and mono-hydroxypiridinone: synthesis, solution and in vivo evaluation.* Journal of Inorganic Biochemistry, 2009, **103**, 288-298.

[173] Rangel, M., Leite, A., Silva, A.M.N., Moniz, T., Nunes, A., Amorim, M.J., Queiros, C., Cunha-Silva, L., Gameiro, P. and Burgess, J., *Distinctive EPR signals provide an understanding of the affinity of bis-(3-hydroxy-4-pyridinonato) copper(ii) complexes for hydrophobic environments.* Dalton Transactions, 2014, **43**, 9722-9731.

[174] Mesquita, R.B.R., Suárez, R., Cerdà, V., Rangel, M. and Rangel, A.O.S.S., *Exploiting the use of 3,4-HPO ligands as nontoxic reagents for the determination of iron in natural waters with a sequential injection approach.* Talanta, 2013, **108**, 38-45.

[175] Suarez, R., Mesquita, R.B., Rangel, M., Cerda, V. and Rangel, A.O., *Iron speciation by microsequential injection solid phase spectrometry using 3-hydroxy-1(H)-2-methyl-4-pyridinone as chromogenic reagent.* Talanta, 2015, **133**, 15-20.

[176] Leite, A., Silva, A.M.G., Nunes, A., Andrade, M., Sousa, C., Cunha-Silva, L., Gameiro, P., De Castro, B. and Rangel, M., *Novel tetradentate chelators derived from 3-hydroxy-4-pyridinone units: Synthesis, characterization and aqueous solution properties.* Tetrahedron, 2011, **67**, 4009-4016.

[177] Moniz, T., Queirós, C., Ferreira, R., Leite, A., Gameiro, P., Silva, A.M.G. and Rangel, M., *Design of a water soluble 1,8-naphthalimide/3-hydroxy-4-pyridinone conjugate: Investigation of its spectroscopic properties at variable pH and in the presence of Fe3+, Cu2+ and Zn2+.* Dyes and Pigments, 2013, **98**, 201-211.

[178] Leite, A., Silva, A.M., Cunha-Silva, L., de Castro, B., Gameiro, P. and Rangel, M., *Discrimination of fluorescence light-up effects induced by pH and metal ion chelation on a spirocyclic derivative of rhodamine B.* Dalton Transactions, 2013, **42**, 6110-6118.

[179] Queirós, C., Leite, A., Couto, M.G.M., Moniz, T., Cunha-Silva, L., Gameiro, P., Silva, A.M.G. and Rangel, M., *Tuning the limits of pH interference of a rhodamine ion sensor by introducing catechol and 3-hydroxy-4-pyridinone chelating units.* Dyes and Pigments, 2014, **110**, 193-202.

[180] Piyamongkol, S., Zhou, T., Liu, Z.D., Khodr, H.H. and Hider, R.C., *Design and characterisation of novel hexadentate 3-hydroxypyridin-4-one ligands.* Tetrahedron Letters, 2005, **46**, 1333-1336.

[181] Chaves, S., Mendonça, A.C., Marques, S.M., Prata, M.I., Santos, A.C., Martins, A.F., Geraldes, C.F.G.C. and Santos, M.A., *A gallium complex with a new tripodal tris-hydroxypyridinone for potential nuclear diagnostic imaging: solution and in vivo studies of 67Ga-labeled species.* Journal of Inorganic Biochemistry, 2011, **105**, 31-38.

[182] Fischer, R., Longo, F., Nielsen, P., Engelhardt, R., Hider, R.C. and Piga, A., *Monitoring long-term efficacy of iron chelation therapy by deferiprone and desferrioxamine in patients with beta-thalassaemia major: application of SQUID biomagnetic liver susceptometry.* British Journal of Haematology, 2003, **121**, 938-948.

[183] Saghaie, L., Sadeghi-Aliabadi, H. and Kafiri, M., *Synthesis and biological evaluation of bidentate 3-hydroxypyridin-4-ones iron chelating agents.* Research in Pharmaceutical Sciences, 2011, **6**, 117-122.

[184] Ceci, A., Baiardi, P., Felisi, M., Cappellini, M.D., Carnelli, V., De Sanctis, V., Galanello, R., Maggio, A., Masera, G., Piga, A., Schettini, F., Stefano, I. and Tricta, F., *The safety and effectiveness of deferiprone in a large-scale, 3-year study in Italian patients.* British Journal of Haematology, 2002, **118**, 330-336.

[185] Song, D., Zhao, L., Li, Y., Hadziahmetovic, M., Song, Y., Connelly, J., Spino, M. and Dunaief, J.L., *The oral iron chelator deferiprone protects against systemic iron overload-induced retinal degeneration in hepcidin knockout mice.* Investigative Ophthalmology & Visual Science, 2014, **55**, 4525-4532.

[186] Guariglia, R., Martorelli, M.C., Villani, O., Pietrantuono, G., Mansueto, G., D'Auria, F., Grieco, V., Bianchino, G., Lerose, R., Bochicchio, G.B. and Musto, P., *Positive effects on hematopoiesis in patients with myelodysplastic syndrome receiving deferasirox as oral iron chelation therapy: A brief review.* Leukemia Research, 2011, **35**, 566-570.

[187] Sánchez-González, P.D., López-Hernandez, F.J., Morales, A.I., Macías-Nuñez, J.F. and López-Novoa, J.M., *Effects of deferasirox on renal function and renal epithelial cell death.* Toxicology Letters, 2011, **203**, 154-161.

[188] Pangjit, K., Banjerdpongchai, R., Phisalaphong, C., Fucharoen, S., Xie, Y.Y., Lu, Z.D., Hider, R.C. and Srichairatanakool, S., *Characterisation of a novel oral iron chelator: 1-(N-Acetyl-6-Aminohexyl)-3-Hydroxy-2-Methylpyridin-4-one.* Journal of Pharmacy and Pharmacology, 2015, **67**, 703-713.

[189] Sheppard, L.N. and Kontoghiorghes, G.J., *Comparative iron binding studies of bis- and tris(3-hydroxy-2-methylpyrid-4-ones) and desferrioxamine.* Inorganica Chimica Acta, 1991, **188**, 177-183.

[190] Streater, M., Taylor, P.D., Hider, R.C. and Porter, J., *Novel 3-hydroxy-2(1H)-pyridinones. Synthesis, iron(III)-chelating properties and biological activity.* Journal of Medicinal Chemistry, 1990, **33**, 1749-1755.

[191] Liu, G., Miller, S.C. and Bruenger, F.W., *Synthesis of Lipophilic 3-Hydroxy-2-methyl-4-pyridinone Derivatives.* Synthetic Communications, 1995, **25**, 3247-3253.

[192] Yokel, R.A., Fredenburg, A.M., Durbin, P.W., Xu, J., Rayens, M.K. and Raymond, K.N., *The hexadentate hydroxypyridinonate TREN-(Me-3,2-HOPO) is a more orally active iron chelator than its bidentate analogue.* Journal of Pharmaceutical Sciences, 2000, **89**, 545-555.

[193] Abergel, R.J. and Raymond, K.N., *Synthesis and Thermodynamic Evaluation of Mixed Hexadentate Linear Iron Chelators Containing Hydroxypyridinone and Terephthalamide Units1.* Inorganic Chemistry, 2006, **45**, 3622-3631.

[194] Chaves, S., Marques, S.M., Matos, A.M.F., Nunes, A., Gano, L., Tuccinardi, T., Martinelli, A. and Santos, M.A., *New Tris(hydroxypyridinones) as Iron and Aluminium Sequestering Agents: Synthesis, Complexation and In Vivo Studies.* Chemistry – A European Journal, 2010, **16**, 10535-10545.

[195] Zhou, T., Kong, X.L., Liu, Z.D., Liu, D.Y. and Hider, R.C., *Synthesis and iron(III)-chelating properties of novel 3-hydroxypyridin-4-one hexadentate ligand-containing copolymers.* Biomacromolecules, 2008, **9**, 1372-80.

[196] Geissler, S., Hellwig, M., Markwardt, F., Henle, T. and Brandsch, M., *Synthesis and intestinal transport of the iron chelator maltosine in free and dipeptide form.* European Journal of Pharmaceutics and Biopharmaceutics, 2011, **78**, 75-82.

[197] Ma, Y. and Hider, R.C., *Novel synthetic approach to fluoro- and amido-disubstituted 3-hydroxypyridin-4-ones.* Journal of Fluorine Chemistry, 2015, **173**, 29-34.

[198] Kovacevic, Z., Yu, Y. and Richardson, D.R., *Chelators to the rescue: different horses for different courses!* Chemical Research in Toxicology, 2011, **24**, 279-282.

[199] Liu, Z.D. and Hider, R.C., *Design of iron chelators with therapeutic application.* Coordination Chemistry Reviews, 2002, **232**, 151-171.

[200] Pippard, M.J., Jackson, M.J., Hoffman, K., Petrou, M. and Modell, C.B., *Iron chelation using subcutaneous infusions of diethylene triamine penta-acetic acid (DTPA).* Scandinavian Journal of Haematology, 1986, **36**, 466-472.

[201] Barton, J.C., *Drug evaluation: Deferitrin for iron overload disorders.* IDrugs, 2007, **10**, 480-490.

[202] Hider, R.C., Kong, X., Abbate, V., Harland, R., Conlon, K. and Luker, T., *Deferitazole, a new orally active iron chelator.* Dalton Transactions, 2015, **44**, 5197-5204.

[203] Neufeld, E.J., Galanello, R., Viprakasit, V., Aydinok, Y., Piga, A., Harmatz, P., Forni, G.L., Shah, F.T., Grace, R.F., Porter, J.B., Wood, J.C., Peppe, J., Jones, A. and Rienhoff, H.Y., *A phase 2 study of the safety, tolerability, and pharmacodynamics of FBS0701, a novel oral iron chelator, in transfusional iron overload.* Blood, 2012, **119**, 3263-3268.

[204] Bergeron, R.J., Wiegand, J., McManis, J.S., Vinson, J.R.T., Yao, H., Bharti, N. and Rocca, J.R., *(S)-4,5-Dihydro-2-(2-hydroxy-4-hydroxyphenyl)-4-methyl-4-thiazolecarboxylic Acid Polyethers: A Solution to Nephrotoxicity.* Journal of Medicinal Chemistry, 2006, **49**, 2772-2783.

[205] Bergeron, R.J., Wiegand, J., McManis, J.S., Bharti, N. and Singh, S., *Desferrithiocin Analogues and Nephrotoxicity.* Journal of Medicinal Chemistry, 2008, **51**, 5993-6004.

[206] Budimir, A., *Metal ions, Alzheimer's disease and chelation therapy.* Acta Pharmaceutica, 2011, **61**, 1-14.

[207] Blat, D., Weiner, L., Youdim, M.B.H. and Fridkin, M., *A Novel Iron-Chelating Derivative of the Neuroprotective Peptide NAPVSIPQ Shows Superior Antioxidant and Antineurodegenerative Capabilities.* Journal of Medicinal Chemistry, 2008, **51**, 126-134.

[208] Mandel, S.A., Amit, T., Kalfon, L., Reznichenko, L., Weinreb, O. and Youdim, M.B., *Cell signaling pathways and iron chelation in the neurorestorative activity of green tea polyphenols: special reference to epigallocatechin gallate (EGCG).* Journal of Alzheimer's Disease, 2008, **15**, 211-222.

[209] Torti, S.V. and Torti, F.M., *Iron and cancer: more ore to be mined.* Nature Reviews Cancer, 2013, **13**, 342-355.

[210] Whitnall, M., Howard, J., Ponka, P. and Richardson, D.R., *A class of iron chelators with a wide spectrum of potent antitumor activity that overcomes resistance to chemotherapeutics.* Proceedings of the National Academy of Sciences, 2006, **103**, 14901-14906.

[211] Becton, D.L. and Bryles, P., *Deferoxamine inhibition of human neuroblastoma viability and proliferation.* Cancer Research, 1988, **48**, 7189-7192.

[212] Zhu, C.-F., Battah, S., Kong, X., Reeder, B.J., Hider, R.C. and Zhou, T., *Design, synthesis and biological evaluation of 5-aminolaevulinic acid/3-hydroxypyridinone conjugates as potential photodynamic therapeutical agents.* Bioorganic & Medicinal Chemistry Letters, 2015, **25**, 558-561.

[213] Bendova, P., Mackova, E., Haskova, P., Vavrova, A., Jirkovsky, E., Sterba, M., Popelova, O., Kalinowski, D.S., Kovarikova, P., Vavrova, K., Richardson, D.R. and Simunek, T., *Comparison of Clinically Used and Experimental Iron Chelators for Protection against Oxidative Stress-Induced Cellular Injury.* Chemical Research in Toxicology, 2010, **23**, 1105-1114.

[214] Mohammadpour, M., Sadeghi, A., Fassihi, A., Saghaei, L., Movahedian, A. and Rostami, M., *Synthesis and antioxidant evaluation of some novel ortho-hydroxypyridine-4-one iron chelators.* Research in Pharmaceutical Sciences, 2012, **7**, 171-179.

[215] Baek, J.H., Reiter, C.E., Manalo, D.J., Buehler, P.W., Hider, R.C. and Alayash, A.I., *Induction of hypoxia inducible factor (HIF-1alpha) in rat kidneys by iron chelation with the hydroxypyridinone, CP94.* Biochimica et Biophysica Acta, 2011, **1809**, 262-268.

[216] Nigam, A., Gupta, D. and Sharma, A., *Treatment of infectious disease: Beyond antibiotics.* Microbiological Research, 2014, **169**, 643-651.

[217] Butler, M.S. and Cooper, M.A., *Antibiotics in the clinical pipeline in 2011.* The Journal of Antibiotics, 2011, **64**, 413-425.

[218] Weinberg, E.D. and Moon, J., *Malaria and iron: history and review.* Drug Metabolism Reviews, 2009, **41**, 644-662.

[219] Biot, C., Castro, W., Botte, C.Y. and Navarro, M., *The therapeutic potential of metal-based antimalarial agents: implications for the mechanism of action.* Dalton Transactions, 2012, **41**, 6335-6349.

[220] Gehrke, S.S., Pinto, E.G., Steverding, D., Pleban, K., Tempone, A.G., Hider, R.C. and Wagner, G.K., *Conjugation to 4-aminoquinoline improves the anti-trypanosomal activity of Deferiprone-type iron chelators.* Bioorganic & Medicinal Chemistry, 2013, **21**, 805-813.

[221] Hershko, C., Gordeuk, V.R., Brittenham, G.M., Thuma, P.E., Theanacho, E.N., Spira, D.T., Hider, R.C. and Peto, T.E.A., *The antimalarial effect of iron chelators: Studies in animal models and in humans with mild falciparum malaria.* Journal of Inorganic Biochemistry, **47**, 267-277.

[222] Pradines, B., Ramiandrasoa, F., Rolain, J.M., Rogier, C., Mosnier, J., Daries, W., Fusai, T., Kunesch, G., Le Bras, J. and Parzy, D., *In vitro potentiation of antibiotic activities by a catecholate iron chelator against chloroquine-resistant Plasmodium falciparum.* Antimicrobial Agents and Chemotherapy, 2002, **46**, 225-228.

[223] Ferrer, P., Tripathi, A.K., Clark, M.A., Hand, C.C., Rienhoff, H.Y., Jr. and Sullivan, D.J., Jr., *Antimalarial iron chelator, FBS0701, shows asexual and gametocyte Plasmodium falciparum activity and single oral dose cure in a murine malaria model.* PLoS One, 2012, **7**, e37171.

[224] Hershko, C., Theanacho, E.N., Spira, D.T., Peter, H.H., Dobbin, P. and Hider, R.C., *The effect of N-alkyl modification on the antimalarial activity of 3-hydroxypyridin-4-one oral iron chelators.* Blood, 1991, **77**, 637-643.

[225] Dehkordi, L.S., Liu, Z.D. and Hider, R.C., *Basic 3-hydroxypyridin-4-ones: potential antimalarial agents.* European Journal of Medicinal Chemistry, 2008, **43**, 1035-1047.

[226] Andayi, W.A., Egan, T.J. and Chibale, K., *Kojic acid derived hydroxypyridinone-chloroquine hybrids: synthesis, crystal structure, antiplasmodial activity and beta-haematin inhibition.* Bioorganic & Medicinal Chemistry Letters 2014, **24**, 3263-3267.

[227] Arantes, J.M., Pedrosa, M.L., Martins, H.R., Veloso, V.M., de Lana, M., Bahia, M.T., Tafuri, W.L. and Carneiro, C.M., *Trypanosoma cruzi: treatment with the iron chelator desferrioxamine reduces parasitemia and mortality in experimentally infected mice.* Experimental Parasitology, 2007, **117**, 43-50.

[228] Francisco, A.F., de Abreu Vieira, P.M., Arantes, J.M., Pedrosa, M.L., Martins, H.R., Silva, M., Veloso, V.M., de Lana, M., Bahia, M.T., Tafuri, W.L. and Carneiro, C.M., *Trypanosoma cruzi: effect of benznidazole therapy combined with the iron chelator desferrioxamine in infected mice.* Experimental Parasitology, 2008, **120**, 314-319.

[229] Arantes, J.M., Francisco, A.F., de Abreu Vieira, P.M., Silva, M., Araújo, M.S.S., de Carvalho, A.T., Pedrosa, M.L., Carneiro, C.M., Tafuri, W.L., Martins-Filho, O.A. and Elói-Santos, S.M., *Trypanosoma cruzi: Desferrioxamine decreases mortality and parasitemia in infected mice through a trypanostatic effect.* Experimental Parasitology, 2011, **128**, 401-408.

[230] Malafaia, G., Marcon, L.d.N., Pereira, L.d.F., Pedrosa, M.L. and Rezende, S.A., *Leishmania chagasi: Effect of the iron deficiency on the infection in BALB/c mice.* Experimental Parasitology, 2011, **127**, 719-723.

[231] Sartori, M., Andorno, S., Rigamonti, C. and Boldorini, R., *Chronic hepatitis C treated with phlebotomy alone: biochemical and histological outcome.* Digestive and Liver Disease, **33**, 157-162.

[232] Georgiou, N.A., van der Bruggen, T., Oudshoorn, M., Nottet, H.S., Marx, J.J. and van Asbeck, B.S., *Inhibition of human immunodeficiency virus type 1 replication in human mononuclear blood cells by the iron chelators deferoxamine, deferiprone, and bleomycin.* The Journal of Infectious Diseases, 2000, **181**, 484-490.

[233] Jang, Y.J., Achary, R., Lee, H.W., Lee, H.J., Lee, C.K., Han, S.B., Jung, Y.S., Kang, N.S., Kim, P. and Kim, M., *Synthesis and anti-influenza virus activity of 4-oxo- or thioxo-4,5-dihydrofuro[3,4-c]pyridin-3(1H)-ones.* Antiviral Research, 2014, **107**, 66-75.

[234] Barral, K., Balzarini, J., Neyts, J., De Clercq, E., Hider, R.C. and Camplo, M., *Synthesis and Antiviral Evaluation of Cyclic and Acyclic 2-Methyl-3-hydroxy-4-pyridinone Nucleoside Derivatives.* Journal of Medicinal Chemistry, 2006, **49**, 43-50.

[235] Drakesmith, H. and Prentice, A., *Viral infection and iron metabolism.* Nature Reviews Microbiology, 2008, **6**, 541-552.

[236] Leal, S.M., Jr., Roy, S., Vareechon, C., Carrion, S., Clark, H., Lopez-Berges, M.S., Di Pietro, A., Schrettl, M., Beckmann, N., Redl, B., Haas, H. and Pearlman, E., *Targeting iron acquisition blocks infection with the fungal pathogens Aspergillus fumigatus and Fusarium oxysporum.* PLoS Pathogens, 2013, **9**, e1003436.

[237] Ibrahim, A.S., Gebermariam, T., Fu, Y., Lin, L., Husseiny, M.I., French, S.W., Schwartz, J., Skory, C.D., Edwards, J.E., Jr. and Spellberg, B.J., *The iron chelator deferasirox protects mice from mucormycosis through iron starvation.* Journal of Clinical Investigation, 2007, **117**, 2649-2657.

[238] Ibrahim, A.S., Gebremariam, T., French, S.W., Edwards, J.E., Jr. and Spellberg, B., *The iron chelator deferasirox enhances liposomal amphotericin B efficacy in treating murine invasive pulmonary aspergillosis.* Journal of Antimicrobial Chemotherapy, 2010, **65**, 289-292.

[239] Albert, A., Rubbo, S.D., Goldacre, R.J. and Balfour, B.G., *The Influence of Chemical Constitution on Antibacterial Activity. Part III: A Study of 8-Hydroxyquinoline (Oxine) and Related Compounds.* British Journal of Experimental Pathology, 1947, **28**, 69-87.

[240] Chew, B.P., Tjoelker, L.W. and Tanaka, T.S., *In vitro growth inhibition of mastitis causing bacteria by phenolics and metal chelators.* Journal of Dairy Science, 1985, **68**, 3037-3046.

[241] Bergan T, B.T., Klaveness J, Klaveness J, Aasen A, J, Aasen A, J., *Chelating Agents.* Chemotherapy, 2001, **47**, 10-14.

[242] Oglesby-Sherrouse, A.G., Djapgne, L., Nguyen, A.T., Vasil, A.I. and Vasil, M.L., *The complex interplay of iron, biofilm formation, and mucoidy affecting antimicrobial resistance of Pseudomonas aeruginosa.* Pathogens and Disease, 2014, **70**, 307-320.

[243] Liu, Y., Yang, L. and Molin, S., *Synergistic activities of an efflux pump inhibitor and iron chelators against Pseudomonas aeruginosa growth and biofilm formation.* Antimicrobial Agents and Chemotherapy, 2010, **54**, 3960-3963.

[244] Ji, C., Miller, P.A. and Miller, M.J., *Iron Transport-Mediated Drug Delivery: Practical Syntheses and In Vitro Antibacterial Studies of Tris-Catecholate Siderophore–Aminopenicillin Conjugates Reveals Selectively Potent Antipseudomonal Activity.* Journal of the American Chemical Society, 2012, **134**, 9898-9901.

[245] Reid, D.W., O'May, C., Kirov, S.M., Roddam, L., Lamont, I.L. and Sanderson, K., *Iron chelation directed against biofilms as an adjunct to conventional antibiotics.* The American Journal of Physiology - Lung Cellular and Molecular Physiology, 2009, **296**, L857-858.

[246] Musk, D.J., Jr. and Hergenrother, P.J., *Chelated iron sources are inhibitors of Pseudomonas aeruginosa biofilms and distribute efficiently in an in vitro model of drug delivery to the human lung.* Journal of Applied Microbiology, 2008, **105**, 380-388.

[247] Sobke, A., Klinger, M., Hermann, B., Sachse, S., Nietzsche, S., Makarewicz, O., Keller, P.M., Pfister, W. and Straube, E., *The urinary antibiotic 5-nitro-8-hydroxyquinoline (Nitroxoline) reduces the formation and induces the dispersal of Pseudomonas aeruginosa biofilms by chelation of iron and zinc.* Antimicrobial Agents and Chemotherapy, 2012, **56**, 6021-6025.

[248] Lin, M.-H., Shu, J.-C., Huang, H.-Y. and Cheng, Y.-C., *Involvement of Iron in Biofilm Formation by Staphylococcus aureus.* PLoS One, 2012, **7**, e34388.

[249] van Asbeck, B.S., Marcelis, J.H., van Kats, J.H., Jaarsma, E.Y. and Verhoef, J., *Synergy between the iron chelator deferoxamine and the antimicrobial agents gentamicin, chloramphenicol, cefalothin, cefotiam and cefsulodin.* European Journal of Clinical Microbiology, 1983, **2**, 432-438.

[250] Neupane, G.P. and Kim, D.M., *In vitro time-kill activities of ciprofloxacin alone and in combination with the iron chelator deferasirox against Vibrio vulnificus.* European Journal of Clinical Microbiology & Infectious Diseases, 2010, **29**, 407-410.

[251] Chan, G.C., Chan, S., Ho, P.L. and Ha, S.Y., *Effects of chelators (deferoxamine, deferiprone and deferasirox) on the growth of Klebsiella pneumoniae and Aeromonas hydrophila isolated from transfusion-dependent thalassemia patients.* Hemoglobin, 2009, **33**, 352-360.

[252] Neupane, G.P. and Kim, D.M., *Comparison of the effects of deferasirox, deferiprone, and deferoxamine on the growth and virulence of Vibrio vulnificus.* Transfusion, 2009, **49**, 1762-1769.

[253] Collins, H.L., Kaufmann, S.H. and Schaible, U.E., *Iron chelation via deferoxamine exacerbates experimental salmonellosis via inhibition of the nicotinamide adenine dinucleotide phosphate oxidase-dependent respiratory burst.* Journal of Immunology, 2002, **168**, 3458-3463.

[254] Thompson, M.G., Corey, B.W., Si, Y., Craft, D.W. and Zurawski, D.V., *Antibacterial activities of iron chelators against common nosocomial pathogens.* Antimicrobial Agents and Chemotherapy, 2012, **56**, 5419-5421.

[255] Visca, P., Bonchi, C., Minandri, F., Frangipani, E. and Imperi, F., *The dual personality of iron chelators: growth inhibitors or promoters?* Antimicrobial Agents and Chemotherapy, 2013, **57**, 2432-2433.

[256] Kim, C.M. and Shin, S.H., *Effect of iron-chelator deferiprone on the in vitro growth of staphylococci.* Journal of Korean Medical Science, 2009, **24**, 289-295.

[257] Zhou, Y.-J., Liu, M.-S., Osamah, A.R., Kong, X.-L., Alsam, S., Battah, S., Xie, Y.-Y., Hider, R.C. and Zhou, T., *Hexadentate 3-hydroxypyridin-4-ones with high iron(III) affinity: Design, synthesis and inhibition on methicillin resistant Staphylococcus aureus and Pseudomonas strains.* European Journal of Medicinal Chemistry, 2015, **94**, 8-21.

[258] Zhang, M.X., Zhu, C.F., Zhou, Y.J., Le Kong, X., Hider, R.C. and Zhou, T., *Design, Synthesis, and Antimicrobial Evaluation of Hexadentate Hydroxypyridinones with High Iron(III) Affinity.* Chemical Biology & Drug Design, 2014, **84**, 659-668.

[259] Qiu, D.-H., Huang, Z.-L., Zhou, T., Shen, C. and Hider, R.C., *In vitro inhibition of bacterial growth by iron chelators.* FEMS Microbiology Letters, 2011, **314**, 107-111.

[260] Xie, Y.-Y., Liu, M.-S., Hu, P.-P., Kong, X.-L., Qiu, D.-H., Xu, J.-L., Hider, R. and Zhou, T., *Synthesis, physico-chemical properties, and antimicrobial evaluation of a new series of iron(III) hexadentate chelators.* Medicinal Chemistry Research, 2013, **22**, 2351-2359.

[261] Xu, B., Kong, X.L., Zhou, T., Qiu, D.H., Chen, Y.L., Liu, M.S., Yang, R.H. and Hider, R.C., *Synthesis, iron(III)-binding affinity and in vitro evaluation of 3-hydroxypyridin-4-one hexadentate ligands as potential antimicrobial agents.* Bioorganic and Medicinal Chemistry Letters, 2011, **21**, 6376-6380.

[262] Zhou, Y.J., Zhang, M.X., Hider, R.C. and Zhou, T., *In vitro antimicrobial activity of hydroxypyridinone hexadentate-based dendrimeric chelators alone and in combination with norfloxacin.* FEMS Microbiol Letters, 2014, **355**, 124-130.

[263] Cronje, L. and Bornman, L., *Iron overload and tuberculosis: a case for iron chelation therapy.* International Journal of Tuberculosis and Lung Disease, 2005, **9**, 2-9.

[264] Bosne-David, S., Bricard, L., Ramiandrasoa, F., DeRoussent, A., Kunesch, G. and Andremont, A., *Evaluation of growth promotion and inhibition from mycobactins and nonmycobacterial siderophores (Desferrioxamine and FR160) in Mycobacterium aurum.* Antimicrobial Agents and Chemotherapy, 1997, **41**, 1837-1839.

[265] Ishida, S., Arai, M., Niikawa, H. and Kobayashi, M., *Inhibitory effect of cyclic trihydroxamate siderophore, desferrioxamine E, on the biofilm formation of Mycobacterium species.* Biological and Pharmaceutical Bulletin, 2011, **34**, 917-920.

[266] Kumar, R.R., Perumal, S., Senthilkumar, P., Yogeeswari, P. and Sriram, D., *A highly atom economic, chemo-, regio- and stereoselective synthesis, and discovery of spiro-pyrido-pyrrolizines and pyrrolidines as antimycobacterial agents.* Tetrahedron, 2008, **64**, 2962-2971.

[267] Kumar, R.R., Perumal, S., Senthilkumar, P., Yogeeswari, P. and Sriram, D., *An atom efficient, solvent-free, green synthesis and antimycobacterial evaluation of 2-amino-6-methyl-4-aryl-8-[(E)-arylmethylidene]-5,6,7,8-tetrahydro-4H-pyrano[3,2-c]pyridine-3-carbonitriles.* Bioorganic & Medicinal Chemistry Letters, 2007, **17**, 6459-6462.

[268] Kumar, R.R., Perumal, S., Senthilkumar, P., Yogeeswari, P. and Sriram, D., *Discovery of antimycobacterial spiro-piperidin-4-ones: an atom economic, stereoselective synthesis, and biological intervention.* Journal of Medicinal Chemistry, 2008, **51**, 5731-5735.

[269] Bairwa, R., Tawari, N.R., Alate, A., Anam, S., Degani, M.S., Ray, M. and Rajan, R.M., *Novel 2-hydrazino-pyrimidin-4(3H)-one derivatives with pseudofunctional- similarity to siderophores as potential antimycobacterial agents.* Medicinal Chemistry, 2013, **9**, 77-83.

[270] Douvas, G.S., May, M.H., Kolnagou, A. and Kontoghiorghes, G.J., *Effects on Mycobacterium avium replication in normal human macrophages by deferiprone (L1) and other iron chelators. Possible implications on toxicity.* Arzneimittelforschung, 2002, **52**, 45-52.

[271] Raja, V.P.A., Perumal, S., Yogeeswari, P. and Sriram, D., *Synthesis and antimycobacterial activity of highly functionalized tetrahydro-4(1H)-pyridinones.* Bioorganic & Medicinal Chemistry Letters, 2011, **21**, 3881-3884.

[272] Coimbra, J.T.S., Moniz, T., Brás, N.F., Ivanova, G., Fernandes, P.A., Ramos, M.J. and Rangel, M., *Relevant Interactions of Antimicrobial Iron Chelators and Membrane Models Revealed by Nuclear Magnetic Resonance and Molecular Dynamics Simulations.* The Journal of Physical Chemistry B, 2014, **118**, 14590-14601.

[273] Corbin, B.D., Seeley, E.H., Raab, A., Feldmann, J., Miller, M.R., Torres, V.J., Anderson, K.L., Dattilo, B.M., Dunman, P.M., Gerads, R., Caprioli, R.M., Nacken, W., Chazin, W.J. and Skaar, E.P., *Metal chelation and inhibition of bacterial growth in tissue abscesses.* Science, 2008, **319**, 962-965.

[274] Silva, A.M.G., Leite, A., Gonzalez, P., Domingues, M.R.M., Gameiro, P., De Castro, B. and Rangel, M., *Use of a porphyrin platform and 3,4-HPO chelating units to synthesize ligands with N4 and O4 coordination sites.* Tetrahedron, 2011, **67**, 7821-7828.

[275] Cardoso, I.C.S., Amorim, A.L., Queirós, C., Lopes, S.C., Gameiro, P., de Castro, B., Rangel, M. and Silva, A.M.G., *Microwave-Assisted Synthesis and Spectroscopic Properties of 4'-*

Substituted Rosamine Fluorophores and Naphthyl Analogues. European Journal of Organic Chemistry, 2012, **29**, 5810-5817.

[276] Moniz, T., Silva, D., Silva, T., Gomes, M.S. and Rangel, M., *Antimycobacterial activity of rhodamine 3,4-HPO iron chelators against Mycobacterium avium: analysis of the contribution of functional groups and of chelator´s combination with ethambutol.* MedChemComm, 2015, **6**, 2194-2203.

[277] Kruger, R.G., Dostal, P. and McCafferty, D.G., *An economical and preparative orthogonal solid phase synthesis of fluorescein and rhodamine derivatized peptides: FRET substrates for the Staphylococcus aureus sortase SrtA transpeptidase reaction.* Chemical Communications, 2002, 2092-2093.

[278] Foley, T.L., Yasgar, A., Garcia, C.J., Jadhav, A., Simeonov, A. and Burkart, M.D., *Preparation of FRET reporters to support chemical probe development.* Organic & Biomolecular Chemistry, 2010, **8**, 4601-4606.

[279] Kottke, T. and Stalke, D., *Crystal Handling at Low-Temperatures.* Journal of Applied Crystallography, 1993, **26**, 615-619.

[280] APEX2, Data Collection Software Version 2.1-RC13, Bruker AXS, Delft, The Netherlands, 2006.

[281] Cryopad, Remote monitoring and control, Version 1.451, Oxford Cryosystems, Oxford, United Kingdom, 2006.

[282] SAINT+, Data Integration Engine v. 7.23a, 1997-2005, Bruker AXS, Madison, Wisconsin, USA.

[283] Sheldrick, G.M., SADABS v.2.01, Bruker/Siemens Area Detector Absorption Correction Program, 1998, Bruker AXS, Madison, Wisconsin, USA.

[284] Sheldrick, G.M., SHELXS-97, Program for Crystal Structure Solution, University of Göttingen, 1997.

[285] Sheldrick, G.M., *A short history of SHELX.* Acta Crystallographica Section A, 2008, **64**, 112-122.

[286] Sheldrick, G.M., SHELXL-97, Program for Crystal Structure Refinement, University of Göttingen, 1997.

[287] Spek, A.L., *PLATON.* Acta Crystallographica Section A, 1990, **46**, C34.

[288] Spek, A.L., *Single-crystal structure validation with the program PLATON.* Journal of Applied Crystallography, 2003, **36**, 7-13.

[289] van der Sluis, P. and Spek, A.L., Acta Crystallographica Section A, 1990, **46**, 194-201.

[290] Yacoby, I. and Benhar, I., *Targeted Anti Bacterial Therapy.* Infectious Disorders - Drug Targets, 2007, **7**, 221-229.

[291] Foley, T.L. and Simeonov, A., *Targeting iron assimilation to develop new antibacterials.* Expert Opinion on Drug Discovery, 2012, **7**, 831-847.

[292] Lounis, N., Truffot-Pernot, C., Grosset, J., Gordeuk, V.R. and Boelaert, J.R., *Iron and Mycobacterium tuberculosis infection.* Journal of Clinical Virology, 2001, **20**, 123-126.

[293] Russell, D.G., *Mycobacterium tuberculosis: here today, and here tomorrow.* Nature Reviews Molecular Cell Biology, 2001, **2**, 569-586.

[294] Spellberg, B., Guidos, R., Gilbert, D., Bradley, J., Boucher, H.W., Scheld, W.M., Bartlett, J.G. and Edwards, J., Jr., *The epidemic of antibiotic-resistant infections: a call to action for the medical community from the Infectious Diseases Society of America.* Clinical Infectious Diseases, 2008, **46**, 155-164.

[295] Wilkinson, R.G., Shepherd, R.G., Thomas, J.P. and Baughn, C., *STEREOSPECIFICITY IN A NEW TYPE OF SYNTHETIC ANTITUBERCULOUS AGENT1,2.* Journal of the American Chemical Society, 1961, **83**, 2212-2213.

[296] Wilson, T.M., *Clinical experience with ethambutol.* Antibiotics and chemotherapy, 1970, **16**, 222-229.

[297] Sreevatsan, S., Stockbauer, K.E., Pan, X., Kreiswirth, B.N., Moghazeh, S.L., Jacobs, W.R., Telenti, A. and Musser, J.M., *Ethambutol resistance in Mycobacterium tuberculosis: critical role of embB mutations.* Antimicrobial Agents and Chemotherapy, 1997, **41**, 1677-1681.

[298] Hoffner, S.E., Heurlin, N., Petrini, B., Svenson, S.B. and Kallenius, G., *Mycobacterium avium complex develop resistance to synergistically active drug combinations during infection.* The European respiratory journal, 1994, **7**, 247-250.

[299] Shafran, S.D., Singer, J., Zarowny, D.P., Phillips, P., Salit, I., Walmsley, S.L., Fong, I.W., Gill, M.J., Rachlis, A.R., Lalonde, R.G., Fanning, M.M. and Tsoukas, C.M., *A Comparison of Two Regimens for the Treatment of Mycobacterium avium Complex Bacteremia in AIDS: Rifabutin, Ethambutol, and Clarithromycin versus Rifampin, Ethambutol, Clofazimine, and Ciprofloxacin.* New England Journal of Medicine, 1996, **335**, 377-384.

[300] van Ingen, J., van der Laan, T., Dekhuijzen, R., Boeree, M. and van Soolingen, D., *In vitro drug susceptibility of 2275 clinical non-tuberculous Mycobacterium isolates of 49 species in The Netherlands.* International Journal of Antimicrobial Agents, 2010, **35**, 169-173.

[301] van Ingen, J., Hoefsloot, W., Mouton, J.W., Boeree, M.J. and van Soolingen, D., *Synergistic activity of rifampicin and ethambutol against slow-growing nontuberculous mycobacteria is currently of questionable clinical significance.* International Journal of Antimicrobial Agents, 2013, **42**, 80-82.

[302] Hoffner, S.E., Svenson, S.B. and Beezer, A.E., *Microcalorimetric studies of the initial interaction between antimycobacterial drugs and Mycobacterium avium.* Journal of Antimicrobial Chemotherapy, 1990, **25**, 353-359.

[303] Solecki, T.J., Aviv, A. and Bogden, J.D., *Effect of a chelating drug on balance and tissue distribution of four essential metals.* Toxicology, 1984, **31**, 207-216.

[304] Cole, A., May, P.M. and Williams, D.R., *Metal binding by pharmaceuticals. Part 1. Copper(II) and zinc(II) interactions following ethambutol administration.* Agents Actions, 1981, **11**, 296-305.

[305] Abbasi Nazari, M., Kobarfard, F., Tabarsi, P. and Salamzadeh, J., *Serum copper (cu) alterations in pulmonary tuberculosis patients under treatment with ethambutol.* Biological Trace Element Research 2009, **128**, 161-166.

[306] Schaible, U.E. and Kaufmann, S.H.E., *Iron and microbial infection.* Nature Reviews Microbiology, 2004, **2**, 946-953.

[307] Kim, H., Lee, C., Kim, M.-G. and Lee, H.-S., *Antibacterial activities of phenethyl isothiocyanate and its derivatives against human oral pathogens.* Journal of the Korean Society for Applied Biological Chemistry, 2009, **52**, 555-559.

[308] Jang, M., Hong, E. and Kim, G.-H., *Evaluation of Antibacterial Activity of 3-Butenyl, 4-Pentenyl, 2-Phenylethyl, and Benzyl Isothiocyanate in Brassica Vegetables.* Journal of Food Science, 2010, **75**, M412-M416.

[309] Sofrata, A., Santangelo, E.M., Azeem, M., Borg-Karlson, A.-K., Gustafsson, A. and Pütsep, K., *Benzyl Isothiocyanate, a Major Component from the Roots of Salvadora Persica Is Highly Active against Gram-Negative Bacteria.* PLoS One, 2011, **6**, e23045.

[310] Neoh, T.L., Yamamoto, C., Ikefuji, S., Furuta, T. and Yoshii, H., *Heat stability of allyl isothiocyanate and phenyl isothiocyanate complexed with randomly methylated β-cyclodextrin.* Food Chemistry, 2012, **131**, 1123-1131.

[311] Lin, C.M., Preston, J.F., 3rd and Wei, C.I., *Antibacterial mechanism of allyl isothiocyanate.* Journal of Food Protection, 2000, **63**, 727-734.

[312] Liu, T.T. and Yang, T.S., *Stability and antimicrobial activity of allyl isothiocyanate during long-term storage in an oil-in-water emulsion.* Journal of Food Science, 2010, **75**, C445-451.

[313] Kim, M.G. and Lee, H.S., *Growth-inhibiting activities of phenethyl isothiocyanate and its derivatives against intestinal bacteria.* Journal of Food Science, 2009, **74**, M467-471.

[314] Ngaini, Z., Mohd Arif, Asyikin, M., Hussain, H., Mei, E.S., Tang, D. and Kamaluddin, D.H.A., *Synthesis and Antibacterial Activity of Acetoxybenzoyl Thioureas with Aryl and Amino Acid Side Chains.* Phosphorus, Sulfur, and Silicon and the Related Elements, 2012, **187**, 1-7.

[315] Pinter, G., Horvath, P., Bujdoso, S., Sztaricskai, F., Keki, S., Zsuga, M., Kardos, S., Rozgonyi, F. and Herczegh, P., *Synthesis and antimicrobial activity of ciprofloxacin and norfloxacin permanently bonded to polyethylene glycol by a thiourea linker.* The Journal of Antibiotics, 2009, **62**, 113-116.

[316] Phetsuksiri, B., Baulard, A.R., Cooper, A.M., Minnikin, D.E., Douglas, J.D., Besra, G.S. and Brennan, P.J., *Antimycobacterial activities of isoxyl and new derivatives through the inhibition of mycolic acid synthesis.* Antimicrobial Agents and Chemotherapy, 1999, **43**, 1042-1051.

[317] Greenstein, R.J., Su, L. and Brown, S.T., *The thioamides methimazole and thiourea inhibit growth of M. avium Subspecies paratuberculosis in culture.* PLoS One, 2010, **5**, e11099.

[318] Upadhayaya, R.S., Kulkarni, G.M., Vasireddy, N.R., Vandavasi, J.K., Dixit, S.S., Sharma, V. and Chattopadhyaya, J., *Design, synthesis and biological evaluation of novel triazole, urea and thiourea derivatives of quinoline against Mycobacterium tuberculosis.* Bioorganic & Medicinal Chemistry, 2009, **17**, 4681-4692.

[319] Sriram, D., Yogeeswari, P. and Madhu, K., *Synthesis and in vitro antitubercular activity of some 1-[(4-sub)phenyl]-3-(4-{1-[(pyridine-4-carbonyl)hydrazono]ethyl}phenyl)thiourea.* Bioorganic & Medicinal Chemistry Letters, 2006, **16**, 876-878.

[320] Nishida, C.R. and Ortiz de Montellano, P.R., *Bioactivation of antituberculosis thioamide and thiourea prodrugs by bacterial and mammalian flavin monooxygenases.* Chemico-Biological Interactions, 2011, **192**, 21-25.

[321] Dixit, P.P., Patil, V.J., Nair, P.S., Jain, S., Sinha, N. and Arora, S.K., *Synthesis of 1-[3-(4-benzotriazol-1/2-yl-3-fluoro-phenyl)-2-oxo-oxazolidin-5-ylmethyl]-3-subst ituted-thiourea derivatives as antituberculosis agents.* European Journal of Medicinal Chemistry, 2006, **41**, 423-428.

[322] Sriram, D., Yogeeswari, P., Dinakaran, M. and Thirumurugan, R., *Antimycobacterial activity of novel 1-(5-cyclobutyl-1,3-oxazol-2-yl)-3-(sub)phenyl/pyridylthiourea compounds endowed with high activity toward multidrug-resistant Mycobacterium tuberculosis.* Journal of Antimicrobial Chemotherapy, 2007, **59**, 1194-1196.

[323] Sarker, M., Talcott, C., Madrid, P., Chopra, S., Bunin, B.A., Lamichhane, G., Freundlich, J.S. and Ekins, S., *Combining cheminformatics methods and pathway analysis to identify molecules with whole-cell activity against Mycobacterium tuberculosis.* Pharmaceutical Research, 2012, **29**, 2115-2127.

[324] Rauen, U., Springer, A., Weisheit, D., Petrat, F., Korth, H.G., de Groot, H. and Sustmann, R., *Assessment of chelatable mitochondrial iron by using mitochondrion-selective fluorescent iron indicators with different iron-binding affinities.* Chembiochem, 2007, **8**, 341-352.

[325] Zhao, Z., Chan, P.S., Li, H., Wong, K.L., Wong, R.N., Mak, N.K., Zhang, J., Tam, H.L., Wong, W.Y., Kwong, D.W. and Wong, W.K., *Highly selective mitochondria-targeting amphiphilic silicon(IV) phthalocyanines with axially ligated rhodamine B for photodynamic therapy.* Inorganic Chemistry, 2012, **51**, 812-821.

[326] Gordon, Y.J., Romanowski, E.G. and McDermott, A.M., *A Review of Antimicrobial Peptides and Their Therapeutic Potential as Anti-Infective Drugs.* Current eye research, 2005, **30**, 505-515.

[327] Epand, R.M. and Epand, R.F., *Bacterial membrane lipids in the action of antimicrobial agents.* Journal of Peptide Science, 2011, **17**, 298-305.

[328] Telang, U., Ji, Y. and Morris, M.E., *ABC transporters and isothiocyanates: potential for pharmacokinetic diet-drug interactions.* Biopharmaceutics & Drug Disposition, 2009, **30**, 335-344.

[329] Zhang, Y., *The molecular basis that unifies the metabolism, cellular uptake and chemopreventive activities of dietary isothiocyanates.* Carcinogenesis, 2012, **33**, 2-9.

[330] Yuan, P., Chen, B.-A. and Liu, D.-L., *Anticancer Mechanisms and Researches of Isothiocyanates.* Chinese Journal of Natural Medicines, 2008, **6**, 325-332.

[331] Tseng, E., Scott-Ramsay, E.A. and Morris, M.E., *Dietary organic isothiocyanates are cytotoxic in human breast cancer MCF-7 and mammary epithelial MCF-12A cell lines.* Experimental Biology and Medicine, 2004, **229**, 835-842.

[332] Hu, K. and Morris, M.E., *Pharmacokinetics of alpha-naphthyl isothiocyanate in rats.* Journal of Pharmaceutical Sciences, 2005, **94**, 2441-2451.

[333] Zhang, Y., *Allyl isothiocyanate as a cancer chemopreventive phytochemical.* Molecular Nutrition & Food Research, 2010, **54**, 127-135.

[334] Faiola, B., Peterson, R.A., Kimbrough, C.L., Jordan, H.L. and Cullen, J.M., *Acute ANIT toxicity in male IL-10 knockout and wild-type mice.* Toxicologic Pathology, 2010, **38**, 745-755.

[335] CLSI, *Methods for dilution antimicrobial susceptibility tests for bacteria that grow aerobically: approved standard, CLSI document M07-A8.* 2009, Eighth Edition.

[336] Lucio, M., Lima, J.L. and Reis, S., *Drug-membrane interactions: significance for medicinal chemistry.* Current Medicinal Chemistry, 2010, **17**, 1795-1809.

[337] Santos, N.C., Prieto, M. and Castanho, M.A.R.B., *Quantifying molecular partition into model systems of biomembranes: an emphasis on optical spectroscopic methods.* Biochimica et Biophysica Acta, 2003, **1612**, 123-135.

[338] Lopes, S.C., Ribeiro, C. and Gameiro, P., *A new approach to counteract bacteria resistance: a comparative study between moxifloxacin and a new moxifloxacin derivative in different model systems of bacterial membrane.* Chemical Biology & Drug Design, 2013, **81**, 265-274.

[339] Bucki, R. and Janmey, P.A., *Interaction of the gelsolin-derived antibacterial PBP 10 peptide with lipid bilayers and cell membranes.* Antimicrobial Agents and Chemotherapy, 2006, **50**, 2932-2940.

[340] Bucki, R., Pastore, J.J., Randhawa, P., Vegners, R., Weiner, D.J. and Janmey, P.A., *Antibacterial Activities of Rhodamine B-Conjugated Gelsolin-Derived Peptides Compared to Those of the Antimicrobial Peptides Cathelicidin LL37, Magainin II, and Melittin.* Antimicrobial Agents and Chemotherapy, 2004, **48**, 1526-1533.

[341] Riske, K.A., Fernandez, R.M., Nascimento, O.R., Bales, B.L. and Lamy-Freund, M.T., *DMPG gel-fluid thermal transition monitored by a phospholipid spin labeled at the acyl chain end.* Chemistry and Physics of Lipids, 2003, **124**, 69-80.

[342] Chia, C.S.B., Torres, J., Cooper, M.A., Arkin, I.T. and Bowie, J.H., *The orientation of the antibiotic peptide maculatin 1.1 in DMPG and DMPC lipid bilayers. Support for a pore-forming mechanism.* FEBS letters, 2002, **512**, 47-51.

[343] Neves, P., Leite, A., Rangel, M., Castro, B. and Gameiro, P., *Influence of structural factors on the enhanced activity of moxifloxacin: a fluorescence and EPR spectroscopic study.* Analytical and Bioanalytical Chemistry, 2007, **387**, 1543-1552.

[344] Lopes, S., Simeonova, M., Gameiro, P., Rangel, M. and Ivanova, G., *Interaction of 5-Fluorouracil Loaded Nanoparticles with 1,2-Dimyristoyl-sn-glycero-3-phosphocholine Liposomes Used as a Cellular Membrane Model.* The Journal of Physical Chemistry B, 2011, **116**, 667-675.

[345] Leite, A., *"Design de ligandos quelantes multifuncionalizados derivados de 3,4-hidroxipiridinonas".* Tese de Doutoramento em Química, Departamento de Química e Bioquímica, Faculdade de ciências da Universidade do Porto, Portugal, **2011**.

[346] Pinheiro, M., Arêde, M., Caio, J.M., Moiteiro, C., Lúcio, M. and Reis, S., *Drug–membrane interaction studies applied to N'-acetyl-rifabutin.* European Journal of Pharmaceutics and Biopharmaceutics, 2013, **85**, 597-603.

[347] Lakowicz, J., *Principles of Fluorescence Spectroscopy*, 1999, Springer, New York.

[348] Merino-Montero, S., Montero, M.T. and Hernández-Borrell, J., *Effects of lactose permease of Escherichia coli on the anisotropy and electrostatic surface potential of liposomes.* Biophysical Chemistry, 2006, **119**, 101-105.

[349] Hwang, T.-L. and Shaka, A.J., *Water suppression that works.Excitation sculpting using arbitrary waveforms and pulse field gradients.* Journal of Magnetic Resonance, Series A, 1995, **112**, 275-279.

[350] Campbell, I.D. and Dwek, R.A., *Biological Spectroscopy*, 1984, Benjamin/Cummings Pub. Co., United kingdom.

[351] Parker, A.E. and Bermudez, L.E., *Expression of the green fluorescent protein (GFP) in mycobacterium avium as a tool to study the interaction between Mycobacteria and host cells.* Microbial Pathogenesis, 1997, **22**, 193-198.

[352] Pinto, J.P., Arezes, J., Dias, V., Oliveira, S., Vieira, I., Costa, M., Vos, M., Carlsson, A., Rikers, Y., Rangel, M. and Porto, G., *Physiological implications of NTBI uptake by T lymphocytes.* Frontiers in Pharmacology, 2014, **5**, Article 24.

[353] Liu, Y., Chen, Y., Liu, S.-X., Guan, X.-D., Wada, T. and Inoue, Y., *Unique Fluorescence Behavior of Rhodamine B upon Inclusion Complexation with Novel Bis(β-cyclodextrin-6-yl) 2,2'-Bipyridine-4,4'-dicarboxylate.* Organic Letters, 2001, **3**, 1657-1660.

[354] Lopes, S., Neves, C.S., Eaton, P. and Gameiro, P., *Cardiolipin, a key component to mimic the E. coli bacterial membrane in model systems revealed by dynamic light scattering and steady-state fluorescence anisotropy.* Analytical and Bioanalytical Chemistry, 2010, **398**, 1357-1366.

[355] Schreier, S., Malheiros, S.V.P. and de Paula, E., *Surface active drugs: self-association and interaction with membranes and surfactants. Physicochemical and biological aspects.* Biochimica et Biophysica Acta, 2000, **1508**, 210-234.

[356] Luckey, M., *Membrane Structural Biology: With Biochemical and Biophysiscal foundations*, 2014, Cambridge University Press, United Kingdom.

[357] Royden, G., Hunt, A. and Tipping, L.R.H., *Trans-bilayer pseudocontact shifts produced by lanthanide ions in the 1H and 31P-nmr spectra of phospholipid vesicular membranes and their temperature variation.* Journal of Inorganic Biochemistry, 1980, **12**, 17-36.

[358] Troutman, M.D. and Thakker, D.R., *Rhodamine 123 requires carrier-mediated influx for its activity as a P-glycoprotein substrate in Caco-2 cells.* Pharmaceutical Research, 2003, **20**, 1192-1199.

[359] Swiss, R. and Will, Y., *Assessment of mitochondrial toxicity in HepG2 cells cultured in high-glucose- or galactose-containing media*, Current Protocols in Toxicology, 2011, p. Chapter 2, Unit2.20. John Wiley & Sons, Inc.

[360] Hynes, J., Nadanaciva, S., Swiss, R., Carey, C., Kirwan, S. and Will, Y., *A high-throughput dual parameter assay for assessing drug-induced mitochondrial dysfunction provides additional predictivity over two established mitochondrial toxicity assays.* Toxicology in Vitro, 2013, **27**, 560-569.

[361] Dykens, J.A., Jamieson, J.D., Marroquin, L.D., Nadanaciva, S., Xu, J.J., Dunn, M.C., Smith, A.R. and Will, Y., *In vitro assessment of mitochondrial dysfunction and cytotoxicity of nefazodone, trazodone, and buspirone.* Toxicological Sciences, 2008, **103**, 335-345.

[362] Decaens, C., Durand, M., Grosse, B. and Cassio, D., *Which in vitro models could be best used to study hepatocyte polarity?* Biology of the Cell, 2008, **100**, 387-398.

[363] Sassa, S., Sugita, O., Galbraith, R.A. and Kappas, A., *Drug metabolism by the human hepatoma cell, Hep G2.* Biochemical and Biophysical Research Communications 1987, **143**, 52-57.

[364] Gerets, H.H., Hanon, E., Cornet, M., Dhalluin, S., Depelchin, O., Canning, M. and Atienzar, F.A., *Selection of cytotoxicity markers for the screening of new chemical entities in a pharmaceutical context: a preliminary study using a multiplexing approach.* Toxicology in Vitro, 2009, **23**, 319-332.

[365] Moreira, A.C., *Phytoestrogens as Alternative to the Hormone Replacement Therapy: Mitochondrial and Cellular Interactions.* Tese de Doutoramento em Biociências, Departamento de Ciências da Vida, Faculdade de Ciências e Tecnologia, Universidade de Coimbra, Portugal, **2013**.

[366] Mersch-Sundermann, V., Knasmuller, S., Wu, X.J., Darroudi, F. and Kassie, F., *Use of a human-derived liver cell line for the detection of cytoprotective, antigenotoxic and cogenotoxic agents.* Toxicology, 2004, **198**, 329-340.

[367] Knasmuller, S., Mersch-Sundermann, V., Kevekordes, S., Darroudi, F., Huber, W.W., Hoelzl, C., Bichler, J. and Majer, B.J., *Use of human-derived liver cell lines for the detection of environmental and dietary genotoxicants; current state of knowledge.* Toxicology, 2004, **198**, 315-328.

[368] van Meerloo, J., Kaspers, G.J. and Cloos, J., *Cell sensitivity assays: the MTT assay.* Methods in Molecular Biology, 2011, **731**, 237-245.

[369] Fotakis, G. and Timbrell, J.A., *In vitro cytotoxicity assays: comparison of LDH, neutral red, MTT and protein assay in hepatoma cell lines following exposure to cadmium chloride.* Toxicology Letters, 2006, **160**, 171-177.

[370] Berridge, M.V., Herst, P.M. and Tan, A.S., *Tetrazolium dyes as tools in cell biology: new insights into their cellular reduction.* Biotechnology Annual Review, 2005, **11**, 127-152.

[371] Galluzzi, L., Aaronson, S.A., Abrams, J., Alnemri, E.S., Andrews, D.W., Baehrecke, E.H., Bazan, N.G., Blagosklonny, M.V., Blomgren, K., Borner, C., Bredesen, D.E., Brenner, C., Castedo, M., Cidlowski, J.A., Ciechanover, A., Cohen, G.M., De Laurenzi, V., De Maria, R., Deshmukh, M., Dynlacht, B.D., El-Deiry, W.S., Flavell, R.A., Fulda, S., Garrido, C., Golstein, P., Gougeon, M.L., Green, D.R., Gronemeyer, H., Hajnoczky, G., Hardwick, J.M., Hengartner, M.O., Ichijo, H., Jaattela, M., Kepp, O., Kimchi, A., Klionsky, D.J., Knight, R.A., Kornbluth, S., Kumar, S., Levine, B., Lipton, S.A., Lugli, E., Madeo, F., Malomi, W., Marine, J.C., Martin, S.J., Medema, J.P., Mehlen, P., Melino, G., Moll, U.M., Morselli, E., Nagata, S., Nicholson, D.W., Nicotera, P., Nunez, G., Oren, M., Penninger, J., Pervaiz, S., Peter, M.E., Piacentini, M., Prehn, J.H., Puthalakath, H., Rabinovich, G.A., Rizzuto, R., Rodrigues, C.M., Rubinsztein, D.C., Rudel, T., Scorrano, L., Simon, H.U., Steller, H., Tschopp, J., Tsujimoto, Y., Vandenabeele, P., Vitale, I., Vousden, K.H., Youle, R.J., Yuan, J., Zhivotovsky, B. and Kroemer, G., *Guidelines for the use and interpretation of assays for monitoring cell death in higher eukaryotes.* Cell Death & Differentiation, 2009, **16**, 1093-1107.

[372] Kroemer, G., Galluzzi, L., Vandenabeele, P., Abrams, J., Alnemri, E.S., Baehrecke, E.H., Blagosklonny, M.V., El-Deiry, W.S., Golstein, P., Green, D.R., Hengartner, M., Knight, R.A., Kumar, S., Lipton, S.A., Malorni, W., Nunez, G., Peter, M.E., Tschopp, J., Yuan, J., Piacentini, M., Zhivotovsky, B. and Melino, G., *Classification of cell death: recommendations of the Nomenclature Committee on Cell Death 2009.* Cell Death & Differentiation, 2009, **16**, 3-11.

[373] Smith, S.M., Wunder, M.B., Norris, D.A. and Shellman, Y.G., *A Simple Protocol for Using a LDH-Based Cytotoxicity Assay to Assess the Effects of Death and Growth Inhibition at the Same Time.* PLoS One, 2011, **6**, e26908.

[374] Weyermann, J., Lochmann, D. and Zimmer, A., *A practical note on the use of cytotoxicity assays.* International Journal of Pharmaceutics, 2005, **288**, 369-376.

[375] Brown, D.M., Johnston, H., Gubbins, E. and Stone, V., *Serum enhanced cytokine responses of macrophages to silica and iron oxide particles and nanomaterials: a comparison of serum to lung lining fluid and albumin dispersions.* Journal of Applied Toxicology, 2014, **34**, 1177-1187.

[376] Amit, A., Chaudhary, R., Yadav, A., Suman, S.S., Narayan, S., Das, V.N.R., Pandey, K., Singh, S.K., Singh, B.K., Ali, V., Das, P. and Bimal, S., *Evaluation of Leishmania donovani disulfide isomerase as a potential target of cellular immunity against visceral leishmaniasis.* Cellular Immunology, 2014, **289**, 76-85.

[377] Decker, T. and Lohmann-Matthes, M.L., *A quick and simple method for the quantitation of lactate dehydrogenase release in measurements of cellular cytotoxicity and tumor necrosis factor (TNF) activity.* Journal of Immunological Methods, 1988, **115**, 61-69.

[378] von Eyben, F.E., Madsen, E.L., Blaabjerg, O., Petersen, P.H., von der Maase, H., Jacobsen, G.K. and Rorth, M., *Serum lactate dehydrogenase isoenzyme 1 and relapse in patients with nonseminomatous testicular germ cell tumors clinical stage I.* Acta Oncologica, 2001, **40**, 536-540.

[379] LDH half time. Available from: http://www.clinlabnavigator.com/lactate-dehydrogenase-ld.html. Accessed 29-10-2015.

[380] da Silva, D.D., Silva, E. and Carmo, H., *Combination effects of amphetamines under hyperthermia - the role played by oxidative stress.* Journal of Applied Toxicology, 2014, **34**, 637-650.

[381] Dias da Silva, D., Carmo, H. and Silva, E., *The risky cocktail: what combination effects can we expect between ecstasy and other amphetamines?* Archives of Toxicology, 2013, **87**, 111-122.

[382] Bergmeyer, H.U. and Bernt, E., *UV-Assay with Pyruvate and NADH*, Methods of Enzymatic Analysis, 1974, p. 574-579. Academic Press, Germany.

[383] Rajapakse, N., Silva, E., Scholze, M. and Kortenkamp, A., *Deviation from Additivity with Estrogenic Mixtures Containing 4-Nonylphenol and 4-tert-Octylphenol Detected in the E-SCREEN Assay.* Environmental Science & Technology, 2004, **38**, 6343-6352.

[384] EC50 definition. Available from: http://www.merckvetmanual.com/mvm/pharmacology/pharmacology_introduction/drug_action_and_pharmacodynamics.html#v3329205?qt=&sc=&alt=. Accessed 6-11-2015.

[385] Balcerzak, Z.M.a.M., *Separation, Preconcentration and Spectrophotometry in Inorganic Analysis*, 2000, First Edition, Elsevier, Netherlands.

[386] Rai, B.L., Dekhordi, L.S., Khodr, H., Jin, Y., Liu, Z. and Hider, R.C., *Synthesis, Physicochemical Properties, and Evaluation of N-Substituted-2-alkyl-3-hydroxy-4(1H)-pyridinones.* Journal of Medicinal Chemistry, 1998, **41**, 3347-3359.

[387] Goswami, L.N., Houston, Z.H., Sarma, S.J., Jalisatgi, S.S. and Hawthorne, M.F., *Efficient synthesis of diverse heterobifunctionalized clickable oligo(ethylene glycol) linkers: potential applications in bioconjugation and targeted drug delivery.* Organic & Biomolecular Chemistry 2013, **11**, 1116-1126.

[388] Mesquita, R.B. and Rangel, A.O., *A review on sequential injection methods for water analysis.* Analytica Chimica Acta, 2009, **648**, 7-22.

[389] Mesquita, R.B.R., Moniz, T., Miranda, J.L.A., Gomes, V., Silva, A.M.N., Rodriguez-Borges, J.E., Rangel, A.O.S.S. and Rangel, M., *Synthesis and characterization of a 3-hydroxy-4-pyridinone chelator functionalized with a polyethylene glycol (PEG) chain aimed at sequential injection determination of iron in natural waters.* Polyhedron, 2015, **101**, 171-178.

[390] Zhang, Z., Rettig, S.J. and Orvig, C., *Lipophilic coordination compounds: aluminum, gallium, and indium complexes of 1-aryl-3-hydroxy-2-methyl-4-pyridinones.* Inorganic Chemistry, 1991, **30**, 509-515.

[391] Queiros, C., Amorim, M.J., Leite, A., Ferreira, M., Gameiro, P., de Castro, B., Biernacki, K., Magalhães, A., Burgess, J. and Rangel, M., *Nickel(II) and Cobalt(II) 3-Hydroxy-4-pyridinone Complexes: Synthesis, Characterization and Speciation Studies in Aqueous Solution.* European Journal of Inorganic Chemistry, 2011, **2011**, 131-140.

[392] Zhou, S., Prebyl, B.S. and Cook, K.D., *Profiling pH Changes in the Electrospray Plume.* Analytical Chemistry, 2002, **74**, 4885-4888.

[393] Girod, M., Dagany, X., Antoine, R. and Dugourd, P., *Relation between charge state distributions of peptide anions and pH changes in the electrospray plume. A mass spectrometry and optical spectroscopy investigation.* International Journal of Mass Spectrometry, 2011, **308**, 41-48.

[394] (IUPAC), I.U.o.P.a.A.C., *Analytical Chemical division, Nomenclature, Symbols, Units and their usage in Spectrochemical Analysis - II. Data Interpretation.* Pure & Appl. Chem. , 1976, **45**, 99-103.

APPENDIX

APPENDIX

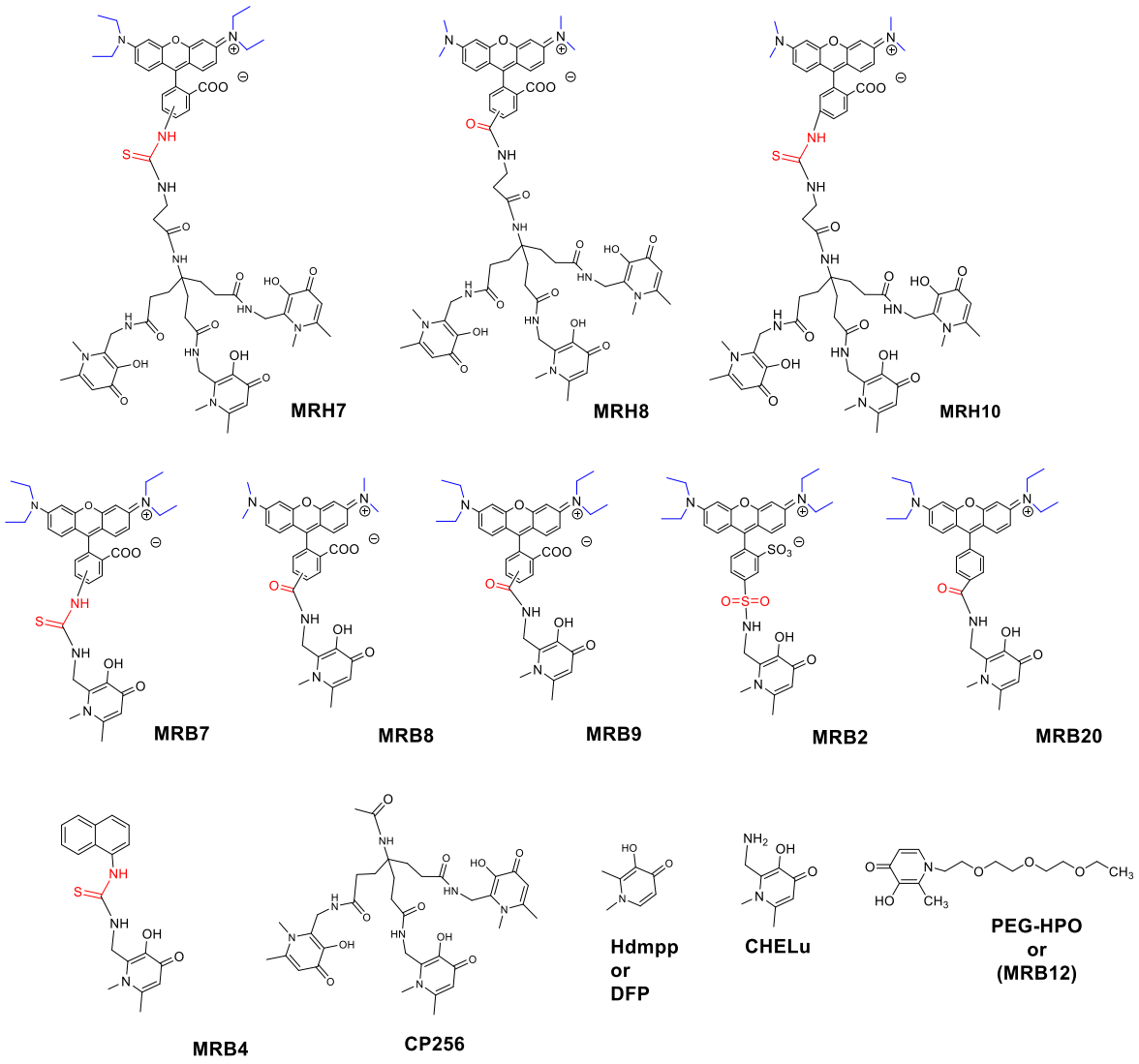

Figure A.1 - Formula of 3,4-HPO chelators referred in the present work.

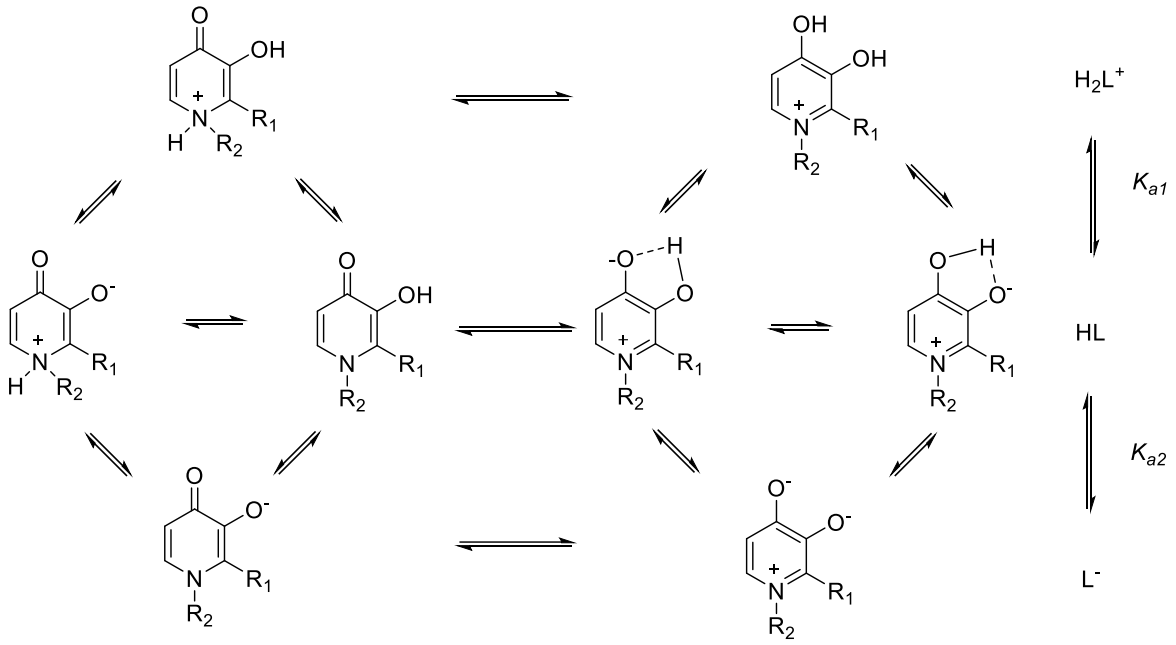

Figure A.2 – Dissociation steps of 3,4-HPO ligands (adapted from reference [345]).


U.PORTO
FACULDADE DE CIÊNCIAS
UNIVERSIDADE DO PORTO